An investigation into the uptake of gold nanoparticles by isolated cells and whole vessels and their influence on function

Teba Mohamed

A thesis submitted in partial fulfilment of the requirements of the Manchester Metropolitan University for the degree of Doctor of Philosophy

School of Healthcare science
the Manchester Metropolitan University

2014

بِسْمِ ٱللَّهِ ٱلرَّحْمَٰنِ ٱلرَّحِيمِ

In the name of Allah, the Most Gracious and the Most Merciful

Knowledge

is Light

Thesis Abstract

Background: Nanoparticles (NPs) of different material composition (silica, gold) have gained increasing attention in drug therapeutics and diagnosis of disease. In particular, Gold nanoparticles (AuNPs) demonstrate potential for cell tracking and imaging diagnostics, however, their impact on cellular and vascular function remains uncertain. The AuNPs emission characteristics can vary when they are suspended in different physiological fluids due to their aggregation; hence, to overcome this effect, organic polymer composite coatings have been applied. The aim of the present study is to investigate the effects AuNPs and their surface modifiers on endothelial cell and murine aortic vascular function, *ex vivo*.

Methods: A number of nanoparticles were fabricated (silica, gold), but AuNPs were selected because they were simple to synthesise and characterise. AuNPs (12±3nm) were synthesised according to the Turkervich method. They were then surface modified with the polymers polyvinylpyrrolidone (PVP) and mercapto-polyethylene glycol - (mPEG) and characterised by transmission electron microscopy (TEM), energy dispersive X-ray spectroscopy (EDAX) and UV-Vis spectroscopy. Silica NPs (SiNPs, 100 and 200 nm) were synthesised using a modification of the Stöber method. They were characterised using TEM and the Malvern Zeta Sizer. Cellular uptake of AuNPs by cultured bovine aortic endothelial cells (BAECs) was visualized using transmission electron microscopy (TEM). The effects of AuNPs on BAEC proliferation, cell viability and apoptosis were determined using the automated cell counter and flow cytometry for cell number counting, exclusion dye propidium iodide (PI) and Annexin V/PI detection, respectively. Aortic vessel rings from male Wistar rats were mounted between two fine steel wires in an organ bath system and constantly superfused in oxygenated physiological salt solution (PSS) at 37^{o}C. Cumulative doses of the endothelial dependent agonist acetylcholine (ACh; 0.01-100µM) and endothelial independent sodium nitroprusside (SNP; 0.1nm-10µM) were added to KCl preconstricted vessels, before and 30 minutes after incubation with modified and non-modified AuNPs.

Results: Maximum cellular uptake of AuNPs was observed 24 hours and 48 hours, after incubation in non-modified and modified AuNPs, respectively. Both non-modified and

modified AuNPs significantly decreased cell viability and proliferation and increased apoptosis up to 24 hours after incubation, whereas no inhibitory effect was observed after 48 hours of incubation. Both modified and non-modified AuNPs influenced cellular signalling and reduced Erk and Akt phosphorylation. Non-modified AuNPs had no overall effect on ACh responses, but significantly reduced responses to SNP. PVP modified AuNPs (AuPVP), but not mPEG modified AuNPs (AumPEG) lead to a significant attenuation in ACh responses (ACh concentration 0.01-100μM; $p<0.05$). AumPEG at 2.9μg/mL had no overall significant effect on either ACh or SNP responses; however, at higher concentration (5.8μg/mL) AumPEG NPs led to a significant reduction in ACh dilator response at most ACh concentrations. PVP alone, at the minimal concentration required to stabilise the AuNPs, reduced ACh dilator responses.

Conclusions: We demonstrate that surface modification of AuNPs using polymers enhances their stability in physiological solutions and culture media, and also reduces cellular uptake by BAECs. Furthermore, we show that cellular and vascular effects of AuNPs depends on the type and concentration of polymer modification used. mPEG modified AuNPs show greater biocompatibility and are less detrimental to vasodilator function, than PVP modified AuNPs, thus showing greater potential use as agents for diagnostic imaging and therapeutics.

Thesis outline

Nanoparticles synthesis (Chapter 2)

Silica Nanoparticles (SiNPs) (100nm) encapsulated with Rhodamine B isothiocyanate (RH) dye

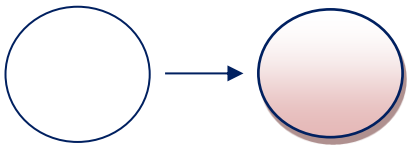

Silica Nanoparticles without dye

Silica Nanoparticles with RH dye

Non -modified gold nanoparticles (AuNPs) and modified gold nanoparticles with A) polyvinylpyrrolidone (PVP) and B) mercapto polyethylene glycol - (mPEG)

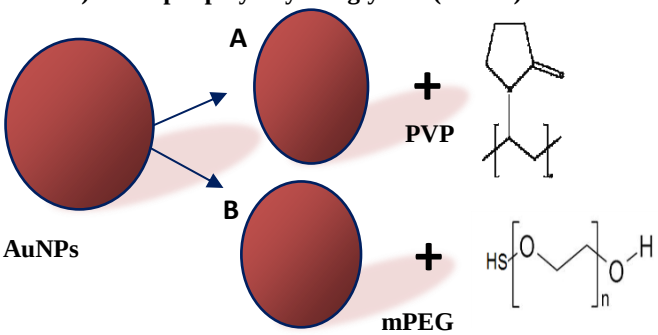

Characterisations (Chapter 3)

A. Scanning electron microscopy (SEM) and transmission electron microscopy (TEM) will indicate the dispersion and sizes of SiNPs.

B. Sizes and stability will also be determined using dynamic light scattering (DLS) and Malvern's Zetasizer.

C. Fluorescence spectroscopy will identify the presence of the encapsulated RH dye on the NPs.

Characterisations (Chapter 3)

A. TEM will indicate the dispersion of modified and non-modified AuNPs and stability will be determined using Ultraviolet-visible spectroscopy (UV-vis).

B. Thermogravimetric analysis for decomposition analysis, infra-red spectroscopy for surface groups attachment.

C. Surface-enhanced Raman scattering (SERs) will also be employed to identify the functional groups attached on AuNPs.

D. Determination of the relative amount of gold in NPs is done by Inductively coupled plasma mass spectroscopy (ICP-MS) and Energy-dispersive X-ray spectroscopy analysis will identify the element of gold in AuNPs.

CELLULAR study (Chapter 4)

Aims

- To determine the effect of mPEG and PVP_Modified gold nanoparticles on bovine aortic endothelial cell's (BAEC) viability, apoptosis, and proliferation.
- To determine the cellular uptake of NPs.

VASCULAR study (Chapter 5)

Aims

- Determine the influence of AuNPs on vascular function using whole aortic vessels *ex* vivo. (Can non-modified and modified AuNPs affect vascular function? Specifically, do they affect: Endothelium dependent (ACh) and endothelium independent (SNP) vasodilator function?).

Discussion and Conclusions (Chapter 7)

List of abbreviations

Acetylcholine	ACh
Alkoxide silica	$Si(OR)_4$
(3aminopropyl) triethoxy silane	APS
Ammonium hydroxide	NH_4OH
Ammonium nitrate	NH_4NO_3
Back-scattered electrons	BSE
Blood–brain barrier	BBB
Bovine Aortic Endothelial Cells	BAEC
Bovine Serum Albumin	BSA
Calcium	Ca^{2+}
Calcium chloride dihydrate	$CaCl_2.2H_2O$
Caveolae-mediated endocytosis	CvME
Central nervous System	CNS
Clathrin mediated endocytosis	CME
Cyclic adenosine monophosphate	cAMP
Cyclic guanosine monophosphate	cGMP
4',6-diamidino-2-phenylindole	DAPI
Debye Landau Verwey Overbeek	DLVO
Diffuse reflectance infra-red Fourier transform spectroscopy	DRIFTS
Dulbecco's Modified Eagle's medium	DMEM
Dynamic light scattering	DLS
Energy-dispersive X-ray spectroscopy analysis	EDAX
Electrochemical Double layer	EDL
Endothelium	ECs
Endothelin receptors A and B	ET_A and ET_B
Endothelium –delivered hyperpolarizing factor	EDHF
Endothelium derived contracting	EDCF
Endothelium derived Relaxing	EDRF
Ethanol	EtOH

Endothelial nitric oxide syntheses	eNOS
Extracellular-signal-egulated kinase	ERK
Ethylenediaminetetraacetic acid dipotassium salt dehydrate	$K_2EDTA.2H_2O$
Fibroblast growth factor	FGF
Fluorescein isothiocyanate	FITC
Fluorescein tagged silica particles	FITC-SiO2
Fourier transform infrared spectroscopy	FTIR
Functionalized carbon nanotubes	*f*-CNT
Gold (iii) chloride sodium	$HAuCl_4$
Gold Nanoparticles	AuNPs
Helmholtz layer	HL
Helacyton gartleri	HeLa
Human Dermal Microvascular Endothelial Cells	HDMEC
Human umbilicalvein endothelial cells	HUVEC
Human liver carcinoma cell line	HepG2
Hydrogen peroxide	H_2O_2
Inductively coupled plasma mass spectroscopy	ICP-MS
Inward rectifier Potassium Channels	K_{IR}
Isopropanol	IP
L-Arginine	L-Arg
Laser Doppler Velocimetry	LDV
Magnetic nano-particle	MNP
Magnesium sulphate heptahydrate	$MgSO_4.7H_2O$
Mercapto polyethylene glycol	mPEG
Mercapto polyethylene glycol modified gold nanoparticles	AumPEG
Mercaptoundecanoid acid	MUA
Michigan Cancer Foundation	MCF-7
Nanoparticle	NP
Nitric oxide	NO
Nitric oxide synthase	NOS
Oxidative phosphorylation	OXPHOS
Phenylephrine	Phe
Phenylmethylsulfonyl fluoride	PMSF

Physiological salt solution	PSS
Photon Correlation Spectroscopy	PCS
Positron emission tomography	PET
Potassium channels	K_{CA}
Potassium chloride	KCl
Potassium phosphate monobasic	KH_2PO_4
Potassium Physiological salt solution	KPSS
Polyethylene glycol	PEG
Polyethylene glycol single-walled carbon nanotube	PEG-SWCNTS
Polyvinilpirrolidine	PVP
Polyvinilpirrolidine modified gold nanoparticles	AuPVP
Porcine brain endothelial cells	PBEC
Propidium iodide	PI
Program cell death	PCD
Protein kinase G	PKG
Quasi Elastic Light	QELs
Sodium orthovanadate	EGTA
Sodium biocarbonate	$NaHCO_3$
Phosphate Buffered Saline	PBS
Radioimmuno-precipitation	RIPA
Reactive oxygen species	ROS
Receptor mediated endocytosis	RME
Rhodamine B isothiocyanate	RH
Smooth muscle cells	SMC
Surface Plasmon Resonance	SPR
Surface-enhanced Raman scattering	SERs
Scanning electron microscope	SEM
Sarcoplasmic reticulum	SR
Serum poor medium	SPM
Sodium nitroprusside	SNP
Silica nanoparticles	SiNPs
Silicon dioxide	SiO_2
Secondary electron imaging	SEI
Standard error of mean	S.E.M
Spinal cord injury	SCI
Standard deviation	SD
Sarcoendoplasmic reticulum Ca2+ ATPase	SERCA
Thermogravimetric analysis	TGA

Sodium chloride	NaCl	Transmission electron microscope	TEM
Targeted drug delivery system	TDDS	Vascular endothelial growth factor	VEGF
Tetraethyl orthosilicate	TEOS		

Contents

Chapter 1: Introduction

Chapter 4: Influence of modified and non-modified gold nanoparticles on cellular function

Chapter 5: Influence of Modified and Non-modified Gold Nanoparticle on Vascular function

List of Figures

List of Tables

List of Equations

Declaration

This thesis contains no material which has been accepted for the award of any other degree or diploma in any university, to the best of my knowledge and belief, contains no material previously published or written by another, except where due reference has been made in the text. In addition, no parts of this thesis have been copied from other sources. I understand that any evidence of plagiarism and/or the use of unacknowledged third party data will be dealt with as a very serious matter.

Signature: Teba Mohamed Date: 20/08/2014

Ethical consideration for experimental animals

The physiological function experiments in this study were performed using animal tissue excised from dead animals (Male Wistar rats, 200-300 g in weight, aged 7-13 weeks), obtained from the BSU, University of Manchester. The Wistar rats were housed under standardised conditions (12 hour light/ dark cycles at 24 ºC). The animals were humanely killed by stunning and cervical dislocation. All procedures are conducted in accordance with institutional guidelines of the MMU and the University of Manchester and the United Kingdom Animals (Scientific Procedures) Act of 1986 (schedule 1 killing- Experiments were performed with the approval of the Review Board of the University of Manchester and the Home Office. A risk assessment for the use and handling of animal tissue was conducted.

This piece of work is dedicated to my loving parents,

(Zubeda Mohamed and Hamid Mohamed);

I will forever strive to make them proud.

They have always been my greatest inspiration and I thank them for their endless support throughout this long journey.

They are the number one reason 1 am where I am today.

I love you.

Acknowledgment

In the name of Allah, the Most Gracious and the Most Merciful

Alhamdulillah, all praises to Allah for the strengths and His blessing in completing this thesis. This thesis has been a long enjoyable journey that has allowed me to expand my scientific knowledge through the various projects explored. The ability for me to pursue this avenue would not have occurred without the support and love that surrounded me. There are many invaluable supporters that have enabled me to succeed, without whom I would have felt lost. I would like to send my heartfelt thanks to my director of studies Dr. May Azzawi. This thesis would never be completed without your help, support, extreme patience, unsurpassed knowledge and constant advice. I am also truly grateful for the guidance and experience of my second supervisor Dr. Debra Whitehead, who has ensure my triumph through the chemistry section of my research investigations. I would also like to thank my third supervisor Dr. Nessar Ahmed for his help in the cell culture investigation of this research thesis. I would also like to express my appreciation to Dr. Sabine Matou - Nasri, for her help in teaching me the step by step procedure for cell culture. I also want to thank Professor Bill Gilmore for his kind support.

I would like to further express my thanks to a very special technical staff who does not have “no” in his vocabulary, thank you Mr Dave Maskew. I am also grateful for the technical help I received from Glenn Ferris.

Words cannot express the gratitude I feel towards my family. I am extremely grateful for the support, love and care I received from both my mother and father. I would also like to thank both my brothers, Abdulrahim and Abdulrahman, for all the support I received from them. I am also grateful to my little cousin Waleed for all the times he took my mind off my thesis by pestering me.

Finally, this is a special thank you to all my friends!

Publications and conferences :

Conferences:

Mohamed T, Whitehead D and Azzawi M 'The influence of PVP and mPEG- Coated Gold Nanoparticles on cellular and vascular function' International Cell Tracking Symposium on the use of nanoparticles as imaging agents for cell tracking University of Liverpool 2013.

Mohamed T, Whitehead D and Azzawi M 'The Effect of gold nanoparticle stabilisers on aortic vessel function Alternative Muscle Club 'AMC' 2011 conference in Univeristy of Oxford.

Mohamed T, Azzawi M, Whitehead D, Jones C, Akbar N, Azhar M 'Attenuation of vasodilator responses, induced by nanoparticle uptake, in rat aortic rings', The physiological society conference, University of Manchester 2010.

Whitehead D, Azzawi M, Farooq A and Mohamed T. Novel nanoparticle systems for use in bioapplications tested using novel physiological systems(microfluidics and nanotech in Drug Discovery conference, 2010.

Publication:

Akbar, N., Mohamed, T., Whitehead D. and Azzawi, M. *'Biocompatibility of amorphous silica nanoparticles: size and charge effect on vascular function, in vitro',* Biotechnology and Applied Biochemistry, 2011, **58(5)**, 353–362.

Mohamed T., Matou-Nasri S., Farooq A., Whitehead D. and Azzawi, M. The influence of polyvinylpyrrolidone and mercapto polyethylene glycol coated gold nanoparticles on cellular and vascular function. In submission.

Farooq, A., Mohamed, T., Whitehead, D. and Azzawi, M. '*Restored endothelial dependent vasodilation in aortic vessels after uptake of ceria coated silica nanoparticles,ex vivo'*. (In Press).

Chapter 1:
Introduction

1. Introduction

1.1 Overview of Nanoparticles and their Applications

According to British Standards Institution (BSI), nanoparticles (NPs) are 'nano-object (material) with all three external dimensions in the nanoscale', where nanoscale is defined as dimension sizes ranging from approximately 1 to 100 nm (BSI, 2011). NPs are one type of nanomaterial, described as a material which has external dimensions or internal/surface structure, all existing in a nanoscale dimension. Due to their small size, nanomaterials are different from the bulk materials and have made a vast impact on the world of nanotechnology.

The fabrication of NPs has witnessed great progress in research and application in the area of nanoscience; the study of matter on an ultra-small scale. NPs are engineered to allow advances in diagnosis and treatment of disease and are used in biomedical applications, including drug and gene delivery (Ghosh *et al*, 2008), bio detection of pathogens (Gu *et al*, 2006), fluorescent biological labels (Huang *et al*, 2009) and tissue engineering (Hachani *et al*, 2013). Moreover, as NPs exist in the same size domain as proteins this makes them suitable agents for biotagging or labelling (Bergman *et al*, 2008; Nitta and Numata, 2013).

NPs have a large surface area to volume ratio and dimensions which gives them the ability fit into cells. Such characteristics of NPs have enabled biomedical scientists to discover that NPs exhibit bioactivity functions. It has been demonstrated that size is one of the characteristics of NPs that influences cell function (Suh *et al*, 1998; Suh *et al*, 2009). In order to allow interaction between biological targets and NPs, NPs have to be coated with layers that act as a bioorganic interface to allow attachment between target site and the NPs and to improve delivery into target tissues (Kamaly *et al*, 2011).

Silica nanoparticles (SiNPs), in particular surface modified silica NPs, the such type of nanoparticles that are currently being explored due to their biocompatibility (Barandeh *et al*, 2012; Akbar *et al*, 2011). Dye doped SiNPs possess important characteristics required to make them an excellent biolabel agent, due to the fact that they are highly photostable with reduced photobleaching effect (Pellach *et al*, 2012), intense luminescence signal, and easy bio-conjugation (Canton *et al*, 2011).

Metal NPs (gold and silver) are also currently being studied for use in biomedical applications due to their unique optical properties, which allow them to be useful in imagining diagnostics. The optical properties are due to their unique interaction with light. The oscillating electromagnetic field of the light stimulates the electrons on the metal particles causing the electrons to oscillate; this effect is referred to as the surface plasmon resonance (SPR) (Mody *et al*, 2010). Using the standard methods of Turkervich and Fern, a wide range of sizes can be fabricated by a chemical reaction involving a reduction of citrate (Kimling *et al*, 2006).

Gold nanoparticles (AuNPs) have been shown to be great potential use in anticancer drug delivery systems and photothermal cancer treatment. They have allowed researchers to easily identify the location of diseases, where cancerous cells have been shown to easily uptake AuNPs (Alkilany *et al*, 2010; Chandra *et al*, 2010; Libutti *et al*, 2010 and Murphy *et al*, 2008). AuNPs are also attractive agents in research as they are easy and inexpensive to synthesise and characterise by UV-spectra and TEM. For instance; a study has looked at quantifying collagen fibril morphology under the influence of AuNPs and were able to identify uptake using TEM (Haidekker *et al*, 2006). Furthermore, AuNPs are widely applicable in radiation research due to their high atomic number (Z). Subsequently, this results in a different mass energy absorption property. For example, in an X-ray analysis of a tissue uptake of AuNPs, the mass energy absorption property of gold is greater than that of the soft tissue. The high atomic number corresponds to a large bound of electrons, which results in high mass absorption coefficient of the gold than the tissue for X-ray. Hence AuNPs are described as being effective X-ray agents (Butterworth *et al*, 2013).

The size, stability and cell specificity of functionalised nanoparticles for targeted drug delivery is dependent on surface modification and can influence the NP's biodistribution and may affect cell function (Suh *et al,* 2009). Other crucial factors, such as cytotoxicity and the efficiency of cellular uptake, are also associated with nanoparticle size. Furthermore, Yu *et al,* (2009) gave evidence that the concentration and size dependent toxic effects are cell specific.

Useful analytical techniques have been introduced to allow characterisation of studied nanoparticles. These include TEM, SEM, and dynamic light scattering (DLS) (Lim *et al,* 2013). The Zeta potential measurements are also necessary to determine the colloidal stability of NPs which signify the repulsive force that is present between NPs. It is used to show the effect of suspension of NPs in a given solution and the resultant stability of functionalised NPs.

1.2 Synthesis of Nanoparticles

Recently, scientists have established different approaches for the synthesis of NPs. Furthermore, the process and chemical reactions in which nanoparticles undergo during synthesis have also been explored. In this study, the focus will be on the formation of nanoparticles from inorganic (Silica) and metal organic (gold) compounds in liquid phase.

A simplified flow chart below (Figure 1.1), illustrated the process that occurs during synthesis of nanoparticles from inorganic compounds (silica).

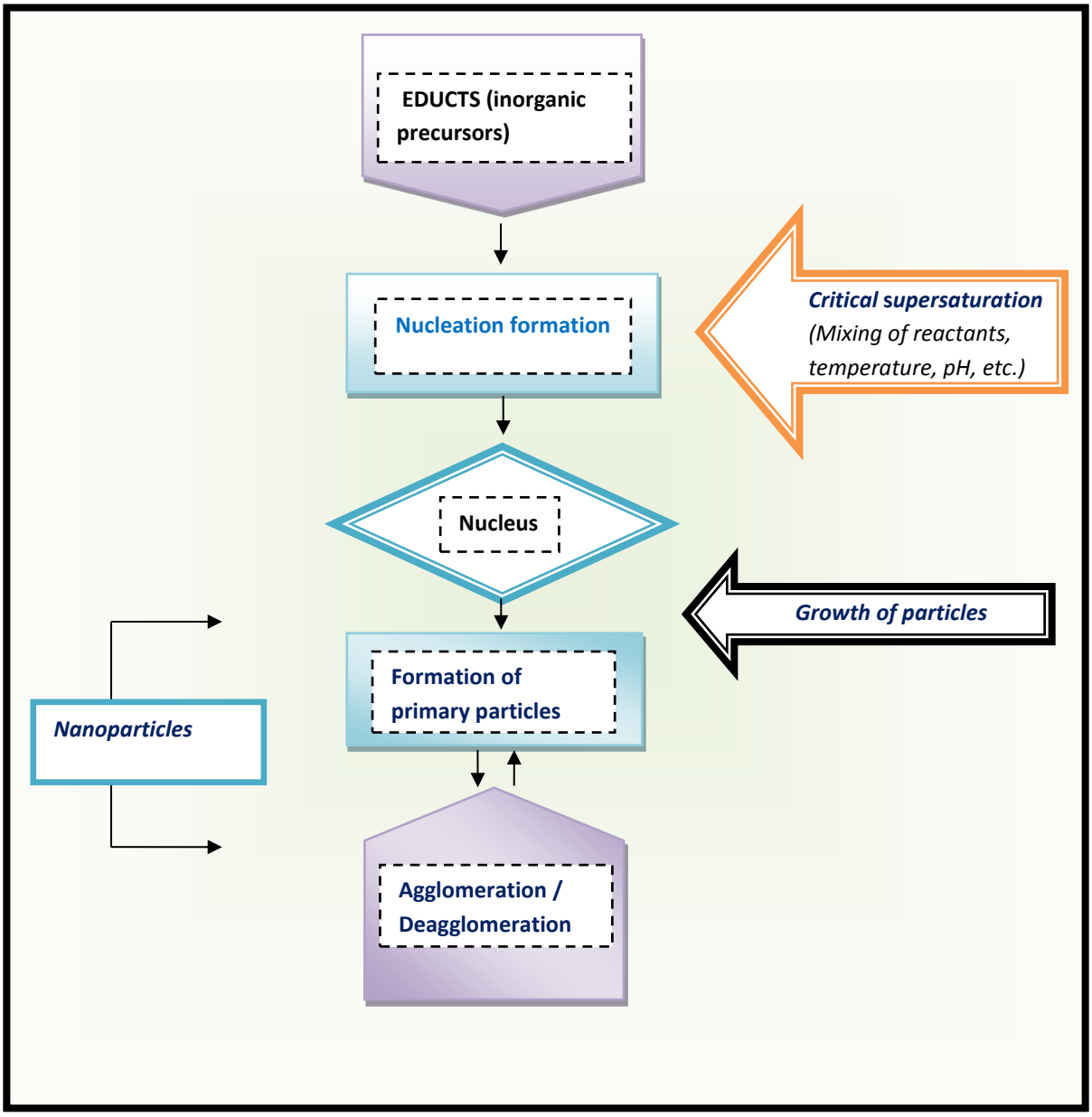

Figure 1.1: Representation the process involved during nanoparticle formation.

The silica nanoparticles (SiNPs) formation can be divided into two stages: nucleation and growth (Rahman and Padvettan, 2012). There are two types of models involved in the growth mechanism of SiNPs being either, monomer addition or controlled aggregation. The monomer addition involves the addition of hydrolyzed monomers, on the primary particle surface. Whereas, controlled aggregation involves expanding the nucleation of particles continuously. During the reaction, the primary particles are formed which then aggregate together, resulting in larger particles known as secondary particles. However, both models lead to the formation of spherical or gel, depending on the reaction condition (Rahman and Padvettan, 2012). The processes of SiNP formation are described in detail in the following section (Section 1.2.1).

1.2.1 Growth mechanisms of Silica nanoparticles

Silica NPs formation is most commonly used in nanotechnology, due to its various structure arrangements and its properties. According to its structure arrangements, the silica material can define whether particles produced are porous or non-porous. The formation of monodispersed silica nanoparticles is currently been described by several models. These include the sol gel method and the microemulsion method. The sol gel method involves developing NPs using inorganic precursors usually metal salts, metal halides and alkoxides ($M(OR)_x$).

The mircoemulsion method, on the other hand involves a system of thermodynamically stable liquid solution which is dispersed with two or more immiscible mixture, for instant water, oil and an amphiphilic molecule such as hydrocarbon based surfactant (Wang and Zhang, 2013). The sol-gel method will be described in more detail below.

1.2.2 Sol-gel method

The sol-gel method allows the manipulation of particle sizes by altering certain parameters including pH, temperature and concentration of reactants. There are several steps that occur before particles are completely fabricated during the sol gel process. The steps include hydrolysis and condensation, and these steps are considered the important stages during NPs formation. It is the rate of either hydrolysis or condensation that influences the rate of reaction. Consequently, the formation of NPs with the desired size is produced. The influence of low pH conditions (acidic), causes slow rate of hydrolysis and slow condensation. Furthermore, gelation is formed. In high pH conditions (basic), a slow rate of hydrolysis occurs, and in turn fast condensation takes place which leads to the formation of colloidal particles (Buckley and Greenblatt,1994).

Originally, it was in 1968 when Stöber *et al* pioneered a method which resulted in the formation of colloidal particles. The Stöber method involves preparation of silica spheres from tetraethylorthosilicate (TEOS) in mixtures of ammonia, water and ethanol. TEOS in the reaction represents the silica precursor which allows the first step of hydrolysis reaction to occur when mixed with alcohol. Ammonia acts as a catalyst once added to the reaction mixtures. The next step of the reaction, known as condensation, occurs when alcohol or water molecules are added in the reaction (Green *et al*, 2003) (Figure 1.2).

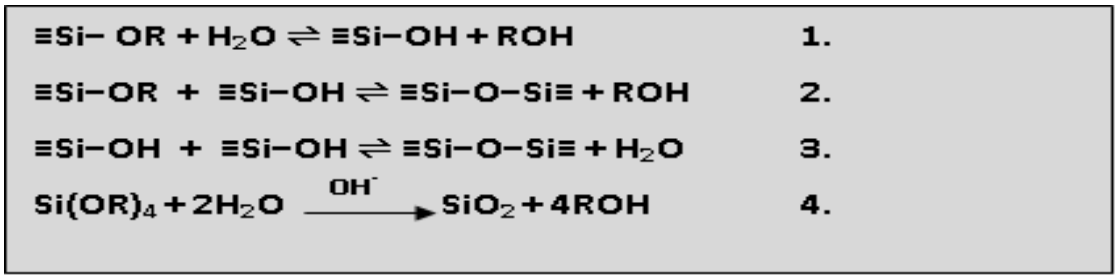

Figure 1.2: The scheme represents the reaction step involved in formation of monodisperesed silica nanoparticles; in order 1. represents the first step hydrolysis, 2. condensation reaction involving alcohol and finally (3) condensation reaction involving water 4. the overall reaction involved in NP synthesis, where R is ethanol (ETOH) ***in the form of C_2H_6O.***

Hydrolysis, previously described, is the first step of the reaction in which TEOS reacts with alcohol. A further second step reaction takes place which involves the condensation of alkoxide silica $Si(OR)_4$ to form monodispersed silica microspheres (Figure 1.3).

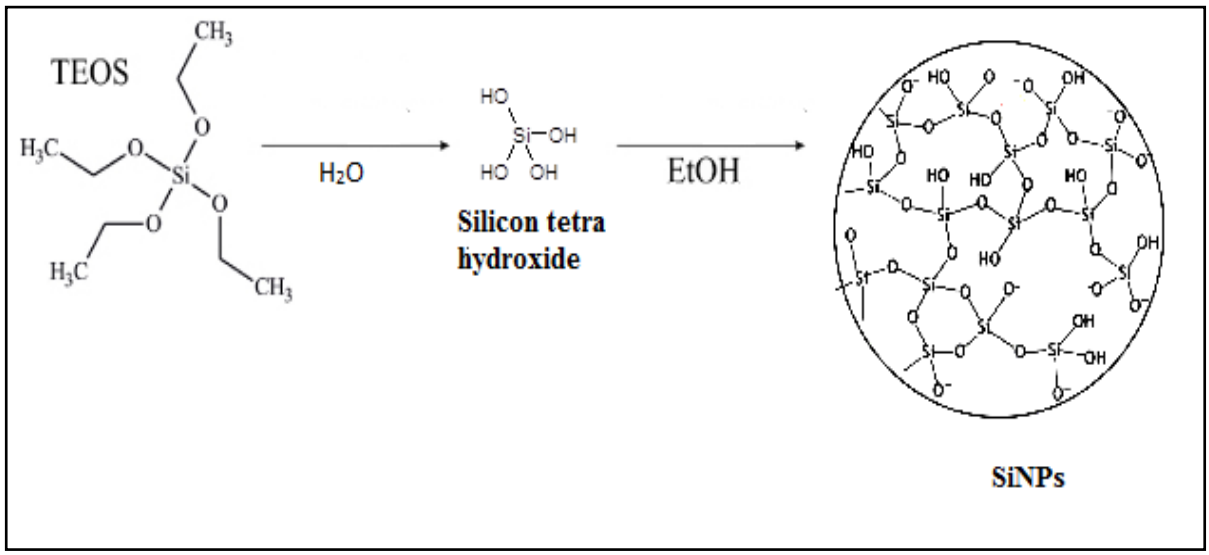

Figure 1.3 Schematic diagramc of Stöber method for the sol-gel reaction forming silica microspheres reaction. Image adapted from Korzeniowska et al (2013).

Studies have reported ways to control the size of the NPs by manipulating the concentration of ammonia, water, alcohol solvent and temperature used in the experiment (Venkatathri, 2007; Geishe, 1993). Geishe, found that parameters such as temperature and ammonia influenced the size of NPs. The decrease of temperature or the increase of ammonia concentration leads to large particle formation. Bogush *et al* (1988), introduced an empirical equation, which was later adapted by Razink *et al* (2007) to directly show that diameter (*d*) of particles is influenced by concentration (mol.l^{-1}) of reactants at 25°C (Figure 1.4).

d=A $[H_2O]^2 exp(-B[H_20]^{1/2})$	**Eq. (1.1)**
Where A and B is defined as:	
A= $[TEOS]^{1/2}(82+151[NH_3]+1200[NH_3]^2-366[NH_3]^3)$	**Eq. (1.2)**
B=$1.05+0.523[NH_3]-0.128[NH3]^{2.}$	**Eq. (1.3)**

Figure 1.4: Empirical equation showing the relationship between the concentration of reactants and the diameter of the particles where in Equation 1.1 Term d is the average particle diameter . Term A is specified in Equation 1.2 later adapted by Razink et al (2007) and, Term B is specified in Equation 1.3.

The sol-gel method is considered advantageous over the microemulsion methods, as it allows the formation of porous particles, for instance; mesoporous NPs. Mesoporous NPs with large surfaced area have been developed. These have been shown to improve the solubility of poorly dissolution drugs *in vitro* and *in vivo* (Lin *et al*, 2005; Martines *et al*, 2005; Lu *et al*, 2007).

1.2.3 Synthesis of gold nanoparticles

It is known that gold (Au) has common oxidation states which includes +1 (Au [I] or aurous compounds) and +3 (Au [III] or auric compounds) (Jain *et al*, 2012). AuNPs are produced from the reduction of chloroauric acid. The process of AuNP synthesis involves dissolving $HAuCl_4$ in water under vigorous stirring conditions at boiling temperature. A reducing agent is then introduced to the reaction. As a result, the Au ions are reduced to neutral Au atoms. In addition, more gold atoms are formed. Subsequently, the atoms start to precipitate in order to form NPs. The gold particles formed then stick to other NPs. If the particles are left under vigorous stirring over a longer period, the particles will eventually aggregate. The length of stirring time influences the size of particles. A number of methods have been developed to allow the fabrication of AuNPs. A well simplified method is known as the Turkevich method (Kimling *et al*, 2006).

1.2.3.1 Turkevich method

The Turkevich method was firstly developed by J. Turkevich *et al* in 1951 and was further improved by G. Frens in 1970s. The Turkevich method produces monodispersed spherical AuNPs in water suspension. Large particles as well as small particles ranging from 10-20 nm can also be achieved using this method. However, it is difficult to produce large monodisperesed spherical particles using this method. The reaction of AuNPs formation involves chlorauric acid in hot water solution, mixed with sodium citrate solution. In this process the gold is reduced by the citrate ions which acts as a reducing agent as well as a capping agent (Ojea-Jiménez and Campanera, 2012). A capping agent is a stabiliser which prevents aggregation of particles. The concentration of sodium citrate influences the diameter of particles produced. Large particles can be obtained using less amount of sodium citrate in the reaction. The particles aggregate into larger particles because the

amount of reducing agents to stabilise the gold particles is reduced. Hence, the particles synthesized by citrate reduction have a negative surface charge due to the weak citrate attachment on the particles. These particles can be characterized without difficulties by their plasmon absorbance band (~ 520 nm for 13 nm particles), (Murawska *et al*, 2012).

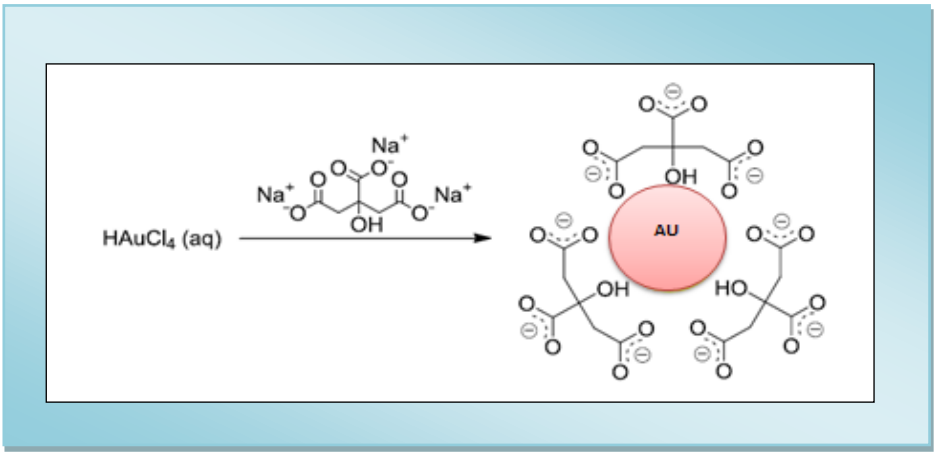

Figure 1.5: Schematic illustration represents the synthesis of AuNPs by reduction of $HAuCl_4$ with sodium citrate.

1.3 Stability of colloidal nanoparticles (Gold and Silica)

Colloidal particles are considered favourable in most studies of NPs. The term colloidal refers to a system whereby particles are finely dispersed in a suspension and are in the size range between 1-1000 nm. Colloidal particles are classified as being irreversible colloid and hydrophobic (water-hating colloid). They tend to remain dispersed in a continuous phase (suspension) due to the minimal interaction between the hydrophobic particles and their suspension (Shaw *et al*, 1992). One common property of colloidal particles is the Tyndall effect. When a beam of light passes through a colloidal solution the light is scattered due to the colloidal particles and this scattering of light is known as the Tyndall effect. Stabilising NPs prevents the attraction between particles known as aggregation. According to Brownian motion, there is a natural kinetic energy in particles which causes random movements of particles in suspension. Hence, the particles collide with each other, subsequently; they may attract or repel (Souza and Miller, 2010).

Debye Landau Verwey Overbeek (DLVO) theory, explains that to prevent aggregation, suspension should acquire greater electrostatic force than van der Waals forces, as colloidal stability is dependent on van der Waals attraction and electrostatic repulsion (Toma *et al*, 2010; Ojea-Jiménez and Puntes, 2009). This is explained in more detail in the next section. Therefore stabilisers are designed to prevent aggregation of particles. This allows particles to be well dispersed in the media. There are different types of aggregations which can occur. These include coagulation, flocculation and gelation. Coagulation refers to particles being packed on each other as clumps. Flocculation type is a reversible aggregation in which, particles are linked together from the weak interaction bonds formed between particles. Finally, gelation aggregation occurs when three dimensional networks are formed by particles which are linked in to branches. This results in the increase of viscosity. Consequently, a solid field network is formed (Figure 1.6) (Hench and West, 1990).

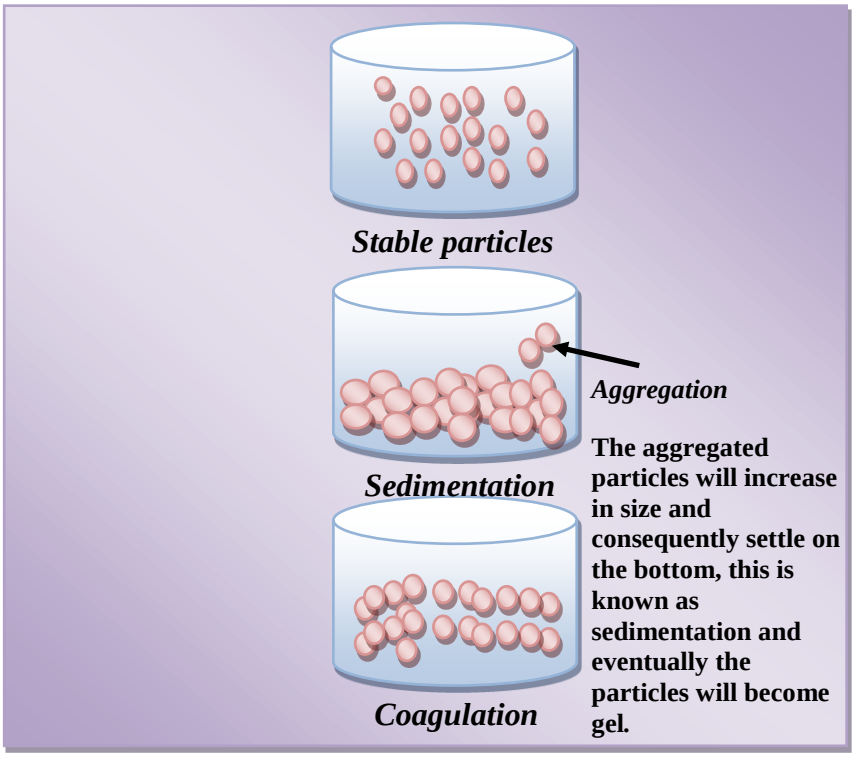

Figure 1.6: Stable colloidal nanoparticles and unstable particles undergoing coagulation and sedimentation.

Stability of particles is considered critical, depending upon the application the particles are used. For instance, if particles are designed for medical applications, the particles need to be stable colloidal in order to increase the uptake of particles by the target cells or tissue. Particle aggregation could increase the risk of toxicological side-effects (Dominguez-Medina *et al*, 2013).

1.3.1 Debye Landau Verwey Overbeek theory

The importance of studying surface characteristics in chemistry is considered one of the critical phases in NP fabrication, as this concepts determines the aggregation of NPs. Studies have considered that particle aggregation has an impact on NP uptakes by cells, thus particle aggregation should be avoided. Surface chemistry has reflected that solutions are used in wide ranges of pH values as well as ionic strengths. Hence the Derjaguin, Landau, Verwey, and Overbeck (DLVO) theory was introduced. DLVO theory stated that colloidal stability in solution is dependent on van der Waals attraction and electrostatic repulsion. DLVO theory is viewed as an acceptable model for stability (Doane and Bruda, 2013; Dukhin *et al*, 2010; Ojea-Jiménez and Puntes, 2009; Park and Borsa, 2004). Particle stability is influenced by the strength of pH and ionic strength of the solution. Furthermore, in order to prevent particles from aggregating, the colloidal particles in suspension should emit a greater electrostatic repulsive force then the van der Waals attraction forces. According to the DLVO theory, the attractive forces (V_{Total}) formed from the electrostatic repulsive and van der Waals attraction forces can be calculated (Equation 2).

$$\boldsymbol{V_{Total} = V_R + V_A} \qquad \textbf{Eq.2}$$

Where (V_R) is electrostatic repulsive force and (V_A) is van der Waals attraction forces, (expressed in Figure 1.7) (Aulton and Taylor, 2013).

Generally, in a lyophobic colloidal system, the electrostatic repulsive force between particles is due to osmotic pressure produced from the overlap between diffuse layer and closer interaction with the charged particles. An increase of the electrolyte concentration causes the reduction of repulsive force. This occurs as a result of the compression on the diffuse layer. A reduction effect on electrostatic repulsive force leads to particle aggregation, as they are able to overcome the electrostatic repulsion energy barrier (Figure 1.7).

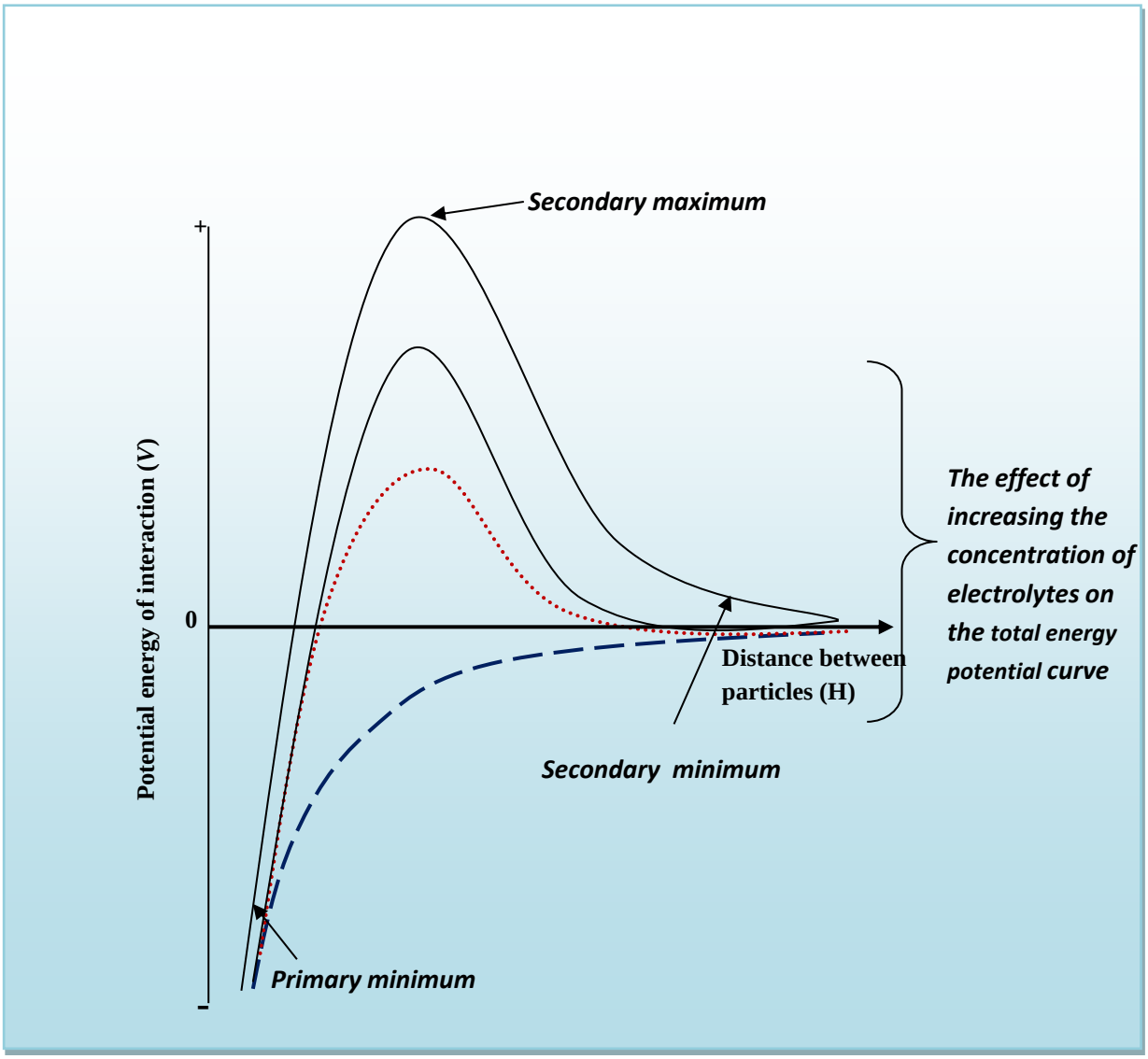

Figure 1.7: The total energy potential of interaction (Vt) between two particles, the schematic expresses the equation VTotal=VR+VA . Additionally, the effect of increasing the electrolyte is shown (Adapted from Aulton and Taylor, 2013)

The curve of potential energy refers to the V_{Total} and distance between the particles. Figure 1.7 illustrates that at a small distance results in the primary minimum, hence indicates the instability of colloidal particles in solution. At a greater inter- particle distance, due to fall off energy, results in the secondary minimum. However, at an intermediate distance, the repulsive energy gives a secondary maximum in the curve and therefore the colloidal solution are well dispersed. Moreover, the addition of the electrolyte in a solution causes the secondary maximum curve to lower and also deepens the secondary minimum curve, which in turn results in flocculation of particles (Aulton and Taylor, 2013).

1.3.2 Influence of surface charge on stability

Surface charges on NPs are known to influence particle stability, flocculation and viscosity (Bizi *et al*, 2012). Understanding surface charge gives insight on interaction between particles. Hence, it is important to determine surface charge including dispersion and stability of particles and to reduce aggregation of the particles. DVLO theory has described in details how surface charge of particles influences the particle characteristics. It describes the behaviour of particles, when interacting with other particles as well as its dispersion ability in solution. For instance, the stability of gold particles can be achieved by surface coating the particles with citrate anions. Similarly, stability of silica particles can also be achieved by coating the particle through subsequent chemical reactions, such as 3-aminopropyltrimethoxysilian (APS). Electrical double layer (EDL) describes the structure of a coating on a surface when interacting with a solution, the interface potential is described as being responsible for forming the EDL. The interface is the boundary which is formed from two different phases i.e. solid to gas, solid to liquid or two immiscible liquids, the interface has different properties compared to the bulk phase. The stern model has been introduced to explain the potential of the EDL which is different to both phases. The model (Figure 1.8) shows the distribution charge of the particles in the electrolyte solutions (Aulton and Taylor, 2013). The surface of the particle adsorbs the monolayer of the electrolyte; this area is known as the inner Helmholtz layer (HL), it causes the surface to be negatively charged. The ions adsorbed are known as dehydrated ions. The monolayer can either be anions or cations and these ions can either be indifferent or specifically adsorbed ions. Indifferent absorption refers to ions which are not involved in specific interaction on the surface, whereas, specifically adsorbed ions by the particle surfaces, causes chemical interaction between the surfaces of the particle (Hubbard, 2002). Stronger interaction between ions and the surface on the particles can also lead to reversal charge on the surface. Whereas, ions with the same overall charge with the particle surface, can lead to greater overall potential (Shaw *et al*, 1992; Aulton and Taylor, 2013).

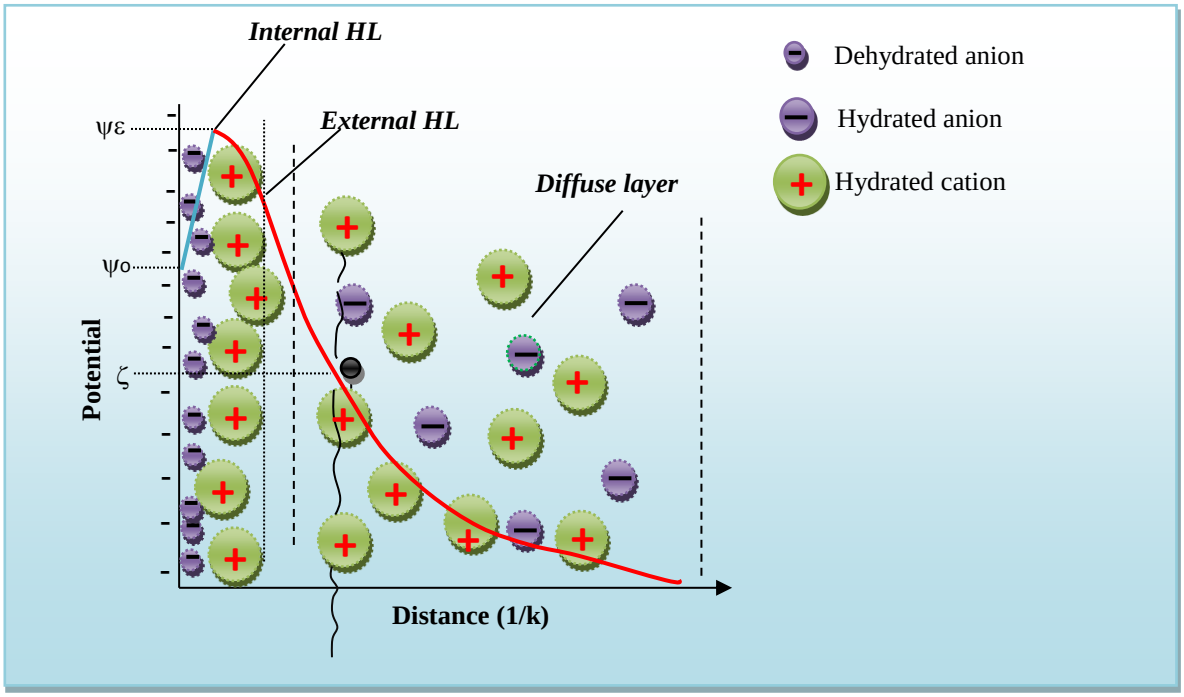

Figure 1.8: Electrochemical double layer on a particle surface in a solution containing electrolytes . Where ψo is surface potential ψε is a stern potential and ζ is zeta potential. (Image adapted from: http://www.silvercolloids.com/Tutorials/Intro/zetaintro.html).

The overlay of different ions and changes in electric potential with distance from the particles surface, also referred to as the thickness of the EDL (1/K) is illustrated in Figure 1.8. K is dependent on the concentration of electrolytes. If concentration of media increases the K increases, resulting in the decrease value of 1/K (Aulton and Taylor, 2013). The inner HL plane is the first layer of the absorbed ions, whereas, the outer Helmholtz plane layer is of non-specifically absorbed, hydrated counter ions. Both the inner and outer HL thickness (δ) are known as the stern layer. The potential changes from ψo to ψε in the stern layer and decays from ψε to zero in the diffuse layer (Figure 1.8) (Nitzsche and Connah, 2012).

1.3.3 Polymeric Stabilisation of nanoparticle surfaces

AuNPs with organic polymer composite coatings have been developed to overcome the effect of interparticle force attraction between gold and water. A polymer molecule creates repulsive force, which counterbalances the attractive force of van der Waals force on the particles when approaching nearby particles. This approach using polymeric stabilisers has aided many studies to overcome aggregation of particles, especially in biomedical application where it has allowed particles to be well dispersed in media. It is crucial for particles to be highly stable, in order for them to carry out their desired properties. For instance, in the delivery of drugs to tissues in order to allow effective release of drugs. Particles have to be highly stable in physiological media in order to prevent aggregation, hence, particles can become internalized by cell (Voliani *et al*, 2012). There are currently two types of polymeric stabilisation, these are steric and depletion stabilisation of colloids. Steric refers to the polymer molecules which form a coating on the particles by attaching on the surface of the particle and forming hairy layers. Consequently, the molecules prevent attraction between particles. It creates a repulsive force causing particles to separate from other particles (Fritz, 2002). On the other hand, the depletion stabilisation involves free polymer molecules in solution which creates repulsive attraction between the approaching particles (Seebergh and Berg, 1994).

1.3.3.1 Polymers

Polymers are chain structured and hydrophilic. They are currently been used in nanotechnology as they have properties which tend to allow the AuNPs to remain well dispersed even at high salt concentrations (Figure 1.9). They cause steric repulsion and prevent coagulation of the colloid particles and therefore make them good stabilisers. (Nagdi *et al*, 2008; Liu *et al*, 2006; Zhang *et al*, 2009; Gasaymeh *et al*, 2010). Many studies on the fabrication of AuNPs built with polymer coatings such as mercapto polyethylene glycol - (mPEG) and polyvinilpirrolidine (PVP) have remarkably proven that nanosized dispersion is enhanced. Interestingly other studies have reported that encrypted polymers target and direct cellular uptake, as well as enhance cytosolic delivery by disrupting endosomal membranes in a pH-dependent fashion. However, the toxicity effect of AuNP stabilisers on vascular function as well as cellular is not known and remains poorly investigated.

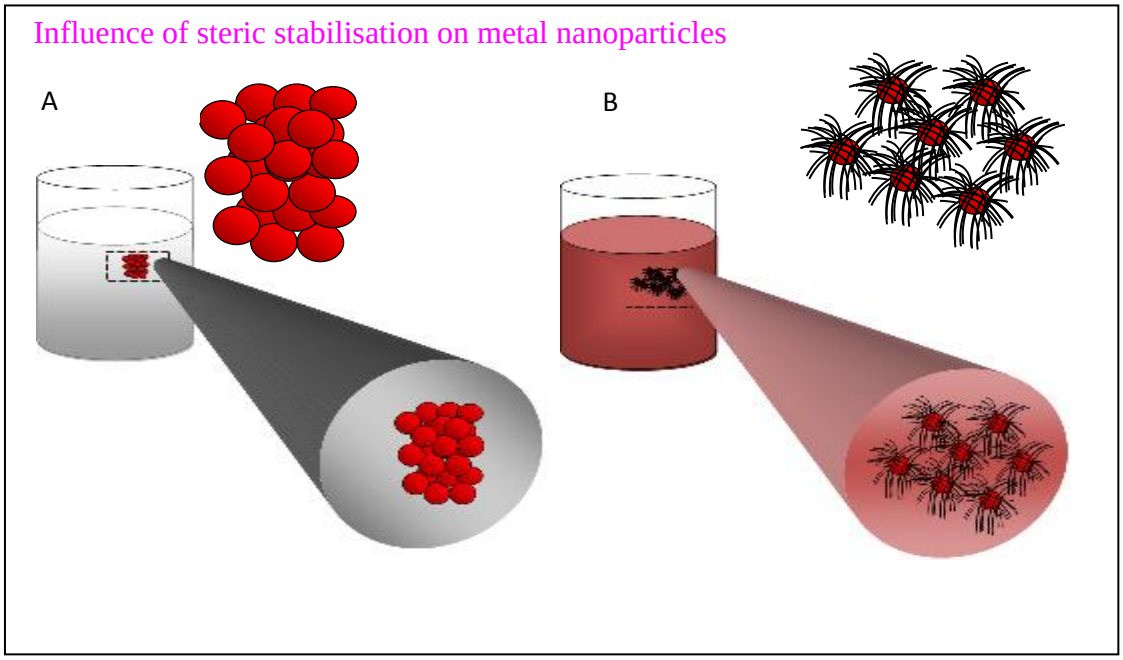

Figure 1.9: Schematic illustration showing the dispersion of A) non-modified AuNPs B) polymer stabilised AuNPs in salt solution.

1.3.3.1.1 Polyvinylpyrrolidone

The polymer compound, polyvinylpyrrolidone (PVP) (Figure 1.10) has a structure and formula of $(C_6H_9NO)_n$ and an average molecular weight of 360,000. It has a long repeating structure. PVP was first discovered by Walter Reppe in 1939, and has been since used in many industrial applications due to its binding abilities. PVP is used in the field of medicine as a blood plasma expander in trauma victims with huge blood loss. It is mostly found in tablets as a binding agents. However, as well as having beneficial properties, large quantities of PVP can be toxic as it has the ability to absorb water. PVP is also known to be lethal as it can cause pulmonary vascular injury if taken by injection other than orally. The molecular structure of polyvinylpyrrolidone (PVP) contains both N and C=O groups. The nitrogen molecule is conjugated with adjacent carbonyl groups. The properties of PVP is determined by its structural formula and is adapted for (a) forming passivating layers around the AuNP core due to the coordination of bond formation between the nitrogen atom of PVP and (b) the polyvinyl groups has a steric repulsion force which prevents agglomeration of the particles (Robinson *et al*, 1990; Astruc *et al*, 2005; Xie *et al*, 2012).

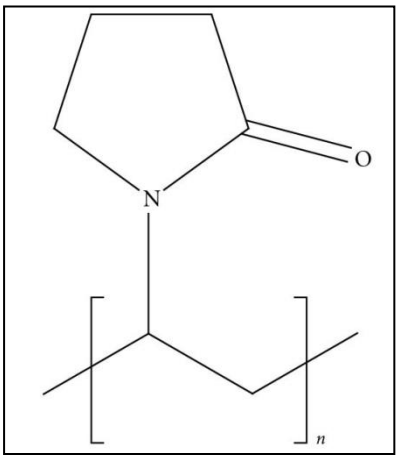

Figure 1.10: The structure of the polyvinylpyrrolidone compound

1.3.3.1.2 Thiol Modified PEG (Mercapto polyethylene glycol - (mPEG))

The molecular formula of PEG is $C_{2n}H_{4n}+2O_n+1$. Polyethylene glycol is a polymer with many applications including industrial and medicinal applications. A series of mercapto compounds containing polyethylene glycol (PEG) group (Figure 1.11), have been synthesised and show advantageous properties such as solubility in water and bio-compatibility. In addition, modified PEG allows chemical bonding to form between PEG and the surface of AuNPs (Figure 1.12), as compared to being physically adsorbed by AuNPs. Many studies are in favour of using PEG for stabilising AuNPs (Manson *et al*, 2011). According to Soel *et al* (2013) the action of PEG chains is related to their affinity to AuCl4(-) ions and conformation on the primary AuNPs. However, Knop and colleagues stated that PEG may also have side effects and complications (Knop *et al*, 2010).

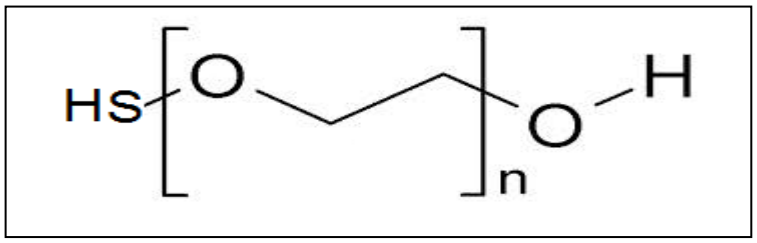

Figure 1.11: The structure of the mercapto polyethylene glycol compound

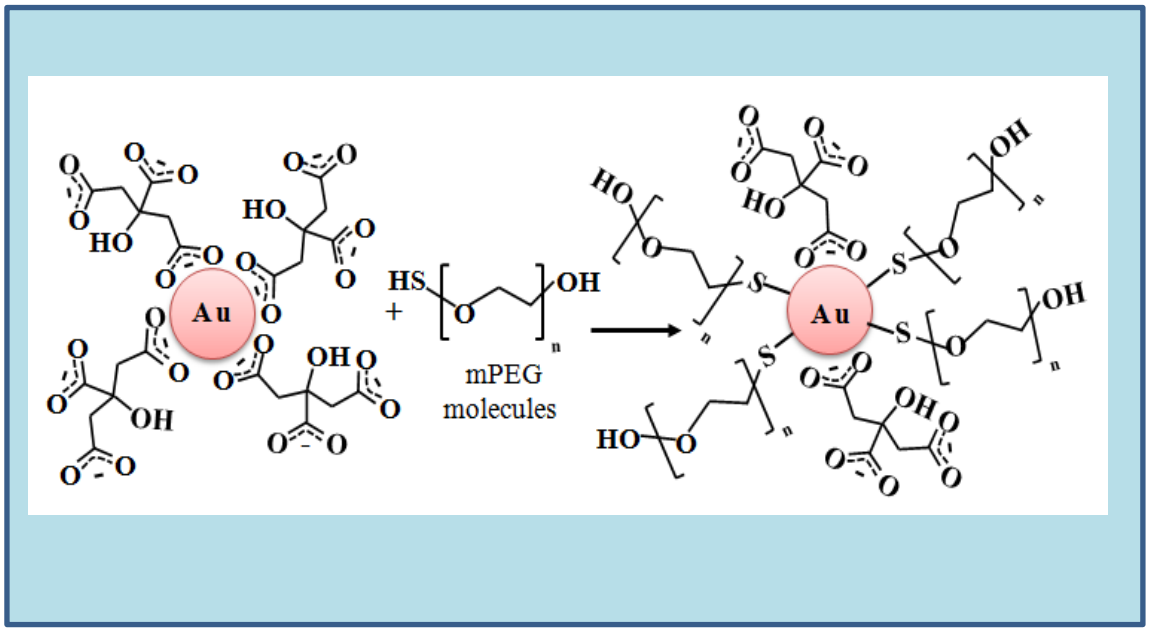

Figure 1.12: Schematic diagram of the reaction of mPEG with AuNPs

1.4 Characterisation of nanoparticles

1.4.1 Electron microscope

Electron microscopes (EMs) are used for characterisation of smaller objects, for example, NPs or cell organelles. The EMs produces a highly magnified image of specimens. There are different types of EM instruments which operate differently from each other. According to the type of EM instrument used, the electron beam can either travel through or over the surface of the specimen. The two common types of EMs are scanning and transmission electron microscope (SEM and TEM) (Figure 1.13), (Staniforth and Aulton, 2007). The following sections (1.4.1.1 and 1.4.1.2) will explain in detail the differences between SEM and TEM.

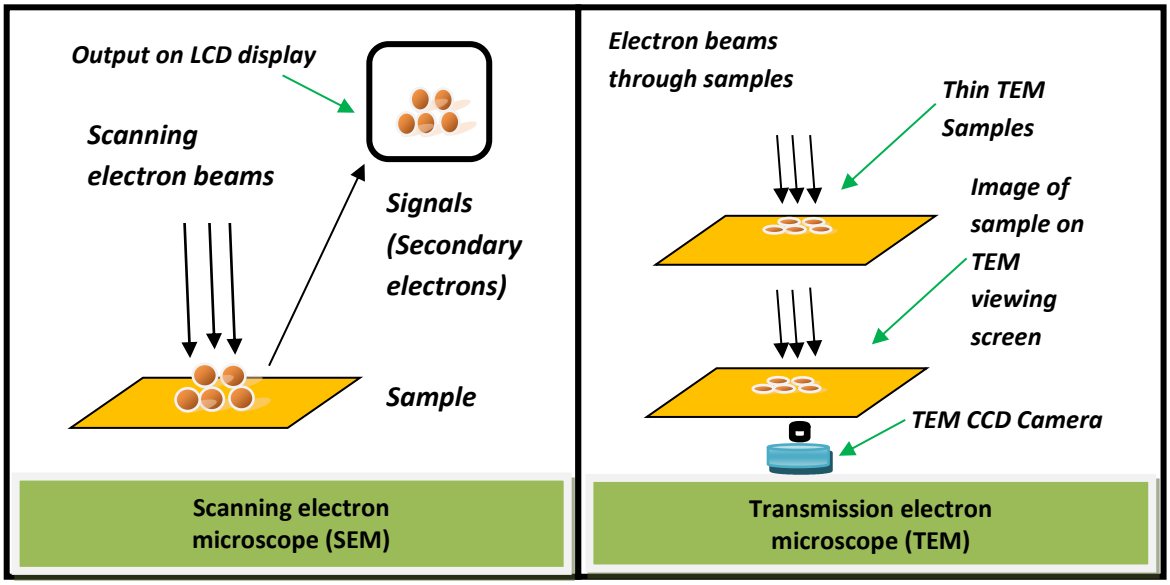

Figure 1.13: An Illustration highlighting the difference in the process of image acquisition between the scanning electron microscope (SEM) and the transmission electron microscope (TEM). In SEM, the electrons interact either on or near to the surface of the specimen to produce an image. In TEM, however, the image is produced when the beam passes through the specimen.

1.4.1.1 Scanning electron microscopy

The scanning electron microscope (SEM) can be used to measure particle sizes. The magnification and resolution of SEMs are lower than TEMs. Unlike the TEM, the resolution of SEM depends on the emission of the instrument (Cortadellas *et al*, 2012). Using a tungsten filament as a source of electrons, the SEM has a spacial resolution of 50-100 nm (Swapp, 2013). The SEM can collect data from an area that ranges from approximately 1 cm to 5 microns in width (Swapp, 2013). Small sized specimens can be imaged at an increased resolution, however, an increased resolution reduces the signal level of detection of the sample, thus the quality of the images is affected (Dunlap and Adaskaveg, 1997).

SEM instruments (Figure 1.14.1) can be used to produce images of both conductive and non-conductive samples. It is essential that conductive samples are coated with metal; this is carried out to prevent the sample from conducting once under the microscope. In the SEM the energy electron is produced from the tungsten filament. There are two types of signals which the SEM produces to analyse the samples, these are known as the back scattered (BSE) and secondary electron imaging (SEI). However, the most common detection used in the SEM is SEI. In this process electrons are produced from the ionisation of atoms within the samples rather than from the primary source of radiation, in this case the tungsten filament. Whereas the BSE beam detects electrons which are reflected from the sample by elastic scattering (Pennycook, and Nellist, 2011). SEM has low vacuum capabilities, hence it is able to produce images of samples which are non-conductive: They are also compatible with samples which contain moisture or oily deposits.

Figure 1.14.1: An image demonstrating an Scanning electron microscope

1.4.1.2 Transmission electron microscopy

Observation of particle morphology and measurement of particles diameter can be conducted using transmission electron microscope (TEM) (Figure1.14.2). TEM instrument was employed for characterisation in the present study. TEM functions by detecting electrons which are transmitted through the specimen. The image of the specimen is produced when the interaction of the beam passes through the specimen. On the other hand, SEM works differently whereby the electrons interact either on or near the surface of specimen and thus produces an image.

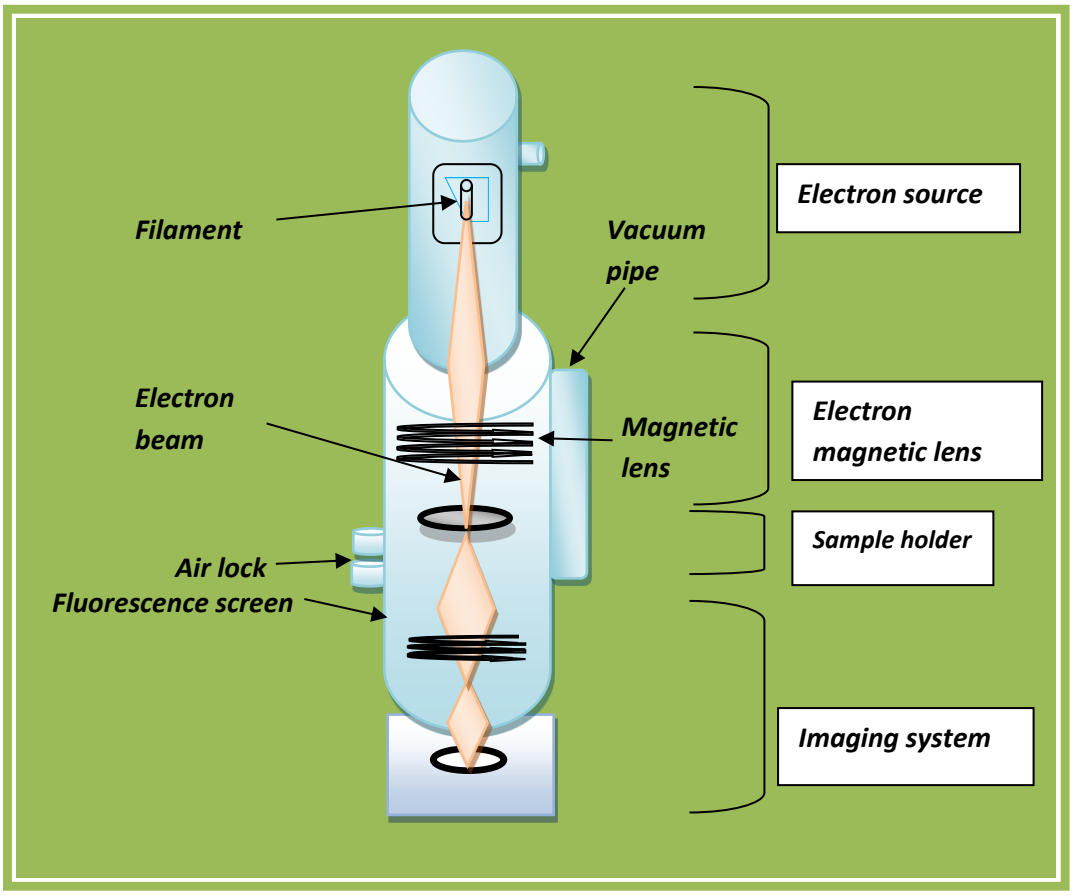

Figure 1.14.2 An illustration image of a TEM consisting of several components: An electron source, an electromagnetic lens, a sample holder, an Airlock chamber and an imaging system. (Image adapted from: http://www.hk-phy.org/atomic_world/tem/tem02_e.html).

As illustrated on Figure1.14.2, TEM consists of several components, including an electron gun which is the electron emission source found on the top column of the TEM, and contains a tungsten filament which generates stream of electrons (electron beam). The TEM contains a vacuum pipe for electrons to travel, and electromagnetic lenses for the operator to control the beam. There is also an airlock chamber for holding a specimen into the vacuum in order to prevent an increase of pressure in other areas of the microscope. Also required is a specimen holder which is designed to hold a standard sized grid in which the sample is placed. An imaging system is present for creating an image from the electrons which exit the system (Pennycook and Nellist, 2011).

1.4.2 Confocal fluorescent microscopy

A fluorescent microscopy is an electromagnetic spectroscopy which works on the principles of fluorescence. It can irradiate an object at specific wavelength. The light at a specific wavelength excites the electrons on an object, in turn light is emitted and detected at a certain wavelength. Using a confocal microscope will show a florescent structure overlaid with a dark background. A confocal microscope has several advantages compared to the conventional microscopy. For instance, the focal plane of a confocal microscope can be controlled, and this allows the imaging system to achieve out-of-focus rejection, a pinhole aperture is present in the system to remove the out of focus interference, when light emitted from the focal plane passes through (Visser and Wiersma, 1994; Shaw, 2006).

Figure 1.15: image of confocal microscopy attachted to computer for analysis

1.4.3 Photon correlation spectroscopy

Malvern Zetasizer Nano ZS is built with the capability of allowing one to optimize and simplify measurement of different types samples. It has the ability to carry out three fundamental techniques: particle size, potential and molecular weight. Particle size measurement is carried out by Photon Correlation Spectroscopy (PCS) measurements, also known as Dynamic light scattering (DLS) and Quasi Elastic Light Scattering (QELS) (Tscharnuter, 2000).

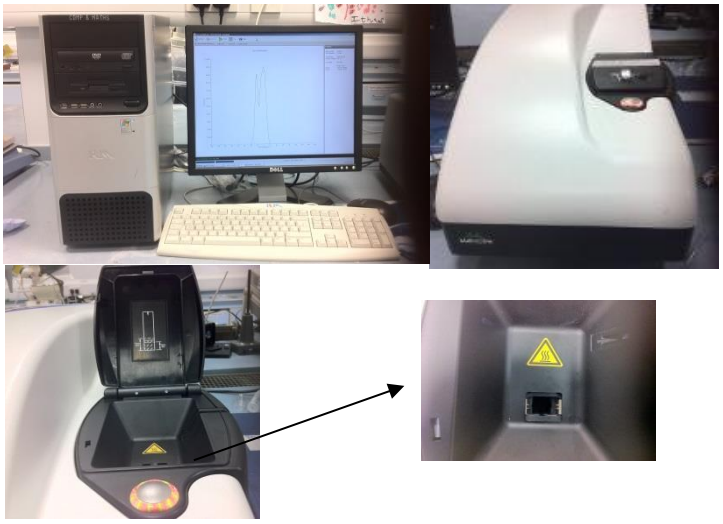

Figure 1.16: Image demonstrates Malvern zetasizer used for photon correlation spectroscopy and zeta potential arrow shows where the cuvette containing sample is placed for measurement.

Malvern Zetasizer Nano ZS determines the size of particle in relation to the measurement of the Brownian motion. The instruments functions by illuminating the sample by a laser. The light which hits the particles in the suspension is then scattered in all direction. The scattered light is then detected and further determines for its rate of diffusion. The average hydrodynamic particle size (Z-Average) is also calculated according to the intensity of the light scattered from the particles using the Stokes-Einstein equation:

$$D = \frac{RT}{N_A} \frac{1}{6\prod \eta r_u} \qquad \textbf{Eq.3}$$

Where N_A is the Avogadro number, T is the constant temperature and η is the viscosity of the solution, and r_u is the radius of the solute expressed in the equation 3. Einstein was the first to derive this equation. According to the Brownian motion, small particles tend to move or diffuse more rapidly than larger particles (Sharma and Yashonath, 2007).

1.4.4 Zeta potential

Zeta potentials of colloidal dispersed nanoparticles were investigated using the Malvern Zetasizer Nano ZS. The zeta potential measurement signifies the repulsive force that is present and is used to show the effect of suspension stability of both surface modified and non-modified NPs; hence the Malvern Zetasizer will be employed in the present study to determine the stability of the non-modified and modified SiNPs in the presence of physiological salt solution (PSS), water and complete medium. During the measurement of zeta potential, electrophoresis takes place on the samples. The velocity of the sample is then measured using Laser Doppler Velocimetry (LDV). It is considered important for a dispersed suspension of nanoparticles to have appropriate repulsive forces between the particles within the suspension. Otherwise, a greater amount of force between the particles may result in the aggregation of the particles (Shaw *et al,* 1992).

1.4.4.1 Electrical double layer

A double layer, also known as electrical double layer (EDL) refers to a structure which appears on the surface of an object such as particles exposed to a fluid. The EDL consists of a cloud of ions with high concentration of counter ions followed by low concentration of co-ions. The layer is described to be a few nanometers in thickness (Kirby and Hasselbrink, 2004). The electrical double layer occurs when the net charge of a particle influences the ions to surround the interfacial region causing a concentrated counter ions to surround the surface of the particle. The counter ions which are attracted to the surface of the particle is referred to as the stern layer, whereas the ions less attached on the outer region are referred to as diffused region. Within the diffused region there is a boundary region where the ions move when the particles move. This boundary is known as a national boundary. Beyond the national boundary, ions do not move with the particles and this region is known as the surface of hydrodynamic shear or the slipping plane. The potential on the boundary region is known as the zeta potential. For a particle to be dispersed in a solution, the given zeta potential value has to be $\leq$ +30Mv or $\geq$ -30mv charged (Shaw *et al*, 1992). Measurement of a Zeta potential is calculated from the electrophoretic mobility in the samples (Figure 1.17), using a micro capillary electrophoresis cell (Figure 1.17.1). The cells are designed with electrodes at each opposite side and are used to promote the potential. When the electrical field is applied to the suspension in the cell, the particles move towards an electrode of the opposite charge. The zeta potential can then be measured by the velocity of the particles, as the velocity it proportional to the charge of the particles in the suspension (Shaw *et al*, 1992).

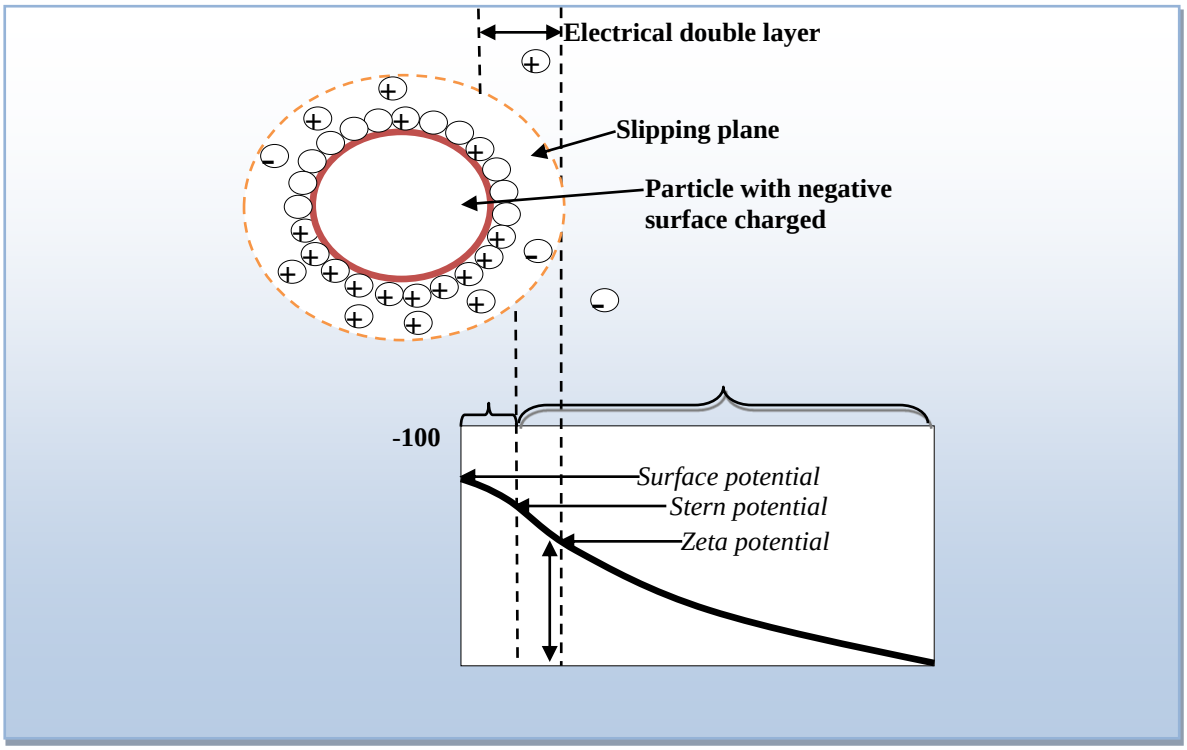

Figure 1.17: The colloidal stability indication by the Zeta potential. (Image adapted from Boonen and Roeven, 2011).

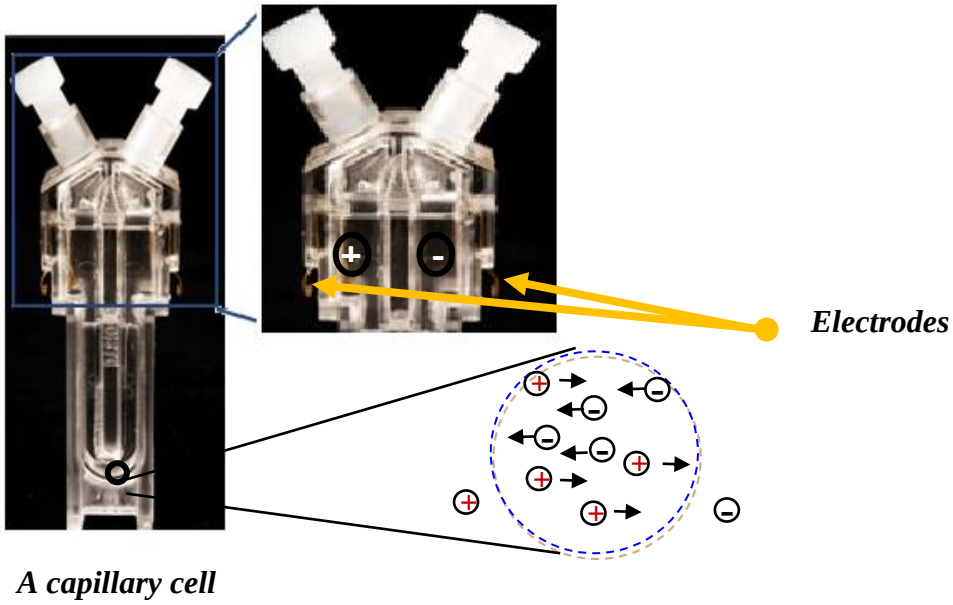

Figure 1.17.1: Samples are held in the capillary cell and their zeta potentials are measured using Laser Doppler Velocimetry (LDV) within Malvern zeta sizer nano series. (Image adapted from (http://www.malvernstore.com/cnb/shop/malvern?productID=11&op=catalogue-product_info-null&prodCategoryID=7)).

1.4.5 Energy-dispersive X-ray spectroscopy analysis

Energy-dispersive X-ray spectroscopy analysis (EDAX) also known as the following acronyms (EDX, EDS, or XEDS), is a technique used for characterizing elements or chemicals within a sample under SEM or TEM. It uses the interaction between source of X-ray excitation and samples to provide analysis. Each element has its unique atomic structure, and this property allows the technique to have the capability of producing a unique set of peaks on its X-ray spectrum. The system detects the X-rays generated as a results of high-energy beam interaction with the samples, which consequently produce charged particles such as electrons or protons. Specimens usually contain atoms which are not excited and have electrons in discrete levels, these electrons are excited by the incident beam. The excited electrons move from their electron shell level, forming an electron hole. The electron from a higher energy level move and fill the holes. The difference from the movement of the high energy electron to filling the hole at the lower shell is released as an X-ray form. Energy-dispersive spectrometer is then used to measure the number and energy of X-rays emitted from the sample. It is the energy of the difference between the lower and higher shell and the atomic structure of the element that characterizes the X-ray energy formed and allows the chemical or element composition of the sample to be measured (Pennycook and Nellist, 2011).

1.4.6 Thermal Gravimetric analysis

Thermal Gravimetric analysis (TGA) is a thermal analysis techniques, which determines the mass change which occur from heating a sample. Thermogravimetry measures the changes in reaction during decomposition and the material becomes volatile with the surrounding atmosphere. The instrument contains four components, each have different functions during the analysis: The furnace, sensor, sample container and the computer. An electrical furnace is used and is purged with suitable gas to burn the sample, consequently allowing decomposition. The thermocouple resistance sensor measures the temperature. The heating is controlled by a system connected to the computer. A ceramic material crucible is used as an inert material; a sample of roughly 10mg is measured on a thermo balance. The balance is electrically sensitive and is designed to avoid the effect of heat (Kealey and Haines, 2002).

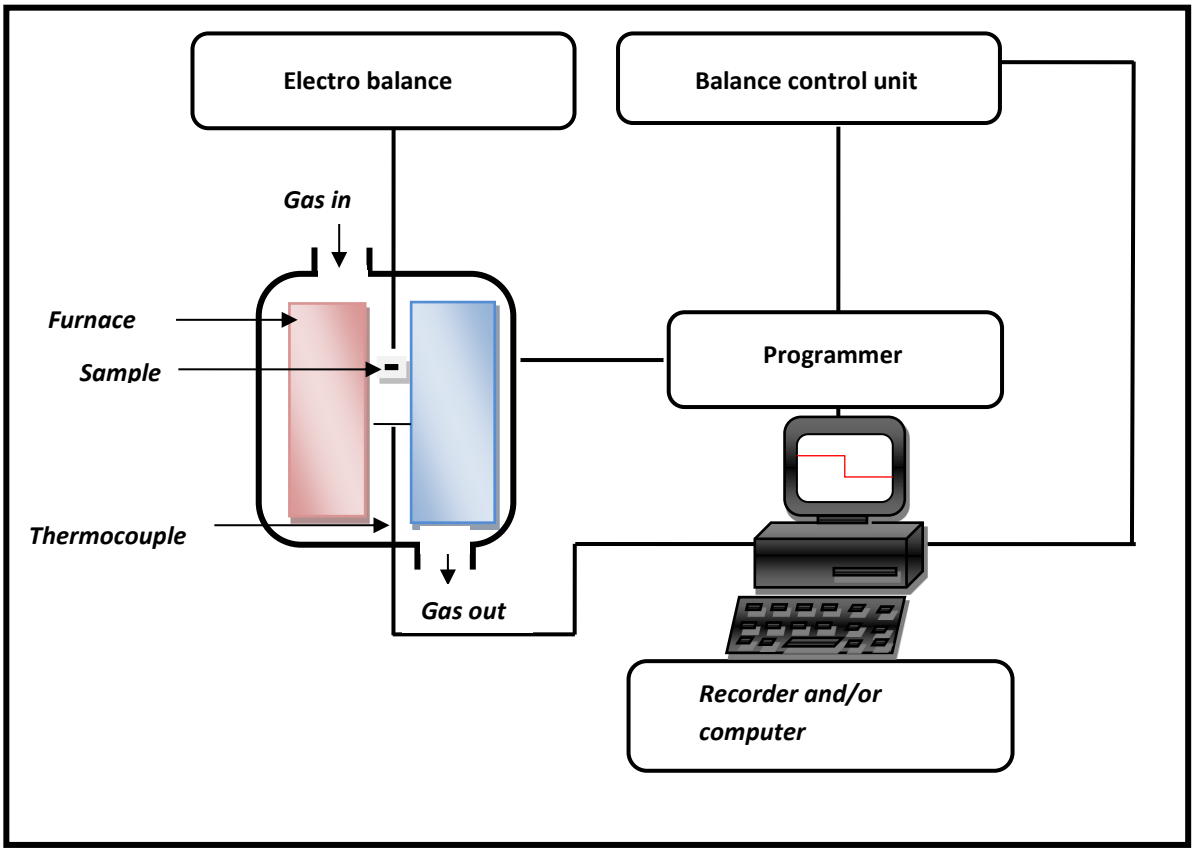

Figure 1.18: Representation of components within the thermogravimetric instrument

1.4.7 Surface Enhanced Raman Spectroscopy

Surface Enhanced Raman Spectroscopy (SERS) is a highly sensitive Raman spectroscopic analytical technique which is similar to the infra-red technique. It looks at the vibration of molecules and produces a spectrum of compounds which are present on the analysed sample. The technique provides the enhanced Raman signal from the analyte molecule, which has beam absorbed on the metal surface from a prepared sample. The excitation laser on the Raman produces a surface plasmon (electron oscillations) on the surface of the metal sample. These surface plasmon are electrical waves which are stationary. The surface plasmon interacts with the analysed sample to enhance the Raman emission and this creates a strong electrical fields which gives an enhanced Raman spectra (Haynes, 2012).

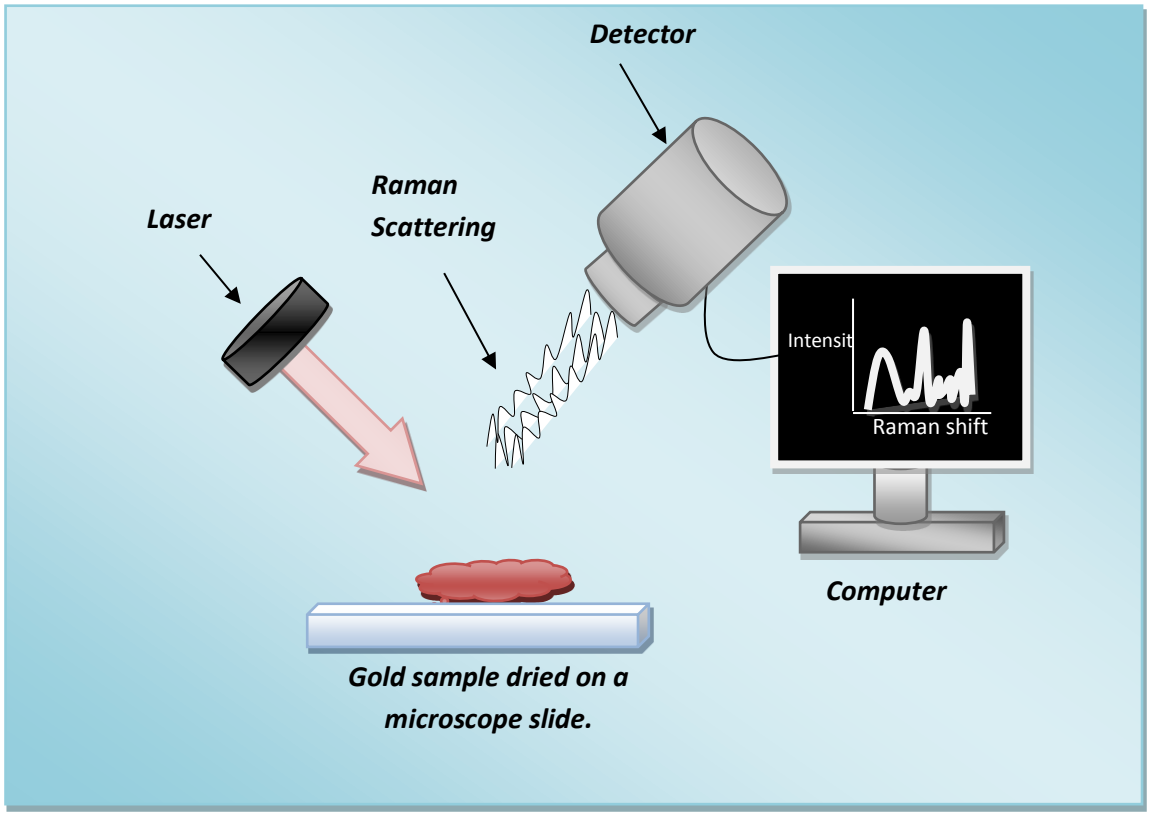

Figure 1.19: Schematic diagram of SER illustrating how the samples are detected

1.4.8 Diffuse reflectance infra-red Fourier transform spectroscopy (DRIFTS)

Using the Thermo Nicolet NEXUS 670 DRIFTS, the Diffuse reflectance infra-red Fourier transform spectroscopy (DRIFTS) analysis was conducted in the present study. The DRIFTS technique is commonly used to obtain a spectrum of absorption emission, photoconductivity or Raman's scattering of a sample in any state (solid, liquid or gas). DRIFTS spectra collects data from a wide range of spectra. This technique is useful for analysis as compared to other spectrometers, such as the dispersive spectrometer which only analyses as at a narrow range of wavelength compared to the DRIFTS which gives a wide range of wavelengths at a time. The infra-red spectroscopy is an important tool for specifying the chemical function of groups present in samples. The instruments work by detecting the vibration caused from the infra-red beam interacting with the samples. Each chemical functional group absorbs the infra-red light at their specific wavelength which as a result causes vibration. The vibration is caused from stretching, contracting and the flexibility of the groups within the samples. The wavenumber band identifies the specific functional groups without interference from the chemical groups within the molecules. The wavelength produced is at a different rate; henceforth the beam produced has a different spectrum. The temperature and pressure within the other chemicals are also not affected. DRIFT is an advantage technique which involves analysing and preparing samples without any difficulties. The techniques directly analyses samples in powder form. The light from the infrared beam is then reflected from the samples. The amount of beam absorbed by the sample is then measured. The reflected light from samples is then collected by either/ or ellipsoid and parabolod mirrors. These mirrors are present in the instruments in order to allow the light absorptions to be processed by a computer to give data of light absorption for each wavelength by the samples (Kealey and Haines, 2002).

1.4.9 Fluorescence spectroscopy

Fluorescence occurs when the molecule of a sample absorbs a photon from the U.V-visible light spectrum resulting in a change to an excited electronic high-energy state. Photons are then emitted once the energy returns to its ground electronic state again. Consequently, the energy within the molecule is lost through heat or vibrational energy, hence the emission wavelength is considered to be longer than the excited molecule wavelength. The difference between the wavelengths is known as the Stokes shift. The fluorescence spectroscopy is used to measure the fluorescence of samples. The spectroscopy involves a light from an excitation source which can be from the LED or laser, passing through a monochromator, in which an excited wavelength of a beam is then selected and passes through the sample held in a cuvette. Once the sample is excited, it then results in the fluorescent light being emitted in all directions. Some of the emitted fluorescent light passes through a second monochromator which is placed at 90°angle to allow the sample to reach the detector, (Glencross *et al*, 2007; Kealey and Haines, 2002).

Figure 1.20: Hitachi fluorescence spectrophotometer F-2500

1.4.10 Ultraviolet-visible spectroscopy

Ultraviolet-visible (UV-vis) spectroscopy, also known as absorption or reflectance spectroscopy is an instrument used to measure the wavelength a sample absorbs or emits. The absorption or reflectance of the sample at a particular wavelength influences the colour observed for the chemical. At that wavelength of the electromagnetic spectrum the molecule undergoes electronic transitions. This analytical technique is complementary to the method used in fluorescence spectroscopy. In fluorescence spectroscopy the transition of the molecules is measured from the excited state to the ground state, while during absorption the transition is from the ground state to the excited state. This instrument contains visible and/or UV light source that split into its component wavelength as it passes through a prism or diffraction grating. The single wavelength beam (monochromatic) will split into two equally intense beams by a half-mirror. The sample beam will pass through the cuvette containing the sample diluted in transparent solvent. While, the reference beam will pass through another cuvette that only contains the solvent. An electronic detector will measure the intensities of these light beams. The intensity of the reference and sample beam is abbreviated as I_0 and I respectively. The UV region of the wavelength is 200 to 400 nm and visible is 400 to 800 nm (Glencross *et al*, 2007).

1.5 Nanoparticles and their application in biomedical science

The integration of nanotechnology into the field of medical science has allowed the development of therapeutic intervention strategies by the use of nanoparticles. NPs have been engineered to allow advances in the treatment of disease through drug delivery (Blanco-Andujar *et al,* 2010) and imaging diagnostics (Jain, 2012). Using NPs has given the potential for providing novel methods in treating diseases which were difficult to target and treat, due to their sizes restrictions (Blanco-Andujar *et al,* 2010). Therapeutic interventions using NPs have been successful in the treatment of cancer (Jain, 2012), diabetes, allergy, infection and inflammation (Nitta and Numata, 2013). There are many reasons for the use of NPs in therapeutic intervention, including the size, since as previously mentioned nanoparticles exist in the same size domain as proteins. The large surface area of the NPs can allow the addition of surface functional groups. In particular, the large surface area, gives NPs greater absorption capability (Jong and Borm, 2008). NP sizes and surface characteristics can thus be modified and controlled, allowing them to be used for targeted drug delivery (Kumar *et al,* 2012) and gene delivery systems (Nitta and Numata, 2013). For example, NPs have been used to enhance delivery across the blood–brain barrier-impermeable probes, to allow *in vivo* optical and magnetic resonance imaging (Koffie *et al*, 2011).

1.5.1 Diagnostic imaging

Gold nanoparticles have been used successfully for imaging diagnostics. A study by Su *et al* (2006) managed to synthesize Au(3) and Cu(1) (gold and copper) nanoshells as contrast agents in Magnetic Resonance Imaging (MRI). Guerrero *et al* (2012) studied the *in vivo* biodistribustion of modified gold nanoparticles with [18F]-fluorobenzoate administered intravenously in rats. Using positron emission tomography (PET) as their analytic technique, they were able to determine that the highest concentration of the radiolabeled conjugate was accumulated in the bladder and urine, where as, less concentration was obtained in the intestine. This finding has as impact in allowing researchers to understand that conjugated NPs can be used for drug delivery, and once these NPs have administrated the drugs to its targeted location, the particles did not accumulate around, but were easily excreted. PET imaging was useful in Guerrero *et al (*2012) study in providing a better

understanding of biodistirbution of gold NPs. AuNPs are considered readily imaged and can be tracked on their fate in cells. However, once these AuNPs are modified, they maybe less useful as agents for diagnostic imaging, Chien and co-workers (2012), justified that non modified AuNPS provided high contrast which allowed them to detect small capillaries *in vivo*, whereas AuNPs modified with mercaptoundecanoid acid (MUA) gave less positive results in detection of small vessels. In their study they used 15.76 mg/ml and 15.5 ± 5.1 nm non modified AuNPs and 31.52 mg/ml and 3.91 nm MUA-modified AuNPs. Nune *et al* (2011) stated that surface functionalization has allowed nanoparticles to be used as probes for molecular imaging.

1.5.2. Drug delivery

Drugs can be delivered in a number of ways such as being dissolved, entrapped, encapsulated or attached to nanoparticles (Chandra *et al*, 2010). Development of the delivery vehicles can vary, as nanoparticles can be colloidal or mesoporous, nanospherical or nanocapsules, and these variations of shape can be obtained depending on the method of preparation. Presently, the use of NPs has shown promising results as agents for effective targeted drug delivery systems (TDDS). TDDS are systems specially designed to safely deliver and release drugs to the targeted site to increase therapeutic effects (Figure 1.21). AuNPs are being used for targeting cancer and are reported to be highly effective (Shenoi *et al*, 2011; Singh *et al*, 2014). Furthermore, AuNPs are also found to acquire antimicrobial properties when conjugated with antibiotics (Ranghar *et al*, 2014). Other reports have described the design of nanoparticles with various materials used as carriers to their targeted location. For instance, Pandey and colleagues (2006) successfully demonstrated that the nanoparticles provided a sustained release of the anti-TB drugs and considerably enhanced their efficacy after oral administration. Voliani *et al* (2012) justified that AuNPs are more efficient for delivery due to their biocompatibility. Using physico-chemically stabilised bioconjugated gold nanoparticles synthesized from Marine Macroalgae, Padina Gymnospora, as a drug delivery system for controlled cancer therapy, Singh *et al* (2014) found that AuNPs induced a death response in the human carcinoma liver cell line, HepG2, however, these gold nanoparticles had less effect on a lung cancer cell line.

Surface modification of NPs, has also gained an interest to increase specific localization of drug delivery with decreased toxic side effects. Poly (D, L-lactide-co-glycolide) coating has been reported to allow modern drug delivery through the blood brain barrier. Such evidence provides relevant uses of polymers as surface modifiers of AuNPs for uses in drug delivery (Tosi *et al*, 2013). PEG-SWCNTs (polyethylene glycol (PEG)-ylated single-walled carbon nanotube) have also been found to be an effective vehicle for cancer drug delivery (Bhirde *et al*, 2010).

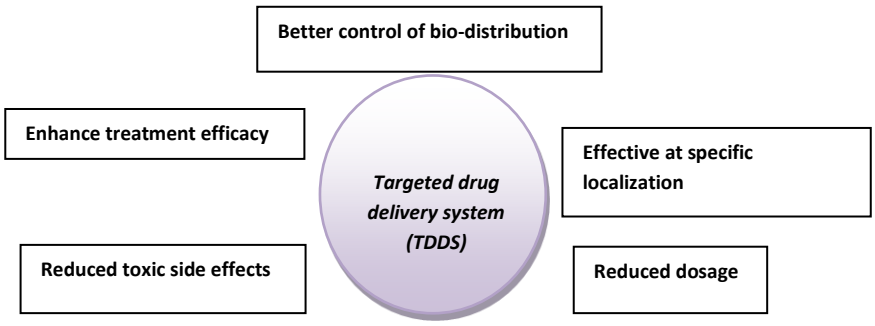

Figure 1.21: The beneficial effect of TDDS

1.5.3 Gene therapy

Gene therapy involves using DNA as a drug to treat diseases. The process involves delivering therapeutic DNA (functional gene) into cells containing defective genes (Pérez-Martínez *et al*, 2012). However, researchers have proclaimed that the major challenge in gene delivery is to further improve the transfection efficiencies of the nonviral carriers such as, gene vectors (Liu and Zhang, 2011). Hence, NPs have currently been shown to represent alternative agents to viral vectors for gene delivery systems. Furthermore, there are important aspects that need to be met by researchers in order to develop effective NPs as genetic delivery systems. For instance, NPs shows to able to adapt themselves to pass genetic material through the blood brain barrier (Pérez-Martínez *et al*, 2012). Investigation into nanoparticles as intracellular delivery vehicles, have found that nanomaterial such as carbon nanotube, have limited efficiency as synthetic vehicles due to their insolubility in water and have tendency to aggregate (Tucknott and Yaliraki, 2002). These findings suggest that such NPs need to be further modified to improve their potential for delivery of genetic material. Functionalised carbon nanotubes (f-CNT), have been developed as

nanovectors and have been reported to be effective for delivering therapeutic molecules (Klumpp *et al*, 2006). Furthermore, different NP composites, such as magnetics have demonstrated the potential to deliver genetic material to neural cells, and are observed to be effective at the central nervous system (CNS). Jeffery *et al* (2009) examined the uptake of magnetic nanoparticles (MNP) using a transection model and found uptake of MNPs in areas of spinal cord injury (SCI) associated with breakdown of the blood–brain barrier (BBB) within 6 hrs of injury. Such findings allow the advance of mediating gene transfer to sites of spinal cord trauma. The type of nanoparticle administration also has an impact as Pérez-Martínez *et al* (2012) reviewed that intravenous administration of the nanoparticles allowed the NPs to reach their targeted location. Recently, Figueroa *et al* (2014) developed AuNP polyamidoamine (PAMAM) conjugates for use as non-viral transfection agents. They reported that AuNP PAMAM conjugates were effective agents for non-viral gene delivery due to high transfection efficiency as well as having low cytotoxicity. Furthermore, Huo*e t al* (2014) successfully delivered 2nm tiopronin-covered AuNPs conjugated with a triplex-forminoligonucleotide (TFO) in the nucleus of MCF-7 cancer cells, to regulate gene expression. They observed that the TFO conjugated NPs were effective in reducing c-myc RNA and c-myc protein and resulted in a greater reduction in cell viability than the non conjugated AuNPs.

In another study, Kim *et al* (2012) also observed that modified AuNP conjugates make promising intracellular gene regulation agents. They found in their study that gold nanoparticles stably functionalized with covalently attached oligonucleotides were able to activate immune-related genes and pathways in human peripheral blood mononuclear cells. Such advantageous findings allow NPs to be used as part of the development of therapeutics and gene delivery systems.

1.5.4. Cancer treatment

According to Jain *et al* (2012) many new nanocomplexes are being developed, however, their full impact for clinical use remains poorly identified. To date, more than 180 nanomaterials have been tested in vitro and in vivo by the NCL (Nanotechnology Characterization Laboratory) (Jain *et al*, 2012). This organization has been collaborating with well-known organizations including the National Cancer Institute, the US Food and

Drug Administration and the National Institute of Standards and Technology, to aid with their research in the study of NPs in cancer treatment. Cancer research has established the advantaged uses of AuNPs in the treatment of cancer, due to their physical and chemical properties. As well as being used for therapy, AuNPs provide a useful tool for imaging diagnostics in cancer therapy.

Studies have established positive results in cancer treatments with AuNPs, furthermore it has been established that tumour cells readily take up AuNPs as compared to healthy tissue (Enhanced retention). This can be observed as being a positive impact, as already researchers are determined to use AuNPs as dose delivery to tumours. Such an example of dose that has been introduced is radiotherapy dose enhancers. The study which involves investigating the effect of AuNPs as dose enhancer has established that AuNPs were biologically effective in allowing radiation to deposit near the directed area targeted by the AuNPs during uptake by tumour cells. A recent study used gold nanoparticles as probes to image mRNA splice variants of the breast cancer susceptibility gene known as BRCA1. They demonstrated that by evaluating the hybridization dynamics of the nanoplasmonic dimers the mRNA splice variant of the cancer gene can be monitered (Lee *et al*, 2014). Such study aims to build understanding on the cellular protein complexes, in addition, it allows for the development of effective genetic diagnosis and gene therapies. Nanorods can be used as ablation components for cancer. As well as non-modified AuNPs, it has become clear that modified NPs can also have a great impact on cancer treatment. For example, polymer coated NPs, PEG in particular, are described to have a prolonged half-life circulation in vivo (Fang *et al,* 2012).

Bio conjugates of AuNPs are found to be useful in cancer therapy, for instance, Bernardi *et al* (2008) synthesized gold-silica for the application of photothermal ablation of tumor cells. They were able to conclude that the use of antibody targeted gold-silica nanoshells as photothermal ablation of cancer cells presents a promising new strategy for the treatment of central nervous system tumors and consequently will result in the reduction of damage and the spread of toxicity to the surrounding normal brain. On the other hand, non-targeted nanoshells did not show cytotoxicity to the tumour cells.

Another study by O'Neal *et al* (2004) found that coating gold nanoshells with PEG resulted in positive in vivo effects for photothermal ablation therapy on a mouse model for colon carcinoma. Sykes *et al* (2014) investigated the impact of AuNP size on active and passive tumor targeting.They used poly(ethylene glycol)-coated NPs as passive and transferrin-coated NPs as active targeting of MDA-MB-435 orthotopic tumor xenografts. The accumulation of actively targeted nanoparticles of 60nm size in the tumor was approximately 2-fold higher than the passive NPs with a similar diameter range. In contrast, there was less accumulation of small NPs of 15 nm diameter size for both active and passive targeting. Sykes *et al* (*2*014) explained that smaller AuNPs are thermodynamicallyless favourable for receptor-mediated endocytosis and are therefore less likely to remain in tumors. They further explain that their study findings will aid in the engineering of the optimal spherical gold nanoparticles for cancer applications.

Finally, an interesting study developed polymer nanoparticles which can carry three different types of drugs (Doxorubicin (DOX), camptothecin (CPT), and cisplatin (Pt)). The NPs are designed as nanoscopic brush arm polymers, with 2 macromolecules featured with PEG that release the drugs DOX and CPT and a cross linker designed for releasing the Pt drug. They demonstrated that such NPs were highly effective in destroying the ovarian cancer cells (OVCAR3) *in vitro* (Liao *et al*, 2014).

1.6 The influence of Nanoparticles on endothelial cellular function

NPs have a large surface area to volume ratio and therefore are very reactive with cellular components. A broad understanding of the effects of NPs on cells after incubation has not yet been achieved. It is therefore of major importance to recognise the effects of NPs and their characteristics on cellular function. The following section will provide a background information on endothelial cells (EC) function and mechanism of NPs uptake by EC. The mechanisms by which NP can lead to cytotoxicity will also be discussed.

.

1.6.1 Regulation of endothelial cell function

ECs make up the luminal layer of all blood and lymphatic vessels (Marcelo *et al*, 2013). They are formed through a process of vasculogenesis which involves activation of receptors for growth factors, including fibroblast growth factor (FGF) and vascular endothelial growth factor (VEGF)(Wang and Zhao, 2010). The structure and integrity of ECs plays a vital role in maintaining the function of both the circulatory system and the vessel wall. ECs are capable of conducting a variety of metabolic and synthetic functions (Sumpio *et al*, 2002), for instance, ECs are involved in the regulation of growth of different cell types, in transporting nutrients and /or waste and the coagulation and fibrinolysis process. ECs also serve as a barrier against the infiltration of bacteria and viruses as well as toxic compounds and molecules (Freese *et al*, 2012). Furthermore, ECs are crucial in immune and inflammatory reactions, as they regulate the movements of lymphocytes and other leukocytes into tissues (Sumpio *et al*, 2002). It has been found that apoptosis of ECs (cell death) can occur as a result of inflammation. During inflammation, ECs are activated by a stimulus (usually a risk factor), which triggers a cascade of events, leading to up-regulation of cell adhesion molecules and recruitment of leukocytes to the lining of the EC (Kluger, 2004). Such events can also lead to endothelial dysfunction (Kolluru *et al*, 2012).

During blood vessel development, ECs interacts closely with smooth muscle cells (SMCs). Such interaction is reflected to have an influence on both development and function of

blood vessels (Bernanke and Velkey, 2002). ECs and SMCs are known to communicate through paracrine signalling. This type of signalling involves cell-cell communication whereby a cell produces a signal in the form of molecules, in order to induce changes to nearby cells, consequently, leading to the alteration of the cell behaviour (Yung *et al*, 2009).

1.6.1.1 Intracellular and Extracellular signalling pathways

ECs contain a large number of cell surface receptors that are responsive to a wide variety of chemical and physical stimuli, including growth factors, cytokines, hormones, transmitters and shear stress. These signals are transmitted into the inside of the cell through different signal transduction pathways. Each type of pathway contains signalling molecules which are important as they convey messages to intracellular spaces. There are three types of chemical signalling by soluble extracellular molecules: endocrine, paracrine, or autocrine (Lodish *et al*, 2000).

The signal molecules derives from extracellular space acts as an adopter which triggers the intracellular events. There are a greater number of molecules involved in the intracellular space for achieving signalling. The first part of cell signalling is a transmembrane protein known as receptor which interacts with the membrane. The second part is the transduction process which passes on the signal. Amplification takes place where one molecule is triggered by other set of molecules and they are usually activated by proteins. There are also other activator molecules known as positive activators (kinases) and negative activators (phosphatases). Most of the signalling pathways involve phosphorylation events. During this event kinase enzymes transfer phosphate groups to the protein causing activation. Phosphorylation of the proteins further results in modulating the activity of a signalling pathway (Cooper, 2000). Interestingly, the kinase enzymes' activities themselves can be inactivated through phosphorylation of scr (non-receptor tyrosine kinases). Furthermore, inactivation of the protein can also occur through a process known as dephosphorylation. The donated phosphate groups are snatched by the phosphatase enzymes resulting in the inactivation of the protein. This process is important to maintain correct responses and prevent production of responses due to errors.

Activation of proteins leads to a cellular response. There are different signal transduction pathways which can activate a particular part of the gene of the nucleus and produce a protein for a particular purpose. Particular signalling molecules have a specific receptor to trigger a particular response. Different pathways are being triggered at all times (Berg *et al*, 2002; Singh and Harris, 2005). Protein Kinase B **(**Akt) and extracellular-regulated kinase (ERK) signalling pathways are examples of intracellular pathways. These pathways and activation of responses are illustrated in Figure 1.22.

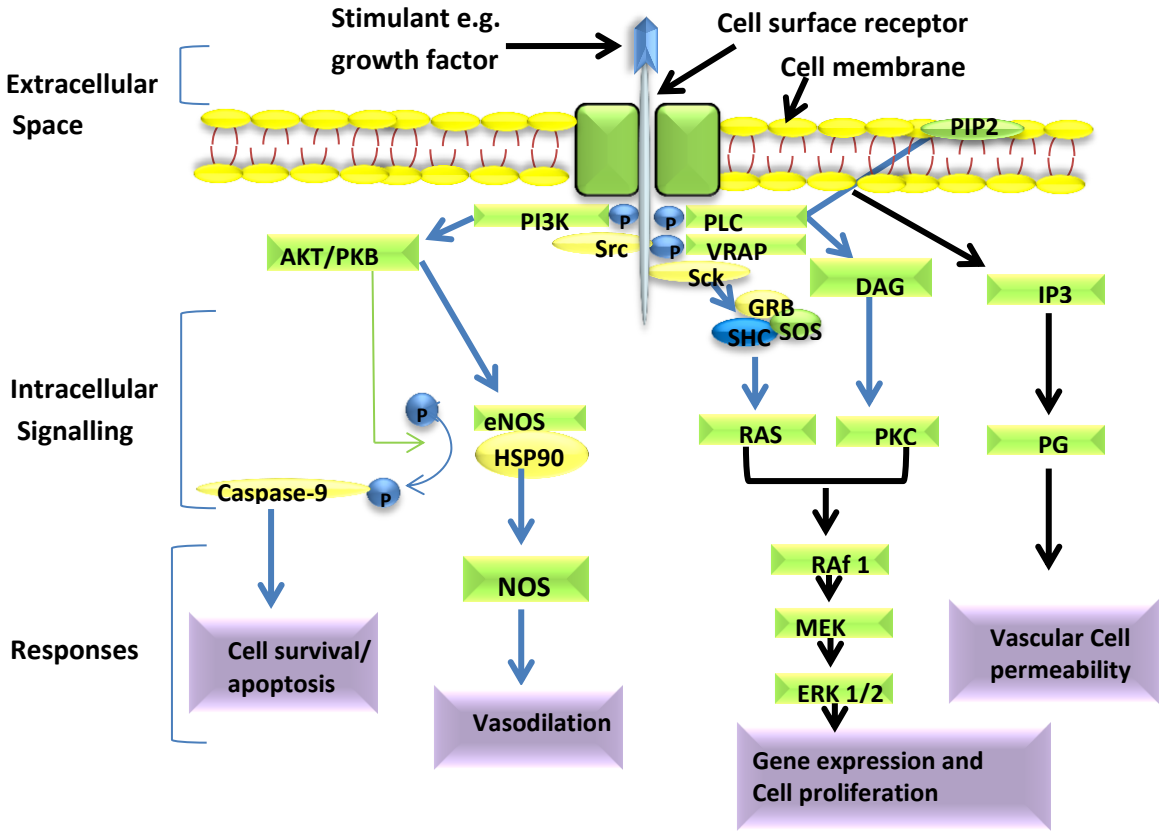

Figure 1.22: Illustrates the activation of ERK pathway induces cellular proliferation, pathway and AKT activation results in apoptosis inhibition by caspase-9 phosphorylation, this pathways also promotes vasodilation through eNOS activation and NO production. The Abbreviations indicate: Akt/PKB, protein kinase B; DAG, diacylglycerol; eNOS, nitric oxide synthase; ERK, extracellular signal-regulated kinase, GRB2, growth factor receptor-bound protein 2; HSP, heat shock protein NO, nitric oxide; P, phosphorylation; PG, prostaglandin; PI3K, phosphatidylinositide 3-kinase; PIP2, phosphatidylinositol 4,5-bisphosphate; PKC, protein kinase C; PLC, phospholipase C; RAS, rat sarcoma; VEGF, vascular endothelial growth factor and VRAP, VEGF receptor-associated protein. Image adapted from Taimeh et al (2013).

1.6.1.2 Cell Death (Apoptosis and necrosis)

The process of cell death involves the death of a cell in any form and can also be mediated by an intracellular program known as program cell death (PCD). PCD serves a fundamental function which results in apoptosis of the cells (Alberts *et al*, 2002). Furthermore, apoptosis is considered an important component in various processes within normal cells, acting as a defense mechanism against harmful agents. This type of cell death can be triggered both by physiological and pathological stimuli (Elmor, 2007; Alberts *et al*, 2002). Another form of cell death is necrosis which is caused by external factors such as trauma. However, necrosis can also be programmed to necroptosis cell death. This mechanism act as a backup for apoptosis, if the signaling of apoptosis is prevented by inhibitors (Miao and Degterev, 2009). A range of stimuli have been established to indicate whether cell death occurs by apoptosis or necrosis (Elmor, 2007).

1.6.2 Nanoparticle uptake by cells

Exposure of NPs to cells can lead to cellular uptake. Using *in-vitro* cell culture model systems, studies have developed some understanding of the effect of NPs on cellular function after exposure.

AuNPs are found to penetrate through skin, in an orderly manner, according to a study based on rat skin. The investigators were able to show that size of NPs had an influence on the way they penetrate into the skin and concluded that infusion kinetics of particles on skin is dependant on NP size. Interestingly, small sized particles were detected in aggregates by TEM in the deeper layer of skin whereas large particles accumulated in the dermis and epidermis (Sonavane *et al*, 2008). In contrast, peptide coupled fullerenes did not penetrate the skin unless the skin is exposed to shear stress (Rouse *et al*, 2007).

NPs without any surface modification can achieve uptake. Furthermore their surface modification increases their dispersion and as a result can also increase their uptake by cells. The key to engineering particles with modified surfaces is to develop particles with optimized properties such as bioavailability (Ghosh *et al*, 2008). In order to reduce the cytotoxic effect of the NPs, their surfaces are also modified with polymer materials such as

Polyvinylpyrrolidone (PVP) or polyethylene glycol (PEG). These polymers have been shown to prevent aggregation of AuNPs and have the ability to prolong their intention within specific targeted organs (Chandra *et al,* 2010; Ojea-jimenez *et al,* 2009; Lui *et al,* 2006; Lui *et al,* 2007). In one study, surface modification with PEG polymer allowed an increase in blood circulation life time (Ghosh *et al,* 2008). AuNPs modified with PEG were efficiently internalized by non-specific endocytosis (Fu *et al,* 2005). Similarly according to Oh *et al* (2011), uptake of PEGylated AuNPs was enhanced according to the diameter of the NPs. This contradicts a statement made by Hauck *et al* (2008), who suggested that PEG polymers may prevent the cellular uptake of nanorods. Manson *et al* (2011) have also found PEGylation of particles reduced uptake of NPs by the reticular endothelial system.

Rauch *et al* (2012) verified that iron oxide NPs with different surface coatings can differentially activate specific cellular signalling pathways in epithelial cells. In a study by Larese *et al* (2009), PVP coated metallic particles (Silver) were found to penetrate into the stratum corneum as demonstrated by TEM analysis. Furthermore, these modified particles also permeated into an aqueous acceptor compartment. Contradicting this study, Arnica *et al,* 2010 found that 50 nm non-polymer modified NPs had the highest uptake by the human prostate cancer cell. However, once these cells were surface modified by PEG, their cellular uptake was reduced.

A recent study has looked at ways of achieving uptake of NPs and ways of predicting highest uptake by cells. Schneider *et al* (2009) indicated that size absorption of NPs through body surface (skin) can be achieved through a formula first established by Potts and Guy in 1993. The concept of the formula is to understand the rule of penetration based on the molecular properties of particles.

$$\log K_p = \log\left(\frac{D}{h}\right) + f \cdot \log P - \beta'' \cdot MW$$

Figure 1.23: Formula established by Potts and Guy explaining the rule of penetration based on the molecular properties of particles, (Schneider et al, 2009).

Where D is diffusivity of the permeant in the membrane (skin), h is the length of the diffusion pathway, MW is the molecular weight, P is the octanol/water partition coefficient (accessibility of P is better than the value of the membrane/water coefficient K_m), and K_p is the permeability coefficient (Figure 1.23).

For effective uptake by cells, one study has shown that the material should be nanosized or less (Oh *et al*, 2011). However, uptake as mentioned previously is not dependent on size only but the morphology and surface charge of both the cell and the NPs. A study by Chithrani *et al* (2006) suggested that the fabrication of AuNPs with citrate leads to a reduced cellular uptake, because surface charge of the NPs were negative due to the citrate stabilizing ligand. They defined that anionic structures are taken up less efficiently when binding to the cell surface than that of neutral or cationic molecules due to electrostatic repulsion. The magnitude of uptake of NPs into cells is also dependent on timing of incubation (Boyoglu *et al*, 2013) and concentration of NPs. For instance, Dragoni *et al* (2012), studied the impact of 5-nm AuNPs modified with PVP on the mammalian liver; they demonstrated that AuNPs were taken up by the endocytotic vesicles of hepatocytes after 30 min of their addition. Similarly, Chawla and Amiji (2003) found that most rhodamine123 loaded poly (ε-caprolactone) (PCL) NPs were internalised within MCF-7 oestrogen receptor positive breast cancer cells after the first 30 minutes of incubation. Hu *et al* (2011) examined the influence of size of fluorescein isothiocyanate (FITC) and rhodamine B isothiocyanate labelled silica NPs on the cellular endocytosis, exocytosis and cell activity of HepG2 cells (Human liver carcinoma cell line), and further determined that their uptake behaviour was dependent on NPs size and concentration as well as incubation time.

1.6.3 Pathways of Nanoparticles uptake by cells

A number of studies have investigated the pathways by which NPs enter the cell (Mukherjee *et al*, 2007; Wang *et al*, 2010; Harush-Frenkel *et al*, 2007; Aderem and Underhill, 1999). It has been demonstrated that cellular internalization of NPs involves several types of mechanisms. These mechanisms are described as pathways. There are two distinctive pathways of NP uptake by the cells; the phagocytic and non-phagocytic

pathways (endocytic pathways). Exocytosis pathways are also common pathways for NPs to enter (Tsai *et al, 2013*). Contents of a cell vacuole are usually released to the exterior through this process. Indeed, it is the surface charge and NP size but not the type of nanomaterial which influences the entry into cells through different pathways. Kim *et al* (2006) demonstrated that 50 nm silica-overcoated magnetic NPs containing an organic fluorescence dye, rhodamine B isothiocyanate, entered cells through energy dependent endocytosis, whereas Lin *et al* (2012), acknowledged that both cationic and neutral surfaced 5 nm AuNPs depended on endocytosis for cellular uptake. Anionic charged NPs, on the other hand, transported through the cell via the paracellular pathway.

1.6.3.1 Phagocytosis

Phagocytosis involves removing pathogen and unwanted debris solid particles and this process is considered crucial in immune defence. The mechanism involves engulfing the solid particles by a phagocyte (cells typically, macrophages, monocytes, neutrophils and dendritic cells). Cells such as epithelial and endothelial can also phagocytose, although less efficiently. An interesting study by Krpetić *et al*, 2010 observed the cellular uptake of gold NPs through the phagocytic pathway. They showed using TEM images that AuNPs were taken up via phagocytosis mechanism by the murine macrophage cells. It has been shown that large NPs or aggregates can be taken up through this pathway (Aderem and Underhill, 1999). It is important to take into account that the characteristics of NPs may also have an effect on phagocytosis. Krpetić *et al*, 2010 found that surface properties of NPs may have an important effect on cellular uptake. They showed that there was an increased movement of macrophages toward 5-aminovaleric acid-modified AuNPs which, overall led to a greater accumulation of NPs in the cytosol. In contrast, Lui *et al* (2013) found that the extent of uptake of negatively charged AuNPs was similar to that of the positively charged AuNPs for phagocytic RAW 264.7 cells. Depending on their application of NPs, studies have looked at surface modification as a tool to either decrease or increase phagocytosis of NPs. Previously, a review by Jong and Borm (2008) identified the advantageous uses of polyethylene glycol (PEG) as a surface modification. The review described studies which have managed to prolong the presence of the polymer in the circulation without being recognized by the mononuclear phagocytic system. Such type of polymer surface modification allows NPs to be implemented as an effective drug delivery agent.

1.6.3.2 Non phagocytic Pathways

Non phagocytic Pathways are different to the phagocytic pathways, and is also known as endocytosis. Most cells undergo non phagocytic pathway mechanisms. There are four mechanisms in which endocytic pathways can be further divided into: clathrin mediated endocytosis (CME), caveolae-mediated endocytosis (CvME), clathrin and caveolae independent endocytosis and macropinocytosis.

1.6.3.3 Clathrin-mediated endocytosis (CME)

Endocytosis is a process by which cells are able to internalize membrane and extracellular materials in the form of a vesicle. Clathrin is a protein which is demonstrated to function in receptor-mediated endocytosis events at the plasma membrane, clathrin-mediated endocytosis is important for nutrient uptake and signal transduction (Le Roy and Wrana, 2005). Once the clathrin has been activated by stimuli it forms a basket-like vesicle and coats the invading particles trapping them in to the cell. This process is known as clathrin-mediated endocytosis (CME). Harush-Frenkel *et al* (2007) studied the effect of negatively and positively charged NPs on uptake and concluded that charge influenced NPs internalization via the clathrin-mediated endocytosis pathway.

1.6.3.4 Caveolae-mediated endocytosis (CvME)

Caveolae are found on the plasma membrane of many types of cells, but enriched in endothelial cell. These are lipid raft shaped, like flask invaginations and appear as membranes that are round in shape with a diameter of 50-80nm. The Caveolae lack a cytoplasmic coat, however, they have the protein caveolin, which helps to characterise the caveolae. In a study by Hao *et al* (2012), they demonstrated that caveolae-mediated endocytosis was the dominant pathway for the intracellular delivery of small-size AuNPs into HeLa cells and were able to determine the internalisation mechanism using fluorescence microscopy. It is reported that inhibition of tyrosine kinase activity inhibits caveolae mediated endocytosis (Kirkham and Parton, 2005).

1.6.3.5 Macropinocytosis

Macropinocytosis is an endocytosis process which allows large amount of uptake of fluid and solid cargo into cytoplasmic vacuoles, known as macropinosomes (Falcone *et al*,

2006). The process is accompanied by membrane ruffling. Macropinocytosis process is often induced by growth factors (Swanson *et al*, 1995). Panariti *et al* (2012) reported that NPs with a diameter up to several hundreds of nanometers prefer to enter the cells via pino- or macropinocytosis process.

1.6.3.6 Clathrin and Caveolae independent endocytosis

Other pathways of clathrin and caveolae independent endocytic are being studied, for instance, flotillin-dependent endocytic pathway are lipid raft-associated proteins and are thought to be involved in clathrin and caveolae independent endocytic. Other internalization routes are based on lipid microdomains. Kasper *et al*, 2012, used immunonoflueresecence staining and detected uptake of amorphous organosiloxane particles by flotillin-1 and -2 containing vesicles. Using a human microvascular endothelial cell line they found colocalisation of NPs with flotillin-1/2 after 4 hours (hrs.), indicating a faster uptake mechanism in these cells was achieved by flotillin-dependent endocytic pathway.

1.6.4 Nano-bio interface

It is important to understand the cellular uptake behaviour of NPs before their use, such as in drug delivery applications. A number of interactions between biomaterials (cells, protein and DNA) and NPs is recalled to have an important role in determining the cellular uptake of NPs. Hence, over decades the number of studies have increased in determining the effect of such interaction between NPs and biomaterials. The nano-bio interface defines the interaction between the surfaces of biocomponents with the NP surfaces. However, their precise effect and complex interaction remains unclear.

Nanomaterials vary in behaviour once they come in contact with biocomponents. Their surface modification can have a great impact on the way they behave. Interaction of NPs with a number of plasma proteins are known to acquire a ‘corona’ (Rahman *et al*, 2013) and can further influence the cellular uptake, inflammation, accumulation, degradation and removal of NPs. Furthermore, size, shape and surface of NPs can affect the NPs capability of protein adsorption and may induce a protein conformational change in the absorbed protein molecule. This can affect protein function (Saptarshi *et al*, 2013). Recently, using a

technique of confocal Raman microscopy, Lopis *et al* (2011) were able to analyses uptake of NPs at a single cell level. They demonstrated that labelling the surface of NPs can interfere with the protein interactions and cellular localization of NPs.

1.6.5 Cytotoxicity of Nanoparticles

Exposure to NPs is inevitable as NPs are becoming more widely used in the chemical, domestic, healthcare and cosmetic industries. Consequently, the study of nanotoxicology is very important (Lewinski *et al*, 2008). In particular, understanding their effect on cell proliferation, viability and cell death is essential (Bancos *et al*, 2012; Selim and Hendi, 2012).

A number of studies have demonstrated the effects of AuNPs on cells. AuNPs can cause impaired viability and proliferation of the cells. For instant, Mukherjee *et al* (2005) were able to determine that AuNPs inhibited VEGF165-induced proliferation of Human umbilical vein endothelial cells (HUVECs). On the other hand, Semi and Hendi (2012) found that the viability of MCF-7 human breast cells was reduced by AuNPs. It has been acknowledged that AuNP cytotoxicity can be influenced by various factors such as size of NPs, incubation time and surface modification as well as concentration of NP. (Soenen *et al*, 2012). It is mentioned that particles size >3 nm possess no toxicity effect. In contrast, particle sizes of 1-2 nm seem to have high toxic effect on both healthy and cancerous cells (Hartung *et al*, 2013). Indeed, AuNPs can lead to induction of reactive oxygen species (ROS) and as a result cause a reduction of cell viability (Vecchio *et al*, 2012). Soenen *et al* (2012), used 4 nm diameter poly(methacrylic acid)-coated AuNPs and found that not only did the concentration of 200 nM NPs reduce cell proliferation and cellular differentiation but also at 50 nM concentration an effect was detected, though, at 10 nM concentration no effect was found. Similarly, Zhang *et al* (2009) observed that at high concentration (>150 mg/mL) AuNPs can cause a sharp decrease in Human erythroleukemia cell (K562) viability, while at low concentration (<75 μg/mL) they had no effect. AuNPs are also known to contribute to cell death, for instance, Selim and Hendi (2012) found that AuNPs induced apoptosis in MCF-7 human breast cells using MTT assay. The degree of

cytotoxicity was dose dependent and at 25µg/mL viability was reduced to 70% after 24 hrs incubation.

In vivo experiments in mice, have found that surface modified AuNPs also induced inflammation and apoptosis (Tsai *et al*, 2013; Tiwari *et al*, 2011). In contrast, using Annexin V/PI double staining to analyse the effect of AuNPs on the cell death program of MG63 Osteoblast-Like cells, Tsai *et al* (2013), found that AuNPs did not alter the cellular apoptosis rate during an eight day incubation period even after high concentrations of NPs were added.

Freese *et al* (2012) studied the cytotoxicity of AuNPs on endothelial cells and investigated whether cytotoxicity effects on Human Dermal Microvascular Endothelial Cells (HDMEC) was due to the concentration of AuNPs applied on the cells. Interestingly, cell viability was not affected significantly, rather it was increased. In contrast when they stabilised the AuNPs with an excess of sodium citrate on their surface they found that high concentration of AuNPs caused decrease in cell viability. Furthermore, they identified that AuNPs had an impact on cell proliferation, and observed that AuNPs had an effect on the amount of nuclear Ki-67, a protein expressed by all cells in the active cell cycle. Similarly, Ng *et al* (2010), found that 20nm AuNPs led to oxidative stress in the embryonic lung fibroblasts which as a result inhibited cell proliferation as well as alteration of the cell cycle gene. They proclaimed that their observation was more likely due to immune reactions. One interesting study indicated that the detrimental effects caused by AuNPs cannot be detected solely by proliferation or apoptosis assays, as AuNPs may be causing an interference of other specific functions within the cells (Mironava *et al*, 2010). The use of protein polymers, to modify the NPs' surface and stabilize it may also affect function. For example, using ethidium bromide/fluorescein diacetate staining technique, for cell viability, Xie *et al* (2012) demonstrated that PVP (10000MW) reduced viability of islet cells by 63.4%, whereas, PEG (5000MW) and PEG (8000MW) both further reduced viability (58.1% and 60.7%, respectively) after 48 hrs incubation. This suggests that cytotoxic effects may depend on chain length. However, Xie *et al* (2012) indicated that PVP polymer was a better cryoprotectant candidate as compared to PEG because PVP

showed a fast dissolution rate in culture medium. Currently there is no information on the effect of PVP and mPEG polymers on endothelial cell function.

1.7 Influence of Nanoparticles on Vascular function

Nanoparticle exposure studies using animals *in vivo*, have demonstrated that NPs can gain entry into the blood stream through a number of routes. They can be inhaled, absorbed or they can penetrate through the skin (Oberdoster *et al,* 2005). NPs can penetrate blood vessels via two modes of exposure: Intravascular and Extravascular. Intravascular (intralumenal) exposure of blood vessels is achieved mainly through directly injecting the NPs into the circulation. These are normally 'engineered' NPs for drug delivery and imaging, where they come in direct contact with the endothelial cell layer lining the vessel wall (Azzawi, 2012). On the other hand, NP inhalation or injection, can lead to extravascular exposure of blood vessels to NPs, where NPs can translocate through extracellular tissues and come in contact with the vessel's outer adventitial layer. NPs translocating through this route include those that are absorbed through the mucosa via inhalation, ingestion or via skin absorption. NP uptake has been shown in areas distal to the exposure sites, and are demonstrated to affect vascular function (Azzawi, 2012). For example, an animal inhalation study reported that titanium dioxide NPs attenuated dilator responses to the agonist acetylcholine [ACh] (Le Blanc *et al,* 2010). NPs can lead to oxidative stress and the generation of reactive oxygen species (ROS) either by simple contact between NPs and cells or by internalisation of the NPs (Roesslein *et al,* 2013). Subsequently, NPs can lead to quenching of the nitric oxide (NO), which is a key vasodilator molecule (Nurkiewicz *et al,* 2009; Park and Park, 2009).

The following sections will provide background information, detailing the mechanisms involved in the regulation of vessel diameter and the techniques used to assess vessel function, *ex vivo.*

1.7.1 Regulation of vascular function

The vascular wall structure (Figure 1.24) includes an inner intima, which contains the endothelium, a middle smooth-muscle cell layer within the media, and an outer adventitia, which mainly supports the tissue (Mulvany, 2002).

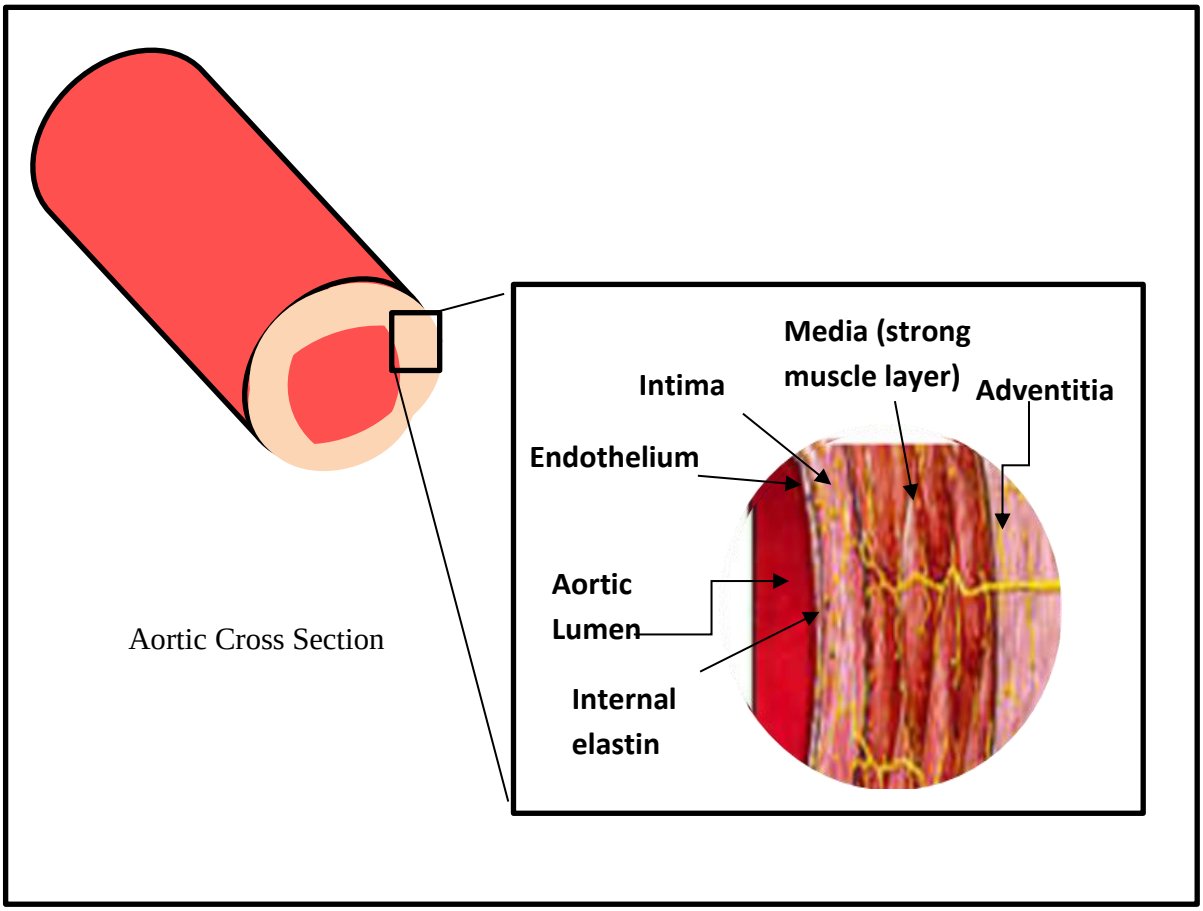

Figure 1.24: A Cross section of aorta containing the inner intima, the media and the adventitia (image adapted from http://www.vcu.edu/hearts/aortic_center.htmhttp://www.vcu.edu/hearts/aortic_center.htm)

Hence, there are multiple layers of SMCs that surround the endothelium. The apposition of the two cell types enables a rapid diffusion of signal derived from one cell to the neighbouring cells. Each layer plays a big part in maintaining the function of the blood vessel. The vascular endothelium layer is presently considered a vital organ and is made up of a number of endothelial cells. It plays a crucial role in the maintenance of vascular smooth muscle tone and structure. Vessel diameter is modulated by the release of vasodilators and vasoconstrictors. Under physiological conditions, a precise and balanced release of relaxing vasodilator and contracting vasoconstrictor factors helps keep arteries

open and blood flowing smoothly. Alterations in this balance, for example a decreased production of dilative agents or an increased production of constrictive agents, lead to impaired vasodilatation with considerable effects on the function and structure of the blood vessels (Boulanger *et al*, 1998).

1.7.1.1 The mechanism of vasoconstriction

Smooth muscle cell contraction leads to vessel constriction (vasoconstriction). Which in turn causes the vessels to decreases its diameter and hence increase vascular resistance, subsequently, this results in the increase in systemic blood pressure. The process of smooth muscle cell contraction is regulated by receptor and the mechanical activation of myosin and actin contractile.Vasoconstriction can be achieved by the binding of angiotensin II and thrombin on the vascular endothelial cells; this activates the endothelium derived factor which then regulates the SM vasoconstriction. A number of potent family of vasoconstrictors, such as Endothelin and phenylephrine (an alpha1 adrenergic receptor agonist), bind to their specific receptors on the smooth muscle cell membrane, which then causes constriction by depolarization from an increase in the release of intracellular-stored Ca^{2+} from the sarcoplasmic reticulum (Ross and Pawlina, 2010). The influx of Ca^{2+} can be blocked by inhibitors of guanylate cyclase and Cyclic guanosine monophosphate (cGMP)-dependent protein kinase Ia (Jorgensen *et al*, 1996). The agonist phenylephrine is sometimes used as a vasoconstrictor to increase the blood pressure in patients with hypotension. The mechanism of agonist mediated vasoconstriction is known as 'Pharmacological coupling'. Vasoconstriction can also be achieved through 'electromechanical coupling' which results from net difference across the membrane resulting from the activity of a number of active and passive ion transport mechanisms in the cell membrane, due to the addition of high potassium solution (Mulvany and Aalkjaer, 1990). The extracellular high potassium concentrations shift the membrane electrical potential from -70 mV to 0 mV, thus leading to depolarisation of the cell and consequent constriction (McCarron *et al*, 2003). According to Webb (2003) for contraction to occur, phosphorylation of the 20-kDa light chain of myosin by the myosin light chain kinase (MLC kinase) is essential to enable the interaction of the protein myosin with actin.

1.7.1.2 The mechanism of vasodilation

One of the most important substances released from endothelial cell is endothelium derived relaxing factor (EDRF), now identified as nitric oxide (NO). The synthesis of NO is controlled by NO synthase and is induced by calcium mobilising agents and fluid shear stress (Boulanger and Vanhout, 1998). Three NO synthase (NOS) isoforms exist: Neuronal NOS (nNOS), inducible NOS (iNOS), and endothelial NOS (eNOS). The latter is constitutively expressed in endothelial cells and is responsible for basal production of NO. NOS is known to have approximately 60% amino acid identity and similar primary structures, (Papapetropoulos *et al*, 1999). NO is formed from the amino acid precursor L-arginine by eNOS. NO involved in a wide variety of regulatory mechanisms of the cardiovascular system (McIntyre and Dominiczak, 1997). It is a diffusible gas and a potent vasodilator. In addition to contributing to endothelium-dependent vascular relaxation, it also plays important roles in maintaining vascular health, including preventing blood clotting and leukocyte adhesion and having antiproliferative and antiapoptotic effects (preventing cell death) on the vascular wall (Pleger *et al*, 2008). Vascular studies have provided convincing experimental evidence that intracellular calcium ions (Ca^{2+}) concentration is the major factor involved in the activation of eNOS synthase in endothelial cells. Intracellular Ca^{2+} is increased in the endothelial cells by agonist-receptor interaction through both extracellular Ca^{2+} influx and Ca^{2+} release from intracellular stores e.g. acetylcholine (ACh). eNOS activity is regulated by its phosphorylation. A number of protein kinases can phosphorylate eNOS, for example, Akt, leading to its activation and NO production. NO that is formed in endothelial cells causes vasodilation by stimulating vascular smooth muscle soluble guanylyl cyclase and elevating cyclic guanosine monophosphate (cGMP) levels.

In vascular SMCs, cyclic adenosine monophosphate (cAMP)-dependent protein kinase (PKA) and cGMP-dependent protein kinase (PKG) are activated by nitric oxide (NO), and lead to Ca^{2+} uptake by sarcoplasmic reticulum (SR) through sarcoendoplasmic reticulum Ca^{2+} ATPase (SERCA) channel and releases Ca^{2+} from SR to the submembrane space through the plasma membrane which activates the calcium-activated potassium channels (K_{CA}) and causes hyperpolarization (Figure 1.25). This hyperpolarization spreads to adjacent SMC causing the blood vessels to dilate (Webb, 2003).

Furthermore, Bolotina *et al* (1994) demonstrated that NO can directly activate calcium-dependnet potassium channels in SMC. Research has shown that inhibition of any site in the L-arginine–NO–guanylyl cyclase pathway can cause an impairment of endothelium-dependent vasodilation (Webb, 2003).

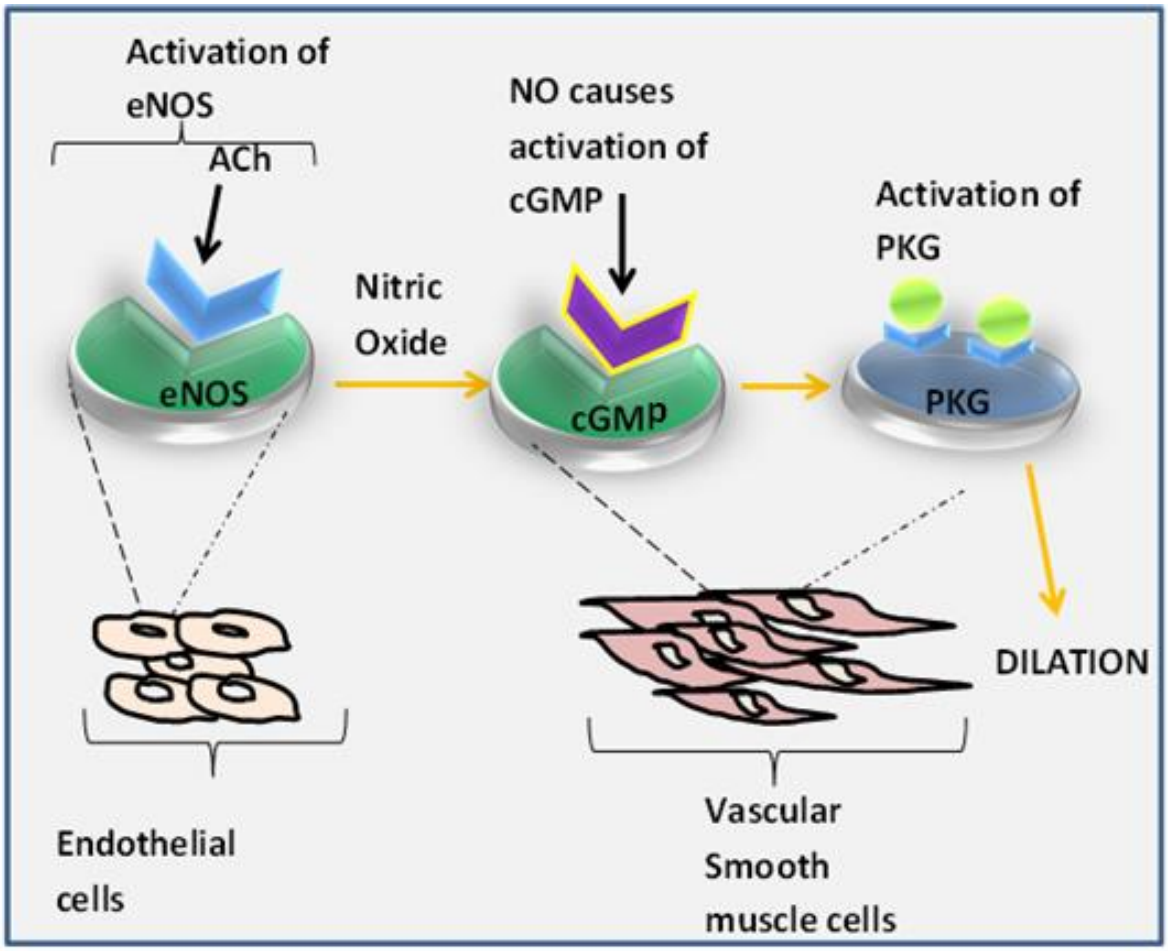

Figure 1.25: The mechanism of vasodilation

1.7.2 Assessment of vascular function

1.7.2.1. Assessment of vessel viability

Experimentally, vessel viability can be assessed *ex vivo* by superfusing vessels in high potassium solution.

1.7.2.2 Assessment of endothelial function-ACh

Acetylcholine (ACh) is an endothelium-dependent vasodilator agonist that acts through different signal transduction pathways (Panza *et al*, 1995). ACh binds to the muscarinic receptor on the surface of endothelial cells, which is coupled to G protein. ACh can act through a number of signal transduction pathways, including the PI3K/Akt pathway, leading to eNOS phosphorylation and activation of NO production (Figure 1.26).

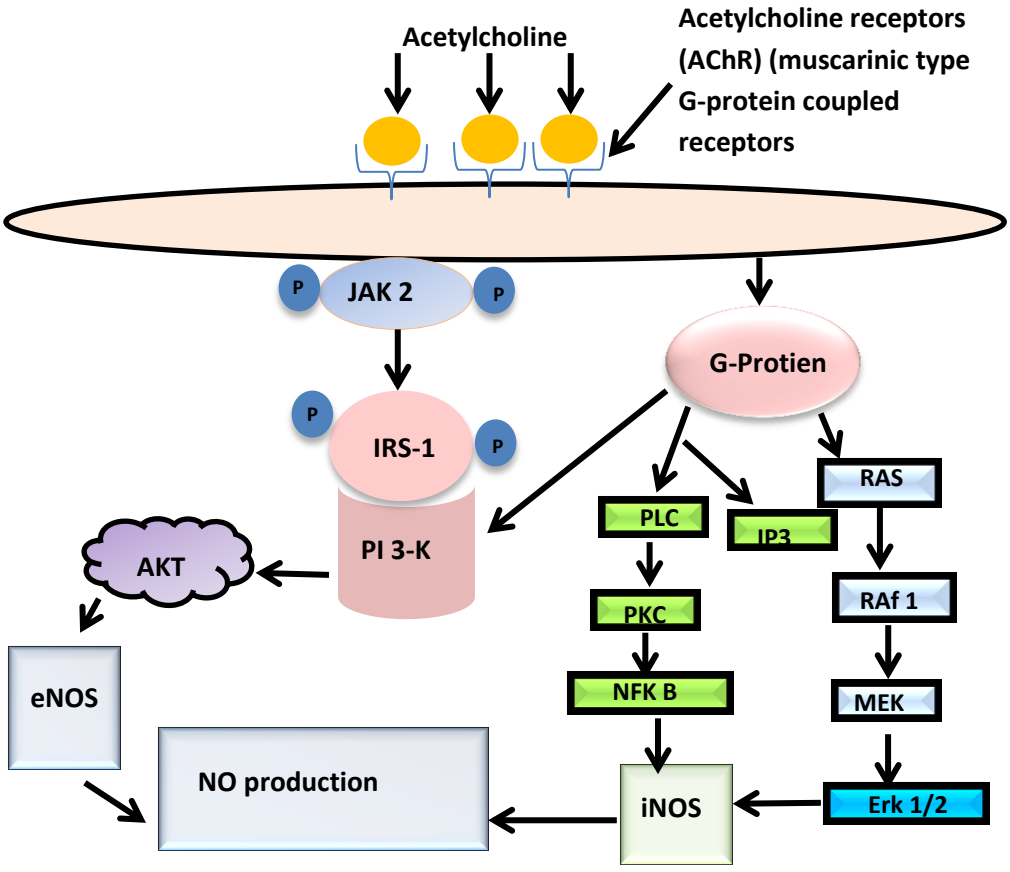

Figure 1.26: The alternative pathways which ACh can induce eNOS and resulting NO pathways. The pathway involves JAK2 /IRS-1 /PI3-K and AKT, other alternative pathways for NO production is PLC/PKC/NFK and RAS/RAf/MEK and Erk 1/2 (Image adapted from Zecchin et al (2007).

ACh binding to its G protein coupled receptor causes a rise in Ca^{2+}, and the cells hyperpolarize as a result from the opening of Calcium activated potassium channels (K_{Ca}). This hyperpolarization spreads to adjacent SMCs leading to arterial dilatation. Even if only a small number of endothelial cells are directly stimulated by the agonist, the entire length of the artery can dilate *in vivo.* The mechanism for this spreading dilatation is intrinsic to the vessel wall, and occurs due to the rapid spread of current through gap junctions. Investigators have found that the rise in endothelial cell Ca^{2+} only occurs within the area where ACh is present, consequently, the cells hyperpolarize along the arterial length (Christense *et al*, 2001). Schffrin *et al* (1998) demonstrated that ACh stimulated a rise in endothelial cell [Ca^{2+}] and hyperpolarization in the rat mesenteric artery endothelial cells. Subsequently, hyperpolarization and relaxation occurred at the adjacent SMCs. Reduced responses to ACh; reflect endothelial dysfunction (Celermajer *et al*, 1997).

The major vasodilator identified within aortic vessels, upon ACh stimulation, is NO. Using an NOS inhibitor N_w-Nitro-L-arginine (L-NNA), Farooq *et al* (2014) demonstrated that most of the dilatory responses of ACh were lost. ACh may also stimulate other vasodilator substances, including endothelial derived hyperpolarising factors (EDHFs). A number of candidate molecules have been identified as EDHFs, including EETs. Furthermore, K^+ are also being classified as EDHF, they were found to extrude from the endothelium and into the myoendothelial gap, where they result in vasorelaxation by activating the vascular smooth muscle inwardly rectifying potassium channels and Na^{2+}, K^+-ATPase pumps. Subsequently, causing the efflux of K^+ from the vascular smooth muscle and finally inducing hyperpolarization (Coates *et al,* 2001; Sokoya *et al,* 2006).

1.7.2.3 Assessment of smooth muscle cell responsiveness-(SNP)

Sodium Nitroprusside (SNP) has the following formula: $Na_2[Fe(CN)_5NO]$, it is a non-selective vasodilator otherwise known as an endothelium independent dilator. The structure of SNP consists of a ferrous ion centre with five cyanide (CN^-) moieties and a nitrosyl group. It acts as a NO donor in the vessels. It breaks down in the tissue and

releases NO. It does this by binding to oxyhaemoglobin and forms methemoglobin while releasing cyanide and NO. The NO diffuses into the muscle cells in the walls of the blood vessels and causes them to relax. When the muscles relax, the blood vessels become wider and the blood pressure decreases (Stoelting and Hillier, 2005).

A study has demonstrated that SNP increased the amplitude of the K_{IR} current of rat-tail small artery smooth muscle cell and induced K_{IR}-mediated vasodilation. The K_{IR} channel were found on the smooth muscle cells (Schubert *et al*, 2004). SNP based drugs are currently used in therapy to lower the pressure of patients, however, a prolong exposure can lead to toxicity effects (Aghababian, 2011).

1.7.3 Assessment of vascular function ex vivo

Vascular function can be assessed *ex vivo* using an organ bath setup. To investigate the ability of the endothelium to produce and release vasodilators, an experimental approach is generally used. Pharmacological agents such as endothelium-dependent, acetylcholine (ACh) and endothelium-independent, sodium nitroprusside (SNP) vasodilators are used to examine dilator responses. Vessels are usually contracted to a steady level *ex vivo* by vasoconstrictors (high potassium or phenylephrine) (Rosas-Hernandez *et al*, 2009), and then are exposed to cumulative concentrations of an agonist drug such as ACh.

Production and release of dilator substances may be assessed by the response to ACh; it is a characteristic for a functioning and healthy endothelium. Similarly a decrease in the maximum dilator response to SNP indicates the lack of SMC sensitivity to NO.

1.7.4 Influence of Nanoparticles on the function of aortic vessel

NP size plays a vital role in cellular uptake and penetration into the vessel through intravascular and extra vascular modes. These particles are then localised in intracellular vesicles (Nasser *et al*, 1996). Studies examining the effect of NPs on vessel function have demonstrated that silver NPs can induce vasoconstriction and block any endothelial-dependent responses by isolated aortic rings (Rosas-Hernandez *et al*, 2009). Similarly using isolated aortic rings *ex vivo*, Farooq *et al* (2014), demonstrated that SiNPs of < 100nm caused attenuation of endothelial dependent (ACh), but not independent dilation (SNP) responses. They further determined that the attenuation response was due to the surface area of the NPs rather than their size. Furthermore, they found that attenuation related to dyed dope SiNPs could be restored using superoxide dismutase (SOD) but this was not the case with non-dye doped SiNPs, therefore suggesting that their mechanisms of dilation for non-dyed and dyed dope SiNPs are different. Similarly, using SiNPs of 100nm and 200nm, our previous published study (Akbar *et al*, 2011) demonstrated that there was no overall detrimental effect on dilatory function. However, once the NPs were surface modified with APS the 200nm lead to a significant reduction in dilatory responses of ACh. This indicated that both size and surface modification of NPs influenced dilatory responses. In a most recent study by Silva *et al* (2014) the effect of coupling AuNPs to NO donors (ruthenium complex) was investigated, demonstrating that NO released from AuNPs was lower than that from the ruthenium complex alone. AuNPs did not impair the vasodilation induced by the NO donors. An *in vivo* study by Khan *et al* (2012) found that administration of 10nm AuNPs did not induce any oxidative stress in the lungs and heart of a rat model, however led to a significant production of lipid peroxidation in the rat liver.

Recently, Goverment and scientific organisations have called for the need to assess toxic effects of NPs in tissues including the heart and blood vessels. At this moment, the author is not aware of any information on the effect of polymer and non-polymer modified AuNPs uptake on aortic vessel function.

1.8. Aims and Objectives

The aim of this project was to synthesise and characterise NPs (silica and gold) and to determine the influence of AuNPs on cellular and vascular function using isolated cells and whole vessels *in vivo* and *ex vivo.*

Specifically the following questions were addressed:

Q1. Will non-modified and polymer modified AuNPs influence endothelial cell function *in vitro?*

Q2. Can non-modified and polymer modified NPs affect vascular function? Specifically, do they affect: Endothelium dependent (ACh) and endothelium independent (SNP) vasodilator function?

Hence, the hypotheses of the present study are:

- AuNPs will influence endothelial cell (EC) viability and proliferation in cell culture, the degree of which depends on the type of polymer modification.
- AuNPs will attenuate dilator function of aortic vessels, the degree of which depends on the type of polymer modification.

In order to answer these questions the following objectives were set out:

1. To synthesise NPs of different material composition (silica, gold) and to characterise them using Ultraviolet-visible spectroscopy (UV-spectra), transmission electron microscopy (TEM), scanning electron microscopy (SEM), thermo-gravimetric analyser (TGA), Photon correlation spectroscopy, Energy-dispersive X-ray spectroscopy (EDAX) and Surface-enhanced Raman spectroscopy (SERS). AuNPs were surface modified using the polymers Polyvinylpyrrolidone (PVP) and mercapto polyethylene glycol (mPEG).

2. To determine the influence of polymer modified AuNPs and non-modified AuNPs on cellular function, *in vitro.* The effect of AuNP uptake on cell viability, proliferation, apoptosis and cell death were investigated using bovine aortic endothial cells (BAECs).

3. To determine the influence of the AuNPs uptake on arterial function using the organ bath system, *ex vivo.* Uptake was verified by TEM and inductively coupled plasma (ICP).

Chapter 2: Methodology

2. Method

2.1 Drugs and chemicals

All chemicals such as: acetylcholine (ACh), sodium nitroprusside (SNP) ammonium hydroxide (NH_4OH), 3-aminopropyltrimethoxysilian, (APS), rhodamine, tetraethylorthosilicate (TEOS), Ethanol absolute, gold (iii) chloride sodium ($HAuCl_4$), rhodamine dye(RH), sodium citrate, thiolated PEG (5000MW), PVP (8000MW) and salts for physiological salt solution (PSS) and high potassium (KPSS) were purchased from Sigma Aldrich chemical company.

2.2 Animal preparation

Male Wistar rats' hearts were collected in a small bottle containing ice cold PSS solution. The rats (150-250g weight) were humanely killed by stunning and cervical dislocation. All procedures were performed in accordance with our institutional guidelines and the United Kingdom Animals Act of 1986, also approved by MMU ethics committee. The animal hearts containing the aortic vessel were removed and placed in ice-cold PSS of the following composition (in mM): sodium chloride (NaCl), potassium chloride (KCl), magnesium sulphate ($MgSO_4$), sodium bicarbonate ($NaHCO_3$), Potassium hydrogen phosphate ($KHPO_4$), dipotassium ethylenediaminetetraacetic acid **(** K_2EDTA), glucose and calcium chloride dehydrate ($CaCl_2.2H_2O$ (pH7.4)). The perivascular adipose tissue was removed from the vessel while being gassed (95% O_2: 5% CO_2) in cold PSS. Aortic rings of 3-4 mm in size were mounted in an organ bath system filled with PSS solution (35 ^oC).

2.3 Nanoparticle Synthesis

2.3.1 Silica Nanoparticles

Before NP synthesis**,** titration of NH_4OH was done to determine the concentration of ammonia (NH_3) in the bottle of NH_4OH (Appendix A: Section2).

Firstly, Silica Nanoparticles were fabricates using methods from previous studies and these methods were subsequently modified (Appendix A: section 4), to determine the influence of modifying certain parameters during NP synthesis.

2.3.1.1 Preparation of dye for silica nanoparticles

The rhodamine dye for silica nanoparticles was prepared using the Stöber method which was further developed by Verhaegh *et al* (1994); briefly 50 µg of rhodamine dye (RH) was added to 0.1136ml of 3-aminopropyltrimethoxysilane (APS) (used as coupling agent) and left stirring in the absence of light for 24 hr under inert atmosphere, until the solution turned orange. This RH dye was used for NP sample termed RH28. Preparation of dye for additional silica nanoparticle samples using different molar ratios of reagent was carried out (*see table 2.1 below*).

Table 2.1: Molar ratio of reagents used for dye preparation in each silica nanoparticle samples.

Sample name	RITC (µg)	APS (ml)	EtOH	Reaction time (hours)
TMNA 100 and 200	**40**	**0.1**	**-**	**3 hrs**
TMRHSI	**3.50**	**0.02**	**0.4ml**	**24hrs**

2.3.1.2 Synthesis of 100nm and 200nm silica nanoparticles

Silica nanoparticles were fabricated using a modified Stöber method. Absolute ethanol (30ml) was added in a 100ml container along with 2ml NH_4OH. An amount of 1.5 ml TEOS was pipetted in the mixture and was left stirring at room temperature. After 10 min 50 µl of the prepared rhodamine dye was added. The solution was left to stir (3hrs); the colour of the solution turned from colourless to a clear, slightly milky pink. This solution was then centrifuged for 25 min at 6000 rpm. The pellet was collected and was then washed and redispersed with deionised water (H_2O) and ethanol. The samples were sonicated using an Ultrasonic Fisherbrand® FB11022 (Germany), and vortexed to dissolve the clumps of particles. Final products were kept in universal tubes and placed in dark storage. This same method was carried out for the production of the non-dyed silica NPs; however, no dye was added to the solution. The sample changed from colourless to slightly milky after 3hrs of stirring. The resultant sample prepared using this method was termed RH28. Additional NPs of varying diameter and morphology were also obtained by reacting different molar ratios of the reagents (*details given in Table 2.2 below*).

Table 2.2: Molar ratio of reagents used for synthesising a variety of silica nanoparticle sizes.

Sample	RITC (µg) + APS	EtOH (ml)	H_2O (ml)	NH_4OH (ml)	TEOS (ml)	Temperature (°C)	Particle Size (nm)	Reaction time (hours)
TMNA 100	5ul	98.30	2.649	8.744	9.946	25	100	3
TMNA 200	5ul	98.70	12.355	4.372	14.94	25	200	24
TMSI	-	90.60	2.808	6.04	3.791	25	100	24
TMRHSI	20ul	-	-		-	25	100	24

2.3.1.3 Surface charging silica nanoparticles with amine group (APS)

The amount of APS needed to coat the whole surface of the silica NPs was weighed out (*An example of APS working out is given in Appendix A: Section 5*) and placed in a beaker along with the sample of the silica nanoparticles. An amount of ethanol worked out (*see table below*) was also added to the mixture and it was placed on the oil bath, which is then placed on the condenser. The particles were left stirring on the oil bath using a magnetic stirrer for 60 min at 40 ^{o}C.

Table 2.3: Amount of APS and ethanol used to functionalise the silica nanoparticles

Sample name	**APS added (µl)**	**Ethanol added (ml)**
TMSI+	**16**	**3.72**
TMRHSI+	**10**	**2.80**
TMNA+ (100nm)	**10**	**2.56**
TMNA+ (200nm)	**2**	**0.63**

2.3.2 Gold Nanoparticle synthesis

Gold nanoparticles were synthesized according to the method by Turkevich *et al* (1951); In brief, 0.02g of $HAuCl_4$ was added to 50ml boiling water heated on a magnetic stirrer. 5ml of a 1% solution of sodium citrate (a reducing agent) was then added to the boiling solution. Heating was continued until the colour of the solution changed from colourless to red. The solution was removed from the hot plate and was left to cool at room temperature for approximately 30 min. The sample was then stored in dark. AuNPs were modified with PVP and mPEG. PEG alone was also prepared for studies on cellular and vascular function

2.3.3 Modification with Polyvinylpyrrolidone

AuNPs were modified with PVP by dissolving 0.0038g of PVP in 1 mL of deionised H_2O, giving a final working concentration of 3.8mg/ml. 500 µL of the stock ($1x10^5$ µM to 10 µM) were prepared and left to stir vigorously with 25mL gold seeds for 24 hours, in order to allow attachment of the polymers to AuNPs. The final working concentration of the sample was 0.076mg/ml in $1x10^5$ µM serial dilution.

2.3.4 Determining the minimum concentration of Polyvinylpyrrolidone required to stabilise NPs

A serial dilution of PVP (1 µM to 0.001 µM) stock was prepared in order to obtain the minimum concentration to prevent aggregation in physiological solution. Each concentration of PVP was incubated with the aortic vessel and their effects on the endothelial dependent and independent dilator responses were assessed.

2.3.5 Determining the minimum concentration of Mecapto polyethylene glycol required to stabilise NPs

A serial dilution of mPEG (5000MW) was prepared from $1.478x10^{-4}$ g/ml of mPEG stock (2.96ml of 0.05g mPEG in 5ml H_2O stock added to 200 ml H_2O) in order to obtain the minimum concentration to prevent aggregation in physiological solutions. pH of all solution was found to be constant at 7.3 in all the mPEG modified AuNPs solutions. The following explains the amount of mPEG used to coat 2 ml AuNPs and its stability after addition in 2ml PSS:

- 7.39x 10^{-5}g /ml of mPEG coated on AuNPs was made up by adding 2 ml of AuNPs in 1 ml H_2O and 0.5 ml of 1.478x10^{-4} g/ml of mPEG stock (2.96 ml of 0.05g mPEG in 5 ml H_2O stock made up to 200 ml with H_2O) added in a vessel of 2ml PSS. Therefore 3.7x10^{-5}g of mPEG is needed for coating 1ml of AuNPs stock. The solution remained stable i.e. no colour change after addition of PSS. The pH of the solution was also measured and gave a pH value of 7.3.

- 7.39x 10^{-6}g/ml of mPEG coated on AuNPs was made up by adding 0.5 ml of AuNPs to 0.25 ml of H_2O and 0.125 ml of 1.478x10^{-5} g/ml mPEG (20 ml of 1.478x10^{-4} g/ml mPEG stock in H_2O (180 ml)). Therefore 3.7x10^{-6}g of mPEG was needed for coating 1ml of AuNPs stock. The stability was then tested with 2 ml PSS after 15 min: there was no colour change.

- 1x10^{-7}g/ml of mPEG coated on Au NPs was made up by adding 0.5 ml of AuNPs to 0.25ml of H_2O and 0.125ml of 1x10^{-6} g/ml mPEG (0.68ml of 1.478x10^{-5} g/ml mPEG stock in H_2O (10ml)) was also added to the solution. Therefore 0.5x10^{-7}g of mPEG was needed for coating 1ml of AuNPs stock. The stability was then tested with 2 ml PSS after 15 min and there was a colour change from pink to blue colour change. This demonstrated instability in PSS.

2.3.6 Modification with Mecapto polyethylene glycol

The concentration of 7.39x 10^{-6} g/ml of mPEG coated on 2ml gold NP stock was made up in and left stirring for 1 hour to allow attachment and 7.4x10^{-8} g/ml of the sample was used for cellular (20 µl) and for vascular (300 µl) function studies.

2.3.7 Preparation of non thiol modified polyethylene glycol (PEG)

Polyethylene glycol (0.001 g) was added to 500 ml distilled water (2x10-6 g in ml). An amount of 166 µl of the sample was added to 15 ml of PSS in the organ bath.

2.4 Characterisation of Nanoparticles

2.4.1 Scanning electron microscopy

Scanning electron microscopy (SEM) was used to confirm the size of the silica nanoparticles. A dilute droplet of nanoparticle (silica) solution was dried onto a clean silicon surface and imaged by scanning electron microscopy (Zeiss FEG SEM). The average nanoparticle size was determined by measuring the diameter of at least 10 NPs with reference to the typography scale found on the micrograph (Akbar *et al*, 2011).

2.4.2 Transmission electron microscopy

The sizes and morphology of the gold nanoparticles were confirmed using transmission electron microscopy (TEM, JEOL JEM-200). A dilute sample was dried on a clean copper grid and the sample was inserted under high vaccum into the microscope (Akbar *et al*, 2011).

2.4.3 Zeta Potential of silica nanoparticles

Using a Malvern Zetasizer Nano ZS instrument, the nanoparticle size of the SiNPs was determined by dynamic light scattering (DLS). Zeta potential was also determined. 1ml of nanoparticle solution containing 0.02% weight was placed into a polystyrene cuvette and placed in to a slot on the a Malvern Zetasizer Nano ZS instrument (Malverin Instruments, UK). The particles were dispersed in water and PSS for their stability analysis.

2.4.4 Analysing the rhodamine B isothiocyanate dye coated silica nanoparticles using fluorescence spectroscopy

The dye molecules encapsulated in silica nanoparticles (TMNA 100nm and RH28) were placed in a Quartz cuvette and determined using fluorescence spectroscopy. The excitation wavelength of the dye was 540 nm and emission at 573 nm.

2.4.5 Determining the stability of the modified and non-modified gold nanoparticles

2.4.5.1 Ultraviolet-visible spectroscopy

To check the stability of the non-modified and modified AuNPs in the presence of PSS, water and complete medium, samples were characterised with UV-vis. Firstly, the instrument was prepared and left for 3-4 minutes in order to set the UV lamp. Two quartz cuvettes were used, one was filled with a solution (H_2O , cell media or PSS) for reference and the second was filled with 1:1 ratio of NPs solution and H_2O, cell media or PSS. The quartz cell was then placed on the sample holder and the sample was analysed.

2.4.6 Assessment of functional groups on gold nanoparticles

2.4.6.1 Energy-dispersive X-ray spectroscopy analysis

EDAX analysis was performed using the Energy-dispersive X-ray spectroscopy analysis system attached to microscope JEOL 5600LV scanning electron microscopy. A droplet of NP samples was dried on a clean aluminium stub and was placed in a sample holder component in the instrument for analysis.

2.4.6.2 Thermogravimetry analysis

Briefly, a solution of PVP modified AuNPs were completely dried to give a pellet. 12 mg of the pellet held in a ceramic crucible was analysed on the thermogravimetry analyser (TGA) to show the number of PVP molecules attached on the AuNPs. A weight of the sample (12mg) was scanned in a temperature range of 0-1000 ^{o}C for TGA at a heating rate of 10^{o}C/min under nitrogen purge. The process involves burning PVP molecules at a certain temperature from AuNPs. The longer it takes for all the PVP molecules to remove from the AuNPs indicates high quantities of PVP chains attached on AuNPs. PVP alone was also analysed as a control.

2.4.6.3 Surface Enhanced Raman Spectroscopy

The functional groups attachted on the modified and non-modified AuNPs were analysed by Surface-enhanced Raman scattering (SERS). For sample preparation, 1ml of the NP solution was drop-coated on the glass slide and left to dry in the oven overnight at 60 ^{o}C, then the Raman spectra were recorded the following day. The spectra were obtained with a microscopic confocal Raman spectrometer (Reinshaw in via Raman microscope) operated with an argon laser (514 nm). The laser intensity was 50 mW.

2.4.6.4 Diffuse reflectance infra-red Fourier transform spectroscopy

DRIFTS were performed to determine the finger prints of the modified and non-modified AuNPs and their stabilisers. Briefly, DRIFTS preparation involved placing an analytic sample on the salt plate (KBr), then another plate was placed on top of the first plate making a "sandwich". The "sandwich" was then mounted on a sample holder. A background spectrum was run using the OMNIC software before the sample was analysed on the system.

2.4.7 Quantification of the relative amount of metal in the modified and non-modified gold Nanoparticles

2.4.7.1 Inductively-coupled plasma mass spectrometry

In order to determine the relative amount of metal in 300 µl of PVP and mPEG modified AuNPS and non-modified AuNPs, the samples were diluted in 5ml of distilled water and analysed using the Inductively coupled plasma mass spectrometry (ICP-MS; Perkin Elmer, UK). Furthermore, the presences of modified and non-modified AuNPs within the aortic vessels after 30 minutes incubation period from the vascular study (section 2.9) were also determined using this technique. Briefly, the vessel was firstly weighed before incubation with the experimental conditions. Afterwards, the concentration of AuNPs, AumPEG and AuPVP used in the organ bath and the double concentration, along with control vessels (in PSS) were incubated with 37 °C PSS under gas condition (95% O_2 /5% CO_2) then the weight of each of the vessels was recorded before being lysed. The amount of 0.5 ml of lysate buffer (containing 0.5g SDS, 0.2925g NaCl, 0.394g Tris, 0.030g tris

(hydroxylmethyl) aminomethane) was added to each tube and tubes were left for 48 hrs at room temperature to allow the tissue to dissolve in the buffer. Each tube was mixed with 1ml of high-purity (70%) nitric acid to allow the vessel tissue to be fully dissolved. The glass tubes were placed in an oil bath at 200°C for 3 hrs. The tubes were then transferred into a 5 ml volumetric flask and the volume made up to 5 ml with distilled water. Volumetric flasks containing the samples were placed within the ICP machine sample tray for analysis.

2.5 *Cellular study of endothelial cells: Cell culture*

2.5.1 Preparation of cell culture medium

The complete medium was prepared by filtering 450ml of the Dulbecco's Modified Eagle medium (DMEM)) containing 4.5 g/l glucose in a 500ml sterile bottle, along with 50ml of 10% foetal bovine serum (FBS) and 5ml of 1% antibiotics (100 U/ml penicillin and 100 µg/ml streptomycin) and finally 5ml of glutamine.

2.5.2 Culture of bovine aortic endothelial cells

Bovine aortic endothelial cells (BAEC) were isolated as previously described (Sattar *et al*, 1994) and seeded in 75-cm^2 flasks pre-coated with 0.1% gelatine and cultured in Dulbecco's Modified Eagle Medium (Lonza, Cambridge, UK) supplemented with 20% foetal bovine serum (Cambrex, Hertfordshire, UK), 2 mM glutamine and 1% antibiotics (100 µg/mL streptomycin, 100 U/ml penicillin), defined as complete medium. The cells were incubated at 37°C in a saturated air humidity with 5% CO_2 incubator, passaged every 2-3 days, using enzymatic digestion with 0.05% trypsin / 0.02% EDTA and split at a ratio of 1:2 or 1:3. At confluence, ECs were identified by their typical cobblestone morphology. The cells were used throughout the study between passages 4 and 9.

2.5.3 Trypsinization of cells

Once the incubated cells reached 80-90% confluence (80% of surface of flask covered by cells) they were trypsinized. It is important to avoid over confluence as this will cause cell death. The medium from the flask was discarded and the cells were rinsed three times with 10 ml sterile phosphate buffer saline (PBS). Afterwards, 5ml of 0.05% trypsin and 0.02% EDTA was added to the flask containing the cells; the flask was gently rolled to ensure trypsin contact with all cells and incubated for cell detachment for 2-3 min. The cells were monitored under the microscope to prevent over-trypsinization which can severely damage the cells. As soon as the cells detached the flask was removed from the incubator and gently tapped to detach all the cells. The cells were then collected in the centrifuge tubes together with the complete medium to inactivate the trypsin. The cells were then centrifuged (HERMILE Z400K) at 1300 RPM for 5 min. The supernatant was discarded

and the cell pellets were re-suspended in fresh complete medium for subculture, (also known as passaging) or in serum poor medium SPM (2.5% FBS).

2.5.4 Process for freezing the cells

The cells were detached from a single T-25 flask with the trypsin and centrifuged at 1300 RPM. The cell pellet was collected and re-suspended by a gentle pipetting with 25 % complete medium and 75% freezing medium made up from 10 % DMSO and 90% FBS. The amount of 1.5 ml was taken from the suspension containing the cells and then transferred to each cryotubes. The cells were first frozen at – 20º C for 30 min then placed in the freezer at -80 ºC for 24 hrs then finally stored in liquid nitrogen (– 196 ºC).

2.5.5 Thawing of cells

The frozen cryotube containing the BAECs was taken from either the liquid nitrogen or the -80 ºC freezer. The cryotube were then disinfected with 70% ethanol spray and were defrosted at 37 ^{o}C under aseptic condition. The cells were gently poured into a T-25 flask containing roughly 3 ml of complete medium and finally, the flask was incubated at 37 ºC in an humidified incubator (5% CO_2; 95% air) changing medium each time, until confluent.

2.5.6 Cell proliferation and Cell viability

Cells were seeded at 2.5x10^4 cells/ml with 500µl of DMEM supplemented in a 24 well plate and were incubated to allow seeding for 4 hrs. The medium was then changed for the experimental conditions (AuNPs, PVP, AuPVP, AumPEG and mPEG). Cells were further incubated at 37^{o}C in humidified 5% CO_2 atmosphere and assessed for morphology and proliferation at periods of 24 and 48 hrs. After incubation period the cells were quantified for the number of cells in a single cell suspension using Coulter counter (Z Series Coulter Counter from Beckman Coulter). At this stage 50 µl of cells were suspended in 10 ml isotonic solution and the reading on the Coulter counter was taken three times. Finally, cell concentration was calculated as following:

Cell concentration/ ml = cell count x **dilution factor**

Viability of cells was determined using two methods: Trypan blue exclusion method and flow cytometer. This is described in details in section 2.5.8.

2.5.7 Cell morphology

Cells were viewed under the light microscope to detect any signs of contamination early on. Furthermore, detachment of the cells from the substrate were also inspected under the microscope, to identify any deterioration of cells which will require a change of medium to further prevent deterioration. The cells were imaged after 24 and 48 hours incubation with modified and non modified AuNPs to show any changes in the morphology such as cell elongation.

2.5.8 Cell Viability

Cell viability was performed based on two methods: Trypan blue exclusion method using Haemocytometer (a) and automated cell counter (b), and propidium iodide (PI) staining using the FACs flow cytometer. The following sections (2.5.8.1, 2.5.8.2 and 2.5.8.3) give more details on the methods used for performing cell viability.

2.5.8.1 Haemocytometer chamber

The cell viability was determined using the haemocytometer chamber and counting the viable cell by a Coulter counter. Proliferation was carried out as described previously. Briefly, the cells were seeded and were added to 24 well plate along with 2 ml complete medium (10 % FBS). The cells were then incubated for 4 hours to allow cell attachment. After 4 hours complete medium was replaced with SPM (2.5% FBS) along with the different experimental conditions: AuNPs (2.9µg/mL), AuPVP (2.9µg/mL), PVP ($5.9x10^{-7}$ µM), AumPEG (2.9 µg/mL) and mPEG ($9.25x10^{-9}$) was added to each well. The cells were then washed with 10 ml of sterile PBS and 150 µl of 1x trypsin was added to each well. A 25 µl volume of the suspension of the cells was mixed with 25 µl volume of trypan blue. Half of the mixture was then placed on the chamber. Finally the chamber was placed in the cell counter to display the results of the viable cells in percentage.

2.5.8.2 Automated cell counter

Cell viability was also determined using TC20 automated cell counter (Bio-rad, UK). Briefly, trypsinized cell suspensions in each well chamber were mixed with trypan blue in a 1:1 ratio. A 25 µl amount of the sample were inserted in a counting slide and placed in a slot on the TC20 cell counter. The cell counter provided a total cell count (with or without trypan blue staining) and cell viability was assessed via trypan blue exclusion method.

2.5.8.3 Determining cell viability with propidium iodide (PI) staining using FACs flow cytometer

A concentration of 1 x 10^6/ml cells incubated in SPM or with the experimental conditions, was washed twice using 2 ml of PBS and centrifuged at 400 x g for 5 min in a 50 ml centrifuge tube. The buffer was then decanted and the pelleted cells were resuspended in 500µL of PBS and placed in a FACs tube. The flow cytometer was then adjusted for the PI setting. Each tube containing the cells after SPM (positive control) or experimental condition was mixed with 5 µl of PI staining solution and left in the dark for 1 minute. Unstained cells were also used as negative control. The samples for the positive control were then determined for PI staining using the FL-2 or FL-3 channel on a FACScan™ instrument. The data for unstained cells were also acquired. The viable cells for the PI stained samples prior to analysis were then set on stop count and examined on a forward scatter versus FL3(PI) dot plot staining.

2.5.9 Confocal analysis of nanoparticle uptake via cells

2.5.9.1 Cell membrane labelling

BAEC membranes were labelled with a fluorescent cell linker kit PKH26 (red dye). Briefly, 2 x 10^6 cells were washed with basal medium (without serum) and centrifuged at 400 g for 5 min at room temperature. After discarding all the supernatant, the cells were gently re-suspended in 100 µl of diluents. Immediately prior to staining, the dye working solution (2x) was added to 100 µl of diluents and the dye mixture was added to the cells. After 5 min with periodic mixing of the cells in the dye solution, the staining was stopped by an equal volume of FBS and left for 1 min. Then, the fluorescent cells in complete medium were centrifuged at 400 g for 10 min. To minimize carryover of residual dye, the cells were transferred into a new sterile conical tube for further centrifugation at 400 g for 5 min. Thus BAECs were ready to be used for confocal microscopy analysis after NP treatment.

2.5.9.2 Cell Nuclei labelling

PKH26 labelled BAEC were seeded at 1x10^5 cells/ml in endothelial cell growth medium on chamber slides previously coated with 0.1% gelatine. Cells were incubated to allow seeding for 4 hrs. The medium was then changed for the experimental conditions (AuNPs, PVP, AuPVP). Cells were further incubated at 37^{o}C in humidified 5% CO_2 for a period of 30 min, 1hr and 18 hrs. After incubation each well was washed with PBS 2x and fixed with 4% Paraformaldehyde for 10 min. The chambers were washed again with PBS and then mounted using DAPI mounting medium. An amount of 300 µl of the diluted DAPI solution (sigma) (1 µl DAPI in 5 ml of PBS) was added to each well, and incubated for 5 min at room temperature. The coverslips where then washed again with PBS. The coverslips were then removed from the wells using fine tweezers and mounted on a microscope slide. AuNP localization was visualised with a Zeiss fluorescent microscope.

2.6 Analysis of Cellular signalling pathways

2.6.1 Protein estimation for western blotting

Determination of the amount of protein extracted from the cell lines for loading in western blotting technique was carried out using a Bradford-based assay. Bio-Rad protein dye was diluted according to the ratio of 1:5 in distilled water (2 ml). Stock 1% BSA was made up at 1 mg/ml (µg/µl) in distilled water as a standard protein and dilution were prepared as shown on Table 2.4. The amount of 10 µl protein lyses from each sample was added with 90 µl of distilled water. The absorbance was measured at 580 nm. The standard curve (Figure 2.1) was calculated to determine the amount of the protein needed to be added.

Table 2.4: Dilution of BSA used for protein estimation

Stock 1% BSA (µg/µl) in distilled water: Distilled water (µl)
0:100
10:90
20:80
40:60

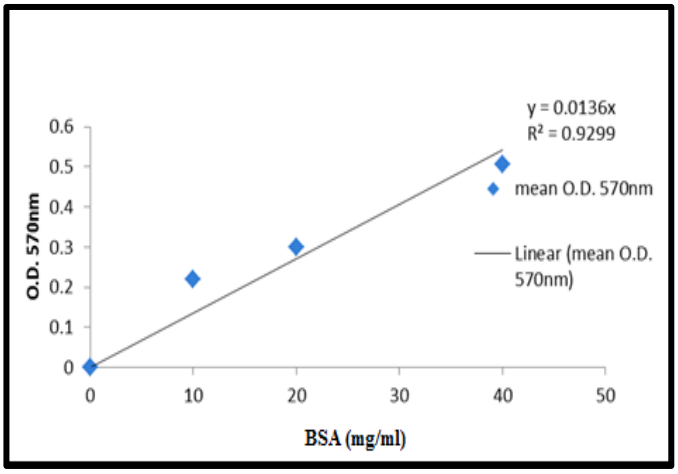

Figure 2.1: The standard curve used to work out protein estimation

2.6.2 Western blotting

BAECs were seeded in complete medium in a 24-well plate at a cell concentration of 10^5/ml/well. After 48 hrs incubation, the medium was renewed with serum poor medium (SPM; medium supplemented with 2.5% FBS) for further 24 hrs incubation, and then NPs were added for 30 min stimulation at 37°C. After fast washing in cold PBS, cells were lysed with 120 µl/well of ice-cold radioimmunoprecipitation (RIPA) buffer (pH 7.5) containing 25 mM Tris-HCl, 150 mM NaCl, 0.5% sodium deoxycholate, 0.5% SDS, 1 mM EDTA, 1 mM sodium orthovanadate (EGTA), 1 mM phenylmethylsulfonyl fluoride (PMSF), 1% Triton X100 and 1 µM leupeptin. Thirty µg of proteins were mixed with 2x Laemmli sample buffer, denatured by boiling in a water bath for 15 min then centrifuged. Samples were separated along with pre-stained molecular weight markers by 12% SDS-PAGE. Proteins were electroblotted onto nitrocellulose filters (1 hr) and the filters were blocked for 1 hr at room temperature in TBS-Tween (pH 7.4) containing 1% BSA. Filters were stained with the following primary antibodies diluted in the blocking buffer, overnight at 4°C on a rotating shaker: rabbit polyclonal antibodies to total extracellular signal-regulated kinase 1/2 (t-ERK1/2), goat polyclonal antibodies to total Akt (t-Akt, 1:1000) mouse monoclonal antibodies to phopsho-ERK1/2 (p-ERK1/2, Tyr204 of ERK1, 1:1000) and rabbit polyclonal antibodies to p-Akt-1/2/3 (Thr308, 1:500) from Santa Cruz Biotechnology. After washing (5x10 min in TBS-Tween at room temperature), the filters were stained with either goat anti-rabbit, rabbit anti-goat or rabbit anti-mouse horse-radish peroxidase-conjugated secondary antibodies diluted in TBS-Tween containing 5% de-fatted milk (1:1000, 1 hr, room temperature) with continuous mixing. After a further 5 washes in TBS-Tween, proteins were visualised using ECL chemiluminescent detection (Geneflow Ltd, Staffordshire, UK) then analysed using GeneSnap software (Syngene, Cambridge, UK).

2.7 Analysis of Cell death

2.7.1 Induction of Apoptosis and quantification using Annexin V-FITC detection kit

Apoptosis was induced by the use of staurosporinse, a potent inhibitor (Sigma Aldrich, UK). Briefly, in bijoux, 2 µl of staurosporine was mixed with 2 ml of DMSO and was later incubated with the BAEC for 2 hrs. This negative control was conducted to determine whether cells underwent apoptosis after exposure to modified and non-modified AuNPs along with their stabilisers after 2 and 24 hrs. The cells were stained as described in the Annexin V FITC Apoptosis Detection Kit (Sigma Aldritch, UK). The percentage of apoptotic cells per sample was determined using the FACs analysis. The samples were analysed in triplicate.

2.8 Cellular uptake of AuNPs

The fate of internalized particles in BAECs was determined by TEM. TEM preparation was as follows. BAECs were incubated with 2.9 µg/mL modified and non-modified 13 nm AuNPs for 30 mins, 2 hrs, 24 hrs and 48 hrs and afterwards were fixed in a solution of 5 ml of 2% paraformaldehyde in 0.1 M PBS (5 ml). The cells were then taken to EM Wellcome Trust facility at the University of Manchester, for ultrathin sectioning and TEM imaging.

2.9 Vascular function study of rat aortic rings using organ bath system

The adult male rat's heart and associated vessels were placed in a dissecting dish containing gassed PSS to keep the tissue viable. The aorta was then isolated from the heart and carefully the tissue surrounding the vessel was removed under a dissecting microscope, 3-4 mm length segments of aortic ring were then cut, and suspended between 2 fine steel wires, connected to a Harvard isometric transducer in an oxygenated bath chamber (Figure 2.1 and Figure 2.2) containing PSS. The segment was then loaded passively to 2g tension for 1hr to equilibrate. The vessel was then preconstricted with KPSS and subsequently dilated with both the endothelium-dependent dilator ACh, and independent dilator SNP. Data were recorded on a computer using the software lab chart 7 (Powerlab system, AD Instruments, UK) (Figure 2.3). *Endothelium dependent relaxation*: Aortic rings were constricted in high potassium solution then dilated at 5 different cummulative concentrations of ACh 10^{-2} to 10^{-5} mol, then incubated with NPs (30 min) and procedures were repeated after NP washout.

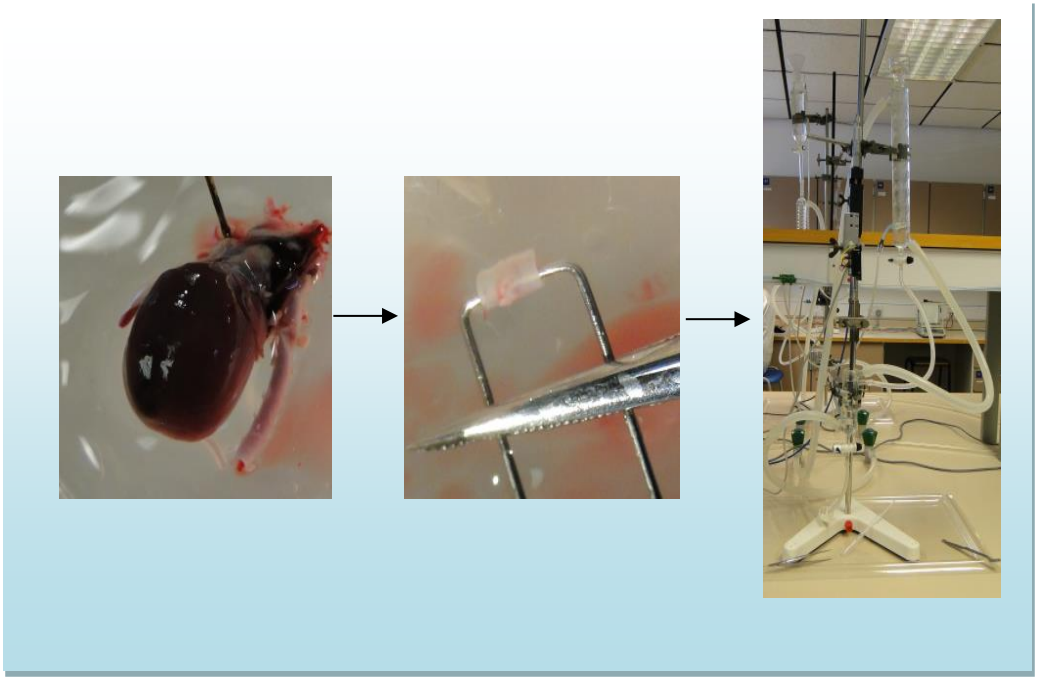

Figure 2.2: Dissection of an aortic ring mounted in an oxygenated organ bath chamber

Endothelium independent dilation: The same protocol as ACh was followed. However vasodilator SNP ($10^{-1}$to 10^{-5} mol) was studied, before and after NPs. The concentration of NPs was calculated (see table 2.4).

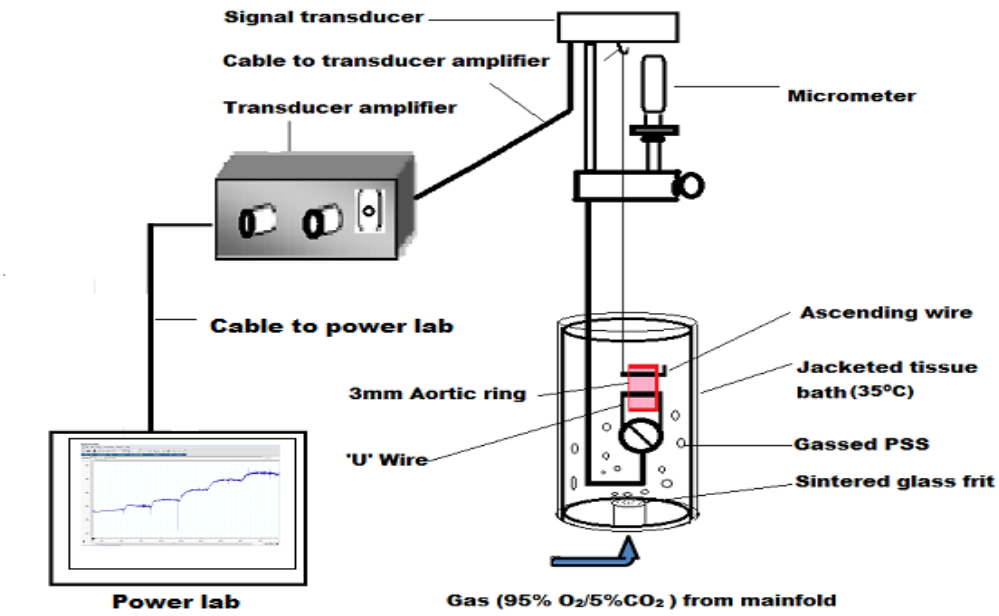

Figure 2.3: Schematic image of organ bath setup

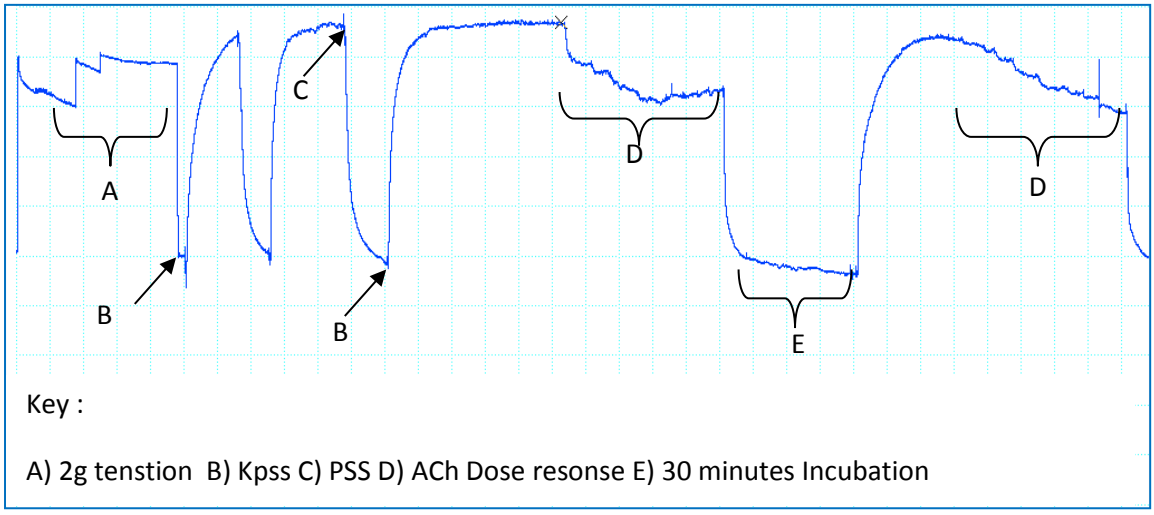

Figure 2.4: An example of data recorded on a computer using the software lab chart 7 (Powerlab system, AD Instruments, UK).

Table 2.5: Calculated surface area and mass of nanoparticles and stabilisers to be added to each experiments

Type of Nanoparticles / Stabilisers	**Surface area /unit mass (m^2)**	**No of particles in organ bath (particles/ml)**	**Mass of NPs added (µg/mL)**
Silica NPs (TMNA, 100nm)	$3.09x10^{-14}$	1.1×10^{11}	**200ug/ml**
PVP- and mPEG-modified and non- modified AuNPs	$4.52x10^{-12}$	$1.698x10^{11}$	**2.9ug/mL**
Double concentration of mPEG modified AuNPs	$4.52x10^{-12}$	$3.396x10^{11}$	**5.8ug/mL**
PVP alone: **Maximum concentration** **used to modify AuNPs** **Minimum concentration used to modify AuNPs**	-	-	**76ug/mL** ($9.5x10^{-6}$uM) **4.75ug/mL** ($5.9X10^{-7}$uM)
PEG alone **mPEG alone**	-	-	**0. 0011 ug/mL** ($1.84x10^{-10}$ uM) **0.074ug/mL** ($9.25x10^{-9}$ uM)

2.10 Tissue fixation and transmission electron microscopy analysis of nanoparticle uptake

TEM was performed to characterise the physical properties of AuNPs and to determine particle sizes, and also to visualise the uptake of AuNPs by the whole aortic vessel. After each aortic functional study, the vessels were fixed in solution containing 2.5% glutaraldehyde in 0.1M sodium cacodylate buffer, pH 7.3 and were allowed to stand in solution for 30 min at 22^{o}C, and were then washed in buffer. The samples were postfixed with reduced osmium (1% OsO_4 + 1.5% $K_4Fe(CN)_6$) for 1 hour, then dehydrated in a series of alcohols (ethanol), infiltrated with TAAB LV resin and polymerised for 24 hours at 60˚C. Ultrathin 70nm sections were cut with Leica 'Ultracut S' ultramicrotome and placed on copper grids. The grids were observed in Tecnai 12 Biotwin TEM at 80kV.TEM sectioning was carried out at Manchester University

2.11 Statistical analysis

Results for both cellular and vascular studies are expressed as mean ±S.E.M (standard error mean). One way anova with Bonferroni correction was used to test for statistical significance ($p<0.05$ taken as significant). The calculation for percentage dilation response of ACh and SNP are calculated as:

$$\frac{\text{(Maximum tension after constriction) – (tension after relaxation)}}{\text{(Maximum tension after constriction)}} \times 100$$

Chapter 3:
Chemical Characteristics of Synthesised Nanoparticles

3. Chemical characteristics of synthesised nanoparticles

3.1 Characteristics of synthesised nanoparticles

A number of nanoparticles (NPs) were fabricated (silica, gold), and surface modified. The NPs were characterized (stability, size, charge) using Ultraviolet-visible (UV-vis) spectroscopy, Malvern's Zetasizer, transmission (TEM) and scanning electron microscopy (SEM). The structures of the functionalised NPs were also determined by infra-red Fourier transform spectroscopy (DRIFTS), Surface Enhanced Raman Spectroscopy (SERs) and Thermogravimetric analysis (TGA). The energy dispersive X-ray spectroscopy (EDAX) was employed to determine the sample's composition. This chapter will describe the results obtained from the NPs analysis.

3.2 Characteristics of synthesised Silica nanoparticles

Silica NPs were firstly fabricated using methods from previous studies (*See Appendix A: Table 2*). The methods were then further modified, and attempts were performed twice to show repeatability. These methods were conducted to show the influence of modifying certain parameters during the NP synthesis.

The attempt of Geishe method for fabricating non-dye doped (100 nm) NPs at 60^{o}C resulted in particles double the expected sizes (200.65±35.65 nm). van Bladdern and Viraj (1992) method for the synthesis of 110 nm NP resulted in the formation of NP hydrodynamic size of 618±45.8 nm. While, van Bladdern *et al* (1992) method resulted in the formation of 371.7±10.3 nm. Then dye doped silica NPs were fabricated using the same methods (van Bladdern and Viraj, 1992; van Bladdern *et al*, 1992) for synthesising non-dye doped silica NPs, with the inclusion of 3-aminopropyltrimethoxysiliane (APS) attached rhodamine B isothiocyanate (RH) dye. Result shows an increase in diameter when RH dye was included. This is due to the APS molecules that are coupled to the dye, as they contain silane groups. The dye doped silica NPs synthesised using van Bladdern and Viraj method gave particles with hydrodynamic diameter of 913.7±52.7, while van Bladdern *et al* method produced particles >1000 nm. Overall, obtaining small size of particles as

demonstrated by van Bladdern *et al* (1992) was difficult. Obtaining small particle sizes is difficult but can be achieved more easily using the microemulsion method.

NPs were synthesised using the Stöber method; furthermore, during synthesis a number of factors were manipulated, including the molar ratio of reagents, pHs, surface charge *and* temperature. NPs were then characterised in water and PSS, to show the influence on the particle diameter. The following section illustrates the results obtained *(See Appendix A: Table 3).*

3.2.1 The influence of surface charge on the hydrodynamic diameter and zeta potential of Silica nanoparticles

The influence of surface charge on the hydrodynamic diameter and zeta potential of nanoparticles in H_2O and physiological salt solution was determined. The seeded growth of the NPs used excessive water and ethanol during synthesis. The following result was obtained:

The TEM images of the SiNPs (sample TMRHSI), showed spherical monodispersed NPs, of 113±12 nm in diameter (Figure 3.1 (B)). The hydrodynamic size, determined by DLS, was slightly larger at 125 nm in diameter. When the sample was dispersed in PSS, the DLS size increased further to 145 nm diameter. Result shows that the zeta potential did not change dramatically compared to NPs dispersed in water. However, the APS surface modified sample of TMRHSI aggregated in both water and ionic salt solution (PSS) (the zeta potential was 9.23 and 5.42 mV, respectively) (*See Appendix A: Table 3*). This observation shows that surface charge can influence stability of particles.

3.2.2 Effect of pH alteration on Silica particle size

It was necessary to investigate the effect of pH alteration on NP size and stability. The results show that altering the pH had an influence on the stability of the NPs (*See Appendix A: Table 3*). The zeta potentials of both dye and non-dye doped 100 nm silica NPs either modified or non-modified with APS, were determined in water and physiological salt solution (PSS). The results show that there is a difference in stability for non APS surface

modified dye doped particles (TMRHSI-) in water suspension after *pH* alteration from 8.64 to 7.4 (zeta potential values before -49.8 and -30.2 after). A similar observation was detected, when dispersed in PSS (zeta potential values before was -37.8 and after it was -23.6 mV) (*Appendix A: Table 3*). At this range, particles remained stable. Once the dye doped NPs were functionalized with APS, the TMRHSI+ characteristic were altered. The hydrodynamic diameter of the NPs were affected, giving a size of 187 nm compared to non APS functionalised NPs at 125 nm in water. Whereas in PSS, the APS modified NPs doubled in size giving a diameter of 256 nm, compared to non-APS modified NPs (145 nm). This shows an increase diameter by a 100 nm. On the other hand, altering the pH did not affect the stability of the APS modified dye doped NPs. Similar observations were seen for the APS modified silica NPs (TMNA 100+ and TMNA 200+) after characterisation in PSS (340.1 nm and 712.8 nm respectively) (*Table 3.1*).

3.2.3 Production of 100nm silica NPs from a minimum amount of ammonia and H_2O

A method was adapted from Stöber to produce 100 nm SiNPs. The NPs were produced from a reaction of ETOH and concentrated ammonia without H_2O added in the process. These samples were named RH28. The hydrodynamic size and zeta potential of the NPs in H_2O and PSS was also recorded and the effect of adding ethanol and ammonia alone during NPs synthesis was determined. The size of NPs obtained (Figure 3.1 D) by SEM indicated that the particles were 100 ±7 nm. Hence this method was the most desirable of all methods for producing 100 nm.

3.2.4 Determining the nanoparticles sizes using DLS vs. Microscopy

The dimension of NPs can be observed using different techniques; here the size and hydrodynamic diameter was investigated with SEM and DLS respectively.

Table 3.1: Determination of nanoparticles sizes using DLS vs. Microscopy and the effect of surface modification on the hydrodynamic diameter and zeta potential of silica nanoparticles (Akbar et al, 2011). (Key: -With out APS, + With APS).

Nanoparticles	**Nanoparticles Size (nm)**			**Zeta potential (mV)**	
	Microscope (SEM)	Hydrodynamic diameter (DLS)			
		In H_2O	*In PSS*	*In H_2O*	*In PSS*
TMNA 100-	97±7.60	103.0	106.0	-44.50	-28.80
TMNA 100+	-	135.6	340.1	66.90	5.45
TMNA 200-	197±7.50	201.6	194.0	-50.00	-21.50
TMNA 200+	-	259.4	712.8	25.50	1.90
RH28	100 ±7 nm	110.0	127	-48.2	-29.5

3.2.5 Scanning electron microscopy to clarify the sizes of silica nanoparticles

The silica NPs were fabricated according to the Stöber method. Some silica NPs were doped with RH and others without. Particle sizes were determined using SEM images and the Malvern's Zetasizer. The SEM indicated that the APS molecules coupled to RH caused the particle size to increase. Silica particles without dye gave a size <100 nm (83±7 nm) whereas with dye the size increased to 113±12 nm (Figure 3.1 A & B). The SEM also identifies the sizes of NPs from modified methods to produce 100-200 nm with dyes (Figure 3.1 C-E). The APS molecules are used to covalently attach the dye molecules to the silica NPs.

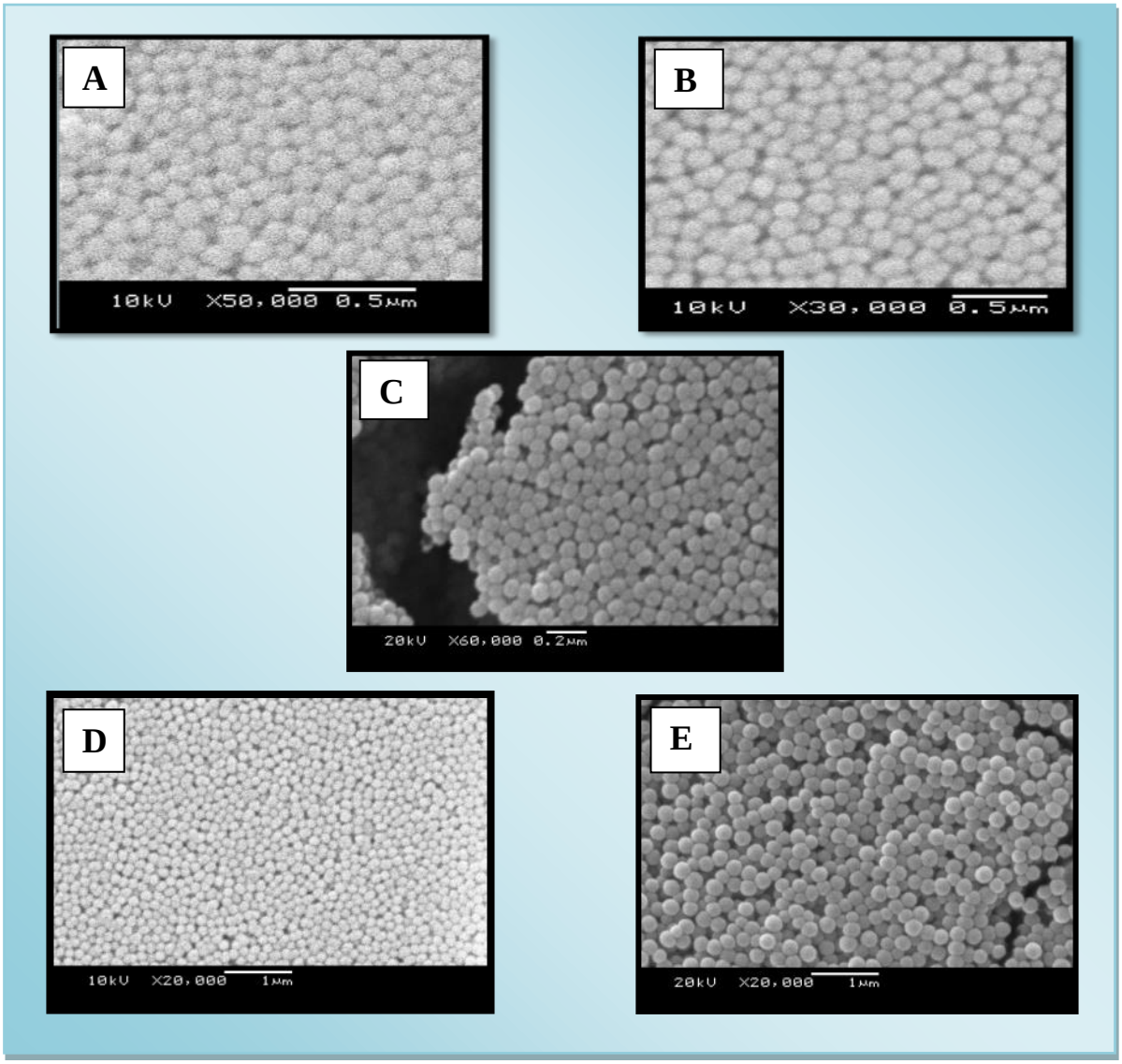

Figure 3.1: Scanning electron microscopy image of silica nanoparticles of (A) TMSI (100nm) non-dye and (B) TMRHSI (100 nm) with dye, (C) TMNA (100nm) with dye (D) RH28 with dye and (E) TMNA (200 nm) with dye

The SEM images in Figure 3.1 confirm the fabrication of colloidal monodispersed SiNPs of close size distribution. The SEM images of silica NPs shows the sample of TMSI non-dye with size distribution of 83±5 nm (Figure 3.1A), the TMRHSI with dye of size distribution of 113.6 ±12 nm (Figure 3.1B); the TMNA (100 nm) sample with the size distribution of 97.9 ±9 nm (Figure 3.1C) and RH28 with dye with the size distribution of 100 ±7 nm (Figure3.1D). Lastly TMNA (200 nm) have a size distribution of 194±9 nm (Figure 3.1E).

Comparing the sizes of the particles obtained from the SEM to those obtained by DLS, it was interesting to observe that sizes were larger by DLS. The particles (TMSI) sample without the dye, gave a reading of 103 nm. However, the size was less when characterised with the SEM 83±5 nm (Figure 1.3A). When the silica NPs were doped with RH dye the size distribution shifted, indicating that the particle sizes increased. Similarly, the DLS reading also indicated that the particles increased to 125 nm for TMRHSI sample. The zeta potential measurement for particles in Figure 3.1A and Figure 3.1B were proven to be stable in H_2O (-80.1 and -49.8 mV, respectively) (*see Appendix A: Table 3*).

3.2.6 Determination of dye present using fluorescence spectroscopy

The fluorescence spectroscopy of the samples prepared with dye (TMNA and RH28) indicates that RH dye is present. Absorption of light at 500-600 nm wavelengths renders the colour of the substance red. Thus, our absorption spectra show a peak obtained at its expected wavelength, indicating that the dye is present (Figure 3.2).

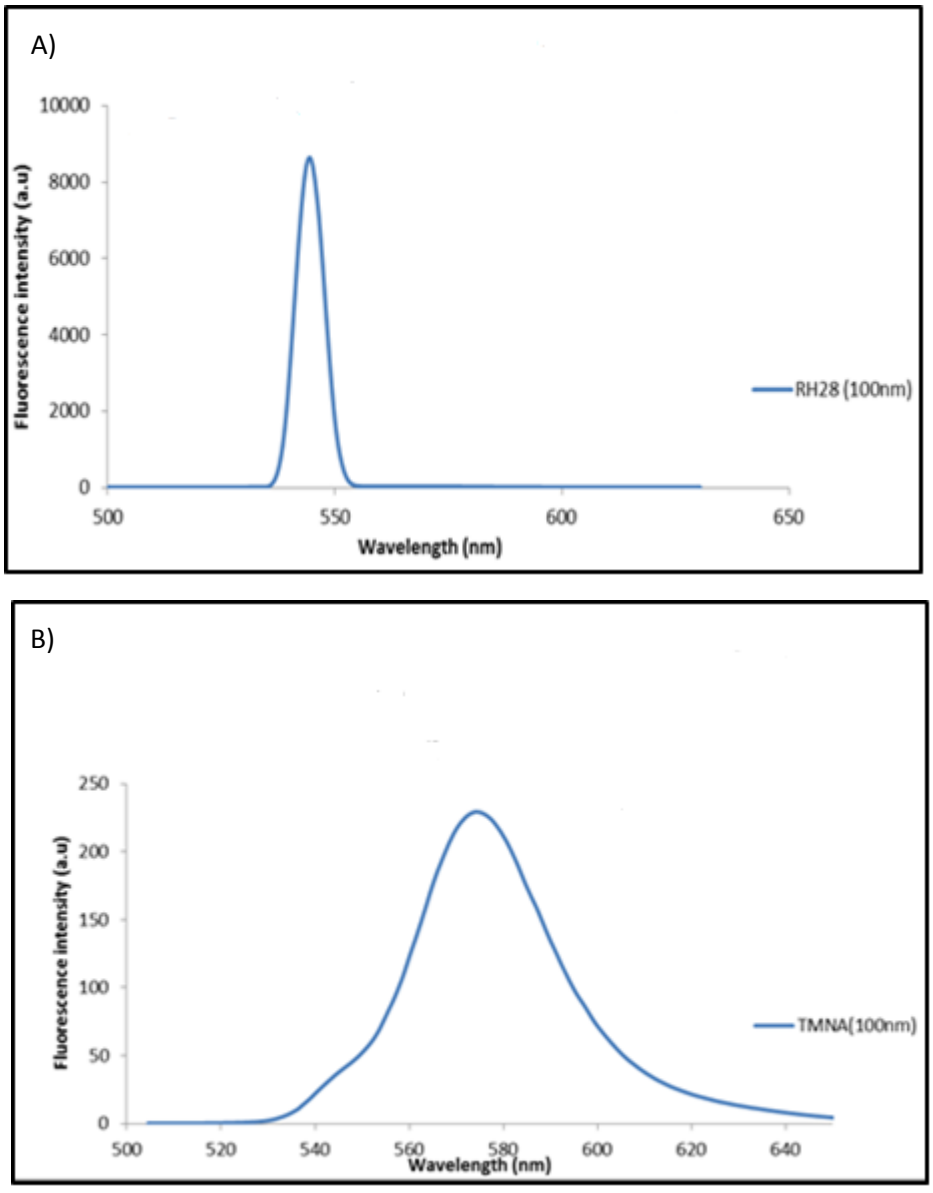

Figure 3.2: The fluorescence spectroscopy indicating the presence of rhodamine B isothioscyanate dye in samples (A) RH28 and (B) TMNA

3.3 Characteristics of synthesised gold nanoparticles

3.3.1 Transmission electron microscopy of modified and non-modified AuNPs

TEM was used to verify the size of the particles. The following images obtained confirm the spherical shape of non- modified AuNPs (Figure 3.3 A) synthesised using Turkevich method. The particles were surface modified with PVP (Figure 3.3 B) and mPEG (Figure 3.3 B). Both polymers caused a wider distribution of particles when compared to non-modified AuNPs. Furthermore, the image shows that the polymer did not affect the spherical structure of AuNPs. The scale bar on the image was used to calculate the particles size, where the individual particles were < 15 nm.

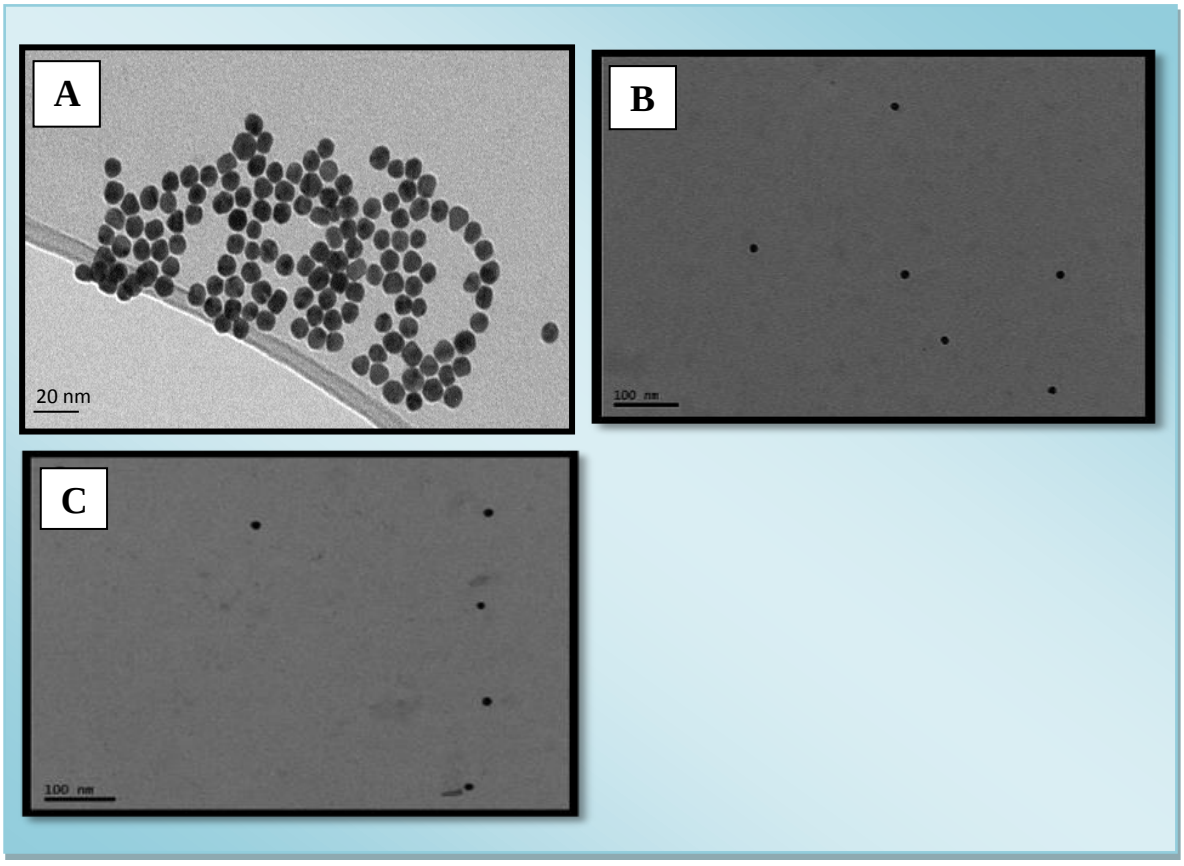

***Figure 3.3:** TEMs shows the distribution of monodispersed black dots which are the non-modified AuNPs, modified AuNPs with b) PVP and c) mPEG*

3.3.2 Determining the stability of modified and non- modified AuNPs in H_2O, complete media and PSS

UV-vis spectra (Figure 3.4A) demonstrated that AuNPs are stable in the presence of H_2O. The surface Plasmon absorption spectra (SPR) trace existed at ~500 to 600 nm wavelength. This is present only for particle size of <50 nm. However, when exposed to PSS media the peak shifted, therefore indicating particle aggregation. When AuNPs were modified with both PVP (Figure 3.4 (B) and Figure 3.5 (C)) and mPEG (Figure 3.6 (1)) the absorption spectra gave the surface Plasmon resonance (SPR) band at ~500-600nm wavelength in water and in PSS, whereby the peak did not shift. Indeed, analysis indicates that AuNPs are very stable after being coated with polymers. After showing that gold alone aggregated in PSS, both PVP (Figure 3.4 C) and mPEG (Figure 3.6 (1) and (2)) stabilizers and demonstrated reduce aggregation of the gold particles in PSS as well as complete media. The polymers PVP and mPEG were used in this study because research has shown that these polymers have favourable properties i.e. preventing aggregation and are also biocompatible.

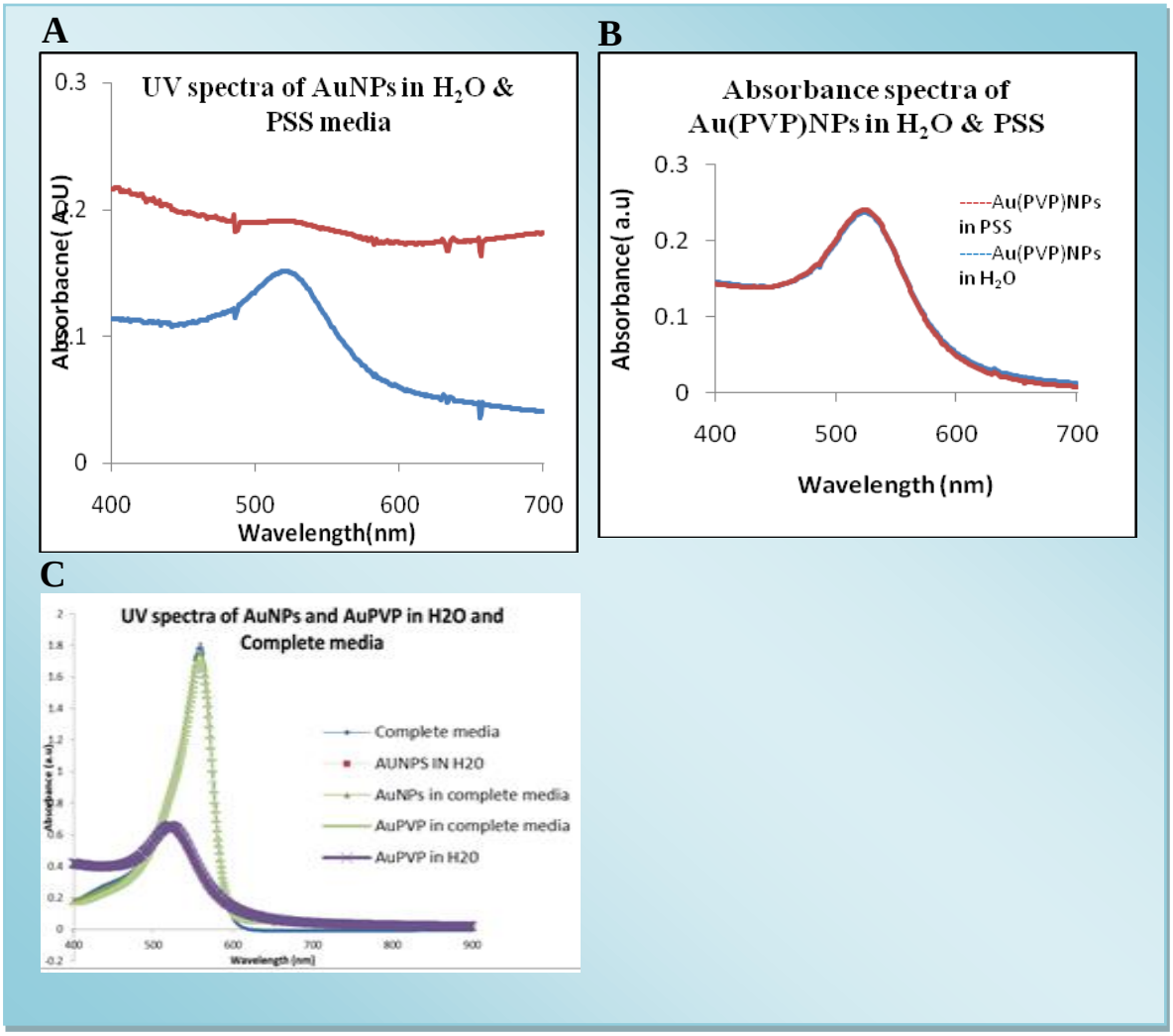

Figure 3.4: (A) Absorption of AuNPs in PSS and H_2O (B) Absorption of Au (PVP) NPs in PSS and H_2O (C) Absorption of Au (PVP) NPs in PSS and H_2O and complete media

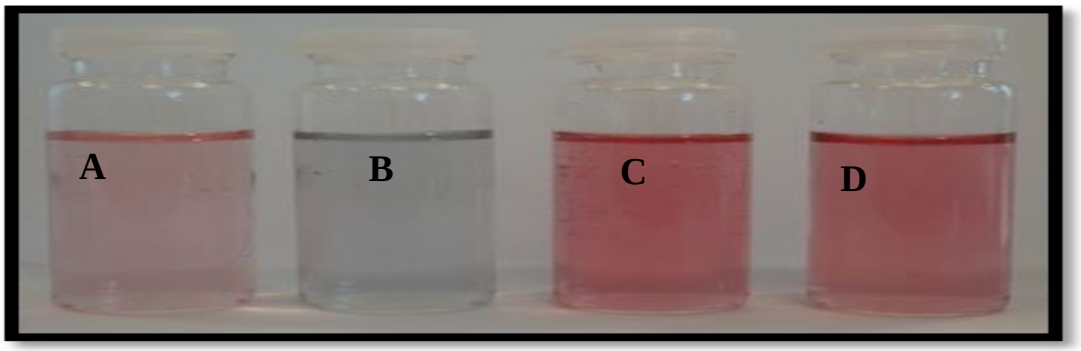

Figure 3.5: Image of AuNPs in solution (A) non-modified AuNPs in water (B) non-modified AuNPs in physiological salt solution showing colour change due to aggregation, (C) PVP modified AuNPs in water and (D)PVP modified AuNPs in PSS.

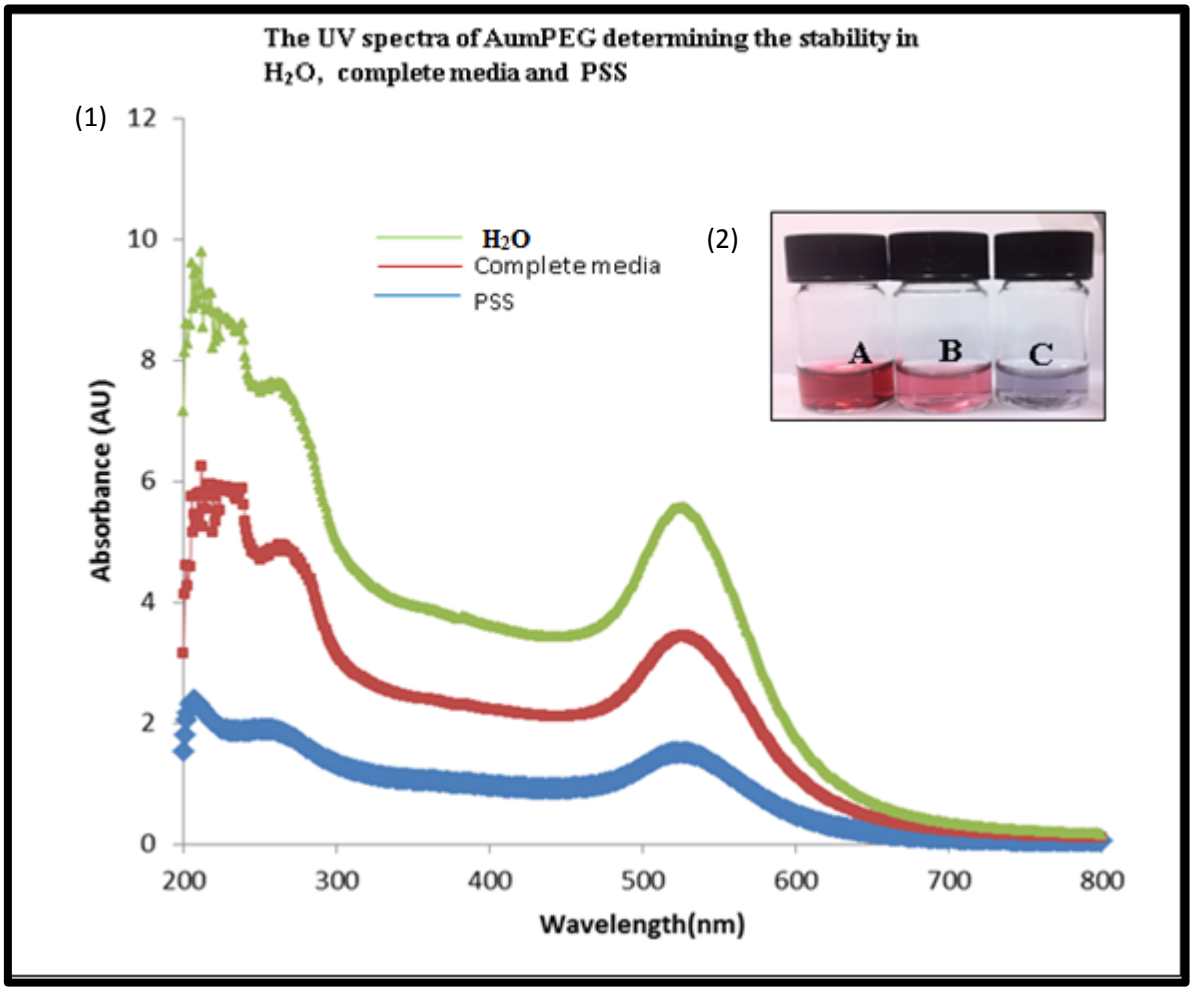

Figure 3.6: 1) Spectra of AuNPs, AuPVP, in H_2O DMEM complete medium and PSS 2) Image of gold nanoparticles in solution (A) mPEG modified in complete media, (B) PEG modified in PSS media, (C) non-modified AuNPs showing a colour change (aggregation) in physiological salt solution.

3.3.3 Quantification of the relative amount of metal in the modified and non-gold Nanoparticles

3.3.3.1 Energy-dispersive X-ray spectroscopy analysis

EDAX analysis was used to determine the elemental composition of the AuNPs sample (Figure 3.7). The EDAX instrument is attached to an SEM that is not able to visualise the small AuNPs due to magnification limits. The result confirms presence of elemental gold within the sample, hence confirms reliability of AuNPs synthesised. The element Au defines gold, Na and Cl from the stabiliser sodium chloride and the Al observation peak is from the aluminium stub used to place the sample on for analysis.

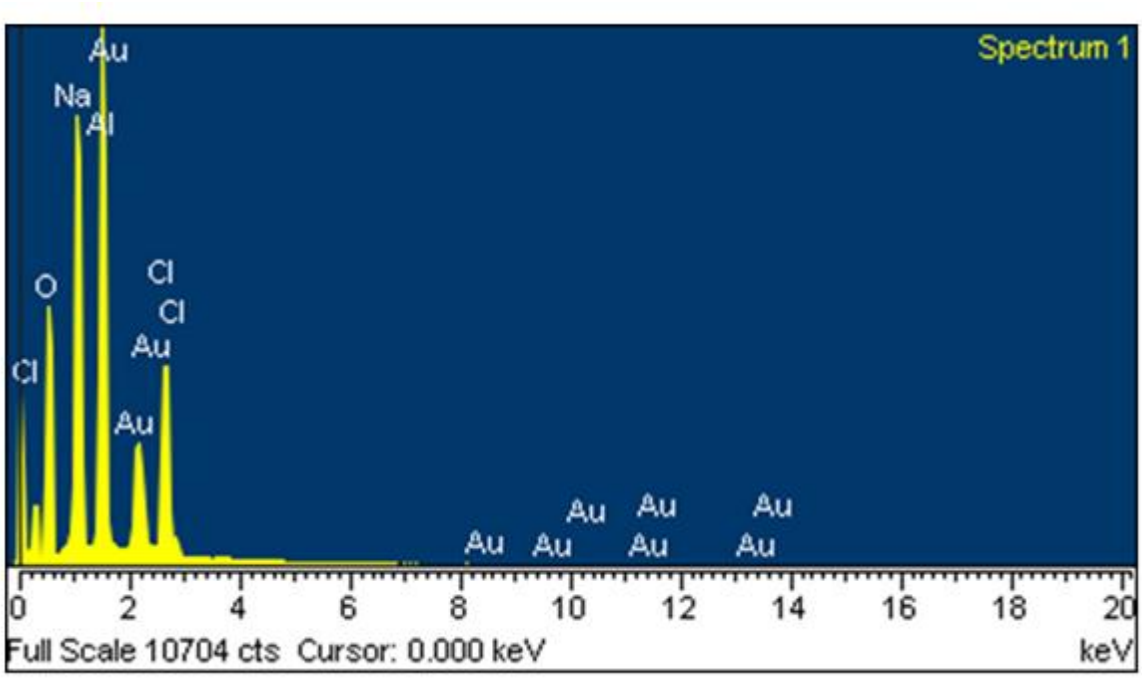

Figure 3.7: Energy-dispersive X-ray spectra of AuNPs

3.3.3.2 Inductively-coupled plasma mass spectrometry

The ICP indicated that the relative amount of gold contained within a 300 µL AuNPs sample was 48.46 ppm, while 600 µL AuNPs sample contained 88.60 ppm. These results were used to quantify the actual concentration of AuNPs within the physiological solution. The actual concentration of AuNPs within the organ-bath was calculated (ppm/ mL) by considering the dilution factor. Furthermore, the uptake concentrations were expressed as percentage. The detail explanation of the vascular uptake of AuNPs is expressed in Chapter 5 Section 5.5 (Figure 3.8, *see Appendix A: Table 4*).

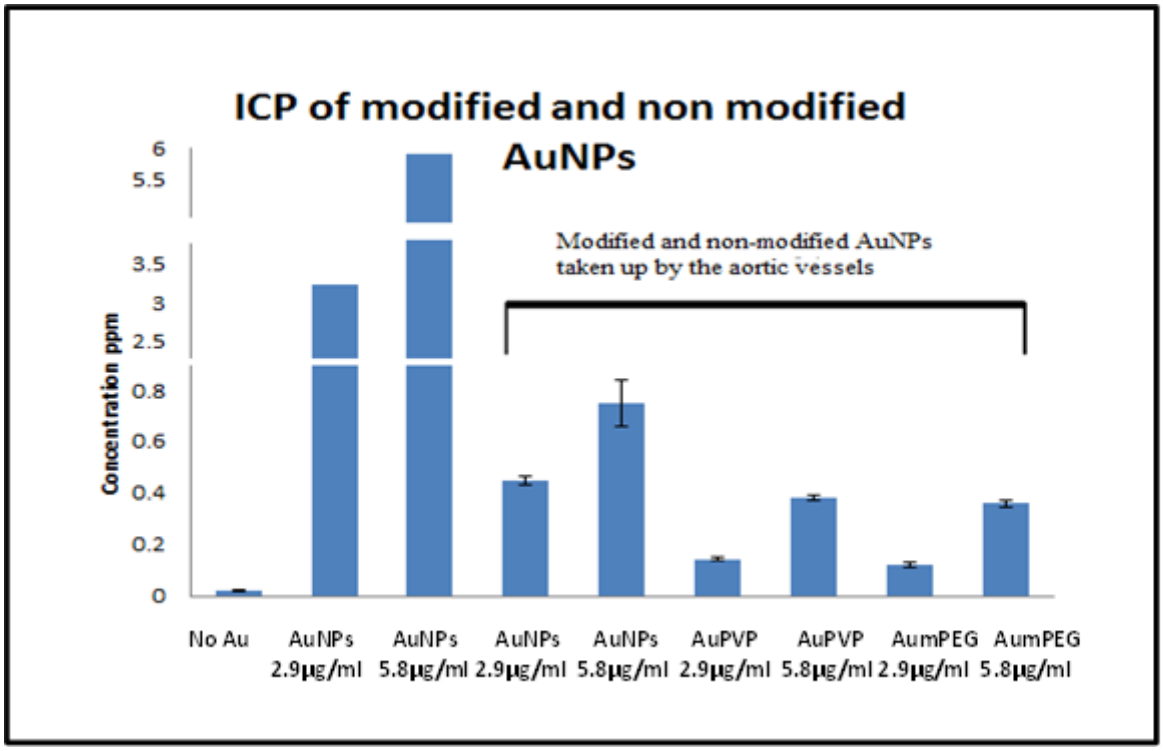

Figure 3.8: Cellular uptake of modified and non-modified gold nanoparticles (N=3) as determined by ICP-MS. Control is calculated as total PPM per mL

3.3.4 Assessments of functional groups on Gold Nanoparticles

3.3.4.1 Thermogravimetric analysis

Thermogravimetric analysis (TGA) was used to determine the presence of PVP on AuNPs by their thermal decomposition. The figure below provides the TGA for PVP modified AuNPs and PVP alone (Figure 3.9). Samples were heated at the rate of 10 °C per min from room temperature to 990°C under nitrogen flow. The initial weight loss observed is due to oligomers that have lower molecular weight, the most common is the loss of water from the moisture absorbed on the sample. Furthermore, residual solvents may be present within the sample. The second weight loss that occurred in PVP alone in the region of 200 to 430 °C is suggestive of the degradation of pure PVP polymer. In the PVP modified AuNPs sample, there was an initial weight loss of -40 % from 150 to 180°C due to water evaporation. The weight loss at approximately 280 to 460 °C and further at 460 to 560 °C may be due to the decomposition of PVP molecules that are attached on the AuNPs. One can notice a different behaviour between the PVP alone and PVP modified AuNPs. PVP alone degraded at a faster rate as compared to PVP modified AuNPs. This higher temperature for polymer decomposition suggest that gold has improved its thermal stability. The weight loss above 800 °C is due to the gold decomposition.

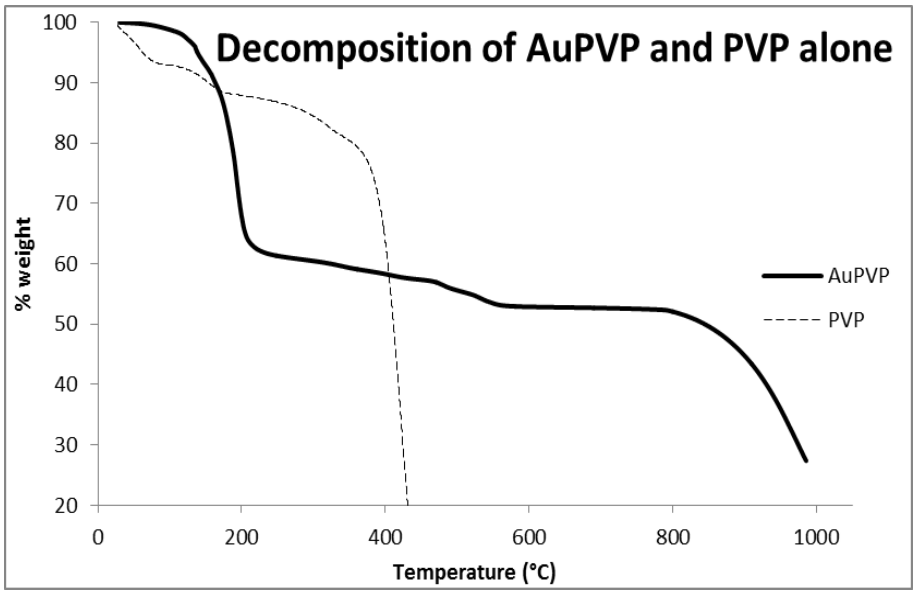

Figure 3.9: TGA analysis of PVP modified AuNPs and PVP alone. Samples were heated at 10 °C heating rate from room temperature to 1000 °C under nitrogen flow

3.3.4.2 Surface Enhanced Raman Spectroscopy

The spectra (Figure 3.10) show the vibration frequency (cm^{-1}) of the functional groups on AuNPs. It identifies the peaks of the groups present within the AuPVP and Au mPEG, and the types of bonds present.This shows that the AuNPs are functionalised, as the wavelength of the functional groups are identified and demonstrated to be present.The results indicate the shifting of C=O peak from 1521 cm^{-1} in the citrate stabilized Au NPs to 1649 cm^{-1}, which is attributed to the hydrogen bonding between the mPEG and the citrate ligands. The peak was shifted to 1609 cm-1 after the surface was stablised with PVP.

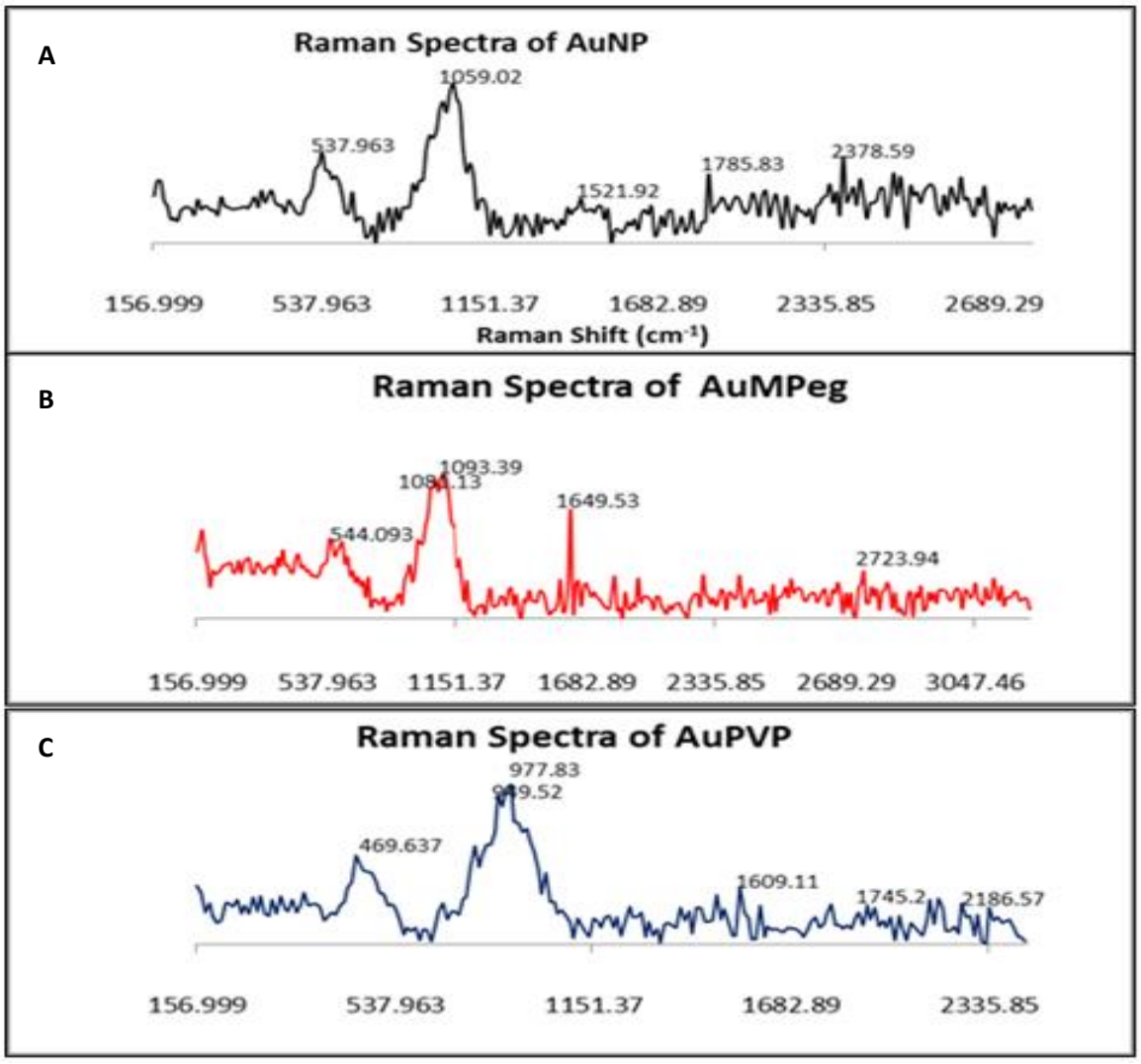

Figure 3.10: The SERs spectra showing the vibration frequency (cm^{-1}) of the functional groups on (A) AuNPs, (B) AumPEG and (C) AuPVP

3.3.4.3 Diffuse reflectance infra-red Fourier transform spectroscopy analysis of the functional groups within the gold nanoparticles.

DRIFTS analysis was carried out to determine the successful attachment of the polymer stabilisers PVP and mPEG on the AuNPs. This analysis is crucial to determine the functional groups present on the modified AuNPs. Appendix A: Figure 12 shows the DRIFTS spectra of (i) PVP (ii) PVP modified AuNPs (iii) mPEG and (iv) mPEG modified AuNPs. These signatures may be recognized as C=O (1660 cm^{-1}) and C\N (1200 cm^{-1}) in PVP, mPEG are recognised by the thiol groups (-SH). The spectrum (*see Appendix A&B: Figure 12*) illustrates the functionalization of citrate reduced gold NPs with PVP in the form of shift of C=O stretching from 1650 cm^{-1} to 1641 cm^{-1}. This may be attributed to the formation of intermolecular hydrogen bonding. Interestingly, analysing the AuNPs complex a distinct absorption bands at 3342.47, 2109.78 and 1634.55cm^{-1} were observed. The C=O peak from 1637 cm-1 is due to the citrate stabilized AuNPs. This stretch indicates the presence of sodium citrate (see table below). The evidence of PVP and mPEG functionalised on AuNPs is also supported by SERs (Section3.44.2) and UV–vis spectroscopy (section 3.3.2).

Table 3.2 : the peaks representing the groups contained within the modified and non-modified AuNPs . PVP and PVP modified AuNPs show similar peaks and mPEG and AumPEG represent similar peaks.

PVP		**AuPVP**		**mPEG**		**AumPEG**		**AuNPs**	
Wavelength (cm^{-1})	**Bond**	**Wavelength (cm^{-1})**	**Bond**	**Wavelength (cm^{-1})**	**Bond**	**Wavelength (cm^{-1})**	**Bond**	**Wavelength (cm^{-1})**	**Bond**
1650	C=O	1600	C=O	2882	-SH	2924	CH_2	3342	O-H
2950	CH_2	2924	CH_2	2860	CH_2	1100-1600	C-O/C-C	1634	C=O
3409	N-H	3370	O-H	1100-1466	C-O/ C-C	3370	O-H	2109	CH_2
1200-1433	C-N/C-C	1200-14720	C-N/C-C	-	-	1641.1	C=O	-	-

Chapter 4:
Influence of Modified and Non-modified Gold Nanoparticles on Cellular function

4. Influence of modified and non-modified gold nanoparticles on cellular function

4.1 Influence of Gold Nanoparticles on Cell proliferation

In order to optimize and examine the effect of modified and non- modified NPs on BAEC proliferation, the cell growth was reduced by exposing the cells to serum-poor medium (SPM). The cell number was determined using an automated Coulter counter (Beckman-Coulter).

In the absence of NPs, there was no significant change in cell proliferation after 48 hrs incubation, as compared with the control (untreated condition) obtained after 24hrs. The addition of unmodified AuNPs (2.92 µg/mL) to SPM, decreased the cell proliferation after both 24hrs and 48hrs significantly ($p<0.001$ and $p=0.01$, respectively). When the BAECs were exposed to PVP modified AuNPs (2.920 µg/mL) after 24hrs and 48 hrs, a significant inhibition was observed ($p<0.01$ and $p<0.001$, respectively (N=3)(Figure4.1).

Similarly, there was a significant inhibition in cell proliferation when BAEC were exposed to PVP ($2.04x10^{-7}$ g/ml)($p<0.01$), PEG (4µg/mL)($p=0.01$), mPEG (7.4X10-8g/ml)($p<0.001$) and AumPEG (2.920 µg/mL), ($p<0.001$) after 24hrs (Fig 5.1). There was a significant decrease in cell proliferation after 48 hrs cell treatment with AuPVP ($p<0.001$), PVP ($p<0.01$), PEG ($p<0.05$), mPEG ($p<0.01$) and AumPEG ($p<0.001$), when compared to the untreated cells after 48 hrs (*See Appendix B: Table 1*).

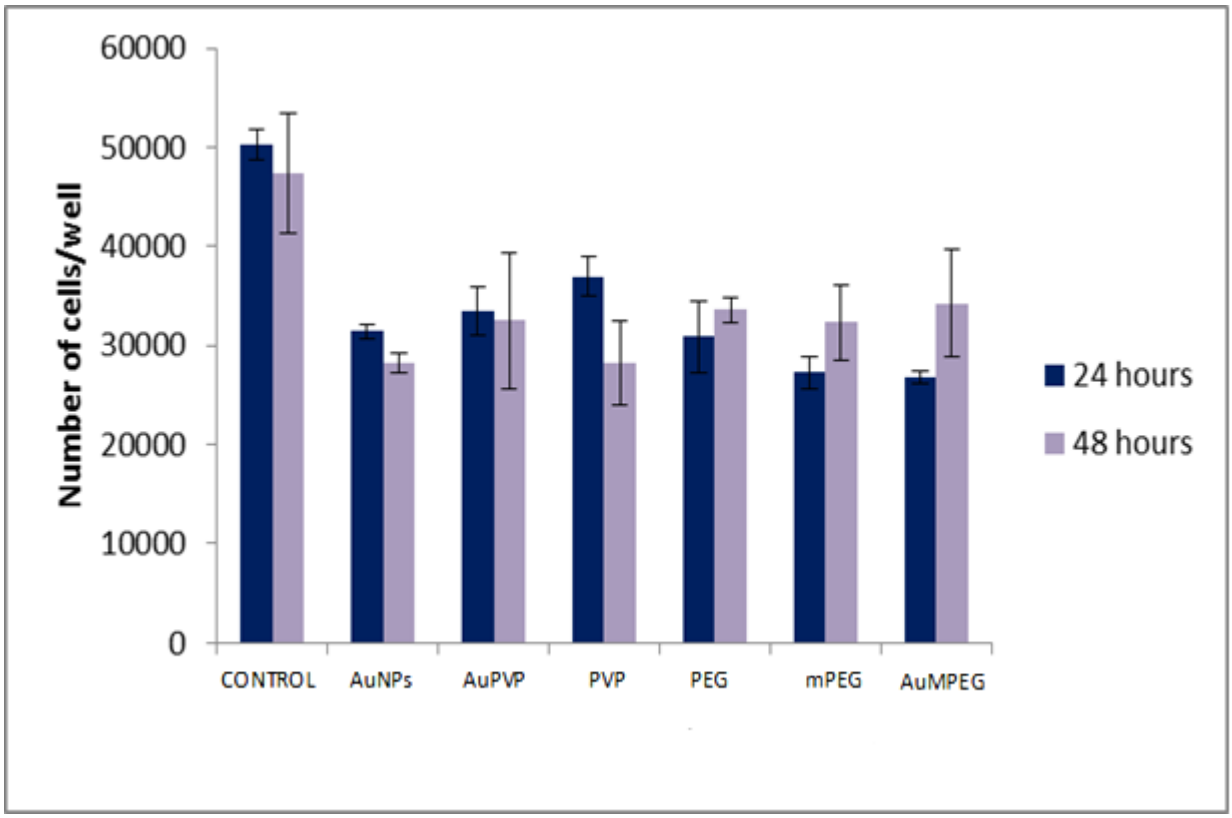

Figure 4.1: The cell proliferation after exposure to modified and non-modified AuNPs and their stabilisers after 24 hours and 48 hours incubation The results are presented as the mean ± SD. Differences at *p<0.05,**p<0.01 and ***p<0.001 are considered statistically significant.

4.2 Determining the Cell viability after incubation with modified and non-modified gold nanoparticles

Determination of the cell viability was based on 2 methods: Trypan blue exclusion method using Haemocytometer (a) and Automated cell counter (b) and propidium iodide (PI) (1 µL of the 100 µg/mL) staining using the FACs flow cytometer.

Cell viability, expressed in percentage, indicates the number of living cells (unstained cells) out of the total cell number (living and dead cells). The addition of modified and non-modifed AuNPs to SPM for 24 hrs did not significantly change cell viability, except PVP and AumPEG which decreased viability by 20% and 10% respsectively, compared with the control. At the end of 48 hrs. cell treatment, AuPVP and PEG decreased viability by 20% and 25% when compared to control (Figure 4. 2A, *see Appendix B:Table 2*).

4.2.1 Determination of Cell viability using the Haemocytometer

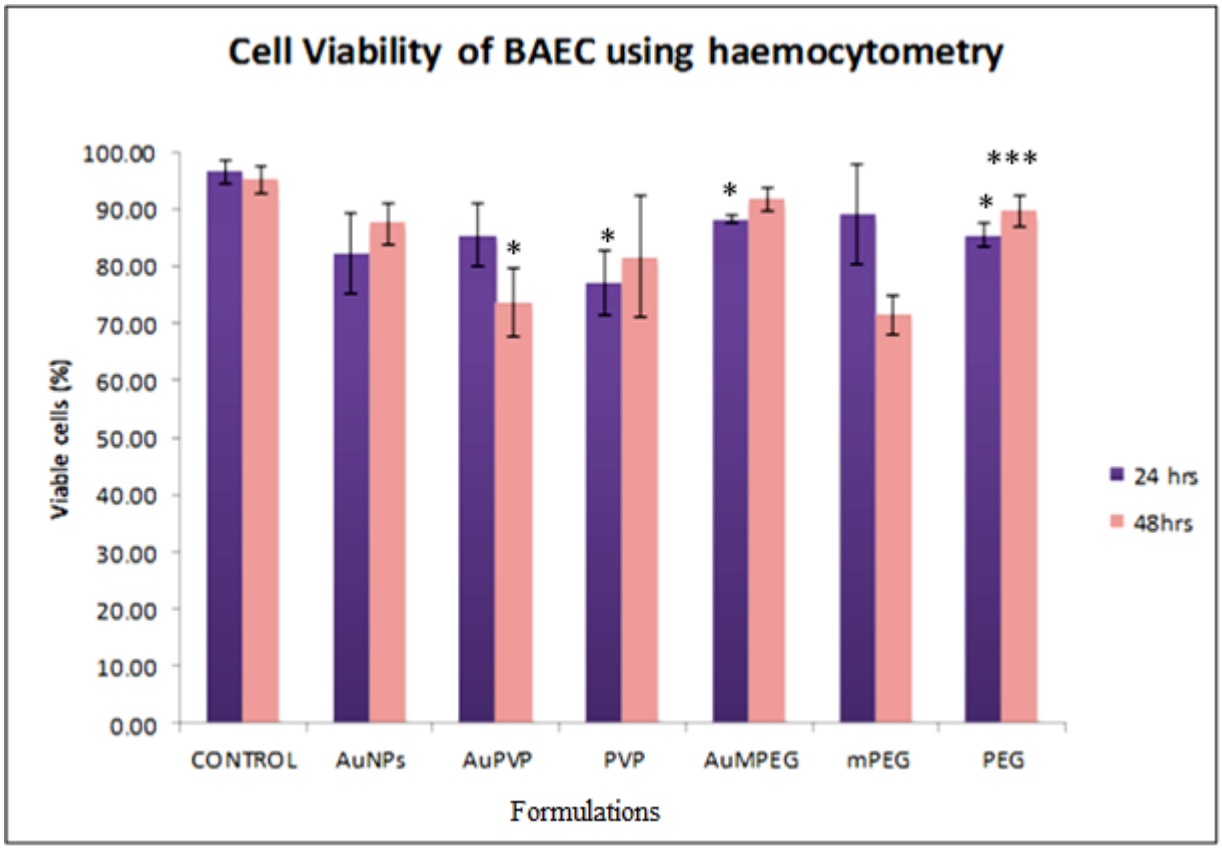

Figure 4.2A: The viability of cells after exposure to modified and non-modified AuNPs and their stabilisers at 24 hours and 48 hours incubation using haemocytometer. The results are presented as the mean ± SD. Differences at *p<0.05, **p<0.01 and ***p<0.001 are considered statistically significant.

4.2.2 Determination of Cell viability using the Automated Cell Counter

In the absence of NPs, no change in cell viability was observed after 48 hrs incubation in SPM, compared with the control (obtained after 24 hrs incubation). Among modified and non-modified NPs, the addition of AuPVP to SPM for 24 hrs significantly decreased cell viability by 15%, compared with the control. At the end of 48 hrs of cell treatment, AuPVP and PEG significantly decreased viability by 40% and 25%, compared with the control, respectively(Figure 4.2B, *see Appendix B:Table 3*).

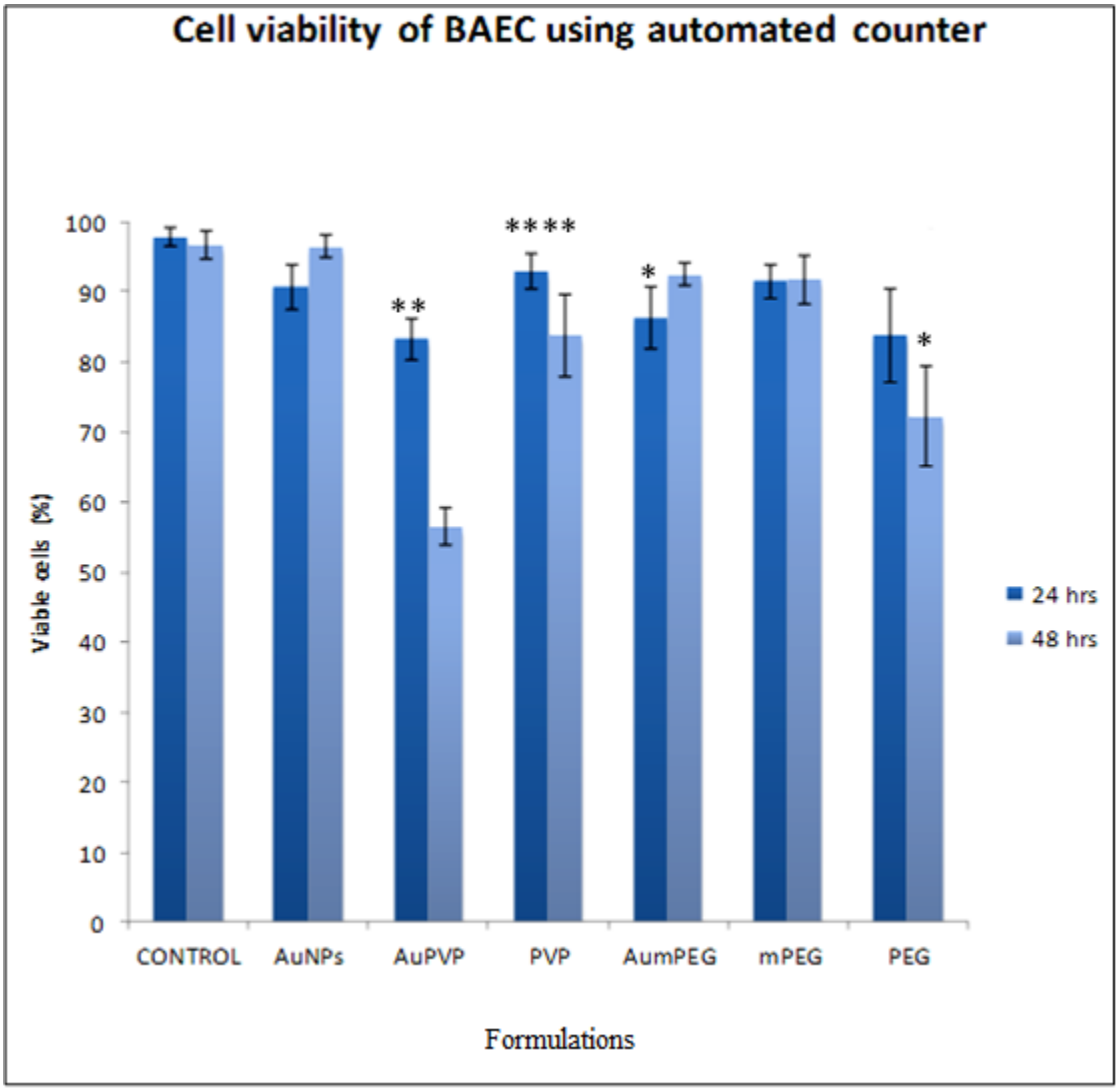

Figure 4. 2B: The viability of cells after exposure to modified and non-modified AuNPs and their stabilisers after 24 hours and 48 hours incubation using automated counter. The results are presented as the mean ± SD. Differences at *p<0.05,**p<0.01and ***p<0.001 are considered statistically significant.

4.2.3 Determination of Cell viability using Fluorescence-activated cell sorting (FACS) flow cytometer

We determined the viability of the BAEC by Fluorescence-activated cell sorting (FACS) after cell treatment with modified and non-modified NPs along with their stabilisers for 30 min, 2 hrs, 24 hrs and 48 hrs In the absence of NPs, short (30 min and 2 hrs) and long (24 hrs and 48 hrs) time exposure did not have a significant effect on cell viability, compared to control (untreated cells). The addition of non-modified and modified NPs to SPM for 24 hrs significantly decreased cell viability by about 20%, compared to the control (untreated cells after 30 min incubation and 24 hrs incubation). In addition, at the end of 48 hrs treatment, the addition of NPs did not change cell viability, except AuPVP which induced 14% and 13% decrease in cell viability, as compared to both controls (Untreated cells after 30 min and 24 hrs incubation)(Figure 4.2C, *see Appendix B: Table 4*).

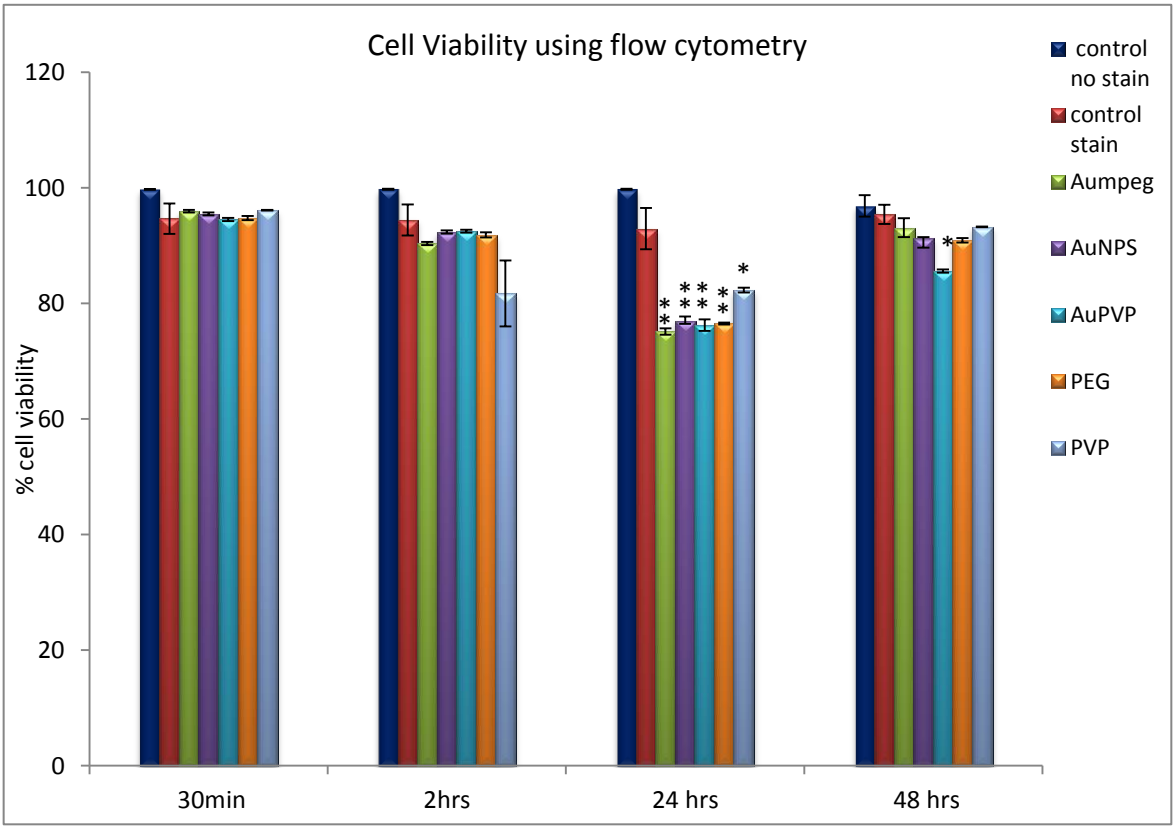

Figure 4.2C: The viability of cells after exposure to modified and non-modified AuNPs and their stabilisers at 24 hours and 48 hours incubation using FACs flow cytometer. The results are presented as the mean ± SD. Differences at *p<0.05,**p<0.01 andP<0.0001 are considered statistically significant.***

4.3 Determination of Apoptosis and necrosis

The apoptotic and necrotic status of BAEC was determined by flow cytometric analysis through fluorescein Annexin V-FITC and PI double staining. Untreated cells were established as a negative control and staurosporine, a protein kinase inhibitor, was used as a positive control for induction of apoptosis. The four quadrants plot were analysed as follows: cells in the lower left quadrant (Annexin-negative/PI-negative) indicate relative amount of living cells (Figure 4.3a and Figure 4.4a). Cells in the lower right quadrant (Annexin-positive/PI- negative) indicate early apoptotic cells and the cells in the upper right quadrant (Annexin-positive/PI-positive) indicate late apoptotic and necrotic cells (Figure 4.3b & Figure 4.4b Figure 4.4c). The cell treatment with staurosporine after 2 hours induced early apoptosis by 59.30% of BAEC population and necrosis by 39.68% (Figure 4.4c), as compared to the negative control (defined by 3% early apoptotic cells and by 15.90% necrotic cells (Figure 4.3a).

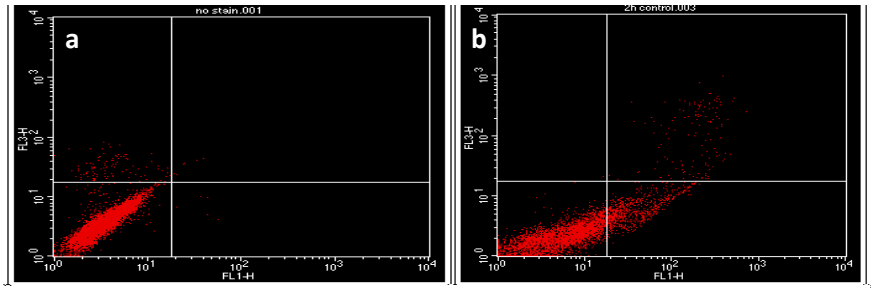

Figure 4.3: Flow analysis of non-induced BAEC cells after incubation with cell media (negative control) stained with a) Annexin-negative/PI-negative and b) Annexin-positive/PI-positive

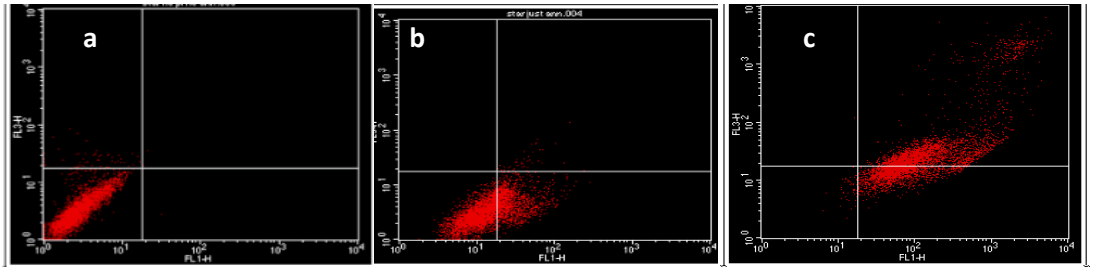

Figure 4.4: Flow analysis of Staurosporine (1µg/ml) (Positive control) induced BAEC cells and stained with a) Annexin-negative/PI-negative, b) Annexin-positive/PI-negative and c) Annexin- positive /PI-positive

4.3.1 Induction of BAEC apoptosis and necrosis after incubation with modified and non-modified AuNPs and their stabilizers

The flow cytometer determined the viability, apoptosis and necrosis of BAEC after 2 hrs and 24 hrs cell treatment with different NPs. In this experiment the non-treated cells were established as a negative control, at both 2 hrs and 24 hrs incubation. The four –quadrant plots are output data obtained from the flow cytometer analysis software (Figure 4.5).

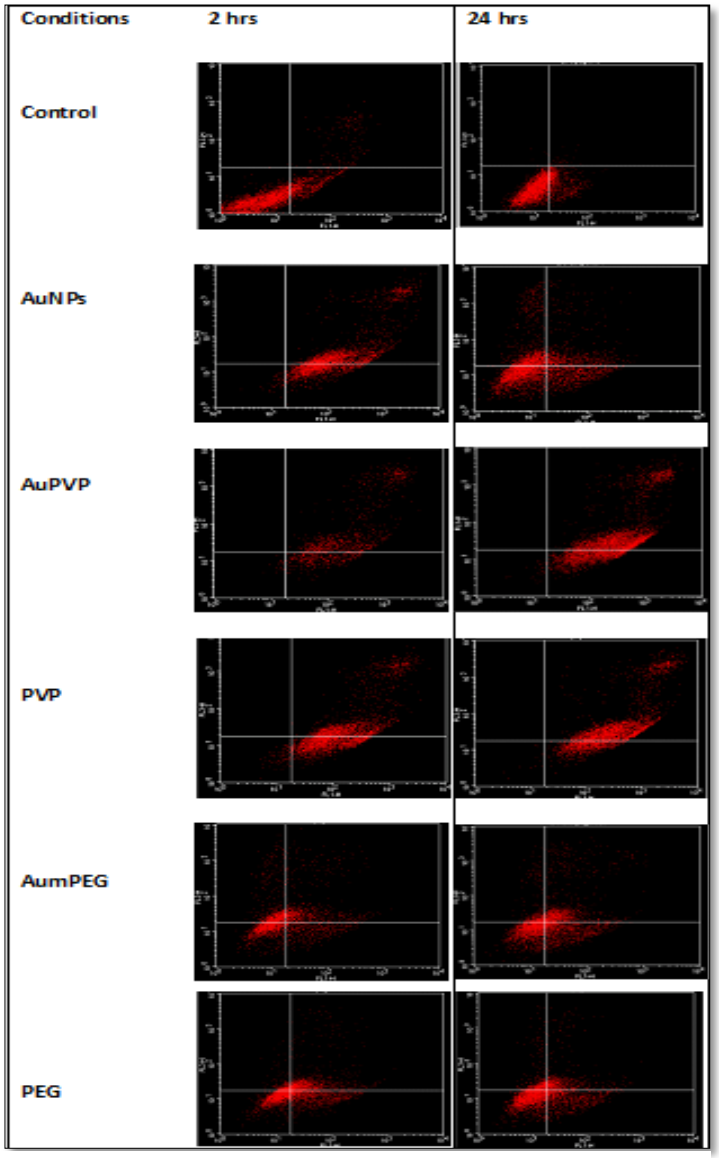

Figure 4.5: Flow analysis of untreated (control) and treated BAEC cells with modified and non-modified and their stabilizers at 2 hrs and 24 hrs. The cells are stained with Annexin- positive /PI-positive

4.3.2 Apoptotic Cells

The percentage of apoptotic cells was measured 2 hrs and 24 hrs after NP incubation, (N=3). The results show that there is a significant difference in the percentage of apoptic cells between the untreated and treated cells with all formulations. However, AuNPs, PVP and mPEG treatment led to greater percentage of apoptotic cells (41.17± 15.82($p<0.01$), 41.62±6.06 ($P<0.001$) and 35.05±7.9% ($p<0.001$) respectively, after 2 hrs incubation. Interestingly, a significant difference in percentage of apoptosis after incubation in modified and non modified AuNPs and their stabilisers was observed when compared to 24 hrs control. Furthermore, AuPVP had a greater increase in percentage number of apoptotic cells (37.47±14.14% ($p<0.001$) (Figure 5.6). There was a reduction in the % number of apoptotic cells after 24 hrs incubation with non-modified AuNPs when compared with 2 hrs incubation but this was not significant (p=NS). Moreover, no overall significant difference in the degree of apoptosis was observed between 2 hrs and 24 hrs incubation (Figure 4.6).

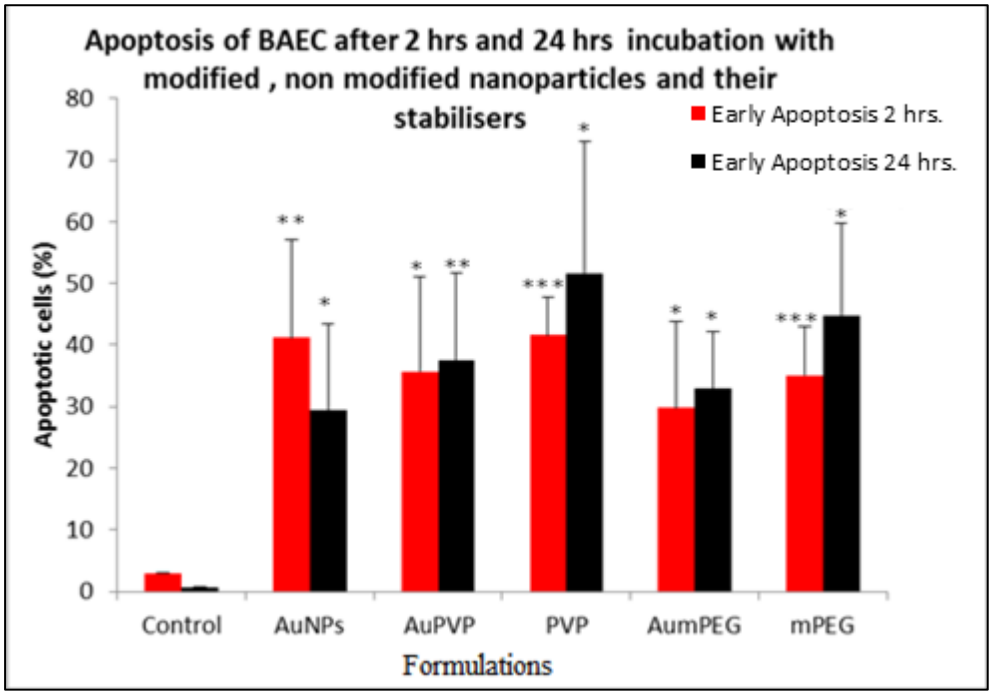

Figure 4.6: Effect of modified, non-modified and their stabilizers on the progressive of apoptosis of BAEC after 2 hrs. and 24 hrs. The results are presented as the mean ± SD. Differences at *p<0.05, **p<0.01 and ***p<0.001 are considered statistically significant.

4.3.3 Necrotic Cells

From the four –quadrant plots (Figure 5.3) the percentage of necrotic cells was determined 2 hrs and 24 hrs after cell treatment. There was a difference in terms of percentage of necrotic cells between the untreated and treated cells with AuNPs, AuPVP and AumPEG at either 2 hrs or 24hrs incubation but this was not significant. However, the exposure of the cells to PVP for 2 hrs resulted in an increase in necrotic cells by 3.0-fold ($p<0.01$), while PVP pro-necrotic effect was reduced at the end of 24 hrs incubation, when compared to the PVP treated cells after 2hrs incubation ($p<0.05$). At the end of 24 hrs of cell treatment AuPVP, PVP and mPEG significantly increased necrotic cells by 28.35±2.97% ($p<0.05$), 23.81±1.42 % ($p<0.05$) and 35.33±3.79% ($p=0.01$) respectively, compared with the control after 24 hrs (Figure 4.7).

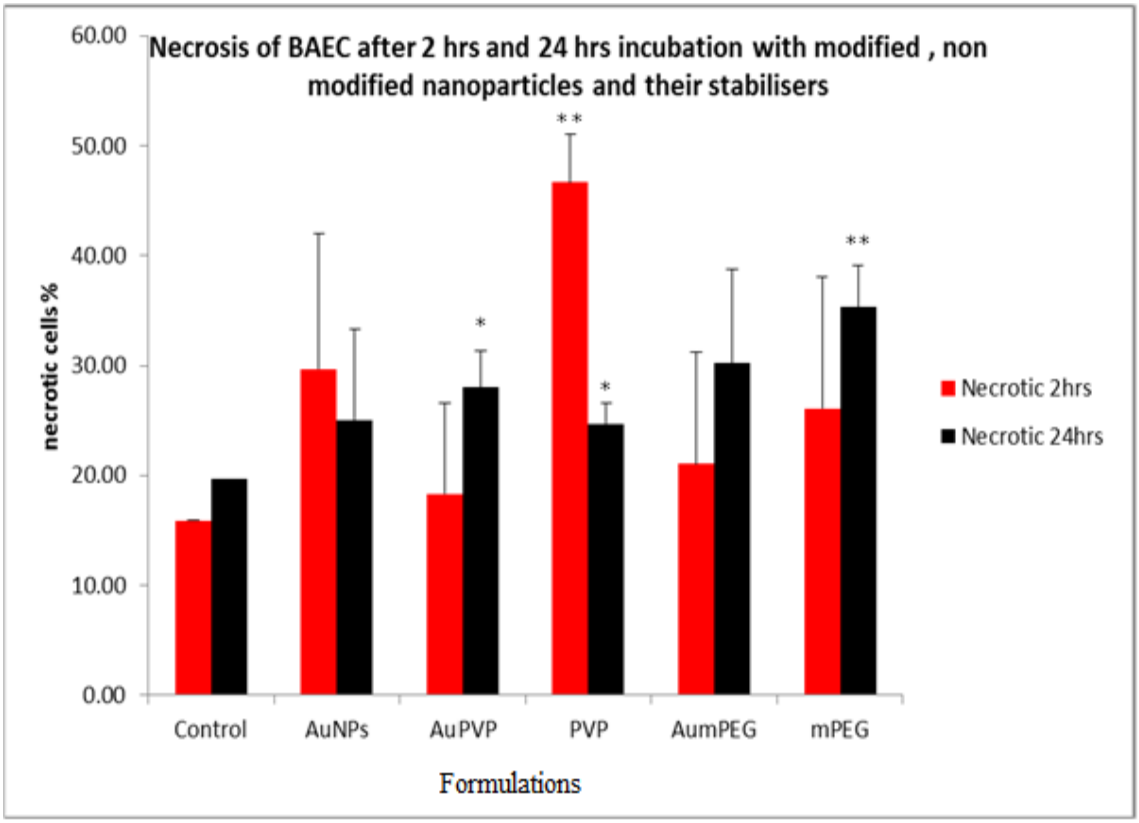

Figure 4.7: Effect of modified, non-modified and their stabilizers on the progressive of necrosis of BAEC after 2 hrs and 24 hrs. The results are presented as the mean ± SD. Differences at *p<0.05 and **p<0.01 are considered statistically significant.

4.4 Influence of Nanoparticles on Cell morphology

BAEC morphology was analysed after 24 hrs and 48 hrs cell treatment with modified and non-modified NPs. The cells treated with most of the NPs did not change the standard polygonal shape of the cells, as observed in untreated cells. However, the cells treated with PVP displayed an elongated shape after 24 hrs (Figure 4.8A) and 48 hrs incubation (Figure 4.8B).

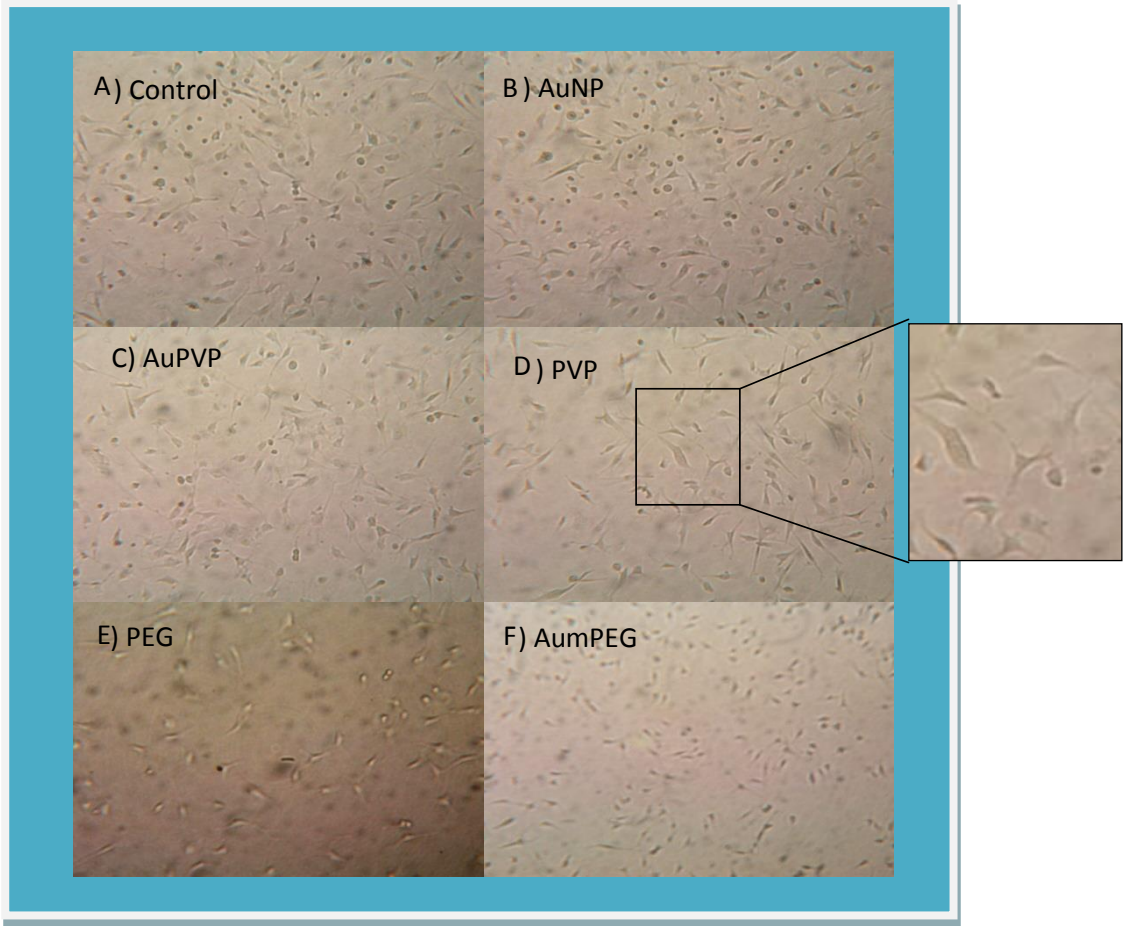

Figure 4.8A: Photomicrograph representing modified and non-modified AuNPs and their stabilisers on BAEC morphology after 24 hours exposure, where: (A) control cells, (B) 2.920 µg/mL AuNPs, (C) 2.920 µg/mL AuPVP, (D) PVP ($5.9X10^{-13}$M), (E) PEG and (F) AumPEG (100x magnification). PVP, but not PEG, caused elongation of the cells (inset).

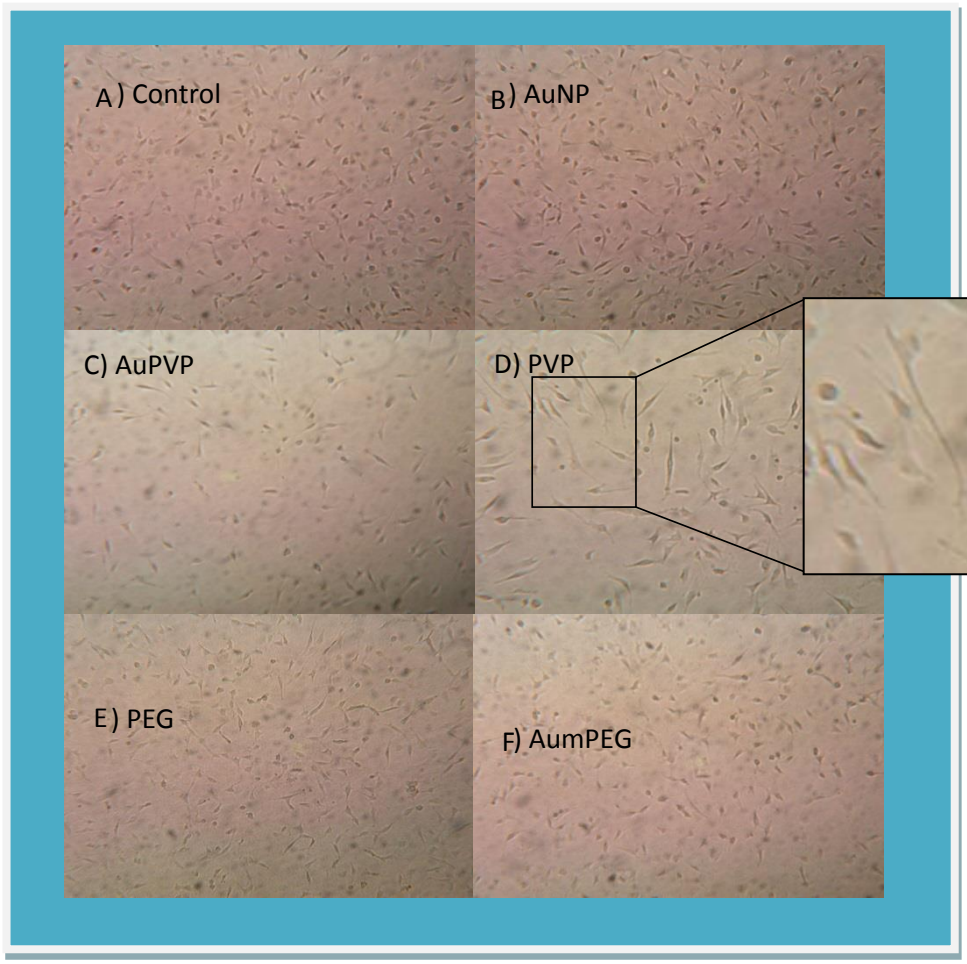

Figure 4.8B: Photomicrograph representing modified and non-modified AuNPs on BAEC cell morphology after 48 hours exposure, where: (A) control cells, (B) 2.920 µg/mL AuNPs, (C) 2.920 µg/mL AuPVP, (D) PVP ($5.9X10^{-13}M$) E) PEG and (F) AumPEG (100x magnification). PVP, but not PEG, caused elongation of the cells (inset).

4.5 Visualisation of AuNPs using Fluorescence microscopy

AuNPs were examined using fluorescence microscopy (13nm) (Figure 5.9A) to determine whether the AuNPs can be observed under the fluorescence microscope, as this will provide the next step in identifying the AuNPs which are taken up by BAEC cells. Also 50nm AuNPs were also examined for comparison (Figure 4.9B). The image below indicates that 13nm gold nanoparticles were difficult to visualise under a fluorescence microscope due to the small size. The few bright spots are due to NP aggregation in PSS. The larger sizes gave a higher intensity than the smaller size NPs.

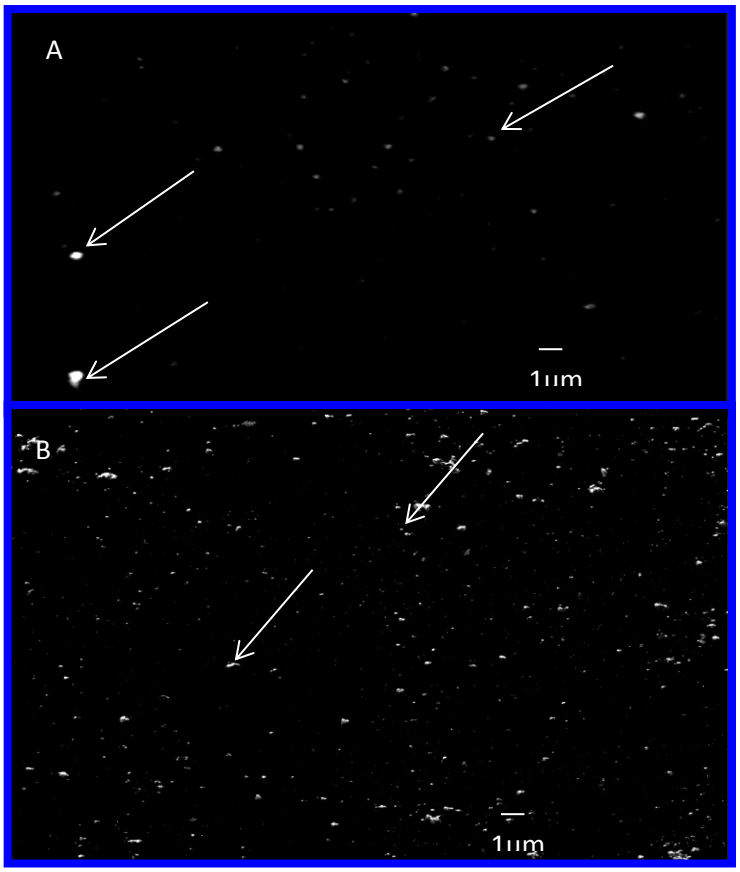

Figure 4.9: Fluorescent imaging of AuNPs prepared in PSS (2.9 µg/ml) for A) 13nm and B) 50nm AuNPs, visualised under a fluorescence microscope (AuNPs are represented by arrows). NPs were invisible due to their flurescence (as bright spots) although size measurements were not possible. In A) Only a few bright spots were identified due to NPs aggregation, in B) many more bright spots are evident. Determination of NP size was confirmed using TEM.

4.5.1 Cellular localization of 13 nm gold nanoparticles

The cellular localization of AuNPs after uptake was investigated using fluorescence microscopy. The image below illustrates uptake after 1 hr and 18hrs incubation. There was a greater number of NP uptake of non-modified AuNPs after 18 hours incubation as compared to the modified AuPVP. Overall, it was difficult to visualise the uptake of 13nm AuNP due to their small sizes. Therefore the localisation of larger non modified AuNPs were investigated for comparison (Figure 4.10).

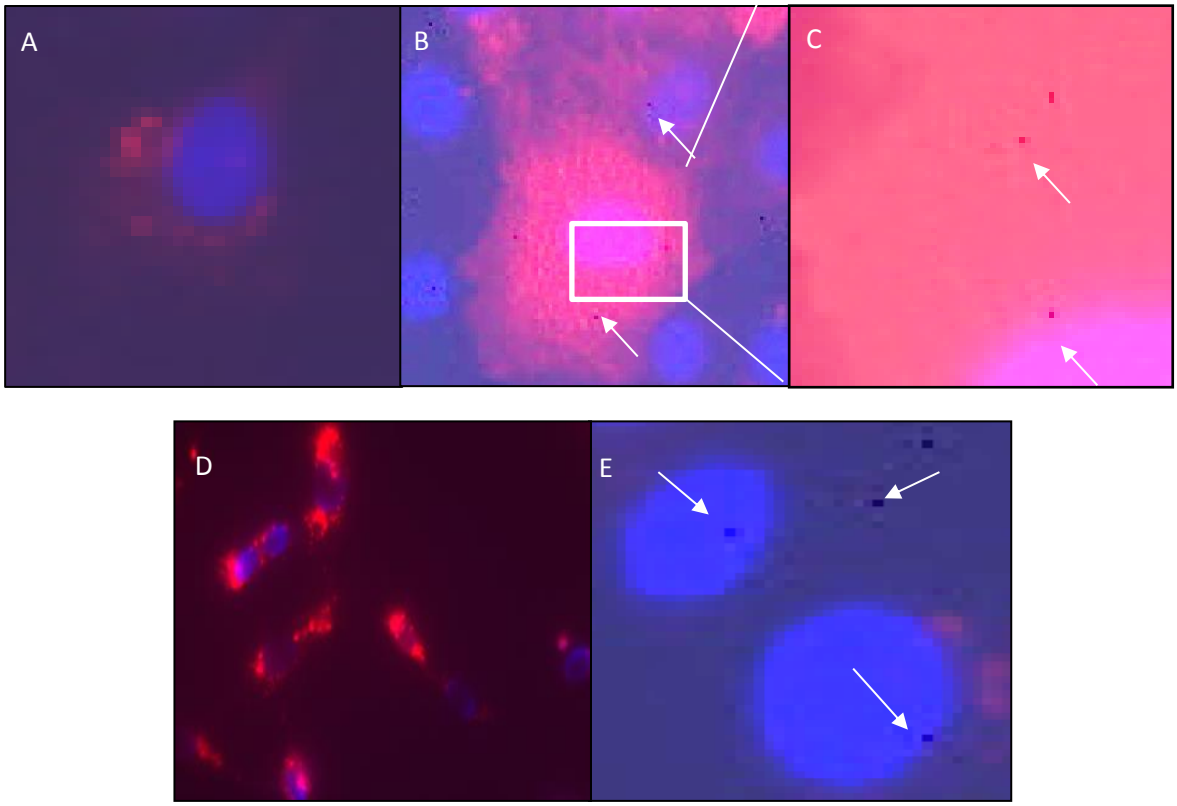

Figure 4.10: Images of BAECs under the fluorescence microscope, after a 1 hour (A-C) and 18 hour (D and E) stimulation with 13 nm AuNPs. Cells were counterstained using DAPI (4', 6-diamidino-2-phenylindole) to identify the nuclei (blue) and the cell membrane fluorescent dye PKH26 (red stain). (A and D) CONTROL; B, C, and E) black spots evident within the nuclear and membrane regions, respectively, suggestive of AuNP uptake (arrows).

4.5.2 Cellular localization of 50 nm AuNPs particles

Localization of 50nm AuNPs could be observed more easily by fluorescent microscopy compared to AuNPs sized 13nm, after 18 hrs. of incubation. The 50 nm AuNPs (Figure 4.11 C) were taken up by the cells and mostly accumulated in the membrane compared to cells treated with small sized 13 nm AuNPs. In addition, using fluorescence microscopy we can also observe that timing also influences uptake of the NPs. We found that after 18hrs, the NPs were particles localised inside the cells, whereas at 30 min and 1 hr, the particles remained outside the nucleus.

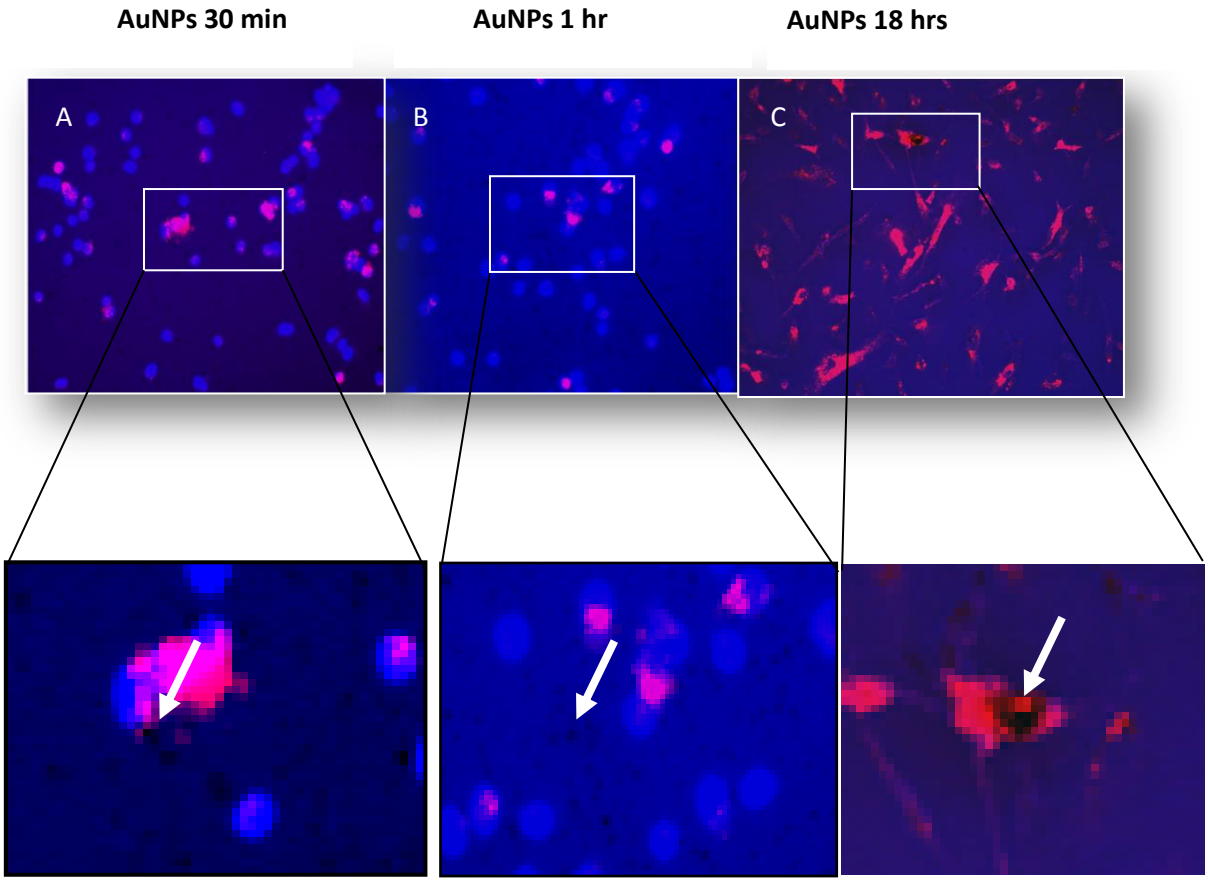

Figure 4.11: Image demonstrates BAEC uptake of 50nm AuNPs after stimulation at (A) 30 min stimulation (B) 1 hr and (C) 18 hrs, black spots evident within the nuclear and membrane regions, respectively, suggestive of AuNP uptake (arrows).

4.6. Determining the membrane integrity of BAECs using confocal microscopy

The influence of modified and non-modified AuNPs on cellular function and integrity of BAEC was determined at 1 time point (24 hrs). The BAECs were stained by red fluorescent dye to determine the integrity of the cell membrane as well as the nucleus. The intensity of the fluorescence illustrates that the control illuminated more than the cells loaded with the AuNPs, PVP AuPVP AumPEG mPEG and PEG. (Figure 4.12).

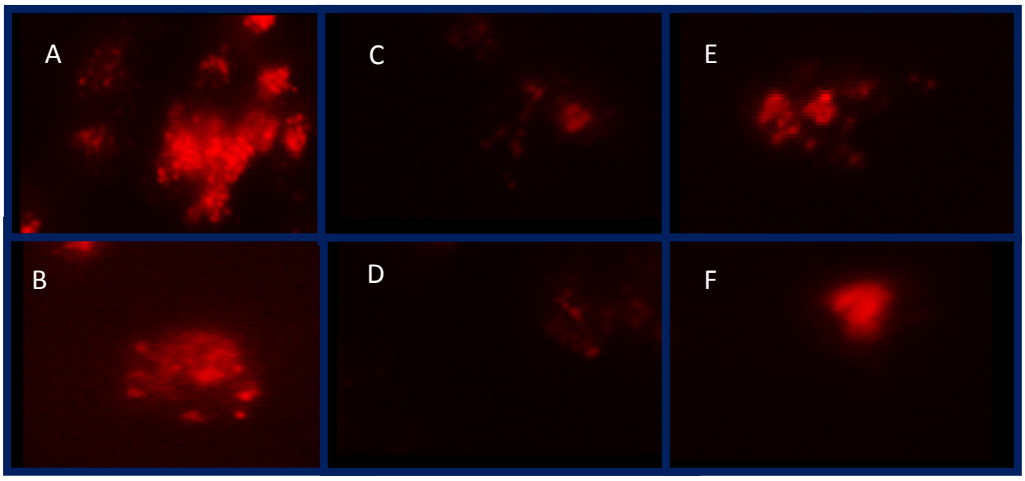

Figure 4.12: Confocal imaging of BAEC after exposure to (A) Control (no nanoparticles exposure) (B) AuNPs (C) AumPEG (D) AuPVP (E) mPEG and (F) PVP. BAEC are stained by the fluroscent dye (PHKH26) (red). Reduced fluorescence intensity is seen after incubation in PVP and mPEG modified AuNPs (C and D).

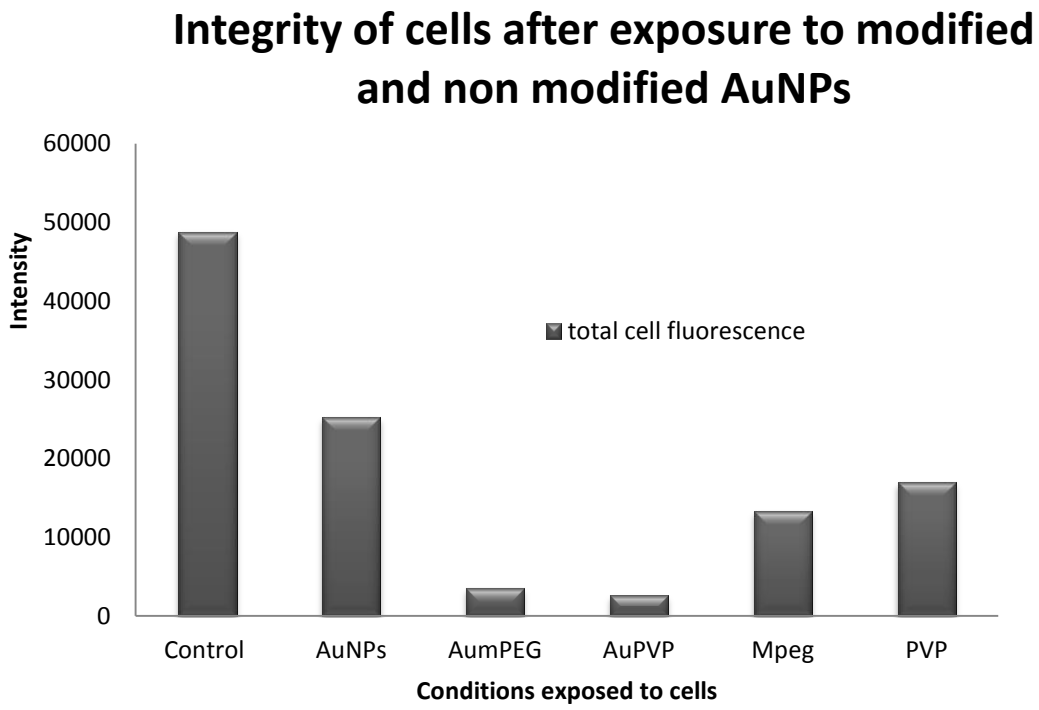

Figure 4.13: Integrity of cells after exposure to SPM (control), (A) AuNPS (B) AumPEG (C) AuPVP (D) mPEG (E) and to PVP (F)

The reduced intensity of the cell fluorescence suggests that that the uptake of NPs may have led to disruption of membrane integrity after application with AuNPs, AumPEG, AuPVP, mPEG and PVP (Figure 4.13).

4.7 Cellular uptake of Modified and non-modified NPs

Transmission electron microscopy (TEM) images clearly show uptake of both non modified and modified AuNPs by BAEC in cell culture and that uptake is influenced by surface modification (Figure 4.14). The result shows that after 30 min exposure there was an indication of AuNPs uptake by the cells (5 particles), although this was not the case for the modified particles. After 2hrs exposure there was clearly an increase of AuNPs uptake (32±5.2 particles). Interestingly, there was a greater number of AuNPs and AuPVP by the cells after 24 hrs incubation (NP number 638±156.12 and 233±91.73 respectively). However, after 48 hrs there was a reverse effect with high uptake of AuPVP (700±91.73 NPs). On the other hand, there seem to be very little uptake of AumPEG but a few particle numbers (16±3.52 NPs) after 48 hrs. Both modified and non-modified NPs were shown to be localised in endosomes, within the cytoplasm, suggestingnthat modified and non-modified NP uptake maybe through endocytosis pathways.

Table 4.1: Number of nanoparticles (AuNPs, AumPEG and AuPVP) taken up by BAEC after incubation at different times (30 min, 2hrs, 24 hrs and 48 hrs).

Incubation time	No of Nanoparticles / cell		
	AuNP	**AumPEG**	**AuPVP**
30 min	5±0	0	0
2 hours	32±5.2	0	55±9.8
24 hours	638±156.12	8±0	234±71.52
48 hours	344±48.52	16±3.52	700±91.73

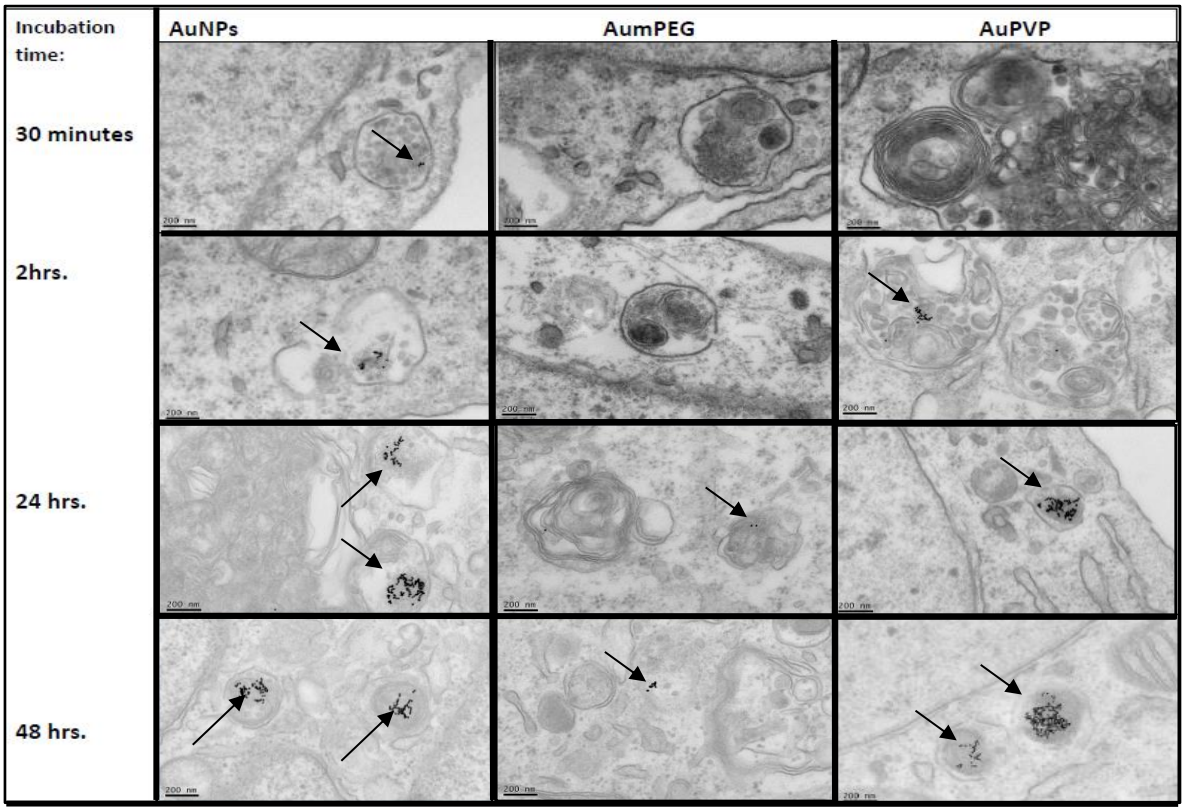

Figure 4.14: TEM images of BAEC uptake of AuNPs AumPEG and AuPVP at different incubation time (30 minutes, 2hrs, 24hrs and 48 hrs) (Arrows represents NPs).

4.8Analysis of Cellular signalling pathways

4.8.1 Influence of ACh on ERK expression

The effect of different concentrations of ACh (1, 10 and 100 µM) on p-ERK1/2 expression was assessed by Western blot analysis. When compared to control, all the ACh concentrations caused an increase in expression of ERK1/2, with 10 µM having the strongest inducer effect on phosphorylation (Figure 4.15).

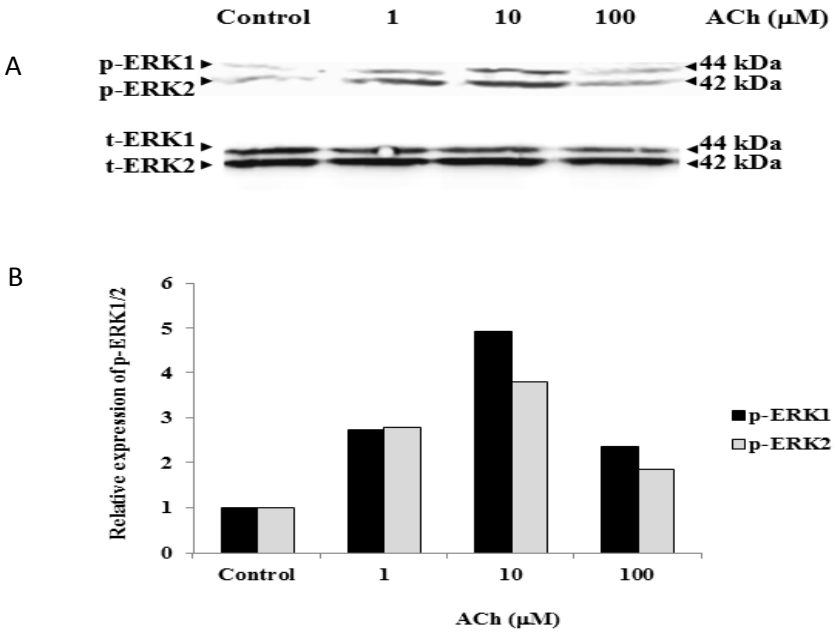

Figure 4.15: ACh activated ERK in BAEC in a concentration dependent manner. A), Western blot showing the effect of 1, 10 and 100 µM ACh on phosphorylation of ERK (p-ERK) in BAEC. Total ERK protein levels were used as a loading control (20µg of protein samples added /well). B, quantitative analysis of the blot shown in A. (ERK-1 [black bars], ERK-2[grey bars]) n=2.

4.8.2 Influence of modified and non-modified AuNPs on ACh-induced p-ERK1/2 expression

Nanomaterials influence cell proliferation and have been suggested to play a role in the phosphorylation or de-phosphorylation of certain regulatory proteins involved in vascular contraction and/or relaxation. Here we stimulated BAEC with Ach in the presence of modified and non-modified AuNPs and examined whether the AuNPs will have any effect on the ERK expression. The expression of ERK was increased after ACh stimulation, however both non- modified and modified AuNPs as well as the polymers alone caused a reduction in expression when compared to ACh control(Figure 4.16). A significant reduction in expression was observed after AuPVP, PVP and AumPEG incubation ($p < 0.05$). Furthermore, modified NPs caused less reduction of p-ERK2 expression than p-ERK1 expression, compared to non-modified NPs

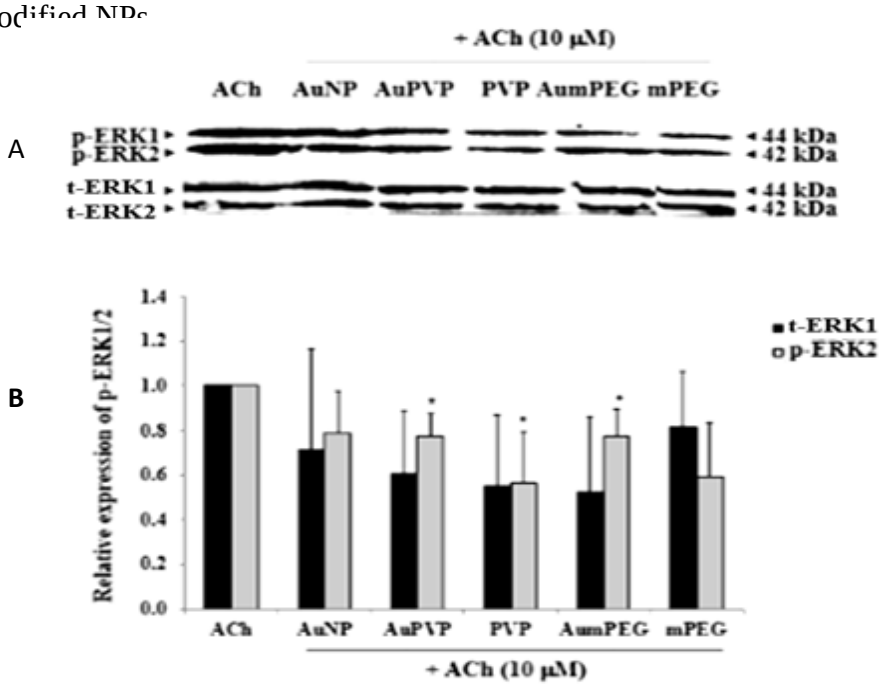

Figure 4.16: Effect of NPs on ACh-induced ERK1/2 phosphorylation in BAEC. A), Western blot showing the effect of AuNPs, AuPVP PVP AumPEG and mPEG after stimulated with 10 µM ACh on phosphorylation of ERK1/2 (p-ERK1/2) in BAEC. Total ERK1/2 protein levels were used as a loading control (20 µg of protein samples added /well). B, quantitative analysis of the blot shown in A. (p-ERK-1 [black bars], p-ERK-2[grey bars] n=3). The results are presented as the mean ± SD. Where differences at *p<0.05 is considered statistically significant.

4.8.3 Influence of ACh on Akt expression

At 10 µM of ACh concentration the p-Akt expression was increased by over 3 fold, (Figure 4.17).

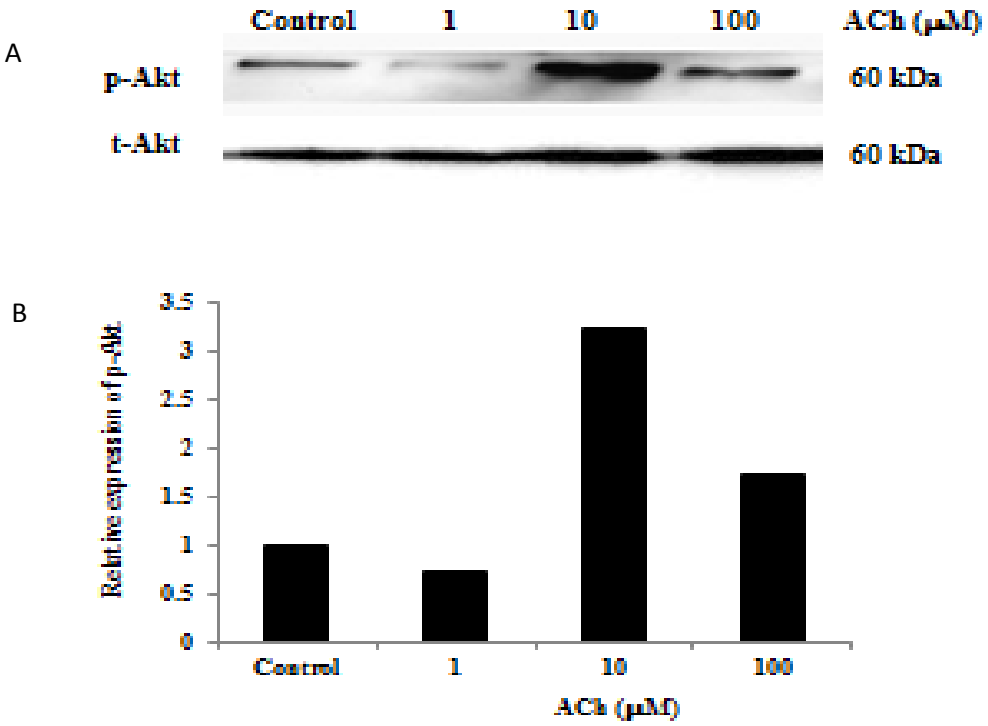

Figure 4.17: ACh activated Akt in BAEC in a concentration manner. A), Western blot showing the effect of 1, 10 and 100 µM ACh on phosphorylation of Akt (p-Akt) in BAEC. Total Akt protein levels were used as a loading control (20 µg of protein samples added /well). Experiments were performed at least twice and a representative example is shown. B, quantitative analysis of the blot shown in A. (Akt-1 [black bars]) n=2.

4.8.4 Influence of modified and non-modified AuNPs on ACh-induced p-Akt expression

The overexpression of p-Akt induced by 10 µM ACh shown in the previous section (section 4.8.3) was again observed. The addition of AuNPs did not alter the positive effect of ACh on p-Akt expression. Both PVP and mPEG modified AuNPs slightly decreased ACh-induced pAkt overexpression, compared with ACh effect alone (Figure 4.18).

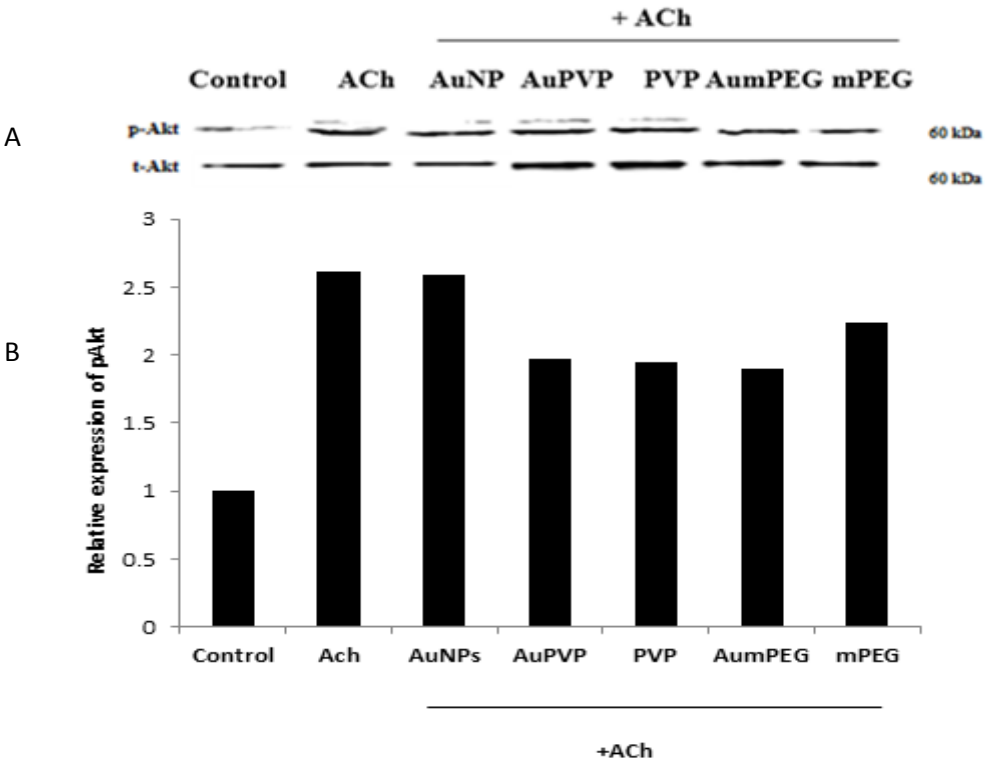

Figure 4.18: Effect of NPs on ACh induced Akt phosphorylation in BAEC. A), Western blot showing the effect of AuNPs, AuPVP, PVP AumPEG and mPEG after stimulation with 10 µM ACh on phosphorylation of Akt (p-Akt) in BAEC. Total Akt protein levels were used as a loading control (20 µg of protein samples added /well). B, quantitative analysis of the blot shown in A (Akt-1 [black bars]) n=2.

Chapter 5:
Influence of Modified and Non-modified Gold Nanoparticle on Vascular function

5. Vascular function studies

All vessels constricted to high potassium solution (KPSS). There was no overall difference in the degree of constriction, before and after AuNP incubation (modified and non- modified) or their stabilisers (Figure 5.1). Vessels that constricted by less than 1g tension, after the equilibration period, were considered non-viable and discarded.

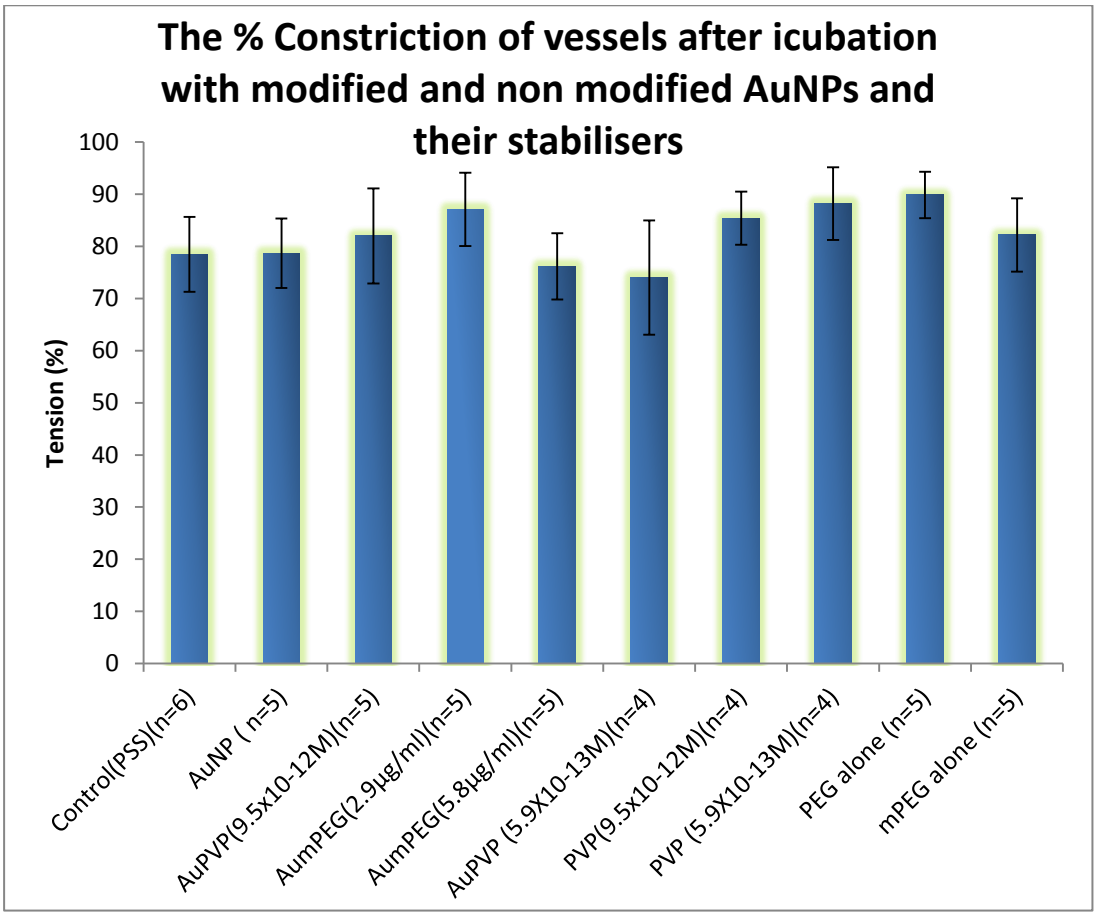

Figure 5.1: The influence of high potassium solution (KPSS) on aortic vessels before and after incubation, where 'n' is the number of vessels

5.1 Control experiments

5.1.1 Repeatability of Acetylcholine responses

To assess repeatability of the dilator responses, two ACh dose responses were carried out on the same vessel, before and after a thirty minute incubation period in PSS. This will determine whether second responses are significantly different from 1st responses and hence inform statistical analysis. The results indicate that there is a difference before and after incubation without any NPs present. A cumulative increase in ACh concentration caused an increased dilation for both 1st and 2nd responses, whereby at the 100µM maximum concentration of ACh, vessel dilation was at 80.29±9.36 % and 68.33±7.86%, before and after PSS incubation, respectively (n=6; NS) Results show some attenuation of dilator responses after incubation in PSS at 3 ACh concentrations only (0.1 µM, 1 µM and 10 µM (Figure 5.2) (*See Appendix C:Table 1*).

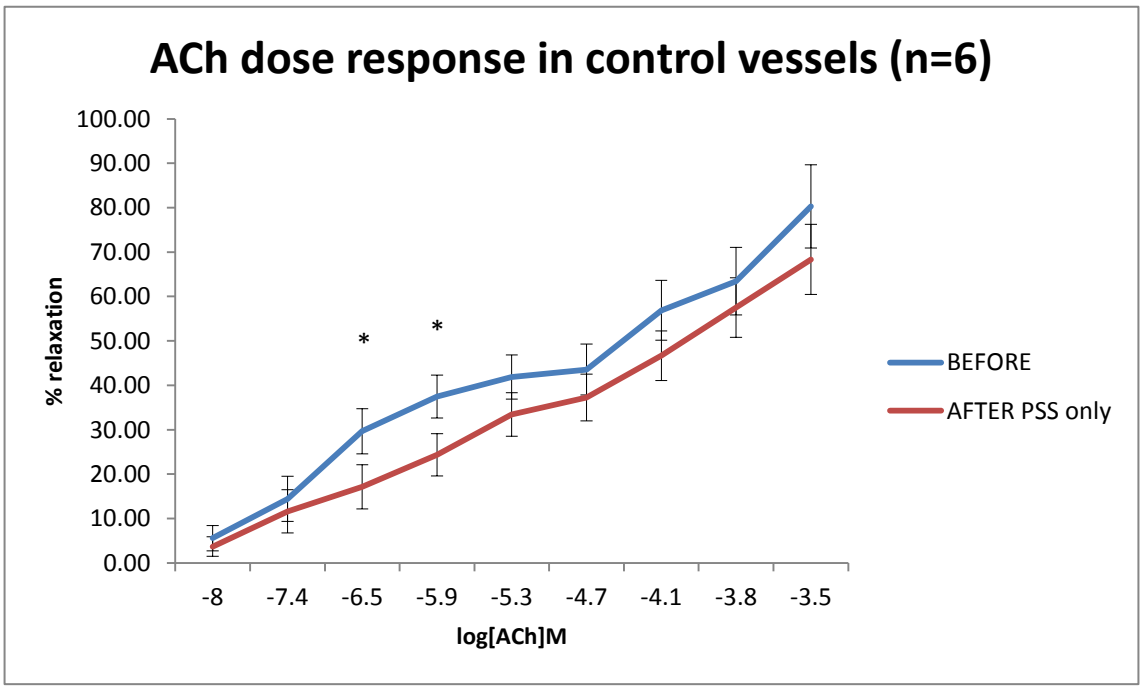

Figure 5.2: Average percentage response of vessels to ACh, before and after incubation in PSS (*P<0.05).

5.1.2 Repeatability of Sodium nitroprusside responses

The effect of the endothelial independent dilator SNP was assessed before and after a 30 minute incubation period in PSS. Results show that incubation in PSS has no overall effect on dilator responses except for 1 dose at 0.01 µM SNP concentration ($p<0.05$). At 0.1 µM SNP maximum concentration, vessel relaxation was only slightly reduced (95.26±3.80 % and 86.50±7.79 % before and after PSS incubation (n=7; NS), (Figure 5.3) *(see Appendix C:Table 2).*

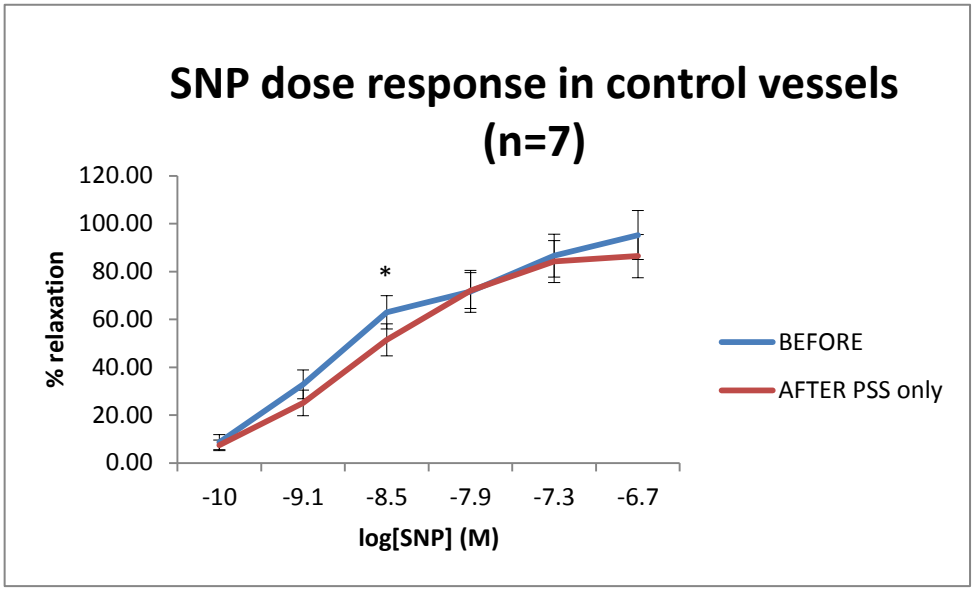

Figure 5. 3: Average percentage dilator response of vessels to SNP, before and after incubation in PSS (*p<0.05).

5.2 Effect of non-modified gold nanoparticles on dilator responses

5.2.1 ACh response after non-modified AuNP incubation

In order to investigate the effect of AuNPs on endothelium-dependent relaxation, aortic vessels were treated with a cumulative concentration of ACh ranging from 0.1-100µM, before and after incubation with AuNPs at $1.68x10^{11}$ NP/mL. The results demonstrated that incubation in AuNPs had no overall effect on dilator responses (n=5) (Figure 5.4; *see Appendix C:Table 3).*

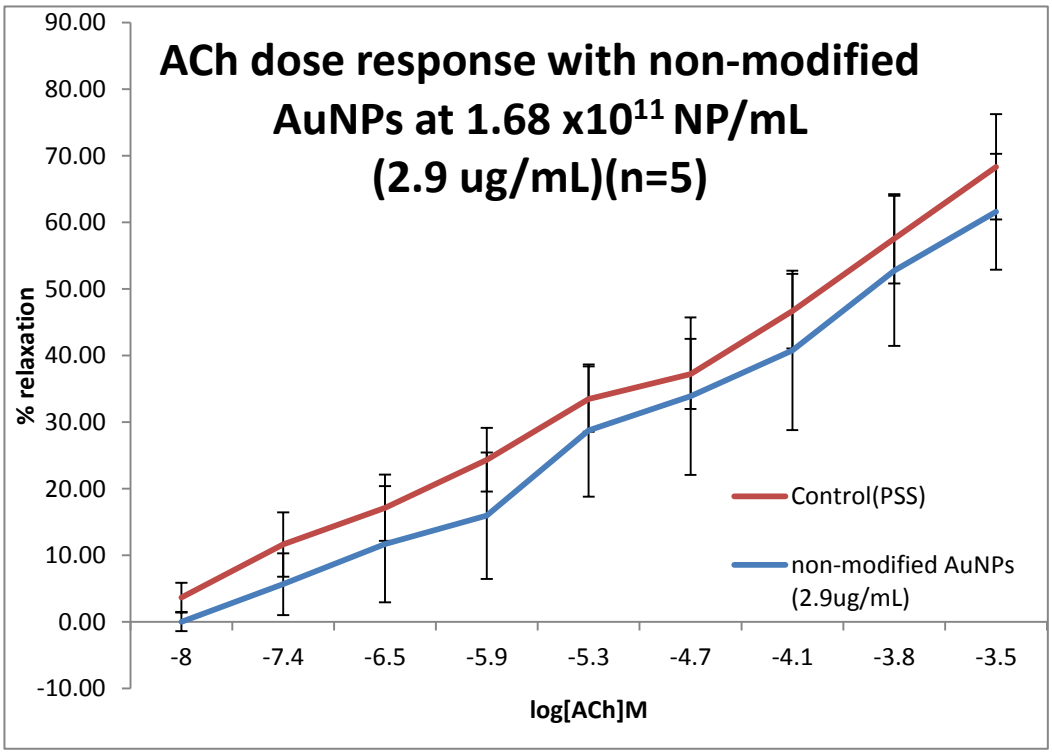

Figure 5.4: Average percentage dilator response of vessels to ACh, after incubation with non-modified AuNPs.

5.2.2 SNP response after non-modified AuNP incubation

There was a significant reduction in dilator response after incubation with AuNPs at all SNP concentrations. This indicates that NPs are inhibiting the effect of SNP (Figure 5.5), *(see Appendix C:Table 4).*

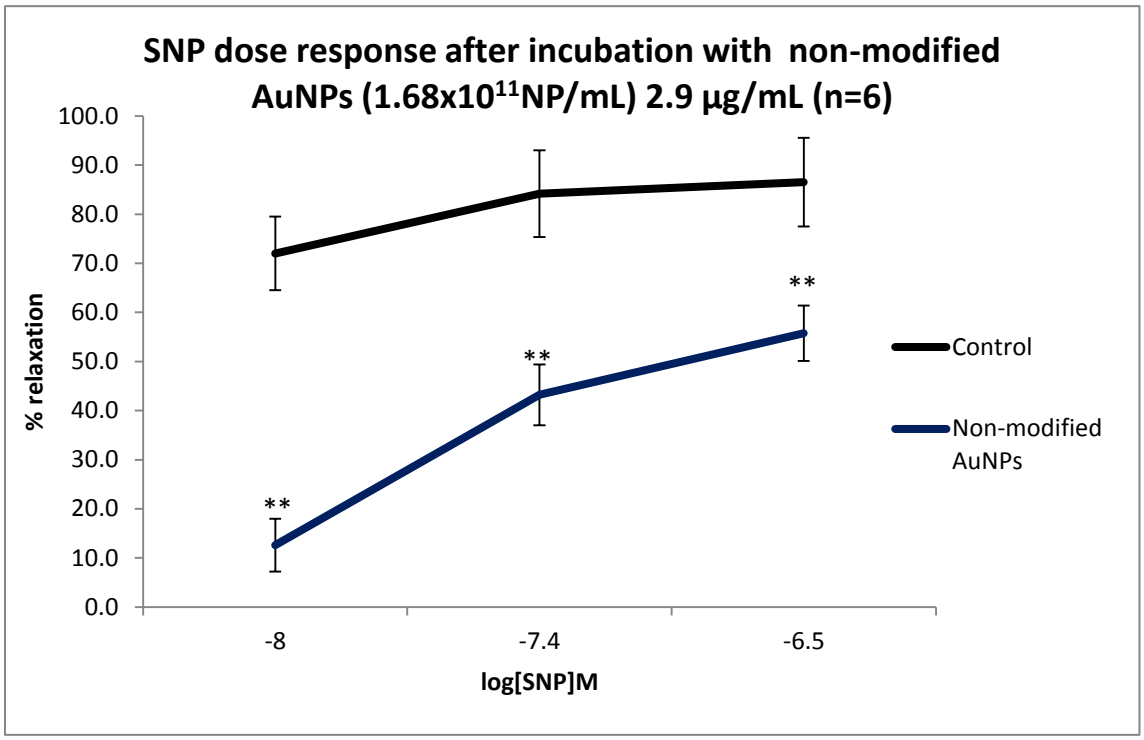

Figure 5.5: Responses of vessels to SNP after incubation with non-modified AuNPs (**P<0.01).

5.3 Effect of Polyvinilpirrolidine modified gold nanoparticles on dilator responses

5.3.1 Initial studies on the influence of Polyvinylpyrrolidone polymer on dilator function

AuNPs were initially coated with 9.5 x10^{-12} M PVP. These NPs were shown to have an effect on the dilation of the aortic vessels. When compared to control vessels, there was a significant reduction in dilator response at 3 ACh concentrations (Figure 5.6),*(see Appendix C:Table 5).*

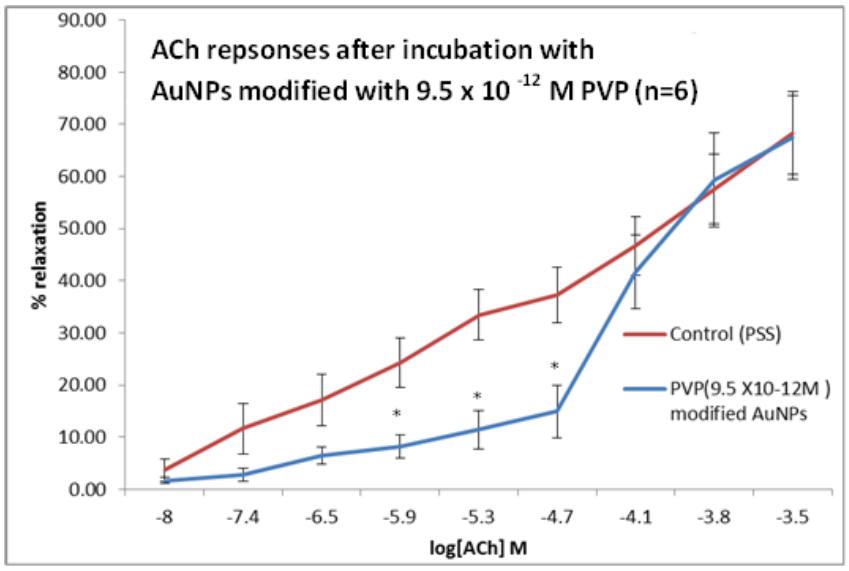

Figure 5.6: Responses of vessels to ACh after incubation with PVP modified AuNPs (*p<0.05)

SNP responses were also assessed. When compared to control SNP responses there was no significant attenuation in dilation (NS) (Figure 5.7).
(See Appendix C: Table 6).

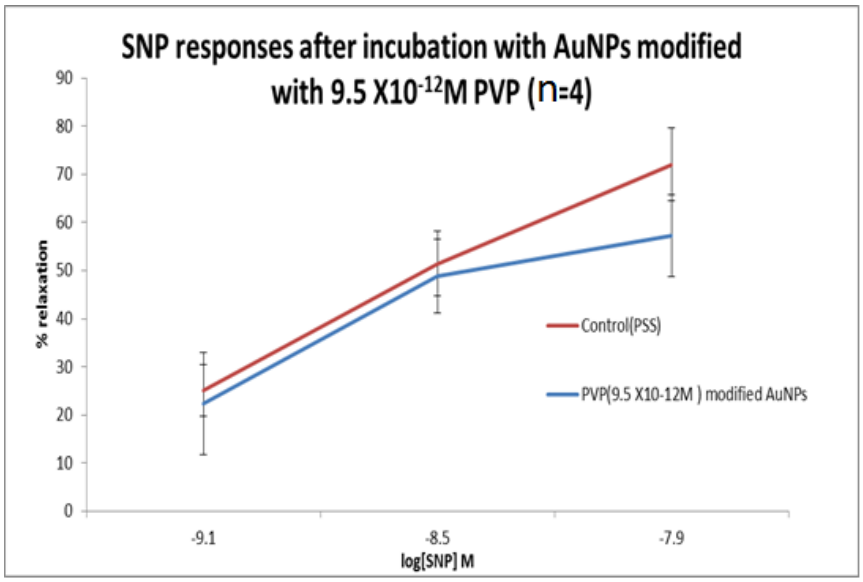

Figure 5.7: Responses of vessels to SNP after incubation with PVP modified AuNPs

5.3.2 Minimum concentration of Polyvinylpyrrolidone needed to stabilize Gold Nanoparticles

To determine the minimum concentration of PVP needed to stabilise the AuNPs, serial dilutions of PVP were used to coat AuNPs. Observation of the colour change from reddish to blueish gave an indication that the NPs had aggregated; no colour change in the solution verified that the NPs were stable. Results demonstrated that a minimum PVP concentration of $5.9x10^{-7}$µM was necessary to prevent aggregation of the AuNPs.

Once the minimum concentration required to prevent aggregation had been verified, the effect of PVP alone on vessel function was assessed to identify a concentration of PVP with minimal detrimental effects on ACh induced dilation. Vessel incubation in PVP alone, at $1.47x10^{-7}$ µM to $3.68x10^{-8}$ µM led to a significant attenuation of ACh dilator responses, while at the lowest concentration examined ($1.84X10^{-8}$µM) no overall attenuation in dilation was observed (Figure 5.8).

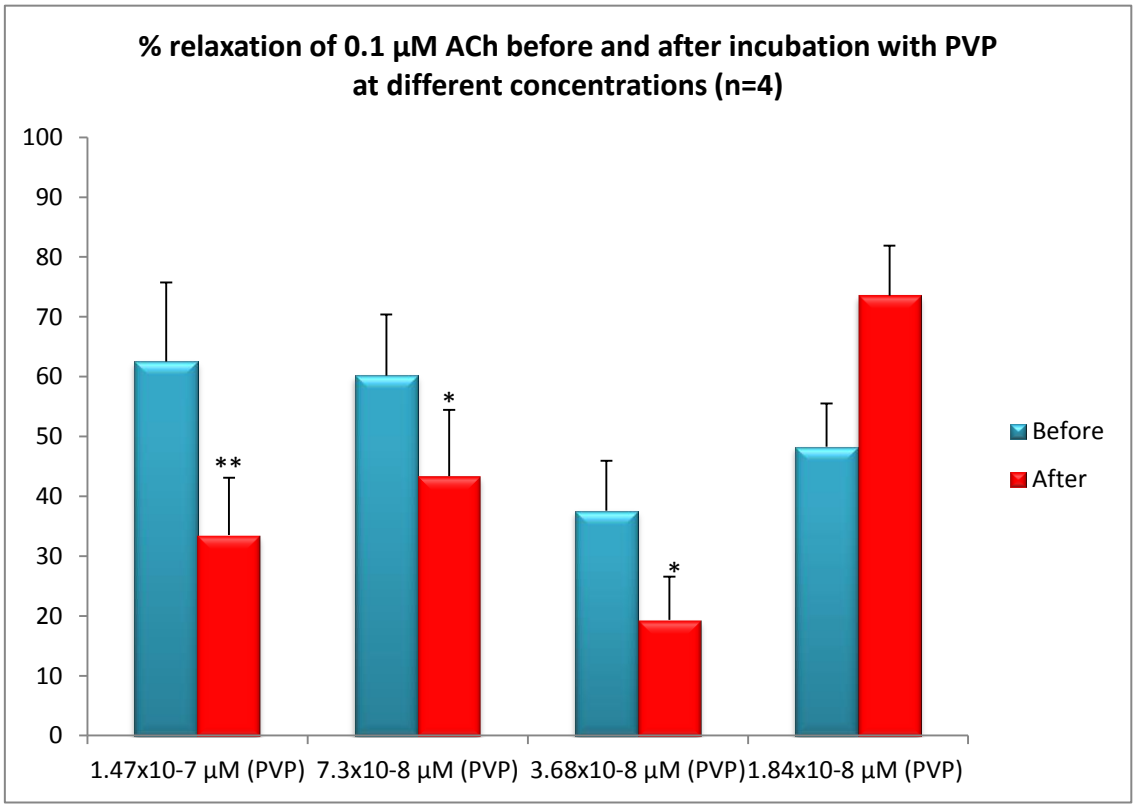

Figure 5.8: Responses to 0.1 µM ACh concentration before and after incubation in serial dilutions of PVP. Where * (p<0.05) and ** (p<0.01)

5.3.3 ACh responses

The effect of PVP alone and PVP modified AuNPs, on ACh dilator responses were compared to the control (PSS). The results show that PVP alone caused a significant reduction in ACh dilator responses at 10 to 100µM [ACh] ($p<0.05$), when compared to PSS incubation (*See Appendix C:Table 9*). PVP modified AuNPs caused a reduction in dilator response, but not significantly

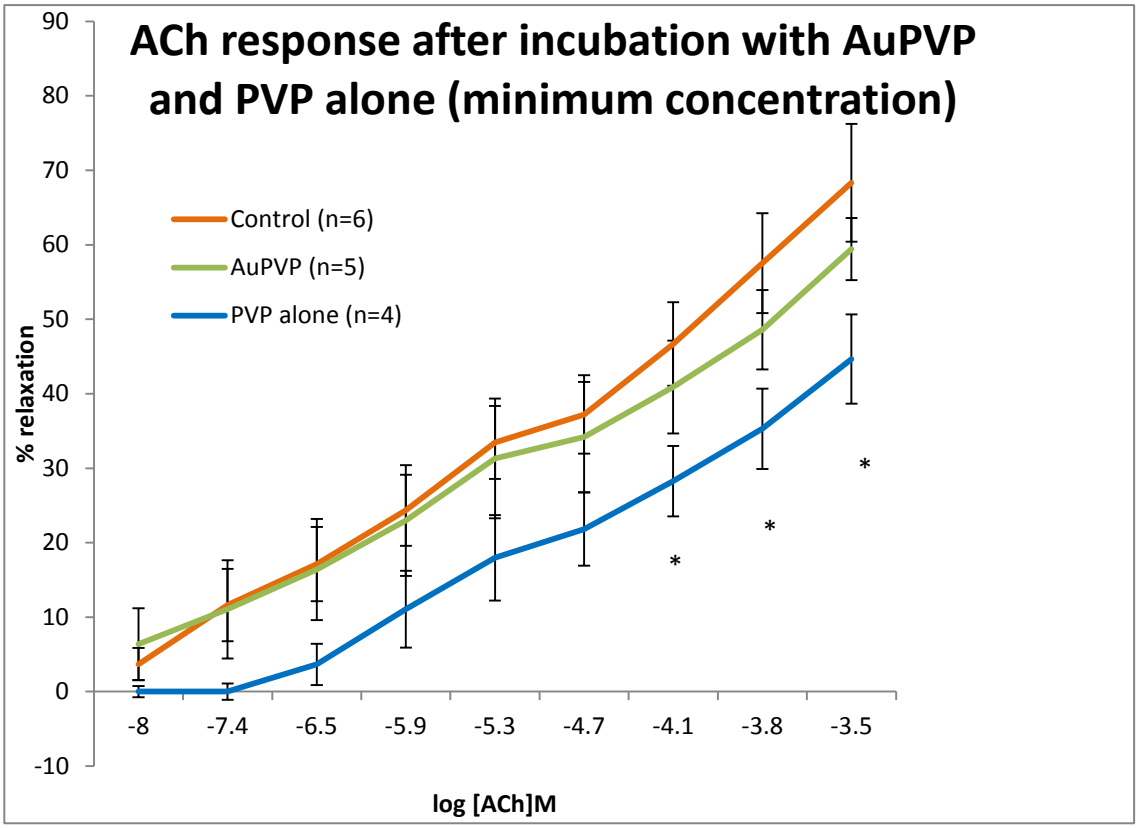

Figure 5.9: Responses of vessels to Ach after minimum concentration of PVP modified AuNPs and PVP alone(* p<0.05).

5.3.4 SNP responses

Vessel incubation in AuPVP affected SNP dilator responses (*see Appendix C: Table 9*). A significant reduction in dilator response was obtained at 0.001 µM to 0.01 µM [SNP] ($p<0.001$) with a further reduction at 0.10 µM ($P<0.01$). Incubation in PVP alone led to a small reduction in response, (NS) (Figure 5.10), (*see Appendix C: Table 10*).

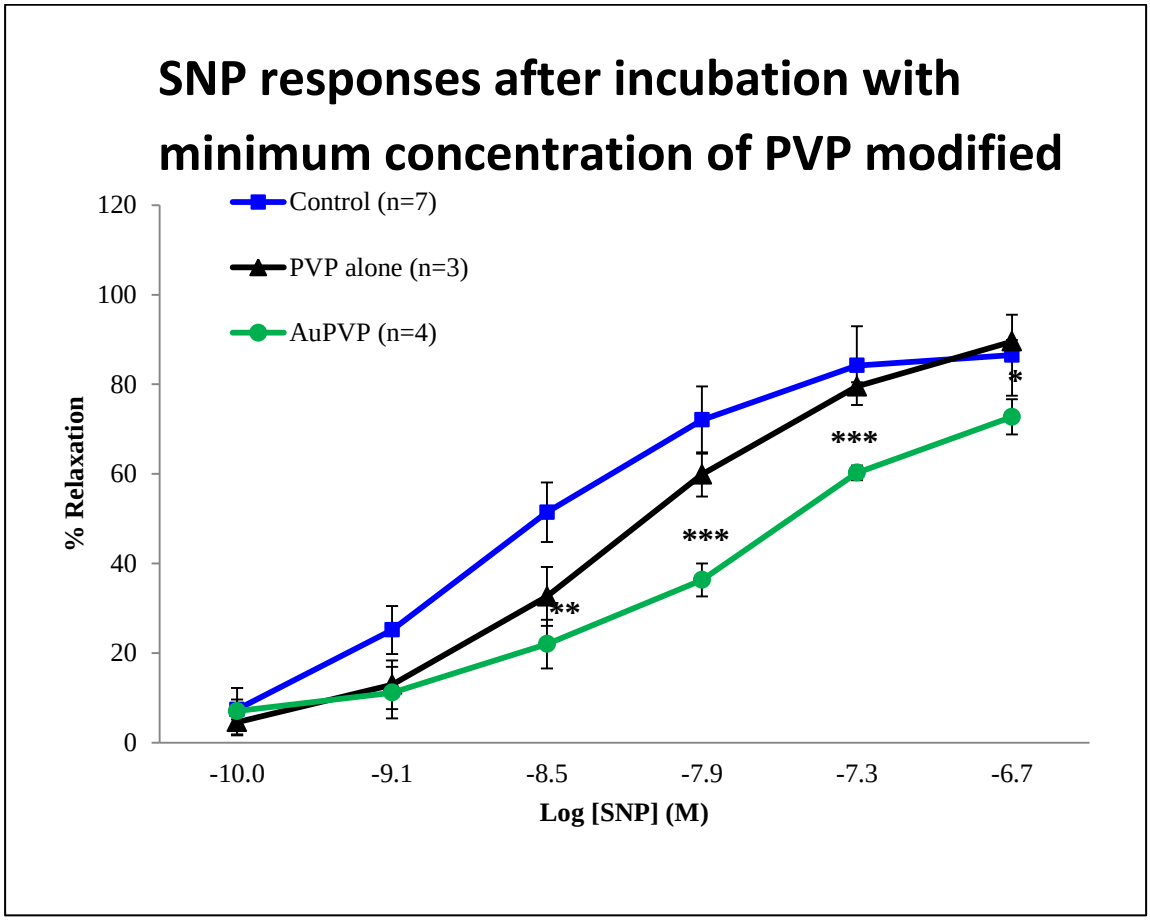

Figure 5.10: responses of vessels to SNP after minimum concentration of PVP modified AuNPs and PVP alone(* p<0.05, ** p<0.0 1 and *** p<0.00 1)

5.4 Effect of polyethylene glycol modified gold nanoparticles on dilator responses

5.4.1 Minimum concentration of polyethylene glycol needed to stabilize Gold Nanoparticles

The results of the PVP effect on vessel function suggests that it attenuates dilator function. Consequently, this study investigated whether other stabilisers had similar effects on dilator responses. Serial dilutions were carried out on mPEG to determine the minimum concentration needed to stabilise AuNPs. Once the minimum concentration required to prevent aggregation had been verified, ACh and SNP responses after incubation with mPEG modified AuNPs were determined (Table 5.1).

Table 5.1: Determining the minimal concentration of mPEG needed to stabilise AuNPs, through colour observation of the solution in physiological salt solution

Concentration of mPEG(g)	Colour observation
$3.7x10^{-5}$g	Clear red -no colour change.
$3.7x10^{-6}$g	Clear red -no colour change.
$0.5x10^{-7}$g	Clear red -blue colour

Findings demonstrated that mPEG coated AuNPs were stable after modification with both concentration of $3.7x10^{-5}$g and $3.7x10^{-6}$g (no colour change, indicating that the NPs were stable). Hence, AuNPs were coated with $3.7x10^{-6}$g of mPEG as the minimal concentration that is necessary to prevent AuNP aggregation.

5.4.2 ACh responses

There was no significant attenuation in ACh responses after incubation with mPEG modified AuNPs (2.9 µg/mL) (*See Appendix C: Table 11*) To determine whether concentration can have an influence on responses, the concentration of the mPEG modified AuNPs was increased (5.8 µg/mL). At this concentration, the dilator responses were significantly reduced ($p<0.001$) compared to PSS control at most ACh concentrations (*See Appendix C: Table 12*). Incubation in PEG alone caused a slight non-significant reduction in ACh dilator responses (Figure 5.11) *(see Appendix C: Table 12).*

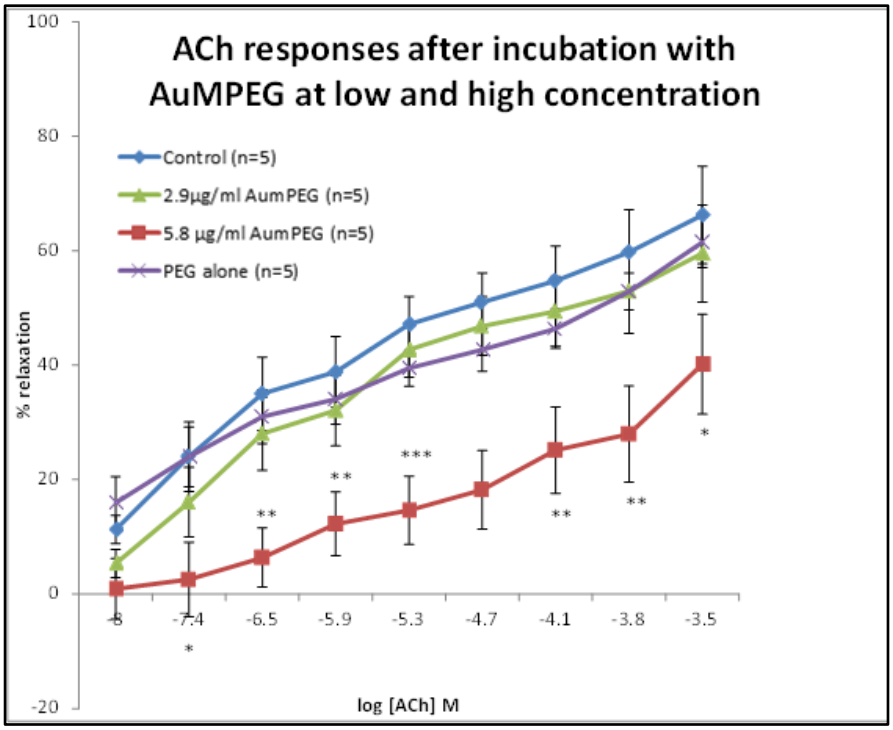

Figure 5.11: Responses to ACh after incubation with mPEG modified AuNPs at low and high concentration and PEG alone. *P<0.05 **P<0.01 and ***P<0.001

5.4.3 SNP responses

Interestingly, SNP dose responses were affected after incubation in PEG alone at the higher SNP concentrations (Figure 5.12)(*See Appendix C:Table 15*). Vessel incubation in mPEG alone (thiol modified PEG) led to a reduction in dilation, only at the highest SNP concentration ($p<0.05$) (Figure 5.13) (*See Appendix C: Table 14*). Vessel incubation in mPEG modified AuNPs at 2.9 µg/mL led to a small non-significant reduction in SNP dilator responses (NS) (*See Appendix C: Table 13*).

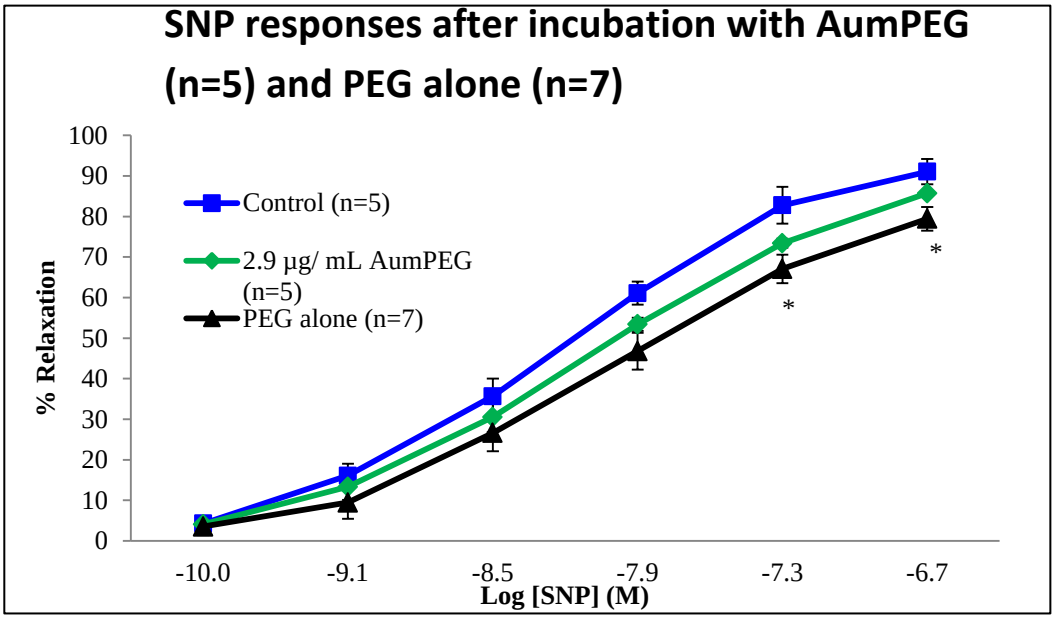

Figure 5.12: responses of vessels to SNP after incubation with PSS, mPEG modified and PEG alone (*p<0.05)

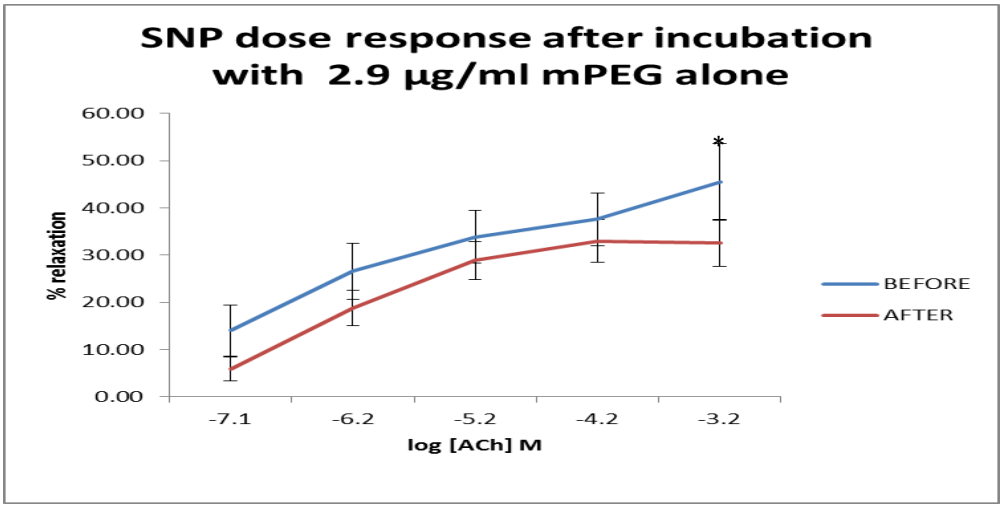

Figure 5.13: responses of vessels to SNP after incubation with mPEG alone(* p<0.05)

5.5 Modified and non-modified gold nanoparticle uptake into vasculature

The uptake of NPs into the vessel wall of aortic vessels after 0.5 hour of vascular lumen exposure was examined using TEM and ICP. The TEM images indicated that the non-modified AuNPs had aggregated and were identified within the lumen of the vessel. They were seen close to the surface of ECs. There was no evidence that the AuNPs had entered the cell (Figure 5.14A). On the other hand, PVP modified NPs were identified within ECs. They were identified within endosomal structures, but not freely within the cytoplasm, suggesting that uptake is by the process of endocytosis (Figure 5.14B). Very few mPEG modified AuNPs were identified in ECs when added at 2.9 µg/mL , (Figure 5.14C). However, once the NP concentration was increased, greater uptake was detected (Figure 5.14D).

ICP analysis indicated a high degree of uptake of non-modifed AuNPs (0.45ppm;13.95%), compared to PVP (0.14ppm;4.4%) and mPEG modified NPs at 2.9 µg /ml. At 5.8µg/mL both uptake of PVP (0.38ppm; 6.46 %) and mPEG (0.35ppm;6.07%) modified AuNPs increased, but was nonetheless still lower than that of the non-modified AuNPs (highest uptake at 0.74ppm;23.95%). The results shown in the chemistry section (section 3.3.3.2) .

5.5.1 Transmission electron microscopy images of nanoparticle uptake by aortic vessels

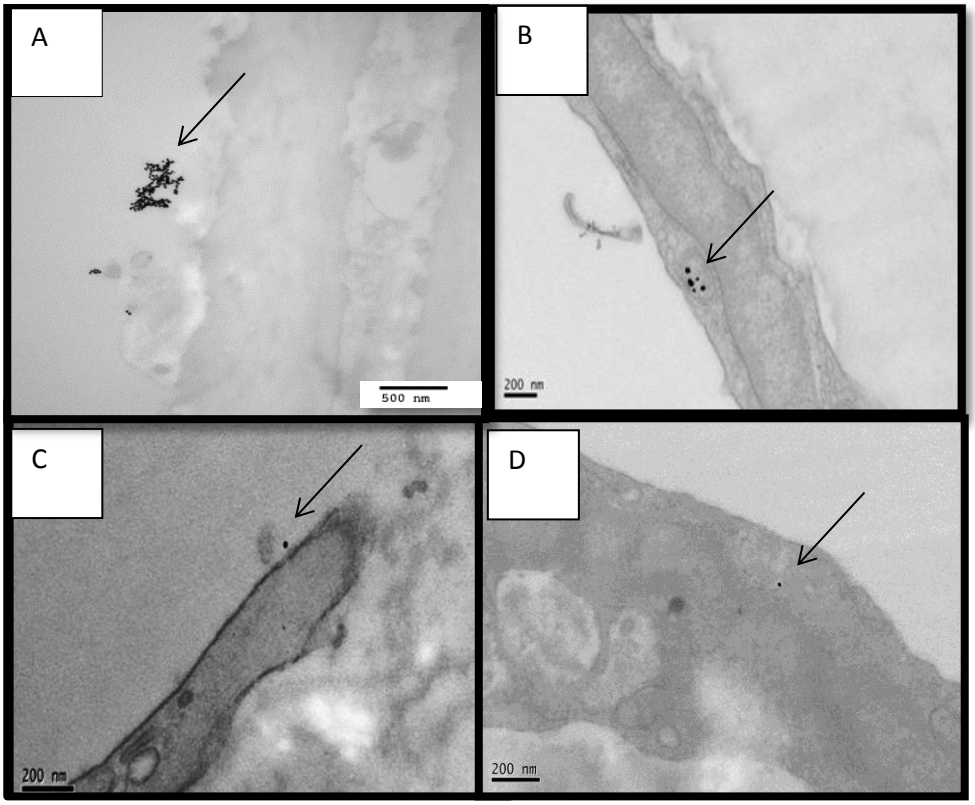

Figure 5.14: Representative TEMs illustrating AuNP uptake by the ECs lining of the vessel wall (A) non-modified AuNPs, (B) PVP modified AuNPs, (C) Low concentration of mPEG modified AuNPs and (D) High concentration of mPEG modified AuNPs, (Arrow represents NPs.)

Chapter 6:
Overall Summary of results

6. Overall Summary of results

6.1 Synthesis and characterisation of Nanoparticles (silica and gold)

NPs of various material compositions (silica and gold), size, charge and stabilisers were fabricated and characterised. The results are summarised as follows:

1. Silica NPs (SiNPs,100 nm and 200 nm, with and without rhodamine dye) were synthesised and their sizes were determined by dynamic light scattering (DLS) and scanning electron microscopy (SEM).
2. Zeta potential measurements demonstrated that the SiNPs were stable in H_2O, physiological *pH* and ionic strength conditions including physiological salt solution (PSS).
3. SiNPs (both dye and non-dye doped) were functionalised with 3-aminopropyltrimethoxysilian (APS). This led to an increase in the hydrodynamic diameter in water and caused aggregation in PSS. Furthermore, Zeta potential value demonstrated the reduced stability of these NPs after APS functionalisation.
4. AuNPs (12±3nm) were fabricated according to the Turkevich method. Size and dispersion of these AuNPs was determined by Transmission Electron Microscopy (TEM). Energy dispersive X-ray spectroscopy (EDAX) identified the presence of gold elements in AuNPs. Inductively coupled plasma mass spectroscopy (ICP-MS) gave the relative amount of gold element present in 300 µl and 600 µl AuNPs samples.
5. AuNPs were surface-modified using the polymers PVP and mPEG. Both diffuse reflectance infra-red Fourier transform spectroscopy (DRIFTS) and Surface Enhanced Raman Spectroscopy (SERS), identified the functional groups on the modified AuNPs. Thermogravimetric analysis (TGA) determined the presence of PVP on AuNPs by studying their thermal decomposition profile.
6. UV spectra demonstrated that non-modified AuNPs were stable in cell culture medium but not in PSS. Once the AuNPs were modified in PVP and mPEG, the AuNPs were stable in both DMEM cell culture media and PSS.

6.2 Influence of gold nanoparticles on cellular function

Cellular study results indicate that:

1. All AuNPs (modified and non- modified) reduced proliferation after 24 hrs incubation. Cell viability (using propidium iodide **(**PI**)** flow cytometric assay) was unaffected after short incubation times with AuNPs (30 min and 2 hrs). At longer incubation times, cell viability was reduced significantly, after 24 hrs incubation in all conditions, and after 48 hrs for AuNPs and AuPVP.
2. Different methods (Haemocytometer chamber, automated cell counter and propidium iodide **(**PI**)** flow cytometric assay) used to test cell viability, gave different results suggesting that NPs may have interfered with cell viability assays.
3. The degree of uptake of AuNPs by BAECs was dependent on incubation time and type of polymer stabilisers used. A greater degree of uptake was observed at a shorter incubation time (30min) with non-modified AuNPs, whereas uptake of AuNPs after PVP modification was highest after longer incubation periods (48 hrs).
4. There was a significant increase in the percentage number of apoptotic cells in all conditions after 2hrs and 24 hrs incubation. AuNPs, PVP and mPEG treatment led to a higher significant increase in percentage number of apoptotic cells after 2 hrs incubation. Furthermore, AuPVP induced a greater increase in percentage number of apoptotic cells after 24 hrs incubation, than AumPEG.
5. PVP resulted in an increase in necrotic cells by 3.0-fold at both 2 hrs and 24 hrs incubation. mPEG also significantly increased necrotic cells by 2-fold, after 24 hrs incubation.
6. Both modified and non-modified AuNPs reduced p-ERK expression, while non- modified AuNPs promoted the Akt signalling pathway. However, AuPVP and AumPEG reduced AKT signalling pathways.

6.3 Influence of gold nanoparticles on vascular function

Vascular study demonstrates that:

1. Non-modified AuNPs had no overall effect on acetylcholine (ACh) responses, however, they significantly reduced responses to sodium nitroprusside (SNP).
2. PVP modified AuNPs (modified using 9.5×10^{-12}M PVP corresponding to the maximum concentration used to stabilise AuNPs) were shown to attenuate the responses to both ACh (significant at 3 dose responses) and SNP (NS) PVP modified AuNPs (at the Least PVP concentration of 5.9×10^{-13}M, which was required to stabilise AuNPs) caused a small reduction in ACh induced dilator responses. SNP responses were, however, significantly attenuated.
3. PVP alone (at the minimal concentration of 5.9×10^{-13}M) caused a significant reduction in ACh dilator responses (at the 3 maximal ACh doses) However, for SNP responses, only a small reduction in dilation was evident.
4. Using serial dilutions, the concentration of PVP that caused minimal attenuated effect on ACh dilator function was determined as $1.84X10^{-8}$ µM, however, this concentration was insufficient to prevent aggregation of the AuNPs.
5. AumPEG at 2.9µg/mL had no overall significant effect on either ACh or SNP responses.
6. Vessel incubation in double the concentration of AumPEG(5.8µg/mL) led to a significant reduction in the ACh dilator response at most ACh concentrations examined.
7. Incubation in mPEG or PEG alone, had no effect on ACh induced dilator responses, but attenuated SNP induced dilation.
8. AuNP uptake by cells within the aortic vessel wall was verified by TEM and ICP. TEM sections had shown the presence of aggregated AuNPs in the lumen of the vessel, but none were identified in the vascular wall. Uptake of PVP modified AuNP was evident by ECs lining the vessel wall. The NPs were seen within endosomes. There was no evidence of AumPEG modified AuNPs at low concentration, however, at high concentration, the occasional NP was seen in the cytoplasm of ECs.

9. ICP analysis indicated a high degree of uptake of non-modifed AuNPs (0.45ppm;13.95%), compared to PVP (0.14ppm;4.4%) and mPEG modified particles at 2.9ug/ml. At 5.8ug/ml both uptake of AuPVP (0.38ppm; 6.46%) and AumPEG (0.35ppm;6.07%), but was nonetheless still lower than that of the non-modified AuNPs (highest uptake at (0.74ppm; 23.95%).

Chapter 7:
Discussion and Conclusion

7. Discussion

In the present study, NPs of different material composition (Gold and silica) and surface modifications were fabricated and characterised. PVP, thiol modified PEG (mPEG), and PEG polymer stabilisers were investigated, however, both PVP and mPEG polymers were chosen to modify AuNPs due to their suggested biocompatibility and assembling abilities on the surface of the NPs. Cell culture and western blotting techniques were employed to determine the effect of modified and non-modified AuNPs on endothelial cell proliferation, viability, apoptosis and signalling pathways. Furthermore, the influence of NPs on the vasodilator function of aortic vessels was also investigated. Our findings demonstrate that the effect on AuNPs on EC function (proliferation, viability and apoptosis) and vasodilator responses of whole aortic vessels, *ex vivo*, was influenced by the type of polymer used to modify the surface of AuNPs. A greater degree of biocompatibility is identified using mPEG modified AuNP, rather than PVP modified AuNPs. However, vascular responses were, nonetheless, dependent to the overall NP concentration used. Our study represents the first description of the influence of 13 nm gold nanoparticles, modified with two different polymers (PVP and mPEG), on EC and vasodilator function of aortic vessels *ex vivo*. Our findings are directly relevant to the current clinical use of AuNPs in imaging diagnostics and will inform the appropriate dosages and surface modifications that will minimise any detrimental effect on cellular and vasodilator function.

7.1 Characteristics of Nanoparticles (Silica and Gold)

NPs of various material composition (silica and gold), size, charge and stabilisers were fabricated and characterised within our laboratories. Both the DLS and SEM techniques were used to verify the size of the silica nanoparticles, while TEM was employed to verify the size of gold nanoparticles due to their small sizes. The stability of SiNPs was also determined using zeta potential measurements. Our results show that the zeta

potential of the SiNPs (with and without rhodamine dye) in H_2O were stable. Interestingly, the sizes of the SiNPs analysed using DLS with the Malvern's Zetasizer gave a slightly larger diameter compared to SEM. Furthermore, the SiNPs were also characterised in PSS to show that they were stable at physiological pH and ionic strength. In addition, the pH of NPs in solution was also examined to show the stability of NPs in various pH conditions. The NPs were stable once the pH were altered to pH 7.4, thus indicating that pH had no effect on the stability of the NPs. When the SiNPs were dispersed in water, the water molecules surrounded the NPs and produced a stern layer, also known as the inner and outer Helmholtz (HL) plane. The other ions which are not directly bound to the particles are also attracted to the negatively charged particles. Repulsion from the stern layer and the counter ions produces a diffuse layer. The point at which these layers meet results in a zeta potential. Once PSS solution is introduced, the ions cause a reduction in the number of water molecules. Both the surface of the silica and the PSS ions compete for the water molecules, resulting in less formation of the hydration layer. Furthermore, a closer interaction of the positively charged ions of the PSS and the water molecules at the surface of the silica results in the reduction of the shorter range of repulsive forces between the silica and the hydration layer. A reduction of zeta potential is therefore achieved.

The APS modified nanoparticles displayed an overall net positive surface charge. However, this caused both the dye and non- dye doped particles to be unstable in PSS solution. We further demonstrated that APS caused the SiNPs to grow larger (Van Blaaderen and Vrij, 1992). Moreover, the DLS analysis also indicated that the rhodamine b isothiocyanate (RH) dye influences the NPs size. An excessive concentration of ammonia and water during the synthesis of the NPs also increases the SiNP size. The seeding growth of the RH28 sample (DLS=110 nm) used less ammonia compared to TMRHSI sample (DLS=125 nm) (2ml vs. 6.04ml of ammonia, respectively) therefore we observed a smaller NP size with RH28. Similarly, Van

Blaaderen *et al* (1992) also demonstrated that NPs increased in size due to excessive concentration of ammonia and water. Ammonia in the reaction is known to act as a catalyst for the hydrolysis and condensation process of the silica precursor (Stöber *et al*, 1968). Furthermore, an increase in the amount of the ammonia resulted in an increase of silanol groups on the surface of the nanoparticles and therefore caused the NP size to increase. Recently, studies have shown that sizes of silica NPs can further be influenced by other parameters besides ammonia. For instance, the optimization of the concentration of silica source (TEOS) and NH_3 as well as the type of solvent (H_2O and ethanol) and the reaction temperature can control the size distribution of SiNPs (Davies *et al*, 2009; Park *et al*, 2002). Indeed, we observed this in our study.

Fabrication of the non-modified AuNPs involved a simple method from Turkevich and particles obtained were 12±3 nm when characterised with TEM. However, AuNPs characterisation with the Malvern Zetasizer was not possible to conduct, as the system in our laboratory was not inbuilt with the laser red HeNe source. This laser source is necessary for detecting the AuNPs samples at the wavelength maxima of 500-600 nm. Nevertheless, substitutes were used for size (TEM), and stability (UV-vis), measurements. Using TEM the non-modified AuNPs were shown to be in aggregates. This aggregation of the non-modified AuNPs was not possible to detect by the naked eyes. Polymer coatings have been developed and have shown advantageous properties in preventing aggregation (Zhang *et al*, 2009). Thus, PVP, and thiol modified PEG (mPEG), polymers stabilisers were employed in our study. Interestingly, PEG molecules have no open bonding on the end of their chain structure, therefore are unlikely to covalently bond to AuNPs; thus PEG molecules are expected to be physically adsorbed on the gold surfaces (Soel *et al*, 2013) whereas, modified PEG (mPEG), assembles on the surface of the particles with ease. Therefore, PVP and mPEG polymers were chosen for AuNPs surface modification in the present investigation. A recent study by Wang *et al* (2013), revealed that non thiol PEG exhibited the maximum

coagulation concentration, whereas thiol-PEG stabilizer accelerated AuNPs aggregation. Indeed this was the case for our mPEG modified AuNPs, therefore fresh mPEG modified AuNPs were made for every cellular and vascular function study. Many studies on the fabrication of gold nanoparticles built with polymer coatings such as PEG, mPEG and PVP have proven that nanosized dispersion is enhanced; this was also observed from our TEM analysis.

To further investigate the stability of the AuNPs, UV-vis was conducted. The characterisation demonstrated that AuNPs aggregated in PSS solution. PSS caused destabilisation and induced a significant color change from red to blue which resulted in the shift in Surface plasmon resonance (SPR). Furthermore, destabilisation of AuNPs could be recognized by the naked eye, however, once the particles were modified with PVP and mPEG, the NPs were able to remain stable in physiological conditions, which was detected visibly as the solution remained red in colour. A slight change in the ionic strength of a medium is known to be the cause of aggregation. Once a capping agent is added to the solution it will result in higher stability (Nativo *et al*, 2008). It is considered that stability in high ionic strength media depends upon PEG length. According to the DLVO theory, greater stability for smaller nanoparticles is achieved through minimal van der Waals attraction energy (Liu *et al*, 2007). In our study, the mPEG used had the length of 5000MW, this length was able to overcome the ionic strength of media. It is has been acknowledged that citrate-stabilized gold nanoparticles prefer to aggregate and precipitate in saline solutions. Dominguez-Medina *et al* (2013) indicated that AuNPs developed a different characteristic in the conditions below the NaCl concentration of many bodily fluids and blood plasma. Furthermore, aggregation was reduced after BSA was introduced to AuNPs in harsh Na+ conditions. Hence, our observation of AuNPs aggregation in PSS are the result of complexing of the citrate anions with Na+ cations in the salt solution. Furthmore, in our study, the non-modified AuNPs remained stable after addition to the cell culture medium. An assumption has

been made that the production of proteins by the cells in cell culture, together with the presence of FBS, are responsible for stabilizing AuNPs (Nativo *et al*, 2008). These proteins absorb on the surface of AuNPs; this in turn provides stability to the particles. Our UV-vis spectra observation do not show any significant red shift or broadening after exposure of the particles to the cell culture medium. AuNPs are considered to have optical scatterings at ranges of 550-600 nm wavelengths, because of the localized surface plasmon resonances (Wang *et al*, 2010). These ranges of wavelengths were also detected in our AuNPs samples.

7.1.2 Assessment of Polyvinilpirrolidine, and Polyethylene glycol attached on gold Nanoparticles

It was crucial to determine functional groups on the surface of the gold nanoparticles after modification. Hence, the diffuse reflectance infra-red Fourier transform spectroscopy analysis (DRIFT) was employed. The evidence forPVP and mPEG functionalisationon AuNPs was demonstrated by their signatures of certain functional groups which were recognized as C=O, C\N (1200 cm−1), in PVP (Gangwar *et al*, 2012), and thiol group (-SH) in mPEG (Yeh *et al*, 2009). These intermolecular bondings are used to identify the functional groups present. The C=O peak observation in citrate stabilized AuNPs was also detected in our study, a similar finding as that made by Wang *et al* (2010). Furthermore, analytical tools such as EDAX were successfully applied in the present study to indicate the presence of AuNPs, and demonstrated that the gold chemical element was present in the nanoparticles. Small traces of Na and Cl from the stabiliser sodium chloride were also detected. SERs analysis was able to identify the functional groups on AuNPs. We identified a slight shift in the peak of C=O peak at 1609cm˙1 on PVP modified AuNPs. However, there is a discrepancy in the documented peak position of carbonyl group of PVP, according to some studies.

For instance, Behera and Ram (2014) identified a slight shift ranging from 1667 to 1662 cm^{-1} in PVP modified AuNPs, and determined that the shift effect was due to charge transfer interaction of PVP molecules with the Au surface. On the other hand, Grzelczak *et al* (2011) and Moran *et al* (2011), identified peaks in the range of 1750-1769 cm^{-1}. However, we can still show that the functional groups on the AuNPs caused shifts in the peaks.

SERs are further used as a tool for ultra-sensitive monitoring of the intracellular distribution of AuNPs (Strem chemicals, Inc. 2013). Furthermore, Hu *et al* (2007) indicated that different-shaped gold nanoparticles possessed different SERS properties. A small variation in the shape/surface of the particles in our study, due to the surface modification with different polymers, may also attribute to a variation in SERs properties. TGA demonstrated the presence of PVP in the PVP-modified AuNPs by their thermal decomposition. The spectra in our study demonstrated that PVP alone degraded above 300 ºC, and completely decomposes at 430^{o}C. The PVP modified AuNPs, demonstrated that PVP on the AuNPs degraded at 280 to 460 ºC and a further weight loss was detected at 460^{O}C to 560^{O}C, this weight loss may also be attributed to the decomposition of PVP. Similarly, *Gangwar et al* (2012) shows a small weight loss at 550^{O}C and indicated that this weight loss was due to to the decomposition of PVP:curcumin coating around the AuNPs. Furthemore, the AuNPs in the present study decomposed at higher temperatures. These findings were similar to those by Gasaymeh *et al (*2010). They found that the metal NPs (silver), started to decompose at higher temperatures. They also demonstrated that PVP alone degraded above 300 ºC, and completely decomposes at 500 ºC.

7.1.3 Inductively coupled plasma Mass spectroscopy (ICP-MS)

Compared to TEM, inductively coupled plasma and mass spectroscopy (ICP-MS), is a more sensitive and accurate technique to quantify small amounts of gold nanoparticles taken up within the rat murine aortic vessels. ICP-MS can detect differences in the

internalized gold concentrations in the order of parts per million (ppm). In our study we analysed the relative amount of metal in the 300µl and 600µl sample of modified and non modified AuNPs and detected the differences at levels of parts per million. Also, the uptake of modified and non-modified particles into cells was also analysed and expressed as percentage uptake. The use of ICP-MS for the detection of internalised nanomaterials within vessels has also been described in other studies. For example, Shukur *et al (*2013) studied the effect of quantum dots on the function of murine mesenteric arteries, and used ICP-MS to identify the relative amount of metal in the QDs samples. Additionally, they detected the QDs uptake by the vessels and expressed their findings as ppm. Our result effectively shows that the double concentration of the AuNPs samples, gave a detection of double relative amount of metal.

.

7. 2 Effect of gold nanoparticles and their stabilisers on cellular function

7.2.1 Cellular uptake of modified and non-modified AuNPs

In our cellular study using BAECs, we observed that modified and non-modified NP uptake is dependent on incubation time and type of stabiliser used; we found cellular uptake of AuNPs by BAEC within 30 min incubation. This may have been facilitated by the fact that non-modified AuNPs were stable in culture media and monodispersed. The greater degree of non- modified NPs uptake could be due to their increased surface area to volume ratio due to smaller NP size, as compared to the modified AuNPs. After 2 hours, the degree of NP uptake increased further. Moreover, a further increased uptake of AuNPs after 24 hours was evident. It was associated with a small non significant decrease in cell proliferation at 24 hours. Freese *et al* (2012) made a similar observation in their study using Human Dermal Microvascular Endothelial Cells (HDMEC). They determined that the cytotoxicity of AuNPs was down to the concentration of AuNPs exposed to the cells. Interestingly, cell viability was not affected significantly, rather it

was increased. Chithrani *et al (*2006) found that AuNP uptake increased in the first 2 hrs after incubation, and slowed down after 4-7 hrs of incubation. In our study, uptake of non-modified AuNPs was reduced over time (after 48hours incubation). This could be due to the distribution of AuNPs amongst dividing cells and/or due to expulsion of the AuNPs from the cells over time. Reduced NP number due to cell division has also been observed in dermal cells cultured in 13 nm AuNPs (Mironava *et al,* 2010). Cell membranes are more likely to take up the NPs by endocytosis if they are monodispersed and colloidal. Which was the case in our study when the non-modified AuNPs were suspended in culture medium

There was a greater uptake of PVP coated AuNPs. According to Hu *et al (*2009) and Chithrani *et al* (2006), uptake of AuNPs by cells is size dependent; this may explain the greater degree of uptake of PVP modified AuNPs. Furthermore Hu *et al* (2009) explained that there are contradictions amongst studies on cellular uptake and stated that chemical and structural differences influenced uptake. Hence, this may explain the variation of uptake observed amongst the modified and non-modified uptake by cells in our study. Qiu *et al,(*2010) found that aging PVP for surface modification resulted in the formation of branched hollow . Interestingly, after 1 and 4 days, their particle size increased to 90–160 nm and 210–490 nm. This indicates that the PVP polymer molecules gradually self-assemble into larger particles in a given solution. Hence, this suggests that during NP modification, PVP self-assembles resulting in larger structure and therefore increases uptake due to their large size. As previously mentioned, cells prefer uptake of larger particles than smaller particles. This may explain our observation of greater uptake number of AuPVPs by the BAEC at longer incubation periods.

There was less uptake of mPEG modified AuNPs, in comparison to PVP modified AuNPs. Uptake was evident after 24 hrs of incubation. In contrast, Nativo *et al (*2008);

suggested that there was no uptake of PEG coated AuNPs at all by (Helacyton gartleri) HeLa cells. Even after prolonged incubation for 24 hours or after an increase in concentration of particles. Particles were also undetectable by TEM and AES. Interestingly, Huang *et al* (2009) found a greater concentration of PEG NPs accumulation in tumour cells, however, they used gamma radiation to promote uptake. The density and the length of PEG chains surrounding the modified AuNPs may influence uptake, as Lipka *et al* (2010), reported PEG (10000MW) prolonged the circulation of AuNPs, but not PEG (750MW). Freese *et al* (2013) also demonstrated that functionalization of AuNPs with poly(2-hydroxypropylmethacrylamide) can influence the uptake behaviour in different endothelial cell types , compared to PEG and glucosamine surface modification. Interestingly, Hu *et al (*2009) stated that a coating of PEG resulted in the reduction of cellular uptake by 1/3 as compared to another polymer coating (poly (N-vinyl caprolactam), which promoted the cellular uptake of NPs. Likewise, Liu *et al* (2007), showed that modified PEG AuNPs led to less cellular internalization of particles. In our study, mPEG modified AuNPs were internalized within the endosomes after uptake. According to Fu *et al* (2005), AuNPs modified with PEG was efficiently internalized by non-specific endocytosis. Moreover, observation shows that modified and non-modified AuNPs accumulated in endocytic vesicles. These findings were similar to Wang *et al* (2010) found that smaller NPs entered the cells through endocytosis and accumulated in the endocytic vesicles. They observed that AuNPs with size of 45 nm had greater interaction with cells compared to larger 70nm and 110nm NPs.

Tsai *et al* (2013), stated that cell uptake of NPs via non-specific endocytosis, results in endocytic vesicles enclosing the NPs. Consequently, the chances of NPs penetrating into the nucleus are reduced. This is confirmed by the lack of visualisation of AuNPs in the nuclei in our study. NP modification may result in a change of particle morphology. Stabilisers may also have an effect on the detection of NPs by TEM. It is acknowledged

that the morphology of NPs may make them difficult to identify, due to the low contrast produced by the mass-thickness (density × thickness) of the modified NP compared to the surrounding organelles within the cell (Garcia *et al*, 2012). This may be a reason in the variation of detection of NP uptake in this study.

7.2.2 Cell proliferation and viability

Researches have stated that AuNPs are biocompatible and non-toxic for cell growth and other biochemical activities of the cell (Wang *et al*, 2012; Tsai *et al*, 2013). Cell proliferation, in this study, was determined by coulter counter measurement. This technique is considered as being most sensitive in determining the decrease in cell number in AuNPs treated cells compared to control (Bancos *et al*, 2012). We show that proliferation was inhibited after incubation with modified and non-modified AuNPs. Similarly, Kalishwaralal *et al* (2011), found that gold nanoparticles significantly inhibited cell proliferation. However, this effect was seen at the concentration of 500 nM (9. μg/mL), whereas we used the dosage concentration of 2.9 μg/mL .

In the present study, cell viability was obtained via haemocytometer, coulters counter and flow cytometer assays. Although we show that cell viability was not affected by AuNP incubation after short incubation times, longer incubation times reduced viability significantly. AuPVP, AumPEG and their stabilisers had similar effect on cell proliferation of BAEC and cell viability when evaluated with flow cytometer. Although it was interesting to observe that the non-modified PEG further inhibited proliferation after 48 hrs. Using the haemocytometer, there was no evidence of any effect of AuNPs on cell viability in our study. NPs have been reported to interfere with cell viability and proliferation assays, (Bancos *et al*, 2012). Using silica nanoparticles (0.001 μg/mL), Bancos *et al* (2012), has shown that they had little interference with flow cytometer and coulter counter assays. NP dosages were less than those used in the present study. Aguilar (2010) reported that 10 μg/mL AuNPs are not toxic to cells *in vitro.*

Freese *et al* (2012), found that cell viability and proliferation of Human Dermal Microvascular Endothelial Cells (HDMEC), was reduced and this profound effect was not due to NPs sizes, but rather due to the influence of concentration of sodium citrate on the NPs surface. In a study on PVP and PEG polymers, Xie *et al* (2012), demonstrated using ethidium bromide/fluorescein diacetate staining technique (for cell viability) that PVP(10000MW) reduced viability of islet cells by 63.4%, whereas, PEG 5000MW and PEG (8000MW) both further reduced viability (58.1% and 60.7%, respectively) after 48 hrs incubation. Furthermore, Xie *et al* (2012) indicated that PVP polymer was a better cryoprotectant candidate as compared to PEG because PVP showed a fast dissolution rate in culture medium.

Our viability observation with the automated cell counter shows that PVP and mPEG both further reduced viability Moreover; we found that incubation timing had an influence on cell viability. Using porcine brain endothelial cells (BPEC), Freese *et al* (2013) found that the cell viability was not affected after treatment with poly (2-hydroxy-propyl-methacrylamide)-coated gold nanoparticles at different concentration. On the other hand, Xie *et al* (2012), found that increasing concentration of the polymers significantly increased the islet viability. In a AuNP study, Ng *et al* (2010) specified that 20nm sized AuNPs led to oxidative stress in the embryonic lung fibroblasts and inhibited cell proliferation as well as alteration of the cell cycle gene. They proclaimed that their observation was more likely due to immune reactions. Oxidative stress induced by AuNPs may lead to cell death and consequently reduce viability. This may explain the reduction in cell viability reflected in our study. Soenen *et al* (2012), found in their study that poly (methacrylic acid),-coated AuNPs reduced cell proliferation and cellular differentiation. These studies further support our findings that the modified AuNPs had an influence on reducing cell function.

7.2.3 Cellular localization of gold nanoparticles

Using confocal microscopy, NPs of 13nm and 50 nm sizes were visualised within the cytoplasm of ECs. Recently, it has been demonstrated that fluorescence intensity can be amplified by Plasmon particles (Dykman and Khlebstov, 2011). This explains the observation of the 13 nm and 50 nm non-fluorescent dyed AuNPs particles by fluorescence microscopy. Furthermore, we observed that 50nm had greater intensity as compared to smaller sized particles. Longer incubation indicated greater number of AuNPs in the membrane. As mentioned previously in the study, AuNPs are widely applicable in radiation research due to their high atomic number (Z). Subsequently, this results in a different mass energy absorption property. Thus the mass energy absorption property of gold is greater than that of the soft tissue. The high atomic number corresponds to large bound of electrons, which results in high mass absorption coefficient for X-ray. Hence AuNPs are described as being effective X-ray agents.

Our observations of the larger sized AuNPs being more easily visualized, may be due to the fact that 50 nm AuNPs had greater atomic number than the small AuNPs and have greater absorption energy than the small particles. We observed uptake of both PVP modified and non-modified 13 nm AuNPs by ECs, where non-modified NPs showed greater uptake within the cytoplasm. Zhang *et al (*2012) stated that 50nm NPs have stronger radiation sensitivity than 17 nm NPs. Chien and co-workers, (2012) justified that non-modified AuNPs provided high contrast which allowed them to detect small capillary species *in vivo,* whereas modified AuNPs with mercaptoundecanoid acid (MUA) gave less positive results in detection of small vessels. Wang *et al* (2013) reported that increasing the capping density of AuNPs can increase the detection sensitivity of AuNPs. Interestingly, using the confocal imaging, demonstrated that images of cells with modified AuNPs had low intensity compared to non-modified AuNPs. Indeed justification can be made that size of AuNPs and weight of polymer stabilisers can influence the contrast of imaging.

7.2.4 Cell apoptosis and necrosis

Apoptosis can be triggered by physiological and pathological stimuli (Elmor, 2007; Alberts *et al*, 2002). Flow cytometric analysis through fluorescein Annexin V-FITC and PI double staining in the present study, revealed that the gold nanoparticles exerted significant cytotoxicity to BAEC- cells in time-dependent manner and was influenced by type of stabilisers used. Similarly, using MTT assay, Selim and Hendi (2012) found that gold NPs induced apoptosis in MCF-7 human breast cells via p53, bax/bcl-2 and caspase pathways. However, they found that significant cytotoxicity was dose dependent, whereby at 200µg/mL , viability was 70% after 24 hrs. The dose used was 3 fold higher as compared to the dose concentration used in the present study (2.9µg/mL). We show that modified AuNPs and their stabilisers significantly induced apoptosis, and after non- modified AuNPs. Similarly, several reviews have stated that 13nm AuNPs coated with PEG (5000MW), induced inflammation and apoptosis of mouse Kupffer cells and macrophages (Tsai *et al*, 2013; Tiwari *et al*, 2011). Knop *et al* (2010) stated that not only does PEG have benefits, but they also have side effects and complications. We observed that mPEG alone significantly increased necrotic cells as well as PVP alone. A contradiction is made by Tsai *et al* (2013), using Annexin V/PI double staining to analyse the effect of AuNPs on the cell death program of MG63 Osteoblast-Like Cells. They found that AuNPs do not alter the cellular apoptosis rate during an eight day incubation period, even after high dose concentration. Likewise, using trypan blue method Soel *et al* (2013), found that PEG modified AuNPs did not have any detrimental effect on the cell viability of EMT-6 mouse mammary carcinoma cell line, therefore proclaimed that PEG-modified AuNPs are not toxic. This finding indicates that AuNPs may be inducing apoptosis in a cell type dependent manner. According to Mironava *et al* (2010), detrimental effects caused by AuNPs cannot be detected solely by proliferation or apoptosis assays, as AuNPs may be causing an interference with other specific functions within the cells. Therefore, this present study,

further looked at the effect of modified and non-modified particles on signalling pathways.

7.2.5 Influence of gold nanoparticles on ERK and Akt pathways

MAP kinase (ERK-1 and ERK-2), is necessary for induction of proliferation in BAEC and is known to accumulate significantly in the nucleus (Roux and Blenis, 2004). Our western blotting study shows that ERK-1 and ERK-2 expression was reduced in all culture condition when compared to incubation in ACh alone.This is supported by our finding that both modified and non-modified AuNPs inhibited cell proliferation of BAEC. Roux and Blenis (2004) revealed that inhibitors of the ERK pathway are emerging in clinical trials as anticancer agents. Based on our findings, we can suggest that modified and non-modified AuNPs make great anticancer agents, due to their ability to inhibit proliferation. Rauch *et al* (2012) demonstrated that NPs can bind to surface membrane receptors and consequently, activate specific cellular signalling pathways. This maybe one mechanism whereby modified and non-modified AuNPs may influence signalling pathways.

In the present study, we noted that non-modified AuNPs did not affect the Akt signalling pathway. However, modified AuNPs reduced Akt signalling pathways. Wang *et al* (2012), studied the metabolic effects of dietary AuNPs in Drosophila larvae, they interestingly found that dietary AuNPs promoted the Akt signalling pathway and altered lipid metabolism, an unexpected *in vivo* effect of nanomaterial on cellular metabolism. Rauch *et al* (2012), demonstrated using superparamagnetic iron oxide NPs that stimulation of ERK and Akt signaling pathways by the NPs was also dependent on surface modification. On the other hand, the concentration used to stimulate the cells in our study may have influenced the outcome.

Furthermore, the study of Wang *et al* (2012) also indicted that endocytosis of AuNPs may promote Akt signalling. We observed greater uptake of non-modified AuNPs than modified AuNPs after 30 min incubation. In the present study Akt signalling was only examined after 30 min of incubation. It is expected that a longer incubation time of cells with NPs will lead to further Akt phosphorylation as we have shown a great degree of uptake of NPs after 24 hrs.

7.3 Effect of stabilisers (Polyvinylpyrrolidone and polyethylene glycol), modified and non-modified particles on vascular function

7.3.1 Gold nanoparticles uptake into vasculature

Examination of EM sections of the aortic vessels, demonstrated that there was no evidence of uptake of non-modified AuNPs by cells of the vasculature after 30 min incubation. However, our ICP results indicated the uptake of gold elements within vessels after exposure to AuNPs at of both concentrations (2.9ug/ml (13%) and 5.8ug/ml (23%)). Considering that the AuNPs aggregated in PSS, indicated that they had increased in size. Interestingly, De Jong *et al* (2010) examined the uptake of 10nm of 250nm AuNPs by tissues after intervenous administration into rats, using TEM. They found that even large particles of 250 nm were impossible to detect in a single TEM section, due to the amount of AuNPs administered being to low; therefore it makes it almost impossible to detect the AuNPs present in one TEM preparation. De Jong *et al* (2010) have suggested that it is ideal to employ additional elemental analysis to positively indicate the presence of AuNPs. Indeed, we have shown using ICP the presence of gold metal. Whether this is due to the presence of AuNPs inside the cytoplasm or whether it is due to AuNPs aggregates attaching to the surface of the EC, cannot be confirmed. Nevertheless, AuNP uptake was detected by TEM once they were

modified with PVP (ICP=4%). However, fewer AuNPs were detected after modification with mPEG (ICP=3%). Our findings also indicated that a greater concentration of polymer monolayers (used to stabilise the NPs) led to a higher degree of PVP modified AuNPs uptake.

An increase in the concentration of mPEG modified AuNP led to increased vascular uptake. They were located in the adventitial layers, as well as the cytoplasm of endothelial cells. None were located in the nucleus of cells, in the elastic lamina or within the smooth muscle cell layer. A number of studies have shown that pegylated particles reduced uptake of particles. For instant, Arnida *et al* (2010) found that 50nm non-polymer modified particles had highest uptake by cells compared to the PEG modified particles. Similarly, Manson *et al (*2011) found less uptake of pegylation of particles by the reticular endothelial system. Nativo *et al* (2008) found no uptake of PEG coated AuNPs at all by by HeLa cells. Terntyuk *et al* (2009) studied the *in vivo* organ and tissue distribution of functionalized nanoparticles in rats and after 24 hours administration of pegylation AuNPs intravenously, and found a maximal AuNPs accumulation in the liver and spleen as compared to 30min administration. Thus, both Terntyuk *et al* (2009) and Boyoglu *et al* (2013) indicated that uptake can be influence by the timing of incubation. Our findings indicated that AumPEG uptake was also concentration dependent. At low concentration there was no uptake of the AumPEG into the vasculature. Swami *et al* (2012) found that PEG modification of the NPs reduced their accumulation in off-target organs such as liver and spleen.

The length, shape, and density of PEG chains on the NPs' surface have been shown to reduce the hydrophilicity and phagocytosis of the NPs (Swami *et al*, 2012). Also, an assumption can be made that modified AuNPs causes the diameter of particle to increase, hence, reducing the chance of uptake into the vasculature. Another plausible explanation for reduced uptake and inability to detect NPs by TEM, maybe due to the

fact that NPs are taken up actively by the cells via nonspecific endocytosis, and are leaving the cells via exocytosis if the particles are unable to be digested by lysosomes after they have been taken up (Tsai *et al*, 2013).

Oh *et al* (2011) identified in their study that the ultimate intracellular destination is further determined by the diameter of particles. Using AuNPs with the diameter ranging from 2.4 to 89 nm, they found that 2.4 nm AuNPs were localised in the nuclear, whereas, 5.5 and 8.2 nm particles were partially delivered into the cytoplasm and > 16 nm AuNPs did not enter the cells and were located at the cellular periphery. This justifies the observation of low or no uptake of NPs into ECs in our study, as non-modified particles aggregated in PSS, subsequently, the particle sizes increased.
Takae *et al* (2005) observed an increase in nanoparticle diameter from 20 to33.3 nm after functionalization with 6,000 Mw PEG. This statement justifies that the modification AuNPs in our present study led to the increase in the NP diameter, consequently, affecting particle uptake.

De Jong *et al* (2010) indicated in their study, that TEM analysis alone is not effective in detecting uptake. Indeed, using ICP-MS we have shown uptake of non-modified AuNPs into vessels, contrary to our TEM results. The aggregation of our non-modified AuNPs may have given a greater reading in ICP-MS, due to the fact that aggregation of NPs involves a greater number of NPs attached. In contrast, our modified AuNPs were well dispersed, therefore less amount of uptake is evident by ICP-MS.

Our ICP-MS results for uptake of modified AuNPs were similar to TEM observation in which we detected less uptake of polymer coated AuNPs, in particular AumPEG. Interestingly, when the concentration of AumPEG NPs was doubled, a higher amount of gold metal from the double amount concentration of AumPEG was detected using ICP-MS.

7.3.2 Effects of gold nanoparticles on aortic dilation responses

The influence of AuNPs on vascular function was studied using the organ bath system.Aortic vessels were incubated in AuNPs at $1.68x10^{11}$ NP/mL (2.9µg/mL), over a 30 minute acute exposure time period. This concentration was also utilised in our cell culture experiments. This exposure time and NP concentration is commonly used in other studies which have identified NP uptake into tissues. For instance, Kempson *et al* (2012), studied the fate of intravenously administered gold nanoparticles in hair follicles, after intravenous administration into mice. After 30 min, the dermal papilla, bulge region, and root sheath all contained NPs. Hainfeld *et al* (2006) used 1.9 nm AuNPs as an x-ray CT contrast agent to detect tumours in mice, and found that AuNPs had accumulated in the organs after just 15 min of intravenous injection. When 10 nm AuNPs were injected intravenously at 5.7 x 10^{12} NP/ml into rats, uptake into most tissues was evident at 24 hours after injection (De Jong et al, 2010). In another *in vivo* study, 13 nm PEGylated AuNPs were injected at the low dose of 1.76 x 10^{11} NPs/ml into mice. These NPs were seen to accumulate in tissues within 30 min after intravenous injection and were shown to induce acute inflammation and apoptosis (Cho *et al*, 2009). A study investigating the effect of coupling AuNPs to NO donors (Ruthenium complex) has demonstrated that NO released from the AuNP-ruthenium complex was lower than that released from the ruthenium complex alone (Silva *et al*, 2014).

7.3.2.1 Influence of non- modified gold nanoparticles on dilator responses

In this study we observed that non-modified AuNPs had no overall effect on the endothelium-dependent (ACh) relaxation of the vessels. AuNP aggregation in PSS and lack of uptake as evidenced by TEM may explain the lack of any detrimental effect on ACh mediated dilation. An important finding from the present study is that unmodified AuNPs significantly attenuated responses to SNP. This suggests that AuNPs may interact directly with the SNP drug. Such interaction has also been suggested for a number of

agonists (Nurkiewicz *et al*, 2009), and confirms the additional need for coating AuNPs before use. AuNPs are able to rapidly catalyse the decomposition of hydrogen peroxide (He *et al*, 2013), whereby, hydrogen peroxide (H_2O_2), is recognized to induce vasorelaxation (Cai, 2005). Another possible suggestion for the attenuated SNP responses is that non-modified AuNPs may reduce the sensitivity of the smooth muscle cells to SNP and interfere with the signalling pathway leading to vasodilation. AuNPs may block the inward rectifier potassium channels (K_{IR}), which therefore reduce the SNP effects on the vascular smooth muscle, (Schubert *et al*, 2004).

7.3.2.2 Influence of Polyvinilpirrolidine- modified gold nanoparticles on dilator responses

Our initial observation showed that non-modified AuNPs aggregated in PSS. Consequently, to overcome this effect and prevent aggregation, AuNPs were modified with the polymers, PVP and mPEG. PVP modification of the AUNPs increased their stability and monodispersion AuPVP NP uptake into the vessel was demonstrated, as individual NPs within the cytoplasm of ECs. Our initial studies demonstrated that when AuNPs were modified with a high concentration of PVP, their uptake induced a significant reduction in ACh dilator responses. Vessel incubation in AuNPs modified with a low concentration of PVP, had no significant effect on ACh dilator responses. The fact that incubation in PVP alone (at the low concentration), caused a significant reduction in ACh dependent dilator responses, suggests that it is the PVP itself which may be influencing dilation. PVP modified AuNPs (at high concentration) may be larger in size than those that were modified with a low PVP concentration, and hence may have interacted with cellular components leading to the attenuated dilation. Furtherrmore, PVP modified NPs may affect the ATP production in the mitochondria as it is acknowledged that the production of relaxant factor by endothelium is dependent on the mitochondrial oxidative phosphorylation (OXPHOS) (Marin-Garcia, 2013). Furthermore, the mitochondria are one of the major organelles targeted by NPs for inducing oxidative

stress (Manke *et al*, 2013). For example, Pan *et al (*2009) demonstrated that non-modified gold nanoparticles of diameter 1.4 nm triggered necrosis by oxidative stress and mitochondrial damage.

Duffin *et al (*2007), has demonstrated, using human models, that NPs enter the circulation and can have direct effects on the endothelium, leading to endothelial dysfunction. They investigated the effects of diesel exhaust inhalation on vascular and endothelial function in humans. After 2 to 6 hrs exposure of the NPs, they found that the vasomotor responses to the vasodilator drugs (ACh, BK and SNP) were attenuated, whilst the responses to Verapamil were not affected, as this type of vasodilator causes relaxation by an endothelium-independent and NO-independent pathways, unlike the other vasodilators used in their study. Therefore in our present study, PVP maybe preventing the AuNPs from quenching NO that is released by the NO donor (SNP). When vessels were incubated in AuNPs modified with a high PVP concentration, they had no influence on SNP responses, however, incubation in AuNPs modified with a low PVP concentration, induced a significant reduction in SNP responses. When vessels were incubated in a low concentration of PVP alone, no effect on SNP responses were noted. This suggests that it is the AuNP itself which maybe interfering with the action of SNP. PVP modification of the AuNPs may thus prevent its interaction with SNP. At low PVP concentration, the polymer monolayer may have been insufficient to fully coat the AuNP and hence allow its interaction with SNP. The interaction of nanomaterials with the function of SNP have been demonstrated previously. For example, Shukur *et al* (2012) demonstrated the attenuation of SNP induced dilation in mesenteric vessels after incubation in quantum dots.

7.3.2.3 Influence of Mecapto polyethylene glycol - modified gold nanoparticles on dilator responses

Polyethylene glycol (PEG) has been demonstrated to prevent cellular uptake of gold nanorods (Hauck *et al,* 2008). Kim *et al (*2007), used PEG coated gold nanoparticles to extend their systemic circulation half-life, whereby nanoparticles injected intravenously into rats showed much longer blood circulation time (> 4 hrs). In our present study we determined the minimum concentration of mPEG required to prevent aggregation of the AuNPs in PSS. mPEG modified AuNPs (at 2.9ug/ml), had no overall influence on endothelium dependent responses. When vessels were incubated at the higher 5.8ug/ml concentration of mPEG modified AuNPs, the dilatory responses were significantly reduced ($p<0.001$). Indeed, uptake of AumPEG by the endothelial cells was also shown to be concentration dependent.A high NP concentration may result in passive transport into the vessels. This is supported by Treuel *et al (*2013); they stated that NPs may enter cells by passive penetration of the plasma membrane.

Vessel incubation in AuNPs modified with mPEG led to a slight but non-significant influence on SNP dilator responses. Since the thiol group on the mPEG is attached to the surface of the AuNPs and the PEG chain molecule is in direct contact with the surrounding tissue**,** we decided to investigate the effect of the non thiol PEG molecule alone on vascular function. ACh responses were not affected after incubation with non thiol modified PEG alone, however, SNP dose responses were affected at high doses, suggesting that PEG may be influencing the sensitivity of the smooth muscle cells to SNP, possibly through blocking the K_{IR} channels(Schubert *et al,* 2004). On the other hand, thiol modified AuNP incubation affected SNP responses only at the highest dose.

Size of the polymer chain may also affect the vascular responses. In our study, PEG (6000 MW) has a greater molecular weight than mPEG (5000MW); indeed, their

weight may contribute towards the influence on responses observed. Nanoparticle morphology may alter after uptake, therefore, this may explain the varied effects of modified particles compared to their stabilizers alone (Garcia *et al*, 2013).

Intracellular degradation of NPs is considered an important factor which may lead to the alteration of the NPs' behaviour, and subsequently, results in the varied biological functionality after interaction with cellular components. Indeed, degradation of modified NPs may lead to variation in effects on cellular function compared to those caused by their stabilisers alone. For instance, Soenen *et al* (2014) studied the effect of nanoparticle degradation on poly(methacrylic acid)-coated quantum dot toxicity and revealed that the quantum dots were partially degraded and released cadmium ions and consequently caused greater particle toxicity. This can explain our observation of the difference in attenuation effects between the modified AuNPs and their stabilisers in our present study.

7.3.2.4 Mechanisms of attenuated vasodilation induced by AuNPs

In order to elucidate mechanisms leading to attenuated vasodilation by AuNPs, cellular studies were conducted on ERK and Akt signalling pathways. Both pathways are reported to be responsible for inducing dilation of vessels, due to their role in stimulating the production of NO by activation of eNOS. For instance, the ERK signalling pathway has been implicated in vasodilator responses associated with retinal arterioles (Yuan *et al*, 2008*).* Stimulation of NO-mediated vasodilation is also linked with the activation of P1EK/Akt pathways (Guo *et al*, 2005*). T*he release of NO results in the activation of guanylyl cyclase in the VSMC, and consequently elevating the cGMP. cGMP is considered an important messenger in inducing vasodilation, as it is involved in activating the K^+ channels which leads to the hyperpolarization and relaxation of the vessels.

When BAECs were stimulated with ACh, AKt and ERK, phosphorylation was maximal at 10μM ACh concentration. This confirms our vascular studies, whereby aortic vasodilation is evident at this concentration. When the BAEC were stimulated with ACh, in the presence of modified and non-modified AuNPs, a reduction in ERK and Akt phosphorylation was observed for PVP and mPEG modified, but not non-modified AuNPs. These findings confirm our vascular function responses for the non-modified AuNPs (no attenuation and PVP modified AuNPs (significant attenuation in dilation). It is not clear why reduced ERK and Akt phosphorylation is not mirrored by reduced dilation due to AumPEG. However, the degree of uptake of modified AuNP by cells in culture was higher than that in vessels and this may explain the difference. Also PVP modified AuNP may act as antagonists and inhibit ERK and AKt stimulation by the ACh receptors; thus reducing the NO production in the EC. Vessel incubation in PVP alone, led to a significant reduction in ACh induced dilation. The reason for this is not clear. The surface chemistry of the polymers is, however, known to influence cell interaction and morphology (Saltzman, 2000). PVP surface groups could bind to protein such as the ACh receptors, acting as an antagonist (Jiang *et al*, 2006). Although PVP has been used to modify NPs to reduce their cytotoxicity, such as grapheme oxides (Zhi *et al*, 2013) and iron oxide NPs (Zhang *et al*, 2010), there is evidence that when PVP is complexed with iodine, the product (PVP-I) can be cytotoxic to cells. For example, Sato *et al* (2014) found that PVP-I induced apoptosis of epithelial cells at $1x10^{-2}$ μM concentration.

The SNP responses were reduced after incubation with non-modified AuNPs, minimal PVP modified AuNPs and PEG stabilisers but not PVP stabilisers. Minimal PVP modification provided a weak stability of AuNPs, hence, justifies the similarity in effect on the SNP responses to non-modified AuNPs. Furthermore, the attenuation of SNP response indicates that non-modified AuNPs and minimal PVP modified AuNPs may similarly compete for the NO released by the NO donors, thus impairing the

vasodilator response as has been recently demonstrated using ruthenium complex as a NO donor. When complexed with AuNPs, NO release was reduced (Silva *et al*, 2014).

7.3.3 Study limitations

The results of our present study maybe have been affected by a number of limitations discussed below.

1. Nanoparticle uptake: NP uptake by vessels may have been affected by the incubation conditions. Using the organ bath system, vessels were constantly gassed in 95 % O_2: 5 % CO_2 within the organ chamber. This could have disturbed the uptake of the AuNPs by the vessels, compared to the steady conditions of exposure in the cell culture environment. A pressure myograph system could be used in future applications, where the vessel is exposed to gassed PSS at source. Additionally, only a few sections were examined under TEM, per exposure condition. A more thorough quantification of serial sections could be done in the future.
2. Cell culture studies were conducted using BAECs. Use of rat aortic endothelial cells would have allowed for a better comparison with rat aortic vascular function studies. Furthermore, the use of human cells and human vessels would allow the translation of the work which would represent an ideal model to determine the direct influence of AuNPs in man.

7.4 Conclusion

In the present study NPs of 2 different material compositions were fabricated and characterised; Silica NPs (SiNPs) and gold NPs (AuNPs). The 13 nm AuNPs were modified using 2 polymers; PVP and mPEG. The SiNPs were successfully utilized as the NPs of choice for an alternative vascular function *ex vivo* study, and the findings were published (Akbar *et al*, 2011). The influence of both modified and non-modified AuNPs on cellular and vascular function ex vivo was examined in this study.

Results demonstrate that AuNPs are rapidly internalised by endothelial cells and whole isolated aortic vessels *ex vivo*, after a 30 min incubation period. Uptake of modified AuNPs by cells was observed to be time dependent, where maximum incubation time (48hrs) resulted in greater uptake of AuPVP, compared to AumPEG. Incubation in polymers alone also affected cellular function. Polymer degradation of internalized polymer modified NPs may take place once inside the cell. In this case, both the AuNPs and their degraded stabilizers may induce different effects on cellular function after uptake compared to polymers alone. This was observed by the cell apoptosis, where PVP and mPEG alone had a greater apoptosis effect compared to AuPVP and AumPEG at 2 hours incubation. Both modified and non-modified AuNPs influenced cellular signalling differently and modulated physiological responses. In the vessel study, unmodified AuNPs attenuated endothelial-independent dilator responses. However, AuNPs aggregated in PSS preventing their uptake into the vasculature and hence did not influence endothelial-dependent dilator responses of murine aortic vessels. Coating of AuNPs with PVP and mPEG polymer (modified AuNPs), prevented aggregation in PSS, however, PVP modified AuNPs led to attenuated endothelial-dependent dilator responses. The mPEG polymer modified AuNPs had no overall influence on endothelial dependent dilator responses, although the influence was concentration dependent. Our findings have important implications for the development of new therapies, since AuNPs are used in therapy and in imaging diagnostics.

7.5 Future work

The results from our study suggest that depending on the coatings and concentration used, AuNPs may affect cellular and vascular function. We have demonstrated that modified and non-modified AuNPs can influence cellular and vascular function by affecting endothelial cell function and influencing cell signalling pathways. Therefore, future studies will involve:

***Additional Cell culture studies*.** Cellular behaviour is influenced by NP dosage; it would be of interest to determine the effect of modified and non-modified AuNPs on cellular function at different dosages. One interesting study indicated that the detrimental effects caused by AuNPs cannot be detected solely by proliferation or apoptosis assays, as AuNPs may be causing an interference of other specific functions within the cells (Mironava *et al*, 2010). Hence it would be of interest to examine the effect of modified and non-modified AuNPs on upregulation of inflammatory markers and also to further explore the cell signalling pathway, including eNOS upregulation and phosphorylation.

Functional studies 1: In the present study, the AuNPs were found to influence endothelial-dependent and independent responses differently, depending on the type and concentration of polymers used to modify the AuNPs. It will be necessary to extend these findings to examine the detailed mechanisms involved in attenuated dilation. The influence of nanoparticle uptake on arterial function can be further investigated using pressure myography technique, which involves mounting vessels under more physiological conditions of pressure and flow. We have determined the type and concentration of stabilizers that will have a minimum cytotoxic effect on large vessels but not on small vessels. So such a study would be interesting, since diameter regulation of these vessels is more important in the control of blood perfusion into tissues. In the present study, non-targeted colloidal gold NPs were examined. It would be interesting to see what effect tagged AuNPs (eg. antibody labelled) may have on cellular and vascular function. Additionally, the effects of modified and non-modified AuNPs on whole

animals *in vivo* are yet to be determined. A detailed analysis and quantification of nanoparticle uptake can be verified by microscopy using thin (confocal) and ultrathin sections (electron microscopy). This will allow detailed quantification of NPs within cells.

Functional studies 2: The influence of SiNPs synthesised in the present study, on vascular function was examined in another study (Akbar *et al*, 2011). The *ex vivo* studies demonstrated that acetylcholine (ACh) induced a concentration dependent dilator response in all pre-constricted vessels. Incubation in 100nm nanoparticles lead to a reduction in the magnitude of the dilator response at higher ACh concentrations, although this was not statistically significant (at 0.1 mM ACh, mean dilation was 37.42±5.50% vs. 45.58±7.02% dilation after incubation in PSS, NS; at 1.0 mM ACh, mean dilation was 40.14±5.74% vs. 53.94±6.26% dilation after incubation in PSS, NS) *ex vivo*. SiNPs were injected into a male Wistar rat and sacrificed after 2 hours. The ACh-induced dilator responses were altered after NPs incubation *in vivo*. There was an improve dilatory response at every ACh dose response. Hence, the degree of ACh dilation after incubation in 100 nm SiNPs *in vivo* was higher than that after incubation in 100 nm SiNPs *exvivo*, at the highest 1.0 mM ACh concentration (74.19% dilation vs. 40.14±5.74%) dilation, after incubation 100nm nanoparticle incubation *in vivo* and *ex vivo* respectively. More *in vivo* experiments are required to confirm the findings. Aortic vessel incubation in 100 nm *ex vivo* had no effect on the endothelial-independent dilator responses (SNP) at any of the concentrations examined (NS). On the other hand, responses were reduced after NPs were incubated i*n vivo*. However, overall n=1 of *in vivo* experiment was conducted therefore, more experiments are needed to clarify the *in vivo* results.

8.REFERENCES

8. REFERENCES

Aderem, A. and Underhill, D.M. (1999) 'Mechanisms of phagocytosis in macrophages.' *Annual Review of Immunology,* 17, pp. 593-623.

Adini I., Rabinovitz I., Sun J. F., Prendergast G. C. and Benjamin L.E. (2003) 'RhoB controls Akt trafficking and stage-specific survival of endothelial cells during vascular development.' *Genes and Development,* 17(21) pp. 2721–2732.

Aguilar, Z. (ed.) (2010) 'Nanomaterials for Medical Applications.' 1st ed., Elsevier, pp. 1-544.

Akbar, N., Mohamed, T., Whitehead, D., Azzawi, M. (2011) 'Biocompatibility of amorphous silica nanoparticles: size and charge effect on vascular function, in vitro.' *Biotechnology and Applied Biochemistry*, 58(5) pp. 353–362.

Alberts, B., Johnson, A., Lewis, J., Raff, M., Roberts, K. and Walter, P. (ed.) (2002) '*Molecular Biology of the Cell*.' 4th ed., New York: Garland Science; pp.1-1616

Alkilany, M.A. and Murphy, C.J. (2010) 'Toxicity and cellular uptake of gold nanoparticles: what we have learned so far?' *Journal of Nanoparticle Research*, 12(7) pp. 2313-2333.

Arnida, A., Malugin, A. and Ghandehari, H. (2010) 'Cellular uptake and toxicity of gold nanoparticles in prostate cancer cells: a comparative study of rods and spheres.' *Journal of Applied Toxicology*, 30(3) pp. 212-217.

Astruc, D., Lu, F. and Aranzaes, J.R. (2005) 'Nanoparticles as Recyclable Catalysts: The Frontier between Homogeneous and Heterogeneous Catalysis.' *Angewandte Chemie International Edition*, 44(48) pp. 7852–7872.

Atomic World; Accessed on 15 January 2014. Available from: http://www.hk-phy.org/atomic_world/tem/tem02_e.html.

Aulton, M.E. and Taylor, K.M.G. (2013) 'Disperse sytems.'(Chapter 5) In: Aulton's Pharmaceutics: The Design and Manufacture of Medicines, pp. 63-92.

Azzawi, M. (2012) 'The nanotoxicological influence of nanoparticles with Special Reference to the Vasculature' In M Slevin, Ed.: *Current advances in the medical application of nanotechnology.* Bentham Publications, pp. 73-84.

Korzeniowska, B. Nooney, R. Wencel, D. and McDonagh, C. (2013) 'Silica nanoparticles for cell imaging and intracellular sensing.' *Nanotechnology* 24(44) Article ID: e442002.

Bancos, S., Tsai, D.-H., Hackley,V.,Weaver, J.L. and Tyner, K.M.(2012)'Evaluation of Viability and Proliferation Profiles on Macrophages Treated with Silica Nanoparticles In Vitro via Plate-Based, Flow Cytometry, and Coulter Counter Assays.' *International Scholarly Research Notices (ISRN) Nanotechnology*, 2012, pp.1-15.

Barandeh, F., Nguyen, P.-L., Kumar, R., Iacobucci, G.J., Kuznicki, M.L., Kosterman,A., Bergey,E. J Prasad, P.N. and Gundawardena, S. (2012) 'Organically Modified Silica Nanoparticles Are Biocompatible and Can Be Targeted to Neurons In Vivo.' *Plos one,* 7(1), Article ID: e29424.

Behera, M. and Ram, S. (2014) 'Inquiring the mechanism of formation, encapsulation, and stabilization of gold nanoparticles by poly (vinyl pyrrolidone) molecules in 1-butanol.' *Applied Nanoscience,* 4(2) pp. 247-254.

Berg, J.M., Tymoczko, J.L.and Stryer, L. (ed.) (2002) *Biochemistry*. 5th ed., New York: W H Freeman. pp. 1-1026.

Bergman, L., Rosenholm, J. and Öst, A. (2008) 'On the Complexity of Electrostatic Suspension Stabilization of Functionalized Silica Nanoparticles for Biotargeting and Imaging Applications.' *Journal of Nanomaterials*, pp. 1-9.

Bernanke, D.H. and Velkey, J.M. (2002) 'Development of the coronary blood supply: changing concepts and current ideas.' *The Anatomical Record,* 269(4) pp.198-208.

Bernardi, R.J., Lowery, A.R., Thompson, P.A., Blaney, S.M. and West, J.L. (2008) 'Immunonanoshells for targeted photothermal ablation in medulloblastoma and glioma: an in vitro evaluation using human cell lines.' *Journal of Neuro-Oncology*, 86(2) pp. 165-72.

Bizi, M. (2012) 'Stability and flocculation of nanosilica by conventional organic polymer.' *Natural Science*, 4(6) pp. 372-385.

Blanco-Andujar, C., Tung L.D and Thanh N.T.K. (2010) 'Synthesis of nanoparticles for biomedical applications.' *Annual Reports on the Progress of Chemistry, Section A* (Inorganic Chemistry), 106, pp. 553-568.

Bogush, G. H., Tracy, M. A. and Zukoski Iv, C. F. (1988) 'Preparation of monodisperse silica particles: control of size and mass fraction.' *Journal of Non-Crystalline Solids*, 104 (1) pp. 95-106.

Böhm, F. and Pernow, J. (2007) 'The importance of endothelin-1 for vascular dysfunction in cardiovascular disease.' *Cardiovascular Research*, 76(1) pp. 8-18.

Bolotina, V. M., Najibi, S., Palacino, J. J., Pagano, P.J. and Cohen, R.A. (1994) 'Nitric oxide directly activates calcium-dependent potassium channels in vascular smooth muscle.' *Nature*, 368(6474) pp. 850-853.

Boonen and Roeven, (2011) 'Synthesis and characterisation of silica-coated magnetite nanoparticles.' *Minor Disciplines Applied Science Course 47: Colloids.* pp.1-23.

Boulanger, C. M. and Vanhoutte, P.M. (1998) 'The endothelium: a modulator of cardiovascular health and disease.' *Dialogues in Cardiovascular Medicine*, 3(4) pp.187-1999.

Boyoglu, C., He, Q., Willing, G., Boyoglu-Barnum, S., Dennis, V. A., Pillai, S. and Singh S. R. (2013) 'Microscopic Studies of Various Sizes of Gold Nanoparticles and Their Cellular Localizations.' *ISRN Nanotechnology*, 2013, pp.1-13.

BSI standards publication, *PAS* 71, pp.1-25.

Buckley, A.M. and Greenblatt, M. J. (1994) 'Sol-Gel Preparation of Silica Gels.' *Journal of Chemical Education*, 71(7) pp. 599-602.

Butterworth, K.T., McMahon, S. J., Taggart, L. E. and Prise, K. M. (2013) 'Radiosensitization by gold nanoparticles: effective at megavoltage energies and potential role of oxidative stress.' *Translational Cancer Research*, 2(4) pp. 269-279.

Cai, H. (2005) 'Hydrogen peroxide regulation of endothelial function:Origins, mechanisms, and consequences.' *Cardiovascular Research*, 68(1) pp. 26-36.

Canton, G., Riccò, R., Marinello, F., Carmignato, S. and Enrichi, F. (2011) 'Modified Stöber synthesis of highly luminescent dye-doped Silica nanoparticles.' *Journal of Nanoparticles Research*, 13(9) pp. 4349-4356.

Casciaro, S., Conversano, F., Ragusa, A., Malvindi, M.A., Franchini, R., Greco, A., Pellegrino, T. and Gigli, G. (2010) 'Optimal enhancement configuration of silica nanoparticles for ultrasound imaging and automatic detection at conventional diagnostic frequencies.' *Investigative Radiology*, 45(11) pp.715-724.

Celermajer, D.S. (1997) 'Endothelial Dysfunction: Does It Matter? Is It Reversible?' *Journal of the American College of Cardiology*, 30(2) pp.325-333.

Chandra, P., Das, D. and Abdelwahab, A.A. (2010) 'Gold Nanoparticles in Molecular Diagnostics and Therapeutic.' *Digest Journal of Nanomaterials and Biostructures*, 5(2) pp. 363 – 367.

Chawla, S J. and Mansoor. M. (2003) 'Cellular uptake and concentrations of tamoxifen upon administration in poly (ε-caprolactone) nanoparticles.' *American Association of Pharmaceutical Scientists*, 5(1) pp. 28–34.

Chien, C.-C., Chen, H.-H., Lai, S.-F., Hwu, Y., Petibois, C., Yang, C.S., Chu, Y. and Margaritondo G. (2012) 'X-ray imaging of tumor growth in live mice by detecting gold-nanoparticle-loaded cells.' *Scientific Reports*, 2, pp.610-616.

Chithrani, B.D, Ghazani, A.A., Warren, C.W. and Chan, W.C.W. (2006) 'Determining the Size and Shape Dependence of Gold Nanoparticle Uptake into Mammalian Cells.' *Nano letters*, 6(6) pp.662-668.

Cines, D.B. , Pollak, E. S., Buck C.A., Loscalzo, J., Zimmerman, G.A. , McEver, R.P., Pober, J. S., Wick, T.M., Konkle, B.A., Schwartz, B.S., Barnathan, E.S., McCrae, K.R., Hug, B.A., Schmidt, A. and Stern, D.M. (1998) 'Endothelial Cells in Physiology and in the Pathophysiology of Vascular Disorders.' *Blood*, 9(10) pp. 3527-3561.

Coats, P., Johnston, F., MacDonald, J., McMurray, J.J. and Hillier, C. (2001) 'Endothelium-derived hyperpolarizing factor: identification and mechanisms of action in human subcutaneous resistance arteries.' *Circulation*, 103(12) pp. 1702-1708.

Cooper, G.M. (ed.) (2000) 'The Cell: A Molecular Approach.' 2nd ed., Sunderland (MA): Sinauer Associates, Available on: http://www.ncbi.nlm.nih.gov/books/NBK9839/5March (Accessed: 4 December 2013).

Cortadellas N, Fernández, E and Garcia A. (2012) 'Biomedical and Biological Applications of SEM.' *Handbook of instrumental techniques from CCiTUB*, pp. 1-9.

Crist, R.M., Grossman, J.H., Patri, A.K., Stern, S.T., Dobrovolskaia, M.A., Adiseshaiah, P. P., Clogston, J. D. and McNeill, S. E. (2013) 'Common pitfalls in nanotechnology: lessons learned from NCI's Nanotechnology Characterization Laboratory.' *Integrative Biology*, 5, pp. 66-73.

Davda, J. and Labhasetwar, V. (2002) 'Characterisation of nanoparticles uptake by endothelial cells.' *International Journal of Pharmaceutics*, 233(1-2) pp. 51-59.

Davies, G.-L, Barry, A. Gun'ko, Y.K. (2009) 'Preparation and size optimization of silica nanoparticles using statistical analyses.' *Chemical Physics Letters*, 468 pp. 239–244.

Doane, T. and Burda, C. (2013) 'Nanoparticle mediated non-covalent drug delivery.' *Advanced Drug Delivery Review*, 65(5) pp. 607-621.

Dominguez-Medina, S., Blankenburg, J., Olson, J., Landes, C.F. and Link, S. (2013) 'Adsorption of a Protein Monolayer via Hydrophobic Interactions Prevents Nanoparticle Aggregation under Harsh Environmental Conditions.' *ACS Sustainable Chemistry and Engineering*, 1(7) pp.833-842.

Dragoni, S., Franco, G., Regoli, M., Bracciali, M., Morandi, V., Sgaragli, G., Bertelli, E. and Valoti, M.(2012) 'Gold nanoparticles uptake and cytotoxicity assessed on rat liver precision-cut slices.' *Toxicological sciences*, 128(1) pp. 186–197.

Duffin, R., Mills, L.N. and Donaldson, K. (2007) 'Nanoparticles-A Thoracic Toxicology Perspective.' *Yonsei Medical Journal*, 48(4) pp. 561–572.

Dukhin, A.S., Ulberg, Z.R., Karamushka, V.I. and Gruzina, T.G. (2010) 'Peculiarities of live cells' interaction with micro- and nanoparticles.' *Advances in Colloid Interface Science*, 159(1) pp. 60-71.

Dunlap, M. and Adaskaveg, J.E. (1997) 'Introduction to the Scanning Electron Microscope: Theory, Practice, & Procedures.' *Facility for advanced instrumentation, U. C. Davis.* pp. 1-50.

Dykman, L.A. and Khlebtsov, N.G. (2011) 'Gold Nanoparticles in Biology and Medicine: Recent Advances and Prospects.' *Acta Naturae*, 3(2) pp. 34–55.

Elmore, S. (2007) 'Apoptosis: A Review of Programmed Cell Death.' *Journal of Toxicologic and Pathology*, 35(4) pp. 495–516.

Estrela-Lopis, I., Romero, G., Rojas, E., Moya, S.E. and Donath, E. (2011) 'Nanoparticle uptake and their co-localization with cell compartments – a confocal Raman Microscopy study at single cell level.' *Journal of Physics: Conference Series*, 304: Article ID: e012017.

Evan, S., Cihui, Z., Amir, N., Hamir, Agatha borne, C., Shea Thompson and Steven A (2011) 'Biodistribution and acute toxicity of naked gold nanoparticles in a rabbit hepatic tumor model.' *Nanotoxicology*. 5(4) pp. 459-468.

Falcone, S., Cocucci, E., Podini, P., Kirchhausen, T., Clementi, E. and Hood, E., Simone, E., Wattamwar, P., Dziubla, T., and Muzykantov, V. (2011) 'Nanocarriers for vascular delivery of antioxidants.' *Nanomedicine*, 6(7) pp. 1257-1272.

Fang, R.H, Che-Ming Jack Hu C.-M.J. and Zhang L. (2012) 'Nanoparticles disguised as red blood cells to evade the immunesystem.' *Expert Opinion on Biological Therapy*, 12(4) pp. 385-389.

Farooq, A., Whitehead, D. and Azzawi, M. (2013) 'Attenuation of endothelial dependent vasodilator responses, induced by dye encapsulated silica NPs, in-vitro.' *Nanomedicine (Lond).* 9(3) pp. 413-425.

Figueroa, E. R., Lin, A.Y., Yan, J., Luo, L., Foster, A. E. and Drezek, R. A.(2014) 'Optimization of PAMAM-gold nanoparticle conjugation for gene therapy.'*Biomaterials.* 35(5) pp. 1725-1734.

Freese, C., Uboldi, C., Gibson, M. I., Unger, R.E., Weksler, B.B., Romero, I.A., Couraud, P.-O. and Kirkpatrick, C.J. (2012) 'Uptake and cytotoxicity of citrate-coated gold nanospheres: Comparative studies on human endothelial and epithelial cells.' *Particle and Fibre Toxicology*, 9(23) pp. 1-11.

Freese, C., Unger, R. E., Deller,R. C., Gibson, M. I., Brochhausen, C., Klok, H.-A. and Kirkpatrick, C.J. (2013) 'Uptake of poly(2-hydroxypropylmethacrylamide)-coated gold nanoparticles in microvascular endothelialcells and transport across the blood–brain barrier.' *Journal of Biomaterial Science*, 1(8) pp. 824-833.

Frens, G. (1973) 'Controlled nucleation for the regulation of theparticle size in monodisperse gold suspensions.' *Nature Physical Science*, 241, pp. 20–22.

Fritz, G., Schädler, V., Willenbacher, N. and Wagner, N.J. (2002) 'Electrosteric Stabilization of Colloidal Dispersions.' *Langmuir*, 18(16) pp. 6381-6390.

Fröhlich E. (2012) 'The role of surface charge in cellular uptake and cytotoxicity of medical nanoparticles.*' International Journal of Nanomedicine*, 7, pp. 5577-5591.

Fu, W., Shenoy, D., Li, J., Crasto. C., Jones. G., Dimarzio, C., Sridhar S. and Amiji, M. (2004) 'Biomedical Applications of Gold Nanoparticles Functionalized Using Hetero-Bifunctional Poly(ethylene glycol) Spacer.*' Material Research Society*, 845,pp. 1-6.

Fulton, D., Gratton, J.P., McCabe, T.J., Fontana, J., Fujio, Y., Walsh, K., Franke, T.F., Papapetropoulos, A. and Sessa, W.C. (1999) 'Regulation of endothelium-derived nitric oxide production by the protein kinase Akt.' *Nature*, 399(6736) pp. 597-601.

García, G.P., Sumbayev, V., Gilliland, D., Yasinska, I.M., Gibbs, B.F., Mehn, D., Calzolai, L. and Rossi, F. (2013) 'Microscopic Analysis of the Interaction of Gold Nanoparticles with Cells of the Innate Immune System.' *Scientific reports*, 1326 (3) pp. 1-7.

Gasaymeh, S.S., Radiman S., Heng, L.Y. and Saion E. (2010) 'Gamma Irradiation Synthesis and Influence the Optical and Thermal Properties of Cadmium Sulfide (CdS)/Poly (Vinyl Pyrolidone) Nanocomposites.' *American Journal of Applied Sciences*, 7(4) pp. 500-508.

Ghosh, P., Han, G., De, M., Kim, C. and Rotello, V. (2008) 'Gold nanoparticles in delivery applications.' *Advanced Drug Delivery Reviews*, 60(11) pp. 1307-1315.

Giesche, H. (1994) 'Synthesis of monodispersed silica powders I & particle properties and reaction kinetics. II. controlled growth reaction and continuous production process.' *Journal of the European Ceramic Society*, 14, pp. 189-15.

Glencross, H., Ahmed, N. and Wang, Q. (2011) 'Biomedical science practice: experimental and professional skills.' *Oxford University Press*, 7, pp. 1-342.

Gliga, A.R., Skoglund, R.., Wallinder, I. O., Fadeel, B. and Karlsson, H.L.(2014) 'Size-dependent cytotoxicity of silver nanoparticles in human lung cells: the role of cellular uptake, agglomeration and Ag release.' *Particle and Fibre Toxicology*, 11(11) pp.1-17.

Green D.L., Lin J.S., Lam Y.F., Hu M. Z.-C., Schaefer D.W. and Harris, M.T. (2003) 'Size, volume fraction, and nucleation of Stöber silica nanoparticles.' *Journal of Colloid and Interface Science*, 266(2) pp. 346–358.

Grzelczak, M., Mezzasalma S.A., Ni, W., Herasimenka, Y., Feruglio, L., Montini, T., Perez-Juste, J., Fornasiero P., Prato, M., and Liz-Marzan, L. M. (2012) 'Antibonding Plasmon Modes in Colloidal Gold Nanorod Clusters.' *Langmuir*, 28, pp. 8826–8833.

Gu, H., Xu, K., Xu, C. and Xu, B. (2006) 'Biofunctional magnetic nanoparticles for protein separation and pathogen detection.' *Chemical Communications (Cambridge, England)*, 7(9) pp. 941-949.

Guerrero, S., Herance, J.R., Rojas, S., Mena, J. F., Gispert, J. D., Acosta, G. A., Albericio, F. and Kogan, M. J. (2012) 'Synthesis and in vivo evaluation of the biodistribution of an 18F-labeled conjugate gold-nanoparticle-peptide with potential biomedical application.' *Bioconjugate Chemistry*, 23(3) pp. 399-408.

Guo, X., Razandi, M., Pedram, A., Kassab, G. and Levin, E.R. (2005) 'Estrogen induces vascular wall dilation: mediation through kinase signaling to nitric oxide and estrogen receptors alpha and beta.' *The Journal of Biological Chemistry*, 280(20) pp. 19704-19710.

Hachani, R., Lowdell, M., Birchall, M. and Thanh, N. T. (2013) 'Tracking stem cells in tissue-engineered organs using magnetic nanoparticle.' *Nanoscale*, 5(23) pp. 11362-11373.

Haidekker, A.M., Boettcher, L.W., Suter, L.D., Rone, R. and Grant, S.A. (2006) 'Influence of gold nanoparticles on collagen fibril morphology quantified using transmission electron microscopy and image analysis.' *BMC Medical Imaging*, 6(4) pp. 1-7.

Hainfeld, J.F., Slatkin, D.N., Focella, T.M. and Smilowitz, H.M. (2006) 'Gold nanoparticles: a new X-ray contrast agent.' *British Journal of Radiology*, 79(939) pp. 248–253.

Haiss, W., Thanh, T.K.N., Aveyard, J. and Fernig, D.G. (2007) 'Determination of Size and Concentration of GoldNanoparticles from UV-Vis Spectra.' *Analytical chemistry*, 79(11) pp. 4215-4221

Hao, X., Wu, J., Shan,Y., Cai, M., Shang, X., Jiang, J. and Wang H. (2012) 'Caveolae-mediated endocytosis of biocompatible gold nanoparticles in living Hela cells.*' Journal of Physics: Condensed Matter*, 24(16) pp. 164207.

Hartung, G.A. and Mansoori, G.A. (2013) 'In vivo General Trends, Filtration and Toxicity of Nanoparticles.' *Journal of Nanomaterial and Molecular Nanotechnology*, 2(3) pp.1-21.

Harush-Frenkel, O., Debotton, N., Benita, S. and Altschuler, Y. (2007) 'Targeting of nanoparticles to the clathrin-mediated endocytic pathway.' *Biochemical Biophysical Research Communications*, 353(1) pp. 26-32.

Hauck, T.S., Ghazan, A.A. and Chan, C.W. (2008) 'Assessing the Effect of Surface Chemistry on Gold Nanorod Uptake, Toxicity, and Gene Expression in Mammalian Cells.' *Small*, 4(1) pp. 153–159.

Haynes, W. M. (2012) 'CRC Handbook of Chemistry and Physics, 93rd Edition 2012-2013.' Section 8: Analytic chemistry, *Taylor and Francis group, CRC press, FL*, pp.1-2664.

He, W., Zhou, Y.T., Wamer, W. G., Hu, X., Wu, X., Zheng, Z., Boudreau, M.D. and Yin, J.J. (2013) 'Intrinsic catalytic activity of Au nanoparticles with respect to hydrogen peroxide decomposition and superoxide scavenging.' *Biomaterials*, 34(3) pp.765-773.

Hench, L.L. and West, J. K. (1990) 'The Sol-Gel Process.' *Chemical Reviews*, 90(1) pp. 33-72.

Hsiai, T.K, (2008) 'Mechanosignal transduction coupling between endothelial and smooth muscle cells: role of hemodynamic forces.' *American journal of physiology-cell physiology*, 294(3) pp.659–661.

Hu, J., Wang, Z. and Li, J. (2007) 'Gold Nanoparticles with Special Shapes: Controlled Synthesis, Surface-enhanced Raman Scattering, and The Application in Biodetection.' *Sensors*, 7(12) pp. 3299-3311.

Hu, L., Mao, Z. and Gao, C. J. (2009) 'Colloidal particles for cellular uptake and delivery.' *Journal of Materials Chemistry*, 19(20) pp.3108–3115.

Huang, S., Li, R., Qu, Y., Shen, J. and Liu, J. (2009) 'Fluorescent Biological Label for Recognizing Human Ovarian Tumor Cells Based on Fluorescent.' *Journal of fluorescence*. , 19(6), 1095-101.

Hubbard, A.T. (ed.) (2002) 'Encyclopedia of Surface and Colloid Science: Por-Z.' *CRC Press*, pp.1-5667.

Huo, S., Jin, S., Ma, X., Xue, X., Yang, ,K., Kumar, A., Wang, P.C. Zhang, J., Hu, Z. and Liang, X.-J. (2014) 'Ultrasmall Gold Nanoparticles as Carriers for Nucleus-Based Gene Therapy Due to Size-Dependent Nuclear Entry.' *ACS Nano*, 8 (6) pp. 5852–5862.

Ignarro, L.J. (2000) ' Nitric oxide: biology and pathobiology.' *Academic Press*, pp. 606-611.

Jackson, T. and Zheng, X. (2010)' A Cell-based Model of Endothelial Cell Migration, Proliferation and Maturation During Corneal Angiogenesis.' *Bulletin of Mathematical Biology*, 72(4) pp. 830-868.

Jain, S., Hirst, D.G. and O'Sullivan, J.M. (2012) 'Gold nanoparticles as novel agents for cancer therapy.' *British Journal of Radiology*, 85(1010) pp. 101–113.

Jeffery, N.D., McBain, S.C., Dobson, J. and Chari, D.M. (2009) 'Uptake of systemically administered magnetic nanoparticles (MNPs) in areas of experimental spinal cord injury (SCI)', *Journal of Tissue Engineering and Regenerative Medicine*, 3(2), 153-160.

Jeon, I.–Y. and Baek, J.-B. (2010) 'Nanocomposites Derived from Polymers and Inorganic Nanoparticles.' *Materials*, 3, pp. 3654-36.

Jiang, Y., Yan, Y.B., and Zhou, H.M. (2006) 'Polyvinylpyrrolidone 40 assists the refolding of bovine carbonic anhydrase B by accelerating the refolding of the first molten globule intermediate.' *Journal of Biological Chemistry*; 281, pp. 9058-65.

Jong, W.H.D and Borm, P.J.A. (2008) 'Drug delivery and nanoparticles: Applications and hazards.' *International Journal of Nanomedicine*, 3(2) pp. 133–149.

Jong,W.H.D., Burger, M.C., Verheijen, M.A. and Geertsma, R. E. (2010) 'Detection of the Presence of Gold Nanoparticles in Organs by Transmission Electron Microscopy.' *Materials*, 3(9) pp. 4681-4694.

Jorgensen, T.D., Dissing, S. and Gromada, J. (1996) 'Cyclic GMP potentiates phenylephrine but not cyclic ADP-ribose-evoked calcium release from rat lacrimal acinar cells.' *Elsevier Science B.V*, 391(1-2) pp. 117-120.

Kalishwaralal, K., Sheikpranbabu, S., BarathManiKanth, S., Haribalaganesh, R., Ramkumarpandian, S. and Gurunathan, S. (2011) 'Gold nanoparticles inhibit vascular endothelial growth factor-induced angiogenesis and vascular permeability via Src dependent pathway in retinal endothelial cells.' *Angiogenesis*, 14(1) pp.29-45.

Kamaly, N., Xiao, Z., Valencia, P. M., Radovic-Moreno, A. F.and Farokhzad, O. C. (2012) 'Targeted polymeric therapeutic nanoparticles: design, development and clinical translation.' *Chemical Society Reviews*, 41(7) pp. 2971-3010.

Kasper, J., Hermanns, M.I., Bantz, C., Utech, S.,Koshkina, O., Maskos, M., Brochhausen, C., Pohl, C., Fuchs, S.,Unger, R.E. and Kirkpatrick, J. (2013) 'Flotillin-involved uptake of silica nanoparticles and responses of an alveolar capillary barrier in vitro.' *European Journal of Pharmaceutics and Biopharmaceutics*, 84(2), pp. 275-287.

Kealey, D. and Haines, P. J. (2002) 'Instant notes: analytical chemistry.' *BIOS Scientific Publishers Limited*, 7, pp. 1-342.

Kempson, I. M., Chien, C.C., Chung, C.Y., Hwu, Y., Paterson, D., de Jonge, M.D. and Howard, D.L. (2012) 'Fate of intravenously administered gold nanoparticles in hair follicles: follicular delivery, pharmacokinetic interpretation, and excretion.' *Advanced Healthcare Materials*, 1(6) pp. 736-741.

Khan, H.A., Abdelhalim, M.A.K., Al-Ayed, M.S. and Alhomida, A.S. (2012) 'Effect of gold nanoparticles on glutathione and malondialdehyde levels in liver, lung and heart of rats.' *Saudi Journal of Biological Sciences*, 19(4) pp. 461–464.

Kim, D., Park, S., Lee, J. H., Jeong, Y. Y., and Jon, S. (2007) 'Antibiofouling polymer-coated gold nanoparticles as a contrast agentfor in vivo X-ray computed tomography imaging.' *Journal of the American Chemical Society*, 129, pp. 7661–7665.

Kim, E.-Y., Schulz, R., Swantek, P., Kunstman, K., Malim, M.H. and Wolinsky, S.M. (2012) 'Gold nanoparticle-mediated gene delivery induces widespread changes in the expression of innate immunity genes.' *Gene Therapy*, 19, pp. 347-353.

Kim, J. S., Yoon, T. J., Yu, K. N., Noh, M. S., Woo, M., Kim, B. G., Lee, K. H., Sohn, B. H., Park, S. B., Lee, J. K. and Cho, M. H. (2006) 'Cellular uptake of magnetic nanoparticle is mediated through energy-dependent endocytosis in A549 cells.' *Journal of Veterinary Science*, 7(4) pp. 321-326.

Kimling, J., Maier, M., Okenve, B., Kotaidis, V., Ballot, H. and Plech, A. (2006) 'Turkevich Method for Gold Nanoparticle Synthesis Revisited.' *Journal of Physical Chemistry B*, 110(32) pp. 15700–15707.

Kirby, B.J and Hasselbrink E.F. (2004) 'Zeta potential of microfluidic substrates:1.Theory, experimental techniques, and effects on separations.' *Electrophoresis*, 25, pp. 187–202.

Kirkham, M. and Parton, R.G. (2005) 'Clathrin-independent endocytosis: New insights into caveolae and non-caveolar lipid raft carriers.' *Biochimica et Biophysica Acta (BBA) - Molecular Cell Research*, 1746(3) pp.350–363.

Kluger, M.S. (2004) 'Vascular Endothelial Cell Adhesion and Signaling During Leukocyte Recruitment.' *Advances in Dermatology*, 20, pp. 163-200.

Klumpp, C., Kostarelos, K., Maurizio Prato., M. and Bianco, A. (2006) 'Functionalized carbon nanotubes as emerging nanovectors for the delivery of therapeutics.' *Biochimica et Biophysica Acta (BBA) – Biomembranes*, 1758(3) pp. 404–412.

Knop, K., Hoogenboom, R., Fischer. D. and Schubert U.S. (2010) 'Poly(ethylene glycol) in drug delivery: pros and cons as well as potential alternatives.' *Angewanted Chemie International Edition* (English), 49(36) pp. 6288-6308.

Koffie, R.M., Farrar, C.T., Saidi, L.-S., William, C.M., Hyman, B.T. and Spires-Jones, T.L. (2011) 'Nanoparticles enhance brain delivery of blood–brain barrier-impermeable probes for in vivo optical and magnetic resonance imaging.' *Proceedings of the National Academy of Sciences*, 108(46) pp. 18837–18842.

Kolluru G. K., Bir, S. C. and Kevil, C. G. (2012) 'Endothelial Dysfunction and Diabetes: Effects on Angiogenesis, Vascular Remodeling, and Wound Healing.' *International Journal of Vascular Medicine*, 2012, pp. 1-30.

Krpetić. Z., Porta. F., Caneva, E., Dal Santo, V. and Scarì, G. (2010) 'Phagocytosis of biocompatible gold nanoparticles.' *Langmuir*, 26(18) pp. 14799-14805.

Kumar, D. P., Subas, D., Subrata, C. and Soumen, R. (2012) 'Formulation and Evaluation of Solid Lipid Nanoparticles of a Poorly Water Soluble Model Drug, Ibuprofen.' *International Research Journal of Pharmacy*, 3(12) pp. 132-137.

Lake, C. L. (2004) 'Pediatric cardiac anesthesia.' 4th ed. Booker *PD Lippincott Williams & Wilkins*, pp. 1-786.

Larese, F. F., D'Agostin, F., Crosera, M., Adami, G., Renzi, N., Bovenzi, M. and Maina, G. (2009) 'Human skin penetration of silver nanoparticles through intact and damaged skin.' *Toxicology*, 255, pp. 33-37.

LeBlanc, A. J., Moseley, A. M., Chen, B. T., Frazer, D., Castranova, V. and Nurkiewicz, T. R. (2010) 'Nanoparticle inhalation impairs coronary microvascular reactivity via a local reactive oxygen species-dependent mechanism.' *Cardiovascular Toxicology*, 10, pp. 27-36.

Lee, K., Cui, Y., Lee, L. P., and Irudayaraj, J. (2014) 'Quantitative imaging of single mRNA splice variants in living cells.' Nature Nanotechnology, 9, pp. 474–480.

LeRoy, C. and Wrana, L. (2005) 'Clathrin mediated Endocytic Regulation of cell signalling.' *Nature Reviews Molecular Cell Biology*, 6, pp. 112-126.

Lewinski, N., Colvin, V. and Drezek, R. (2008) 'Cytotoxicity of nanoparticles.' *Small,* 4(1) pp. 26-49.

Liao, L., Liu, J., Dreaden, E. C., Morton, S. W., Shopsowitz, K. E., Hammond, P. T. and Johnson. J. A. (2014) 'A Convergent Synthetic Platform for Single-Nanoparticle Combination Cancer Therapy: Ratiometric Loading and Controlled Release of Cisplatin, Doxorubicin, and Camptothecin.' *Journal of the American Chemical Society*, 136(16) pp. 5896-5899.

Libutti, S. K., Paciotti, G. F., Byrnes, A. A., Alexander, H. R., Gannon, Jr. W. E., Walker, M., Seidel, G. D.,Yuldasheva, N. and Tamarkin, L. (2010) 'Phase I and Pharmacokinetic Studies of CYT-6091, a Novel PEGylated Colloidal Gold-rhTNF.' *Nanomedicine clinical cancer research*, 16(21) pp. 6139-6149.

Lim, J., Yeap, S.P., Che H.X. and Low, S.C. (2013) 'Characterization of magnetic nanoparticle by dynamic light scattering.' *Nanoscale Research Letters*, 8, pp. 381-425.

Lin, A., Sabins, A., Kona, S., Nattama, S., Patel, H., Dong, J. F. and Nguyen, K. T. (2010) 'Shear regulated uptake of nanoparticles by endothelial cells and development of endothelial-targeting nanoparticles.' *Journal of Biomedical Materials Research Part A*, 93(3) pp.833-842.

Lin, I.-C., Liang, M., Liu, T.-Y., Monteiro, M.J. and Toth, I. (2012) 'Cellular transport pathways of polymer coated gold nanoparticles.' *Nanomedicine: Nanotechnology, Biology and Medicine*, 8(1) pp. 8–11.

Liongm, M., Zinkm, J.I. and Tamanoi, F. (2007) 'Mesoporous silica nanoparticles as a delivery system for hydrophobic anticancer drugs.' *Small Journal*, 3, pp. 1341-1346.

Lipka, J., Semmler-Behnke, M., Sperling, R. A., Wenk, A., Takenaka, S., Schleh, C., Kissel, T., Parak, W.J.and Kreyling, W..G. (2010) 'Biodistribution of PEG-modified gold nanoparticles following intratracheal instillation and intravenous injection.' *Biomaterials*, 31(25) pp. 6574-81.

Liu, C. and Zhang, N. (2011) 'Nanoparticles in gene therapy principles, prospects, and challenges.' *Progress in molecular biology and translational science*, 104, pp. 509-571.

Liu, Q., Liu, H., Zhou, Q., Liang, Y., Yin, G. and Xu, Z. (2006) 'Synthesis of nearly Monodispersive gold nanoparticles by a sodium diphenylamine sulfonate reduction process.' *Journal of Materials Science*, 41, pp. 3657-3662.

Liu, Y., Shipton, M.K., Ryan, J., Kaufman, E.D., Franzen, S. and Feldheim, D.L. (2007) 'Synthesis, Stability, and Cellular Internalization of Gold Nanoparticles Containing Mixed Peptide−Poly (ethylene glycol) Monolayers.' *Analytical Chemistry*, 79(6) pp. 2221–2229.

Lodish, H., Berk, A., Zipursky, S.L., Matsudaira, P., Baltimore, D. and Darnell, J. (2000) 'Molecular Cell Biology.' 4th ed., New York: W.H. Freeman; Section 20.1, *Overview of Extracellular Signaling*. Available on: http://www.ncbi.nlm.nih.gov/books/NBK21475.

Malvern; Available on: http://www.malvernstore.com/cnb/shop/malvern?productID=11&op=catalogue-product_info-null&prodCategoryID=7 (Accessed: 29 November 2013).

Manke, A., Wang, L. and Rojanasakul, Y. (2013) 'Mechanisms of Nanoparticle-Induced Oxidative Stress and Toxicity.' *Biomedical Research International*, 2013, pp. 1-15.

Manson, J., Kumar, D., Meenan, B.J. and Dixon, D. 2011 'Polyethylene glycol functionalized gold nanoparticles: the influence of capping density on stability in various media.' *Gold Bulletin*, 44(2) pp. 99-105.

Marcelo, K.L., Goldie, L.C. and Hirschi, K.K. (2013) 'Regulation of endothelial cell differentiation and specification.' *Circulation Research*, 112(9) pp. 1272-1287.

Marín-García, J. (2012) 'Mitochondria and Their Role in Cardiovascular Disease.' *Springer*, USA, pp.1-519.

Martines, M.U, Yeung, E., Persin, M., Larbot, A., Voorhout, W.F., Kübel, C.K.U., Kooyman, P. and Prouzet, E. (2005) 'Hexagonal mesoporous silica nanoparticles with large pores and a hierarchical porosity tested for HPLC.' *C. R. Chimie* 8, pp. 627-634.

McCarron, G.J., Bradely, K.N. and Muir, T.C. (2003) 'Ca $^{2+}$ signalling and Ca $^{2+}$ activated K^{+} in smooth muscle' in Chadwick, J. D. and Goodie, J. A. (e.ds.) Role of the Sarcoplasmic Reticulum in Smooth Muscle, Novartis Foundation Symposia: Devon, *John Wiley & Sons*, pp. 52-64.

McIntyre, M. and Dominiczak, A.F. (1997) 'Nitric oxide and cardiovascular disease.' *Postgraduate Medical Journal*, 73, pp. 630- 634.

Meldolesi, J. (2006) Macropinocytosis: regulated coordination of endocytic and exocytic membrane traffic events.' *Journal of Cell Science*, 119(22) pp. 4758-4769.

Miao, B. and Degterev, A. (2009) 'Methods to analyze cellular necroptosis.*' Methods in Molecular Biology*, 559, pp.79-93.

Mironava, T., Hadjiargyrou, M., Simon, M., Jurukovsk, V. and Rafailovich, M.H. (2010) 'Gold nanoparticles cellular toxicity and recovery: Effect of size, concentration and exposure time.' *Nanotoxicology*, 4 (1) pp. 120-137.

Mody, V., Siwale, R., Singh, A. and Mody, H. R. (2010) 'Introduction to metallic nanoparticles.'*Journal of pharmacy & bioallied sciences*, 2(4) pp. 282-289.

Moran, C.H., Rycenga, M., Zhang, Q. and Xia, Y. (2011) 'Replacement of Poly(vinyl pyrrolidone) by Thiols: A Systematic Study of Ag Nanocube Functionalization by Surface-Enhanced Raman Scattering.' *Journal of physical chemistry. C, Nanomaterials and interfaces*, 115(44): 21852–21857.

Mukherjee, P., Bhattacharya, R., Bone, N., Yean, K., Lee, Y. K., Patra, C. R., Wang, S., Lu, L., Secreto, C., Banerjee, P.C., Yaszemski, M. J., Kay, N. E. and Mukhopadhyay, D. (2007) 'Potential therapeutic application of gold nanoparticles in B-chronic lymphocytic leukemia (BCLL): enhancing apoptosis.' *Journal of Nanobiotechnology*, 5(4) pp. 1-13.

Mukherjee, P., Bhattacharya, R., Wang, P., Wang, L., Basu, S. and Nagy, J. A. (2005) 'Antiangiogenic Properties of Gold Nanoparticles.' *Clinical Cancer Research*, 11(9) pp. 3530-3535.

Mulvany M.J. and Aalkjaer, C. (1990) 'Structure and function of small arteries.' *Physiological. Reviews,* 70, pp. 921-961.

Mulvany, M.J. (2002) 'Small Artery Remodeling and Significance in the Development of Hypertension News in Physiological Sciences.' *News in physiological sciences,* 17, pp.105-109.

Murawska, M., Skrzypczak A. and Kozak, M. (2012) 'Structure and Morphology of Gold Nanoparticles in Solution Studied by TEM, SAXS and UV-Vis.' *Acta Physica Polonica A*, 121(4) pp. 888-892.

Murphy, C.J., Gole, A. M., Stone, J.W., Sisco, P.N., Alkilany, A. M., Goldsmith, E. C. and Baxter, S. C. (2008) 'Gold nanoparticles in biology: beyond toxicity to cellular imaging.' *Accounts of chemical Research,* 41, pp. 1721–1730.

Nasser, T.K., Wilensky, R.L., Mehdi, K. and March, K.L. (1996) 'Microparticle deposition in periarterial microvasculature and intramural dissections after porous balloon delivery into atherosclerotic vessels: quantitation and localization by confocal scanning laser microscopy.' *American Heart Journal*, 131(5) pp. 892-898.

Nativo, P., Prior, I.A. and Brust, M. (2008) 'Uptake and Intracellular Fate of Surface-Modified Gold Nanoparticles.' *ACSNano*, 2(8) pp. 1639–1644.

Ng, C.T., Li, J.J., Perumalsamy, R., Watt, F., Yung, L.Y.L. and Bay, B.H. (2010) 'Localizing cellular uptake of nanomaterials in vitro by transmission electron microscopy' in Microscopy: Science, Technology, Applications and Education Méndez-Vilas, A. and Díaz, J. *Formatex*, pp. 316-320.

Ngadi, N., Abrahamson, J., Fee, C. and Morison, K. (2000) 'QCM-D Study on Relationship of PEG CoatedStainless Steel Surfaces to Protein Resistance.' *International Journal of Chemical and Biological Engineering*, 1(3) pp. 125-129.

Nitta, S.K. and Numata, K. (2013) 'Biopolymer-Based Nanoparticles for Drug/Gene Delivery and Tissue Engineering.' *International Journal of Molecular Sciences*, 14(1) pp. 1629-1654.

Nitzsche, R. and Connah, M. (2012). The use of the Malvern Zetasizer for the measurement of Zeta Potential. Available on: http://www.silver-colloids.com/Tutorials/Intro/zetaintro.html (Accessed: 2nd March 2014).

Nune, S.K., Gunda, P., Thallapally, P.K., Lin. Y.-Y., Forrest, M.L. and Berkland, C. J. (2009) 'Nanoparticles for biomedical imaging.' *Expert Opinion on Drug Delivery*, 6(11) pp. 1175–1194.

Nurkiewicz T.R., Porter, D.W., Hubbs, A.F., Stone, S., Chen, B.T., Frazer, D.G., Boegehold, M.A. and Castranova, V. (2009) 'Pulmonary Nanoparticle Exposure Disrupts Systemic Microvascular Nitric Oxide Signaling.' *Toxicological Sciences*, 110(1) pp. 191-203.

O'Neal, D.P., Hirsch, L.R., Halas, N.J., Payne, J.D. and West, J.L. (2004) 'Photo-thermal tumor ablation in mice using near infrared-absorbing nanoparticles.' *Cancer Letter*, 209, pp. 171–176.

Oberdorster, G., Maynard, A., Donaldson, K., Castranova, V., Fitzpatrick, J., Ausman, K., Carter, J., Karn, B., Kreyling, W., Lai, D., Olin, S., Monteiro-Riviere, N., Warheit, D. and Yang, H. (2005) 'Principles for characterizing the potential human health effects from exposure to nanomaterials: elements of a screening strategy.' *Particle and Fibre Toxicology*. 2, pp. 8-21.

Oh, E., Delehanty, J.B., Sapsford, K.E., Susumu, K., Goswami, R., Blanco-Canosa J.B., Dawson, P.E., Granek, J., Shoff, M., Zhang, Q., Goering, P.L., Huston, A. and Medintz, I.L. (2011) 'Cellular uptake and fate of PEGylated gold nanoparticles is dependent on both cell-penetration peptides and particle size.' *ACS Nano*, 5(8) pp. 6434-48.

Ojea-Jiménez, I. and Campanera, J.M. (2012) 'Molecular Modeling of the Reduction Mechanism in the Citrate-Mediated Synthesis of Gold Nanoparticles.' *Journal of Physical Chemistry C*, 116(44) pp. 23682-23691.

Ojea-Jiménez, I. and Puntes, V. (2009) 'Instability of Cationic Gold Nanoparticle Bioconjugates: The Role of Citrate Ion.' *Journal of the American Chemical Society*, 131(37) pp. 13320-13327.

Panariti, A., Miserocchi, G. and Rivolta I. (2012) 'The effect of nanoparticle uptake on cellular behavior: disrupting or enabling functions?' *Nanotechnology, Science and Applications*, 5, pp. 87–100.

Pandey, R., Sharma, S. and Khuller, G.K. (2006) 'Oral poly(lactide-co-glycolide) nanoparticle based antituberculosis drug delivery:Toxicological and chemotherapeutic implications.' *Indian Journal of Experimental Biology*, 44, pp. 459-467.

Panza, J.A., García, C.E., Kilcoyne, C.M., Quyyumi, A.A. and Cannon, R.O. (1995) 'Impaired Endothelium-Dependent Vasodilation in Patients With Essential Hypertension Evidence That Nitric Oxide Abnormality Is Not Localized to a Single Signal Transduction Pathway.' *Circulation*, 91, pp. 1732-1738.

Papapetropoulos, A., Rudic, R.D. and Sessa W.C., (1999) 'Molecular control of nitric oxide synthases in the cardiovascular system.' *Cardiovascular Research*, 43(3) pp. 509-520.

Park W and Borsa T. (2004) 'Synthesis and Self-Assembly of Metal-Coated Nanoparticles.' *Materials Research Society Symposium Proceedings*, 820, pp. 289-294.

Park, E.J. and Park, K. (2009) 'Oxidative stress and pro-inflammatory responses induced by silica nanoparticles in vivo and in vitro.' *Toxicology Letters*, 84(1) pp. 18-25.

Park, S.K., Kim K. D. and Kim H. T. (2007) 'Preparation of silica nanoparticles: determination of the optimal synthesis conditions for small and uniform particles.' *Colloids and Surfaces A*, 197, pp. 7–17.

Pellach, M., Goldshtein, J., Ofra Ziv-Polat, O. and Margel, S. (2012) 'Functionalised, photostable, fluorescent polystyrene nanoparticles of narrow size-distribution.' *Journal of Photochemistry and Photobiology A: Chemistry*, 228, pp. 60– 67.

Pennycook, S.J. and Nellist, P.D. (2011) 'Scanning transmission electron microscopy: imaging and analysis.' *Springer New York*, pp. 1-762.

Pérez-Martínez, F.C., Carrión, B. and Ceña, V. (2012) 'The use of nanoparticles for gene therapy in the nervous system.' *Journal of Alzheimer's disease*, 31(4), 697-710.

Pleger, S.T., Harris, D.M., Shan, C., Vinge, L.E., Chuprun, J. K., Berzins, B., Pleger,W., Druckman, C., Volkers, M., Heierhorst, J., Øie, E., Remppis, A., Katus, H. A., Scalia, R., Eckhart, A. D., Koch, W.J and Most, P. (2008) 'Endothelial S100A1 Modulates Vascular Function via Nitric Oxide.' *Circulation Research*, 102, pp. 786-794.

Qiu, P. and Mao, C. (2010) 'Biomimetic branched hollow fibers templated by self-assembled fibrous polyvinylpyrrolidone structures in aqueous solution.' *ACS Nano*, 4 (3) pp. 1573–1579.

Rahman, I.A. and Padvettan, V. (2012) 'Synthesis of silica nanoparticles by sol gel: size-dependent properties, surface modification, and application in silica-polymer nanocomposities-a review.' *Journal of Nanomaterials*, pp. 1-15.

Rahman, M., Laurent, S., Tawil, N., Yahia, L., Mahmoudi, M. (2013) 'Protein-Nanoparticle Interactions.' *Springer Series in Biophysics*, 15, pp. 21-24.

Ranghar, S., Sirohi, P., Verma, P. and Agarwal, V. (2014) 'Nanoparticle-based Drug Delivery Systems: Promising Approaches Against Infections.' *Brazilian Archives Of Biology And Technology*, 57(2) pp. 209-222.

Rauch, J., Kolch, W. and Mahmoudi, M. (2012) 'Cell Type-Specific Activation of AKT and ERK Signaling Pathways by Small Negatively-Charged Magnetic Nanoparticles.' *Scientific Reports*, 2, Article ID 868.

Razink, J.J. and Schlotter, N.E. (2007) 'Correction to 'Preparation of monodisperse silica particles: Control of size and mass fraction' by G.H. Bogush, M.A. Tracy and C.F. Zukoski IV, *Journal of Non-Crystalline Solids*, 104, (1988) 95–106.' *Journal of Non-Crystalline Solids*, 353, pp. 2932-2933.

Robinson, B.V., Sullivan, F.M., Borzelleca, J.F. and Schwartz, S.L. (1990) 'PVP: A Critical Review of the Kinetics and Toxicology of Polyvinylpyrrolidone (Povidone).' *Lewis Publishers*, Chelsea, MI, pp. 1-209.

Roesslein, M., Hirsch, C., Kaiser, J.-P., Krug, H.F. and Wick, P. 'Comparability of in Vitro Tests for Bioactive Nanoparticles: A Common Assay to Detect Reactive Oxygen Species as an Example.' *International Journal of Molecular Sciences*.2013, 14(12) pp. 24320-2433.

Rosas-Hernandez, H., Jimenez-Badillo, S., Martinez- Cuevas, P.P., Gracia- Espino, E., Terrones, H., Terrones, M., Hussain, S.M., Ali, S.F. and Gonzalez, C. (2009) 'Effects of 45-nm silver nanoparticles on coronary endothelial cells and isolated rat aortic rings.*' Toxicology letters*, 191(2-3) pp. 305-313.

Ross, M.H. and Pawlina, W. (2010) Histology: A Text and Atlas. 6th e.d., Minnesota: *Lippincott Williams & Wilkins.* pp. 1-974.

Rouse, J. G., Yang, J., Ryman-Rasmussen, J. P., Barron, A. R. and Monteiro-Riviere, N. A. (2007) 'Effects of Mechanical flexion on the penetration of fullerene amino acid-derivatized peptide nanoparticles through skin*.' Nano Letters*, 7, pp. 155-160.

Roux, P. P. and Blenis, J. (2004) 'ERK and p38 MAPK-Activated Protein Kinases: a Family of Protein Kinases with Diverse Biological Functions.' *Microbiology and Molecular Biology Reviews*, 68(2) pp. 320-344.

Saltzman, W.M. (2000) 'Cell interactions with polymers In Textbook of Tissue Engineering.' 2nd edition, Lanza, R.P., Langer, R. and Vacanti, J. (Ed.), *Academic Press*, NY, pp. 221-235.

Saptarshi, S.R., Duschl, A. and Lopata, A.L. (2013) 'Interaction of nanoparticles with proteins: relation to bio-reactivity of the nanoparticle.' *Journal of Nanobiotechnology,* 11(26) pp. 1-12.

Sato, S., Miyake, M., Hazama, A. and Omori, K. (2014) 'Povidone-iodine-induced cell death in cultured human epithelial HeLa cells and rat oral mucosal tissue.' *Drug and Chemical Toxicology*, 37(3) pp. 268-275.

Sattar, A., Rooney, P., Kumar, S., Pye, D., West, D.C., Scott, I. and Ledger, P. (1994) 'Application of angiogenic oligosaccharides of hyaluronan increases blood vessel numbers in rat skin.' *Journal of Investigative Dermatology*, 103, pp. 576-579.

Schaper, W. and Buschman, I. (1999) 'Anteriogenesis, the good and bad of it.' *Cardiovascular Research*, 43, pp. 835−837.

Schiffrin E.L. (1998) 'Remodeling of Resistance Arteries in Hypertensive Patients: Effects of Antihypertensive Therapy.' *Scandinavian cardiovascular journal*, 32(2) pp. 15 – 21.

Schneider, M., Stracke, F., Hansen, S. and Schaefer, U.F. (2009) 'Nanoparticles and their interactions with the dermal barrier.' *Dermatology-Endocrinology*, 1, pp. 197 – 206.

Schroeder, A., Goldberg, M.S., Kastrup, C., Wang, Y., Jiang, S., Joseph, B.J., Levins, C.G., Kannan, S.T., Langer, R. and Anderson, D.G. (2012) 'Remotely activated protein-producing nanoparticles.' *Nano Letters*, 12(6) pp. 2685-2689.

Schubert, R., Krien U., Wulfsen I., Schiemann, D., Lehmann, G., Ulfig, N., Veh, R.W., Schwarz, J.R. and Gago, H. (2004) 'Nitric oxide donor sodium nitroprusside dilates rat small arteries by activation of inward rectifier potassium channels.' *Hypertension*, 43(4) pp. 891-896.

Seebergh J.E. and Berg, J.C. (1994) 'Depletion flocculation of aqueous, electrosterically-stabilized latex dispersions.' *Langmuir*, 10(2) pp. 454–463.

Selim, M.E. and Hendi, A.A. (2012) 'Gold Nanoparticles Induce Apoptosis in MCF-7 Human Breast Cancer Cells.' *Asian Pacific Journal of Cancer Prevention*, 13(4) pp. 1617-1620.

Seol, S.K., Kim, D., Jung, S., Chang, W.S. and Kim, J.T. (2013) 'One-Step Synthesis of PEG-Coated Gold Nanoparticles by Rapid Microwave Heating.' *Journal of Nanomaterials*, (2013), Article ID 531760.

Shah, V., Shah, S., Shah, H., Rispoli, F.J., McDonnell, K. T., Workeneh, S., Karakoti, A., Kumar, A. and Seal, S. (2012) 'Antibacterial Activity of Polymer Coated Cerium OxideNanoparticles.' *Plos One*, 7(10) pp. 47827-473.

Sharma. M. and Yashonath, S. (2007) 'Size Dependence of Solute Diffusivity and Stokes-Einstein Relationship: Effect of van der Waals Interaction', *Diffusion Fundamentals*, 6, pp. 1-15.

Shaw, D. J. (1992) 'Introduction to Colloid & Surface Chemistry.' 4th ed, *Butterworth Heinemann*, pp. 1-306.

Shaw P.J. (2006) 'Comparison of Widefield/Deconvolution and Confocal Microscopy for Three-Dimensional Imaging, Chapter 23 1-467.' Handbook of Biological Confocal Microscopy, 3rd ed, James B. Pawley, (E.d), *SpringerScience and Business Media*, New York.

Shenoi, M. M., Shah, N.B., Griffin, R.J., Vercellotti, G.M. and Bischof, J.C. (2011) 'Nanoparticle preconditioning for enhanced thermal therapies in cancer.' *Nanomedicine*, 6(3) pp. 545-63.

Shukur, A., Rizvi, S.B., Whitehead, D., Seifalian, A. and Azzawi, M. (2013) 'Altered sensitivity to nitric oxide donors, induced by intravascular infusion of quantum dots, in murine mesenteric arteries.' *Nanomedicine: Nanotechnology, Biology, and Medicine*, 9(4) pp. 532-539.

Silva, B.R., Lunardi, C.N., Araki, K., Juliana, C., Silva, D., Lusiane, M. and Bendhack. (2014) 'Gold nanopartical modifies nitric oxide release and vasodilation in rat aorta.' *Journal of Biological Chemistry*, 7, pp. 57-65.

Singh, M., Kumar, M., Manikandan, S., Chandrasekaran, N., Mukherjee, A. and Kumaraguru, A. K. (2014) ' Drug Delivery System for Controlled Cancer Therapy Using Physico-Chemically Stabilized Bioconjugated Gold Nanoparticles Synthesized from Marine Macroalgae.' *Padina Gymnospora, Journal of Nanomedicine and Nanotechology*, 5(2) pp.1-7.

Singh, A.B. and Harris, R.C. (2005) 'Autocrine, paracrine and juxtacrine signaling by EGFR ligands.' *Cellular Signaling*, 17, pp. 1183-1193.

Soenen, S.J., Manshian, B.B., Montenegro, J.-M., Amin, F., Meermann, B., Thiron, T., Cornelissen, M., Vanhaecke, F., Doak, S., Para W.J., De Smedt, S.C.; Braeckmans, K. (2012) 'Cytotoxic Effects of Gold Nanoparticles: A Multiparametric Study.' *ACS Nano, 6*(7) pp. 5767-5783.

Soenen S.J., Montenegro, J. -M., Abdelmonem, A.M., Manshiand, B.B., Doak, S.H.,Wolfgang J. P., De Smedt, S.C. and Braeckmans, K. (2014) 'The effect of nanoparticle degradation on poly (methacrylic acid)-coated quantum dot toxicity: The importance of particle functionality assessment in toxicology.' *Acta biomaterialia*, 10(2) pp. 732-741.

Sonavane G, Tomoda K, Sano A, Ohshima H, Terada H, Makino K.(2008) 'In vitro permeation of gold nanoparticles through rat skin and rat intestine: effect of particle size.' *Colloids and Surfaces B: Bio interfaces*, 65(1) pp. 1-10.

Sokoya, E.M., Burns, A.R., Setiawan, C.T., Coleman, H.A, Parkington.C. and Tare, M. (2006) 'Evidence for the involvement of myoendothelial gap junctions in EDHF-mediated relaxation in the rat middle cerebral artery.' *American Journal of Physiology - Heart and Circulatory Physiology*, 291, pp. 385-393.

Souza, G.R. and Miller, H. (2012) 'Chapter 2: Elastic Light Scattering of Biopolymer/ Gold Nanoparticles Fractal Aggregates.' Book es C.D. (ed.), Reviews in Plasmonics, *Springer*, pp. 39-68. Available on: http://www.springer.com/cda/content/document/cda_downloaddocument/9781461408833-c1.pdf?SGWID=0-0-45-1252451-p174132423 (Accessed: 3 January 2014).

Sterm chemicals, INC. (2013) 'Medical and Pharmaceutical Applications for Nanomaterials and nanoparticles-supplier data by strem chemicals.' Available on: www.azonano.com/article.aspx?ArticleID=1336 (Accessed: 20 January 2014).

Stöber, W., Fink, A. and Bohn, E. (1968) 'Controlled Growth of monodisperes silica spheres in the Micron size range.' *Journal of Colloid and Interface Science*, 26, pp.62-69.

Stoelting, R.K. and Hillier, S.C. (2005) 'Pharmacology & Physiology in Anesthetic Practice.' 4th ed., Philadelphia: *Lippincott Williams and Wilkins*, pp. 1-850.

Suh, H., Jeong, B., Liu, F. and Kim, S.W. (1998) 'Cellular uptake study of Biodegradable nanoparticles in vascular smooth muscle cells.' *Pharmaceutical Research*, 15, pp.1495-1498.

Suh, W.H., Suslick, K. S., Stucky, G.D. and Suh, Y.H. (2009) 'Nanotechnology, Nanotoxicology, and Neuroscience.' *Progress in Neurobiology*, 87, pp. 133-170.

Sumpio, B.E., Riley, J.T. and Dardik, A. (2002) 'Cells in focus: endothelial cell.' *International Journal of Biochemistry and Cell Biology*, 34(12) pp.1508-1512.

Sun, C., Leeb, J. and Zhang, M. (2008) 'Magnetic Nanoparticles in MR Imaging and Drug Delivery.' *Advanced Drug Delivery Reviews*, 60, pp.1252–1265.

Swami, S., Shi, J., Gadde, S., Votruba , A. R., Kolishetti, N. and Farokhzad O.C. (2012) 'Nanoparticles for Targeted and Temporally Controlled Drug Delivery. In Svenson S. and Prud'homme, R.K. Multifunctional Nanoparticles for Drug Delivery Applications Nanostructure Science and Technology.' US, *Springer*, pp. 9-29.

Swapp, S. (2012) 'Geochemical Instrumentation and Analysis: Scanning Electron Microscopy (SEM).' *University of Wyoming*. Available at :http://serc.carleton.edu/18401 (Accessed: 8 July 2014).

Sykes, E.A., Chen, J., Zheng, G. and. Chan, W.C.W. (2014) 'Investigating the Impact of Nanoparticle Size on Active and Passive Tumor Targeting Efficiency.'*ACS Nano,* 8(6) p. 5696–5706.

Swanson, J.A. and Watts, C. (1995) 'Macropinocytosis.' *Trends in cell biology*, 5(11) pp. 424-428.

Taimeh, Z., Loughran, J., Birks, E.J. and Bolli R. (2013) 'Vascular endothelial growth factor in heart failure.' *Nature Reviews Cardiology*, 10, pp. 519-530.

Takae, S., Akiyama, Y., Otsuka, H., Nakamura, T., Nagasaki, Y. and Kataoka, K. (2005) 'Ligand density effect on biorecognition by PEGylated gold nanoparticles: regulated interaction of RCA120lectin with lactose installed to the distal end of tethered PEG strands on gold surface.' *Biomacromolecules*, 6(2) pp. 818–824.

Terentyuk, G., Akchurin, G., Maksimova, I., Shantrokha, A., Tuchin, V., Maslyakova, G., Suleymanova, L., Kogan, B., Khlebtsov, N. and Khlebtsov, B. (2009) 'Tracking gold nanoparticles in the body Biomedical Optics & Medical Imaging.' *International society for optics and photonics (SPIE)*, (4).

Tiwari, P.M., Vig, K., Dennis V.A. and Singh S. R. (2011) 'Functionalized Gold Nanoparticles and Their Biomedical Applications.' *Nanomaterials*, 1, pp. 31-63.

Toma H.E., Zamarion, V.M., Toma, S.H. and Araki K. (2010) 'The coordination chemistry at gold nanoparticles.' *Journal of the Brazilian Chemical Society*, 21(7) pp.1158-1176.

Tosi, G., Bortot, B., Ruozi, B., Dolcetta, D., Vandelli, M. A., Forni, F. and Severini, G.M. (2013) 'Potential use of polymeric nanoparticles for drug delivery across the blood-brain barrier.' *Current Medicinal Chemistry*, 20(17) pp. 2212-25.

Treuel, L., Jiang, X. and Nienhaus, G. U. (2013) 'New views on cellular uptake and trafficking of manufactured nanoparticles.' *Journal of the Royal Society Interface*, 10(82), Article 20120939.

Tsai S.-W., Liaw, J.-W., Kao1 Y.-C., Huang, M.-Yu., Lee, C.-Y., Rau, R.,Huang, C.Y., Wei, K.-C. and Ye, T.-C. (2013) 'Internalized Gold Nanoparticles Do Not Affect theOsteogenesis and Apoptosis of MG63 Osteoblast-LikeCells: A Quantitative, In Vitro Study.' *Plos one*, 8(10) pp. 6545-6557.

Tscharnuter, W. (2000) 'Photon CorrelationSpectroscopy in Particle Sizing' in Encyclopedia of Analytical Chemistry. R.A. Meyers , *John Wiley & Sons Ltd, Chichester*, (Ed.) pp.5469-5485.

Tucknott, R. and Yaliraki, S.N. (2002) 'Aggregation properties of carbon nanotubes at interfaces.'*Chemical Physics*, 281, pp. 455–463.

Turkevich, J., Stevenson, P. C. and Hillier, J. (1951) 'A study of the nucleation and growth processes in the synthesis of colloidal gold.' *Discussions of the Faraday Society*, 11, pp. 55-75.

Van Blaaderen, A. and Vrij, A. (1992) 'Synthesis and characterization of colloidal dispersions of fluorescent, monodisperse silica spheres.' *Langmuir*, 8(12) pp. 2921–2931.

Van Blaaderin, A. and Vrij, A. (1993) 'Synthesis and characterisation of monodisperese colloidal organo-silica spheres.' *Journal of colloid and interface science,* 156, pp. 1-18.

Van Blaadern, A., Van Geest, J., Vrij, A. (1992) 'Monodisperese colloidal silica spheres from tetraalkoxysilanes particle formation and growth meachanism.' *Journal of colloid and interface science* , 154 (2) pp. 481-501.

Van Hove, C.E. Van der Donckt, C., Herman, A.G., Bult, H. and Fransen, P. (2009) 'Vasodilator efficacy of nitric oxide depends on mechanisms of intracellular calcium mobilization in mouse aortic smooth muscle cell.' *British Journal of Pharmacology*, 158(3) pp. 920–930.

Vecchio, G., Galeone, A., Brunetti, V., Maiorano, G., Sabella, S., Cingolani, R. and Pompa, P. P. (2012) 'Concentration-Dependent, Size-Independent Toxicity of Citrate Capped AuNPs in Drosophila melanogaster.' *Plos one,* 7(1) e29980.

Venkatathri, N. (2007) 'Preparation of silica nanoparticle through coating with octyldecyltrimethoxy silane.' *Indian Journal of Chemistry,* 46, pp. 1955-1958.

Verhaegh, N.A.M. and Van Bladderen, A. (1994) ' Dispersions of rhodamine-labelled silica spheres - Synthesis, characterization, and fluorescence Confocal Scanning Laser Microscopy.' *Langmuir*, 10, pp. 1427-1438.

Verrier, E.D. and Boyle, E.M. 'Endothelial Cell Injury in Cardiovascular Surgery.' *Annals of Thoracic Surgery*, 1996, 62, pp. 915-922.

Visser, Taco D.; Wiersma, Sjoerd H. (1994) 'Electromagnetic description of image formation in confocal fluorescence microscopy.' *Journal of the Optical Society of America A: Optics, Image Science, and Vision,* 11(2) pp.599-608.

Voliani, V., Signore, G., Nifosí, R., Ricci, F., Luin. S. and Beltram, F. (2012) 'Smart Delivery and Controlled Drug Release with Gold Nanoparticles: NewFrontiers in Nanomedicine.' *Recent Patents on Nanomedicine*, 2(1) pp. 34-44.

Wang, F., Phonthammachai, N., Mya, K.Y., Tjiu, W. and He, C. (2011) 'PEG-POSS Assisted Facile Preparation of Amphiphilic Gold Nanoparticles and Interface Formation Janus.' *Chemical Communications*, 47(2) pp. 767-769.

Wang, Y. and Zhao, S. (2010) 'Vascular Biology of the Placenta.' San Rafael (CA): Morgan & Claypool Life Sciences, Accessed 01 February 2014, Available from: http://www.ncbi.nlm.nih.gov/books/NBK53247.

Webb, C,R. (2003) 'Smooth muscle contraction and relaxation.' *Advances in Physiology Education*, 27, pp. 201-206.

Xie, D., Jules, S., Weng,Y., Zhou, Y., Sidner, R.A. and Pescovitz, M. (2012) 'Poly(ethylene glycol) and poly(N-vinlypyrrolidone) for improved porcine islet cryopreservation.' *Journal of Biomedical Science and Engineering*, 5, pp. 263-269.

Yeh, J.-M., Huang, K.-Y., Lin, S.-Y., Wu, Y.-Y., Huang, C.-C. and Liou, S.-J. (2009), 'Noncovalent Interaction between Gold Nanoparticles and Multiwalled Carbon Nanotubes via an Intermediatory.' *Journal of Nanotechnology*, 2009, pp. 1-7.

Yuan, Z., Hein, T.W., Rosa, R. H. and Kuo, L. (2008) 'Sildenafil (Viagra) Evokes Retinal Arteriolar Dilation: Dual Pathways via NOS Activation and Phosphodiesterase Inhibition.' *Investigative Ophthalmology & Visual Science*, 49, pp. 720–725.

Yung, Y.C., Chae, J., Buehler, M.J., Hunter, C.P. and Mooney, D.J. (2009) Cyclic tensile strain triggers a sequence of autocrine and paracrine signaling to regulate angiogenic sprouting in human vascular cells.' *Proceedings of the National Academy of Sciences of the United States of America*, 106(36) pp. 5279-84.

Zecchin, H.G., Priviero, F.B., Souza, C.T., Zecchin, K.G., Prada, P.O., Carvalheira, J.B., Velloso, L.A., Antunes, E. and Saad, M.J. (2007) 'Defective insulin and acetylcholine induction of endothelial cell-nitric oxide synthase through insulin receptor substrate/Akt signaling pathway in aorta of obese rats.' *Diabetes*, 56(4) pp.1014-24.

Zhang X, Guo M, Wu H, Sun Y, Ding Y, Feng X, Zhang L. (2009) 'Irradiation stability and cytotoxicity of gold nanoparticles for radiotherapy.' *International Journal of nanomedicine*, 4, pp.165-73.

Zhang, H. L., Wu, S. H., Tao, Y., Zang, L. and Su, Z. (2010) 'Preparation and Characterization of Water-Soluble Chitosan Nanoparticles as Protein Delivery System.' *Journal of Nanomaterials*, 2010, Article ID 898910 pp. 1- 5.

Zhang, X.-D., Di, Wu, D., Shen, X., Chen, J., Sun, Y.-M., Liu, P.-X. and Liang, X.-J. (2012) 'Size-dependent radiosensitization of PEG-coated gold nanoparticles for cancer radiation therapy.'*Biomaterials*, 33(27) pp. 6408-6419.

Zhi X, Fang H, Bao C, Shen G, Zhang J, Wang K, Guo S, Wan T, Cui D. (2013) 'The immunotoxicity of graphene oxides and the effect of PVP-coating.' *Biomaterials*, 34(21) pp. 5254-61.

9. Appendix

9.1 Appendix A-Chemistry

1. Equation used for working out sphere of particles

$$V = \frac{4}{3}\pi r^3 \qquad [1]$$

Equation 3.1: ***Equation used to calculate the volume of a sphere***

V is volume of sphere π is 3.14 and **r** is the radius of the nanoparticles in cm.

This equation is used to work out the number of particles per mL.

$$m = V \times D \qquad [2]$$

Equation 3.2: ***Equation used to work out mass of a nanoparticles sphere***

m is mass of a nanoparticles sphere, **V** is volume of a sphere and **D** is the density of material used to make the nanoparticles.

$$N = \frac{m}{V} \qquad [3]$$

Equation 3.3: ***Equation used to work out the number of particles within a solution***

V is the volume of a sphere at a given diameter, **m** is the mass of dried nanoparticle product (1mL).

2. Working out total number of mPEG 5000MW and PVP (8000MW) molecules needed to cover area of the gold surface area

Equation used to *working out the surface area of a sphere* :

$$4\prod r^2 = 4x\prod(6x10\text{-}7)^2 = 4.52x10\text{-}12cm^2$$

Calculation for *working out the area of 1 monolayer of mPEG or PVP:*

Assume to cover particles with 1 monolayer, mPEG or PVP will take up 1 nm, therefore area of 1 monolayer is L x h $(1x10\text{-}7)^2 = 1x10^{-14}cm^2$

Chains of mPEG or PVP required to cover an area of a particle:

$4.52x10\text{-}12cm^2$ / $1x10^{-14}cm^2$ =452 chains

Calculation for working out* the *total chains of mPEG orPVP required to cover an area of a particle:

Working out weight of 1 molecule of mPEG:

5000 RMM / 6.022 x 10^23. =$8.303x10^{-21}$g

$8.303x10^{-21}$g x 452 chains=$3.75\ x10^{-18}$g of mPEG required to cover an area of a particle.

Working out weight of 1 molecule of PVP:

8000 RMM / 6.022 x 10^23. =$1.328\ x\ 10^{-20}$

$1.328x10^{-20}$g x 452 chains=$6.00\ x10^{-18}$g of PVP required to cover an area of a particle.

3. Titration of NH_4OH with HCl to determine the concentration of ammonia (NH_3) in the bottle of NH_4OH before synthesising nanoparticles

1.5 ml of NH_4OH unknown concentration was added in a 250ml volumetric flask, then made up to 250cm^3 with water. The (25cm^3) burette is then filled up with 25 ml of 0.1 HCl. Then 20ml of NH_40H from the stock solution of 250ml was transferred into a 100ml conical flask using a glass pipette. Methyl red indicator (2 drops) was added in the flask containing the 20ml of NH_4OH. A magnetic stirrer was introduced in the NH_4OH solution inorder to aid with the stirring of the solution. The flask was then place under the burette then 0.1M HCl was added in to the flask drop wise until the solution changes colour from yellow to pinkish. The value in which it took for the HCl to change the colour of the solution in the flask was recorded. The procedure was repeated 3 times . The average was recorded to work out the % of NH_3 and concentration of NH_4OH (See Table 1).

Table 1: Volume of HCl used in titrating of NH_4OH for determining the % of ammonia

Amount of NH_4OH(cm^3)titrated with HCl	Volume of HCl used to titrate (cm^3)
20	17.5
20	17.49
20	17.4
	AVERAGE :17.46

3.1 Working out the concentration of NH4OH and the %NH3 in the 1L bottle of NH4OH:

$NH_4OH+HCl \rightarrow NH_4Cl + H_2O$

(M X mL) NH_4OH=(M X mL)HCL

M X 20mL=0.1x17.46

Concentration of NH_40H=0.0873 mol/l

g/l= RMM X n

- 35 X 0.0873 =3.0555g/l

(M X mL) NH_4OH (before)=(M x mL) NH_4OH (after)

Volume (1000mL) x Density(0.9) =Mass (900g of **NH_4OH before**)

Working out the mass of **NH_4OH**

M X 1.5=0.0873x250cm^{-3}

Mass of NH_4OH **after** (509.25g) =14.55 X 35

% of NH_4OH =509.25/900 x100=56.65%

Gram of NH_3 : mass (g) =RMM X n

- **Therefore 17x14.55=247g of NH3**

Working out the mass of NH_4OH

% of NH_3 247g of NH_3/900g x100

- **Therefore 27% of NH_3 in the 1L bottle of NH_4OH**

4. Silica NPs fabricated using methods from previous Studies

USING METHOD FROM GIESCHE 1993

Silica produced at the size of 100nm under the temperature of ***$60^{O}C$***

Material

0.8M NH_3

0.2M TEOS

3M H_2O

USING METHOD FROM VAN BLAADEREN AND VRIJ 1992

Silica produced at the size of 110nm under the temperature ***$20^{O}C$***

(Adapted by adding Rhodamine dye(0.001g)

Material

0.07M APS

0.15M TEOS

2.96M H_2O

1.10M NH_3

USING METHOD FROM VAN BLAADEREN, GEEST AND VRIJ (1992) *Silica produced at the size of 35nm under the temperature of* ***$20^{O}C$***

(Adapted by adding APS)

Material

1.2M NH3

0.0016M TEOS

2.98M H_2O

5. An example of the calculation of the amount of APS needed to coat sphere with one monolayer

Area of Sio2 sphere particle with the diameter of 103nm

- $2.7x10^{13}$ *for 1ml* $3.33x10^{-6} x\, 2.7x10^{13}\, cm^2 = 8998.87cm^2$ *molecules*

$8998.87cm^2/40x10^{-16} = 2.24x10^{18}$*molecules*

Mass of an APS molecule=RMM/Avogadro's number

- $222/6.0221x10^{23} = 3.69x10^{-22}$ g

Mass of APS needed=Number of APS molecules x Mass of an APS molecule

$2.24x10^{18} x 3.69x10^{-22}$

$8x10^{-4}g/222=3.7x10^{-7}$moles

$C = 3.7x10^{-7}/0.0230dm^3$

$1.61x10^{-4}M$ = n/100ml=0.0161g of APS=16uL

$0.001xV1=2.76x10^{-5}Mx23.06$

V1=3.72mL of ethanol

Table 2: Hydrodynamic size of silica nanoparticles, in water from adapted method which were repeated n=2

Method	NH_4OH (mL)	H_20 (mL)	ETOH (mL)	TEOS (mL)	Rhodamine dye (g)	APS (uL)	TEMP ^0C	PARTICLE SIZE nm (DLS)		DURATION OF REACTION NH_4OH
								WITH DYE	WITHOUT	
Geische 100nm	4.533	1.722	69.28	20	-	-	60°C	-	200.65 ± 35.65	24 hr
Bladdern and viraj (1992)	6.233	0.272	55.969	3.35l	0.001g	189	20°C	913.7±52.7	618 ± 45.8	24 hr
Bladdern et al (1992)	8.394	0.151	57.134	0.033	0.001g	9.46	20°C	Aggregat-ed to large sizes >1000nm	371.7 ± 10.3	24hr

Table 3: The effect of surface charge on the hydrodynamic and potential of nanoparticles in H_2O and potassium physiological salt solution using Stöber method

		Hydrodynamic diameter (DLS)				*Charge*	*pH of sample*	*Zeta potential (mV)*			
SAMPLE NUMBER	***SAMPLE***	***Size in H_2O***	***Size in H_2O (pH 7.4)***	***Size in PSS***	***Size in PSS (pH 7.4)***			***Zeta potential in water***	***Zeta potential in PSS***	***Zeta potential in water (pH 7.4)***	***Zeta potential in PSS (pH 7.4)***
1	**TMSI- (WITHOUT DYE)**	**103.3**	**133**		**275.1**	**-**	**8.30**	**-80.1**	**-10.7**	**-59.7**	**-29.8**
2	**TMSI+ (WITHOUT DYE)**	**137**	**-**	**222**		**+**	**6.63**	**18.2**	**5.82**	**18.97**	**-4.99**
3	**TMRHSI- (WITH DYE)**	**125**	**-**	**145**		**-**	**8.64**	**-49.8**	**-37.8**	**-30.2**	**-23.6**
4	**TMRHSI+(WITH DYE)**	**187**		**256**		**+**	**6.80**	**9.23**	**5.42**	**-7.18**	**-6.91**

$^-$ Without APS

$^+$ With APS

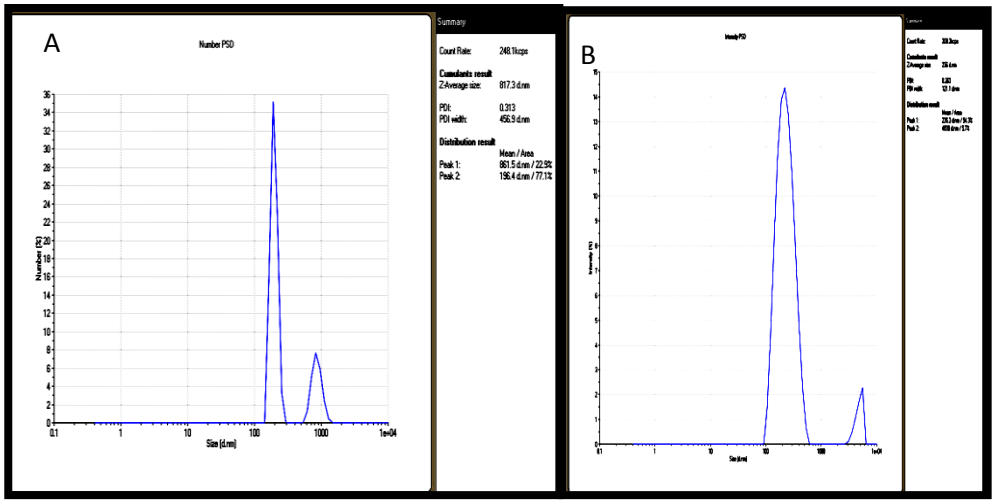

Figure 1: The photon correlation spectroscopy analysis (A and B)showing the hydrodynamic diameter of GEISHE (1993) METHOD for 100nm silica nanoparticles in H_2O.

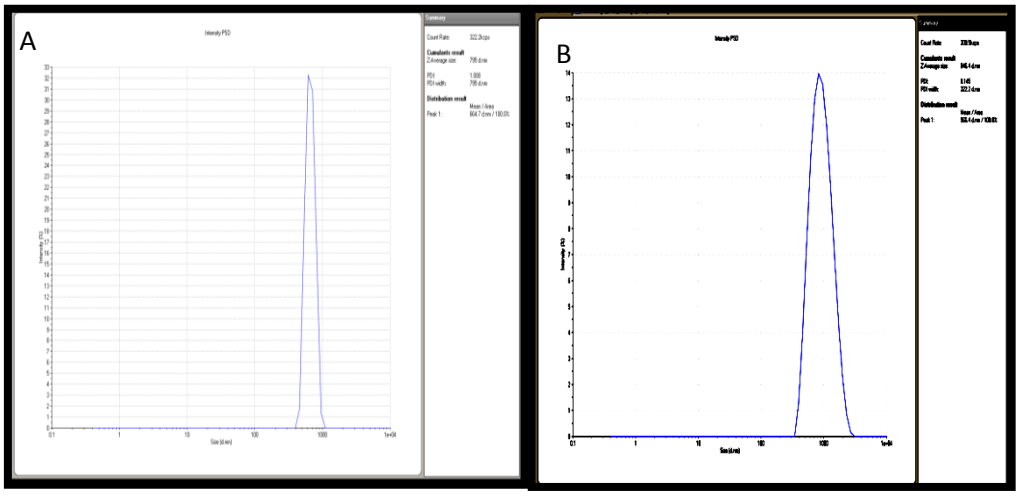

Figure 2: The photon correlation spectroscopy analysis showing the hydrodynamic diameter of Van Bladdern and Viraj (1993) METHOD for 110nm silica nanoparticles in H_2O. Sample A and B with dye

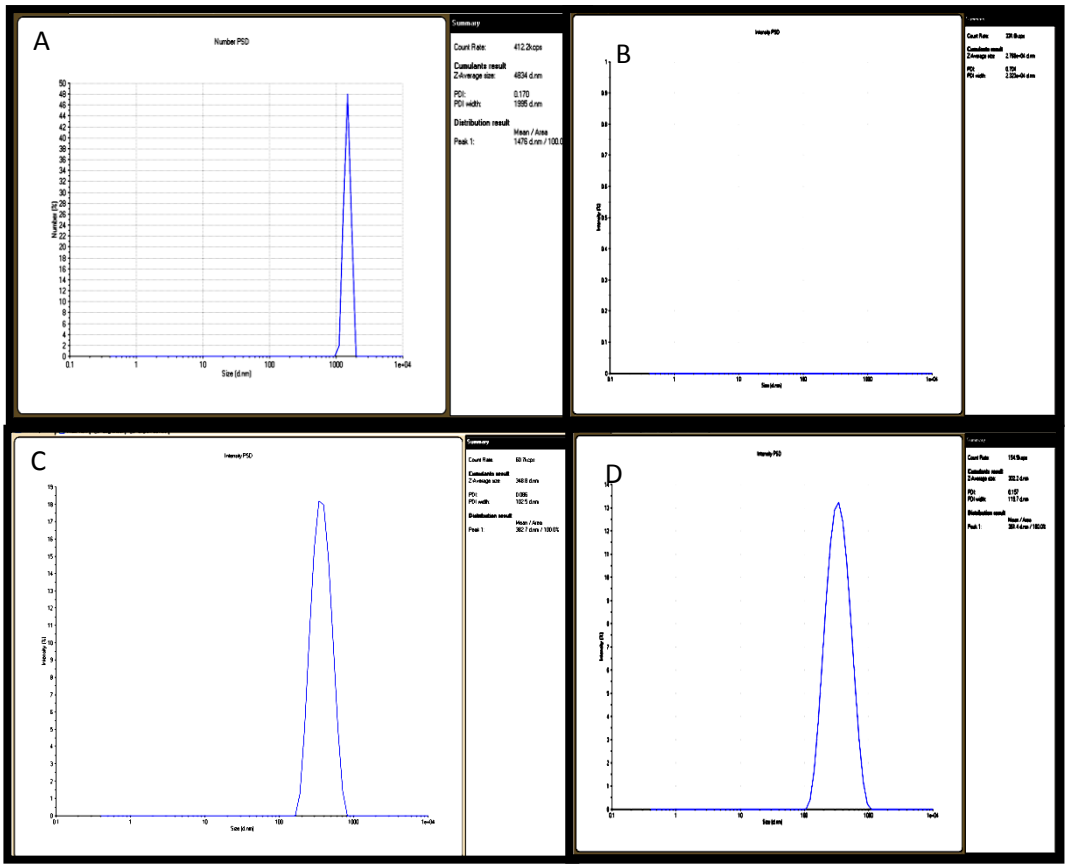

Figure 3: The photon correlation spectroscopy analysis showing the hydrodynamic diameter of Van Bladdern et al (1992) METHOD A) and B)with dye C) and D) without dye

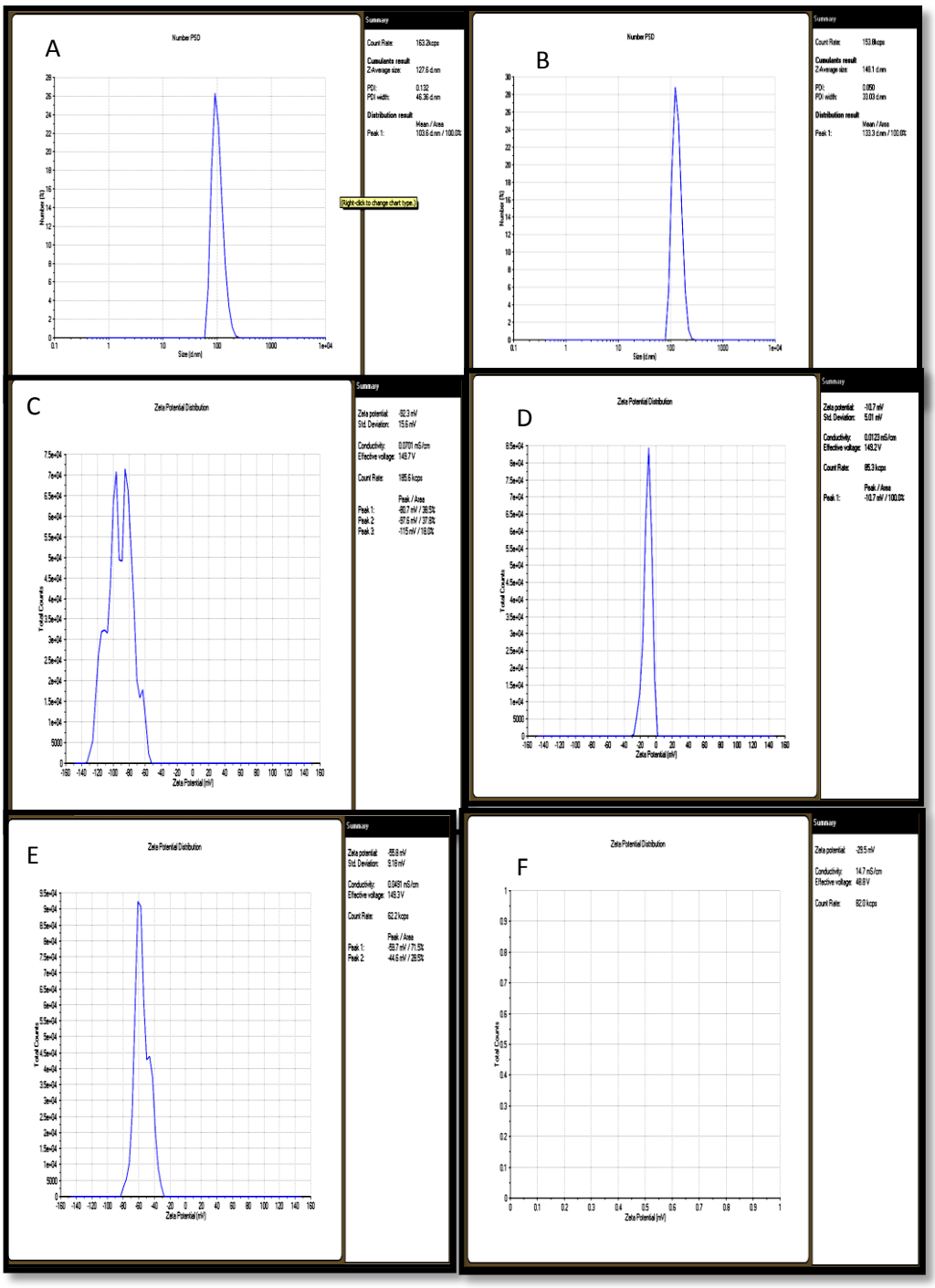

Figure 4: The photon correlation spectroscopy analysis showing the hydrodynamic diameter and stability of TMSI-(WITHOUT DYE) in A) H_2O B)PSS) C) Zeta potential in H_2O D) Zeta potential pss E) Zeta potential in water (pH 7.4) and F) Zeta potential inPSS (pH 7.4)

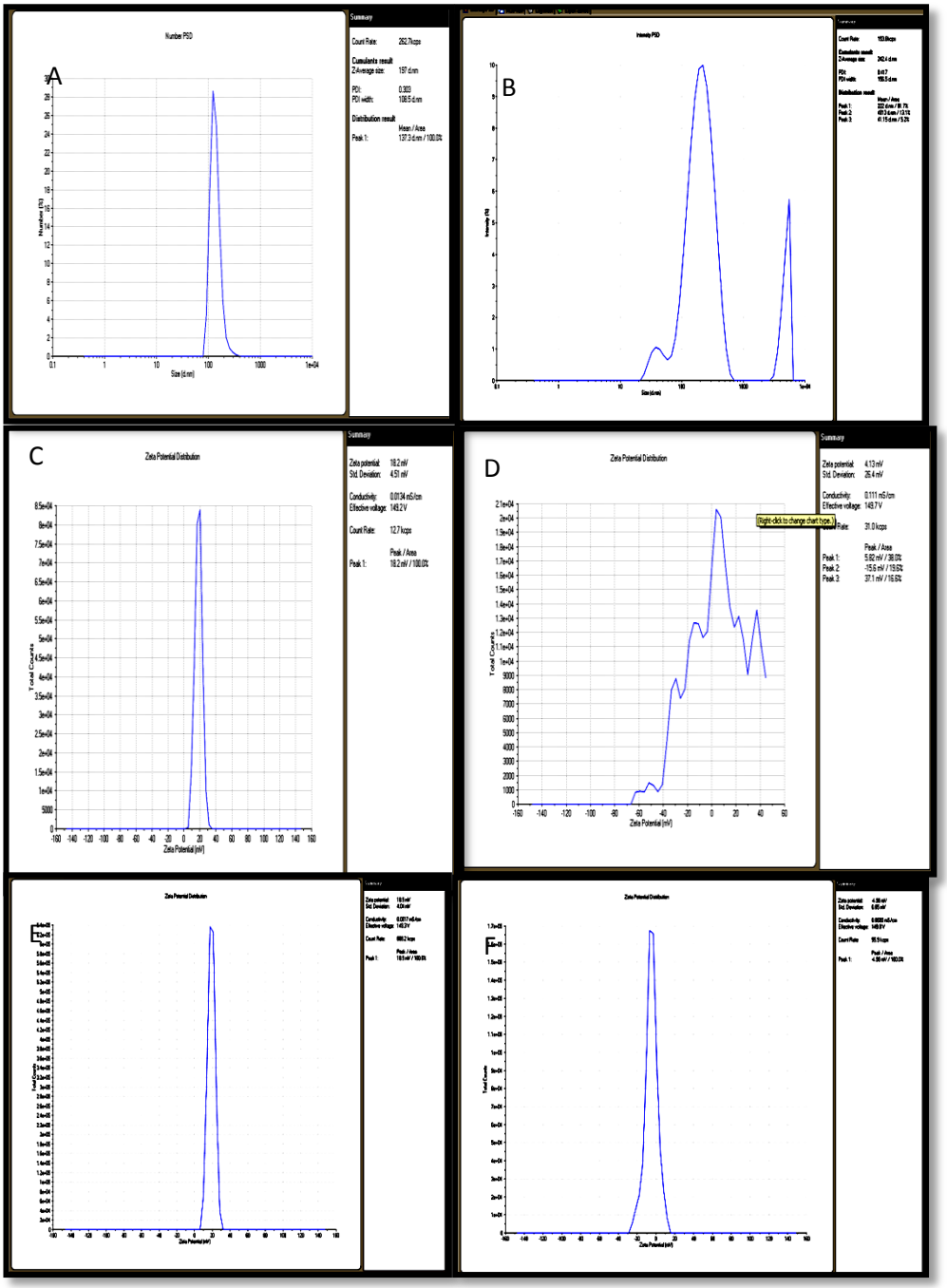

Figure 5: The photon correlation spectroscopy analysis showing the hydrodynamic diameter and stability of TMSI+(WITHOUT DYE) in A) H_2O B) PSS) C) Zeta potential in H_2O D) Zeta potential pss E) Zeta potential in water (pH 7.4) and F) Zeta potential in PSS (pH 7.4)

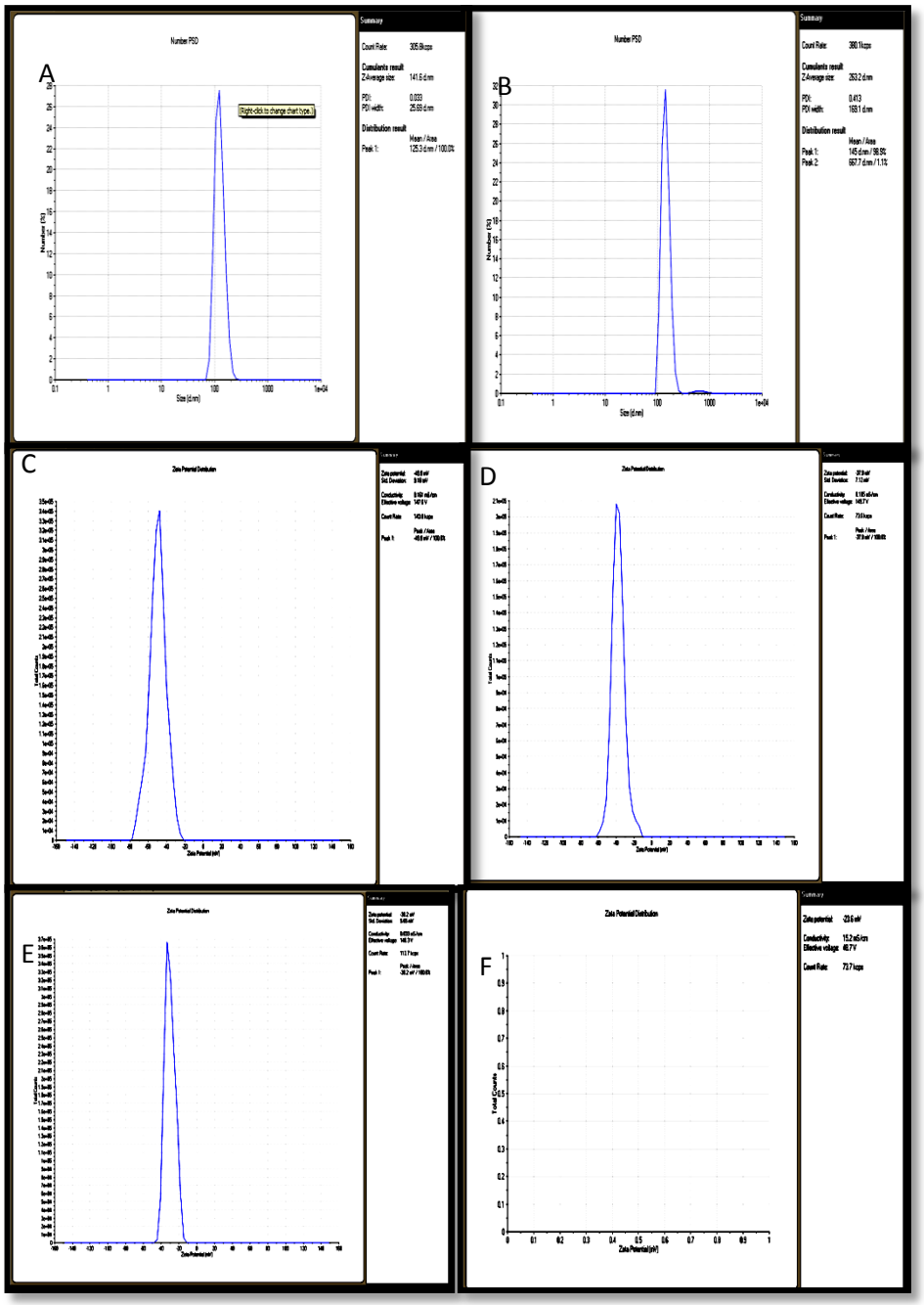

Figure 6: The photon correlation spectroscopy analysis showing the hydrodynamic diameter and stability of TMRHSI-(WITH DYE) in A) H2O B) PSS, C) Zeta potential in H2O, D) Zeta potential pss, E) Zeta potential in water (pH 7.4) and F) Zeta potential inPSS (pH 7.4)

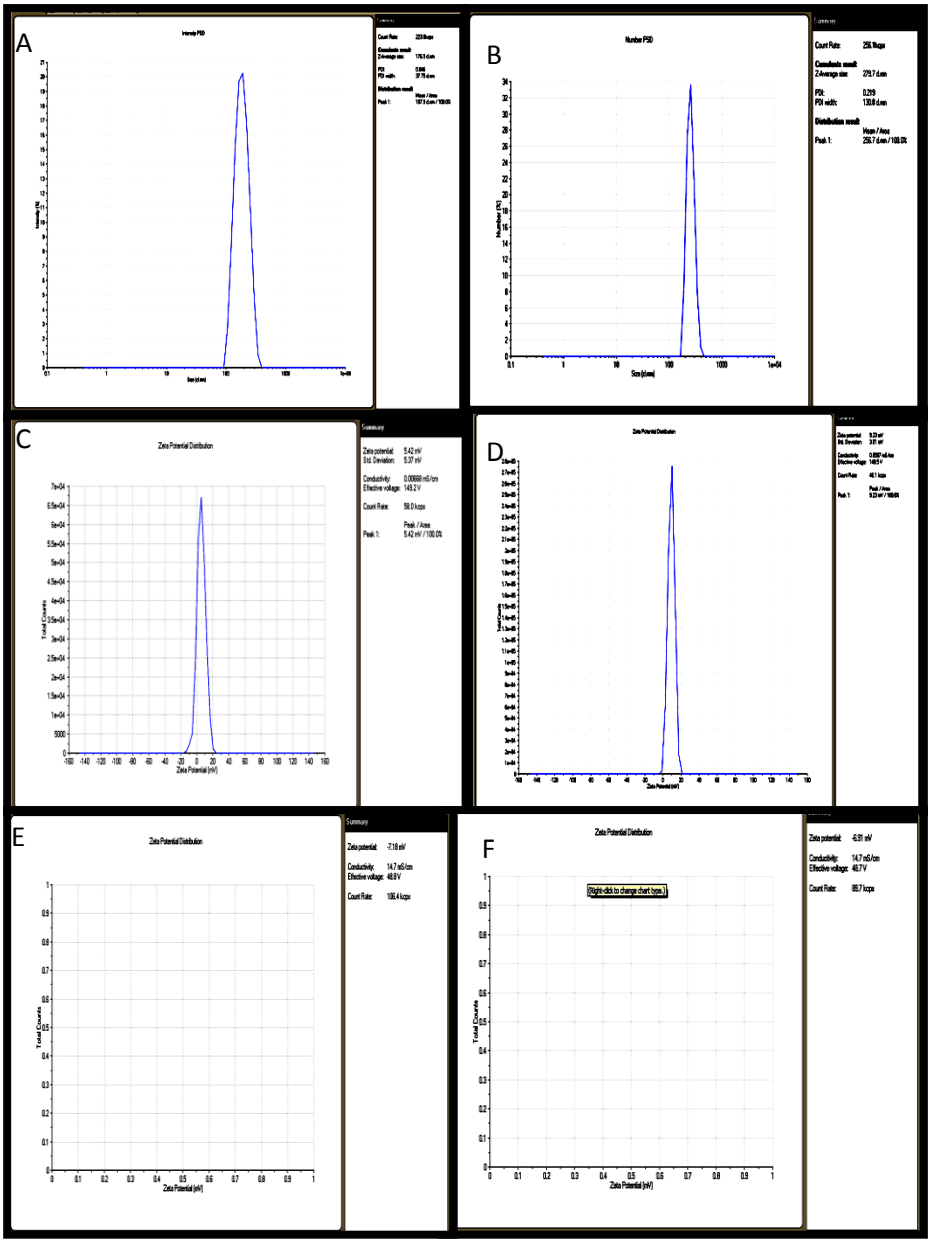

Figure 7: The photon correlation spectroscopy analysis showing the hydrodynamic diameter and stability of TMRHSI+(WITH DYE) in A) H_2O B)PSS) C) Zeta potential in H_2O)D Zeta potential pss)E) Zeta potential in water (pH 7.4)F) Zeta potential inPSS(pH 7.4)

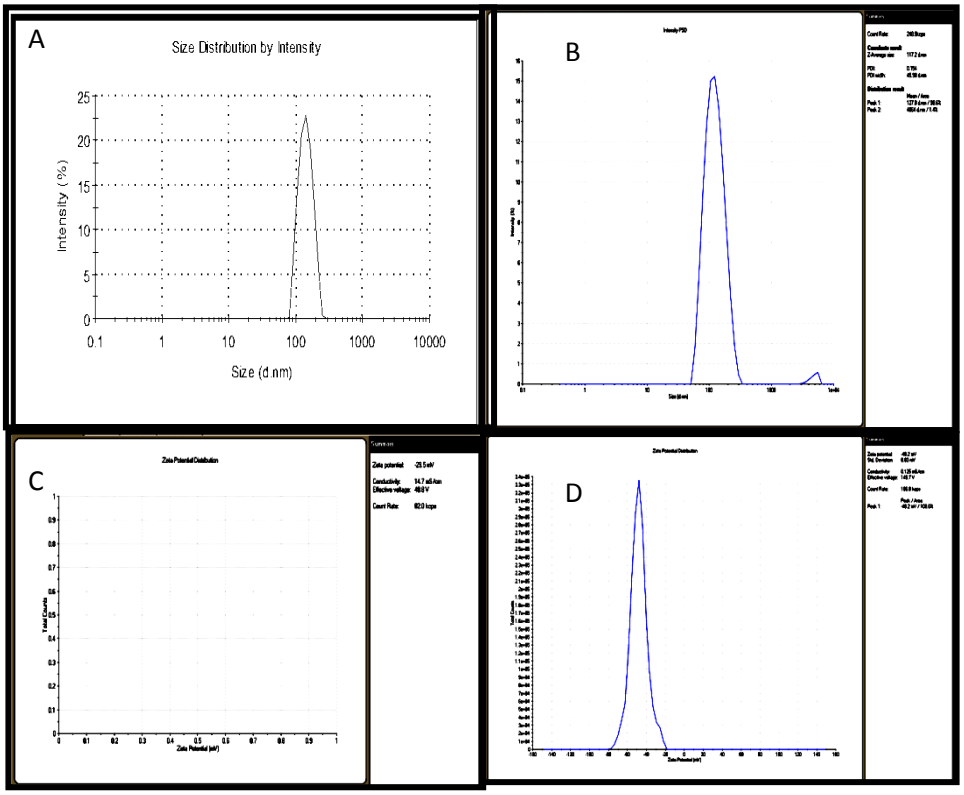

Figure 8: The photon correlation spectroscopy analysis showing the hydrodynamic diameter and stability of RH28) in A) H_2O, B) PSS , C) Zeta potential in H_2O and D) Zeta potential in PSS)

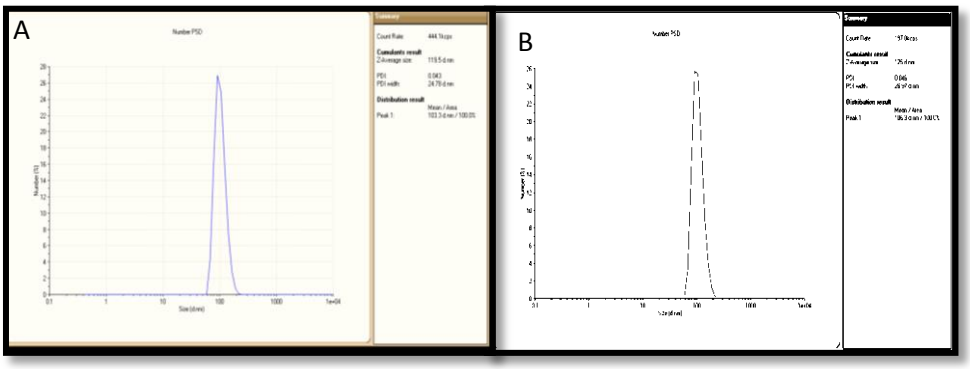

Figure 9 : The photon correlation spectroscopy analysis showing the hydrodynamic diameter and stability of TMNA- 100nm in A) H_2O and B) PSS

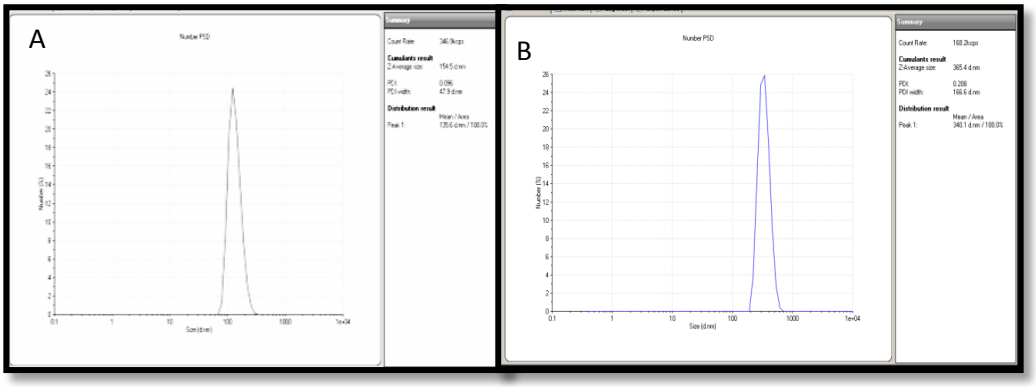

Figure 10 : The photon correlation spectroscopy analysis showing the hydrodynamic diameter and stability of TMNA+ 100nm in A) H_2O and B) PSS

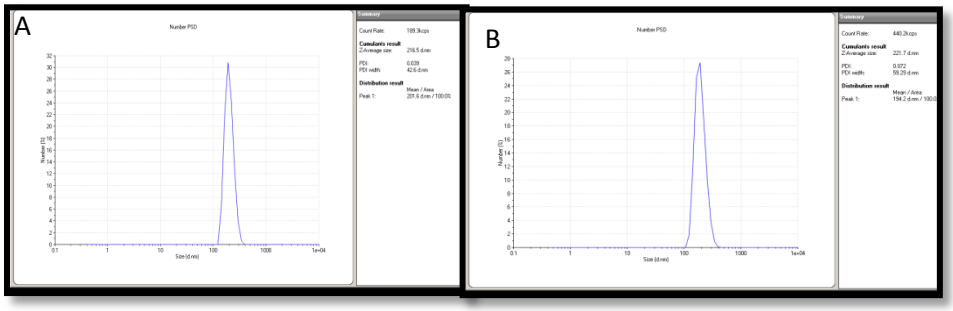

Figure 11 : The photon correlation spectroscopy analysis showing the hydrodynamic diameter and stability of TMNA- 200nm in A) H_2O and B) PSS

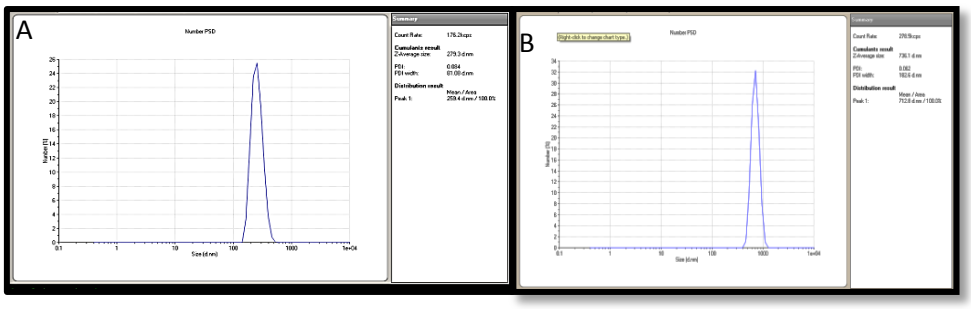

Figure 12 : The photon correlation spectroscopy analysis showing the hydrodynamic diameter and stability of TMNA+ 200nm in A) H_2O and B) PSS

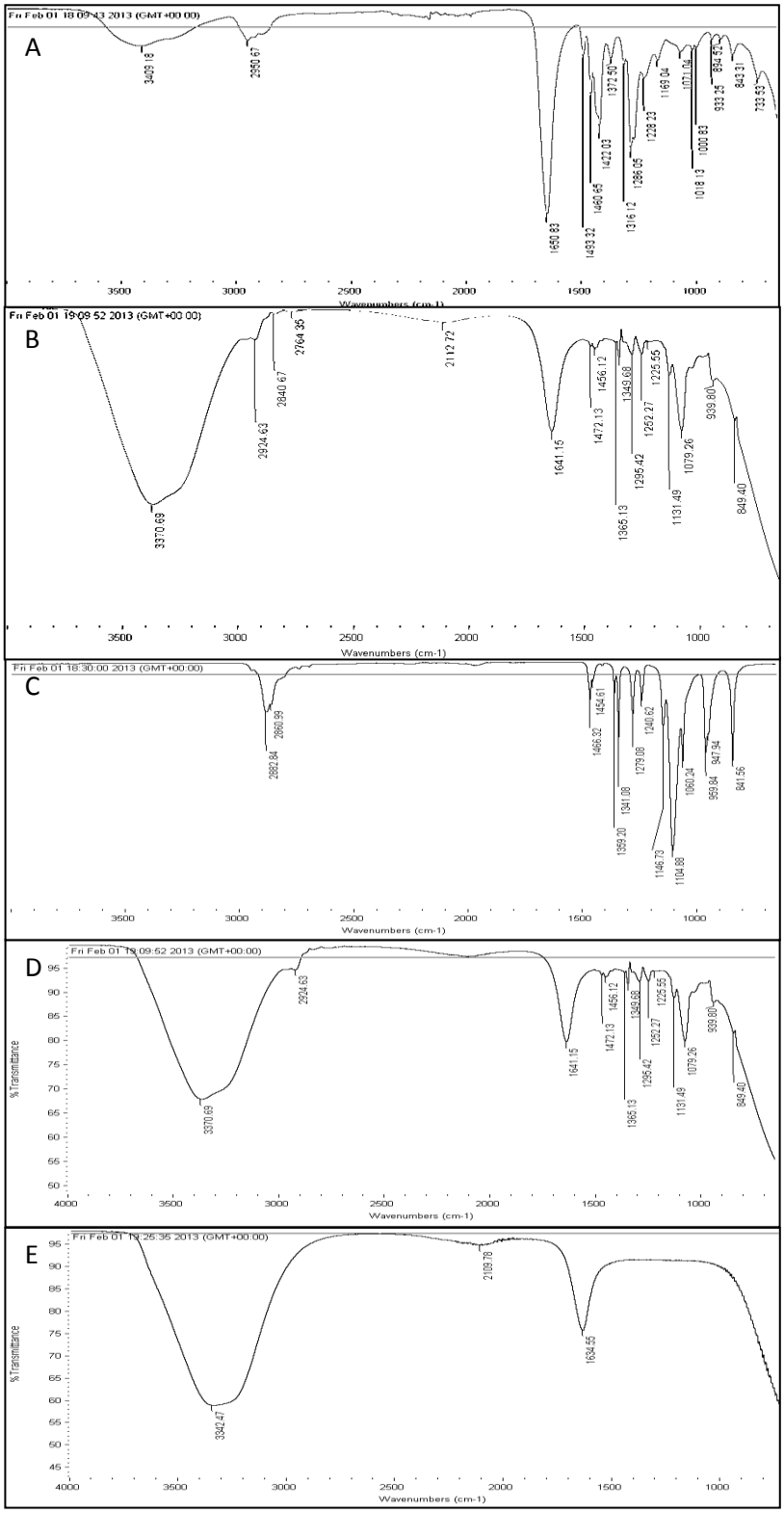

Figure 12: DRIFTS OF A)PVP ALONE and B)PVP modified AuNPs C)mPEG ALONE D) mPEG modified AuNP and E) AuNPs

Table 4: Determining the relative amount of AuNPs in both 300ul, 600ul sample and uptake by aortic vessels

***AuNPs in aortic vessels**

Sample Name	Average concentration of AuNPs (ppm)	Percentage of AuNPs uptake (%)
Control	0.024	0.004
300ul of AuNPs	3.231	100.000
600 ul of AuNPs	5.907	100.000
AuNPs(2.9ug/mL)*	0.451	13.957
AuNPs(5.8ug/mL)*	0.747	23.121
Aupvp(2.9ug/mL)*	0.143	4.426
Aupvp (5.8ug/mL)*	0.382	6.466
AuMPEG(2.9ug/mL)*	0.123	3.811
AuMPEG (5.8ug/mL)*	0.359	6.070

9.2 Appendix B-Cellular study

Table1: The cell proliferation after incubation with modified and non-modified AuNPs and their stabilisers at 24 hrs. and 48hrs using Coulter Counter, Where *p<0.05, **p<0.01 and *** p<0.001

24 hours	control	AuNPs	AuPVP	PVP	PEG	mPEG	AumPEG
Average	50327	31430	33504	36936	30861	27307	26778
PAIRED TTEST	-	8.85E-05***	0.00184**	0.008746**	0.012335**	0.00146**	0.0003**
48 hours	control	AuNPs	AuPVP	PVP	PEG	mPEG	AumPEG
Average	47391	28216	32494	28256	33606	32366	34216
PAIRED TTEST	-	0.012392997**	0.00419**	0.000901***	0.031656*	0.00289**	0.000580***

Table 2: The viability of cells after incubation with modified and non-modified AuNPs and their stabilisers at 24 hrs. and 48hrs using haemocytometer, Where *p<0.05 and ***p<0.001

Condition	Viability of cells after incubation (%)		P-Value		
	24 hrs.	48 hrs.	24 hrs. (Control vs.)	48 hrs. (Control vs.)	24 hrs. vs. 48 hrs.
CONTROL	96.53±2.11	95.14±2.50	-	-	0.693
AuNPs	82.15±7.06	87.50±3.60	0.123	0.157	0.537
AuPVP	85.42±5.51	73.61±6.05	0.133	0.030*	0.223
PVP	77.08±5.51	81.60±10.62	0.030*	0.283	0.725
AuMPEG	88.19±0.69	89.58±2.75	0.030*	0.210	0.651
mPEG	89.24±8.76	71.53±3.47	0.464	0.346	0.801
PEG	85.42±2.08	91.67±2.08	0.020*	0.005***	0.027*

Table3: The viability of cells after incubation with modified and non-modified AuNPs and their stabilisers at 24 hrs. and 48hrs using automated Cell Counter , Where *p<0.05, **p<0.01 and *** p<0.001

Condition	Viability of cells after incubation (%)		P value		
	24 hrs.	48hrs	24 hrs. (Control vs.)	48 hrs. (Control vs.)	p-value (24hrs Vs. 48hrs)
CONTROL	97.75±1.31	96.75±1.97	-	-	0.688
AuNPs	90.75±3.22	96.5±1.50	0.091	0.923	0.157
AuPVP	83.25±2.95	56.5±2.62	0.004**	1.81E-05****	0.001***
PVP	93±2.48	83.75±5.89	0.142	0.081	0.198
AumPEG	86.25±4.40	92.5±1.50	0.046*	0.200	0.228
Mpeg	91.5±2.32	91.75±3.54	0.058	0.264	0.955
PEG	83.75±6.66	72.25±7.08	0.084	0.016*	0.282

Table 4: The analysis of FACs flow cytometer used to determine the viability of cells after incubation with modified and non-modified AuNPs and their stabilisers at 24 hrs. and 48hrs Where *p<0.05, *p<0.01, *** p<0.001

Condition	Incubation time				p-value			
	30min	2 hrs	24 hrs	48 hrs	30min Control vs. 24 hrs	30min Control vs. 48 hrs	24 hrs Control vs. 24 hrs	24 hrs Control vs. 48 hrs
control no stain	99.72 ± 0.03	99.75 ± 0.10	99.76 ± 0.067	96.87 ± 1.85	0.057	0.705	-	0.289
control stain	94.65 ± 2.61	94.44 ± 2.67	92.81 ± 3.54	95.40 ± 1.64	0.002**	0.819	0.119 (CONTROL no stain V.S CONTROL Stain)	0.473
Aumpeg	95.95 ± 0.22	90.36 ± 0.27	75.12 ± 0.57	93.09 ± 1.65	0.003**	0.641	0.003**	0.344
AuNPS	95.50 ± 0.24	92.33 ± 0.31	77.02 ± 0.72	91.29 ± 0.16	0.003**	0.269	0.006**	0.053*
AuPVP	94.5 ± 0.27	92.50 ± 0.24	76.22 ± 1.00	85.58 ± 0.27	0.002**	0.026*	0.005**	0.312
mPEG	94.79 ± 0.36	91.84 ± 0.43	76.51 ± 0.14	90.92 ± 0.37	0.009**	0.232	0.005**	0.453
PVP	96.13 ± 0.06	81.73 ± 5.71	82.33 ± 0.41	93.25 ± 0.06	5e-6***	0.621	0.021*	0.289

9.3 Appendix C-Vascular study

Table 1: Average ACh response of vessels before and after incubation without NPs (PSS) (n=6) for 30 min.

ACh concentration	log[ACh]	AVERAGE % RELAXATION BEFORE	AVERAGE % RELAXATION AFTER	Paired t-test
$1x10^{-8}$	-8	5.57	3.68	0.19416
$4x10^{-8}$	-7.4	14.43	11.62	0.06665
$3.20x10^{-7}$	-6.5	29.66	17.14	0.01109
$1.28x10^{-6}$	-5.9	37.46	24.34	0.01950
$5.12x10^{-6}$	-5.3	41.85	33.45	0.06156
$2.05X10^{-5}$	-4.7	43.56	37.22	0.10887
$8.19X10^{-5}$	-4.1	56.88	46.66	0.04676
$1.11x10^{-4}$	-3.8	63.46	57.53	0.14439
$2.3x10^{-4}$	-3.5	80.29	68.33	0.09005

Table 2: Average SNP response of vessels before and after incubation without NPs (PSS) (n=7) for 30 min.

SNP concentration	Log[SNP]	AVERAGE % RELAXATION BEFORE	AVERAGE % RELAXATION AFTER	Paired t-test
$1x10^{-10}$	-10	7.72	7.4	0.954391
$8x10^{-10}$	-9.1	32.86	25.1	0.262224
$3.2x10^{-9}$	-8.5	62.95	51.4	0.010003
$1.28x10^{-8}$	-7.9	71.68	72.0	0.976534
$5.12x10^{-8}$	-7.3	86.64	84.2	0.624957
$2.05x10^{-7}$	-6.7	95.26	86.5	0.005734

Table 3: Average ACh response of vessels before and after incubation with AuNPs(n=5)and Control (n=6) for 30 min.

ACh concentration	log[ACh]	AVERAGE % RELAXATION BEFORE	AVERAGE % RELAXATION AFTER	Paired t-test	Un-paired t-test
$1x10^{-8}$	-8	0.94	-0.64	0.404263	0.326256
$4x10^{-8}$	-7.4	4.29	5.66	0.800694	0.490163
$3.20x10^{-7}$	-6.5	8.05	11.67	0.723299	0.566694
$1.28x10^{-6}$	-5.9	17.50	15.95	0.894688	0.550331
$5.12x10^{-6}$	-5.3	23.88	28.75	0.611694	0.840879
$2.05X10^{-5}$	-4.7	29.73	33.90	0.659485	0.927022
$8.19X10^{-5}$	-4.1	41.37	40.77	0.934868	0.807125
$1.11x10^{-4}$	-3.8	55.96	53.51	0.784643	0.953815
$2.3x10^{-4}$	-3.5	65.92	61.84	0.706617	0.77778

Table 4: Average SNP response of vessels before and after incubation with AuNPs (n=6) Control (n=7) for 30 min.

SNP concentration	log[SNP]	AVERAGE % RELAXATION BEFORE	AVERAGE % RELAXATION AFTER	Paired t-test	Un paired t-test
1x10-8	-8	44.48	12.59	0.018	0.004
4x10-8	-7.4	85.59	43.22	0.001	0.002
3.20x10-7	-6.5	91.06	55.76	0.001	0.005
1.28x10-6	-5.9	92.40	65.33	0.002	
5.12x10-6	-5.3	94.70	67.57	0.005	
2.05X10-5	-4.7	95.13	69.36	0.021	
8.19X10-5	-4.1	96.13	72.11	0.037	

Table 5: Average ACh dose response before and after incubation with AuNPs modified with maximum concentration ($9.5x10^{-12}$ M) PVP(n=6) Control (n=6) for 30 min.

ACh concentration	log[ACh]	AVERAGE % RELAXATION BEFORE	AVERAGE % RELAXATION AFTER	Paired t-test	unPaired t-test
$1x10^{-8}$	-8	3.51	1.60	0.121	0.498321
$4x10^{-8}$	-7.4	7.89	3.03	0.058	0.227925
$3.20x10^{-7}$	-6.5	22.09	6.38	0.030	0.195211
$1.28x10^{-6}$	-5.9	22.63	8.15	0.020	0.053898
$5.12x10^{-6}$	-5.3	30.56	13.62	0.003	0.016295
$2.05X10^{-5}$	-4.7	31.89	19.14	0.055	0.04547
$8.19X10^{-5}$	-4.1	37.53	41.29	0.653	0.544344
$1.11x10^{-4}$	-3.8	65.43	65.01	0.973	0.477948
$2.3x10^{-4}$	-3.5	88.44	76.55	0.291	0.399664

Table 6: Average SNP dose response after incubation with AuNPs modified with maximum concentration ($9.5x10^{-12}$ M) PVP(n=4) and Control (n=7) for 30 min.

SNP concentration	log[SNP]	AVERAGE % RELAXATION BEFORE	AVERAGE % RELAXATION AFTER	Paired t-test	Unpaired t-test
$8X10^{-10}$	-9	43.11	22.29	0.19005	0.826427
$3.2X10^{-9}$	-8.5	64.84	42.46	0.07872	0.649323
$1.28 x10^{-8}$	-8	70.09	52.19	0.06204	0.213642
$3.20x10^{-7}$	-6.5	73.74	56.97	0.02641	
$2.05X10^{-5}$	-4.7	75.33	61.98	0.02072	
$8.19X10^{-5}$	-4.1	94.49	78.74	0.03673	

Table 7: Average ACh dose response before and after incubation with AuNPs modified with minimum $5.9x10^{-13M}$ PVP (n=4) and Control (n=6) for 30 min.

ACh concentration	log[Ach]	Average % relaxation BEFORE	Average % relaxation AFTER	Paired t-test	Unpaired t-test
$1x10^{-8}$	-8	0.9	6.390185	0.42265	0.6458
$4x10^{-8}$	-7.4	3.45	11.04747	0.185214	0.952266
$3.20x10^{-7}$	-6.5	17.71	16.38699	0.273383	0.939431
$1.28x10^{-6}$	-5.9	28.79	22.97609	0.046869	0.892133
$5.12x10^{-6}$	-5.3	40.83	31.30602	0.016905	0.834884
$2.05X10^{-5}$	-4.7	42.74	34.18649	0.060844	0.759937
$8.19X10^{-5}$	-4.1	45.87	40.90224	0.01984	0.486673
$1.11x10^{-4}$	-3.8	47.76	48.59497	0.108319	0.244744
$2.3x10^{-4}$	-3.5	50.21	59.44046	0.233044	0.192812

Table 8 : Average ACh dose response after incubation with minimum $5.9X10^{-13}$ PVP alone (n=4)and Control(PSS)(n=5) for 30min.

ACh concentration	log[ACh]	CONTROL (PSS) n=5	PVP alone min conc (n=4)	Unpaired t-test
$1x10^{-8}$	-8	3.68	-0.69	0.203875
$4x10^{-8}$	-7.4	11.62	0.27	0.147566
$3.20x10^{-7}$	-6.5	17.13	3.660	0.1224
$1.28x10^{-6}$	-5.9	24.34	11.07	0.190325
$5.12x10^{-6}$	-5.3	33.44	17.96	0.148184
$2.05X10^{-5}$	-4.7	37.22	21.81	0.12204
$8.19X10^{-5}$	-4.1	46.66	28.25	0.053435
$1.11x10^{-4}$	-3.8	57.52	35.29	0.040891
$2.3x10^{-4}$	-3.5	68.32	44.65	0.045597

Table 9: Average SNP dose response after incubation with AuNPs modified with $5.9x10^{-13}$M PVP (n=4) and Control (PSS) (n=5) for 30 min.

SNP concentration	Log[SNP]	CONTROL (PSS) n=5	Average % relaxation AFTER $5.9x10^{-13}$M PVP(AuNPs)	Unpaired t-test
$1x10^{-10}$	-10	7.39	7.03	0.954
$8x10^{-10}$	-9.10	25.13	11.13	0.1555
$3.2x10^{-9}$	-8.49	51.42	22.00	0.0107
$1.28x10^{-8}$	-7.89	72.02	36.29	0.00019
$5.12x10^{-8}$	-7.29	84.18	60.23	3.31E-05
$2.05x10^{-7}$	-6.69	86.51	72.72	0.0288

Table10: Average SNP dose response AFTER incubation with minimum concentration ($5.9X10^{-13}$) PVP alone (n=3) and Control(PSS)(n=5) for 30min.

SNP concentration	log[SNP]	AVERAGE % RELAXATION AFTER Control (PSS) n=5	AVERAGE % RELAXATION AFTER PVP ALONE ($5.9X10^{-13}$)	Unpaired t-test
$1x10^{-10}$	-10	7.39	4.56	0.447
$8x10^{-10}$	-9.10	25.13	12.91	0.158
$3.2x10^{-9}$	-8.49	51.42	32.61	0.060
$1.28x10^{-8}$	-7.89	72.02	59.86	0.063
$5.12x10^{-8}$	-7.29	84.18	79.52	0.133
$2.05x10^{-7}$	-6.69	86.51	89.56	0.341

Table 11: Average ACh response AFTER incubation with AumPEG (2.9 µg/mL) and Control (PSS) (n=5) for 30 min.

ACh concentration	log[ACh]	AVERAGE % RELAXATION AFTER (5.8 µg/mL) AumPEG (n=5)	AVERAGE % RELAXATION AFTER CONTROL (PSS) n=5	Unpaired t-test
$1x10^{-8}$	-8.00	0.91	11.28	0.0883
$4x10^{-8}$	-7.40	2.55	24.01	0.0116
$3.20x10^{-7}$	-6.50	6.37	35.00	0.0008
$1.28x10^{-6}$	-5.90	12.25	38.81	0.0025
$5.12x10^{-6}$	-5.30	14.63	47.12	0.0007
$2.05X10^{-5}$	-4.70	18.22	50.98	0.0022
$8.19X10^{-5}$	-4.10	25.16	54.72	0.0097
$1.11x10^{-4}$	-3.80	27.96	59.74	0.0122
$2.3x10^{-4}$	-3.50	40.17	66.22	0.0298

Table 12: ACh response AFTER incubation with AumPEG (5.8µg/mL)(N=5) and control (PSS) (n=5) for 30 min.

ACh concentration	log[ACh]	AVERAGE % RELAXATION AFTER (5.8 µg/mL) AumPEG (n=5) CONTROL (PSS) n=5	AVERAGE % RELAXATION AFTER (5.8 µg/mL) AumPEG (n=5)AumPEG (2.9 µg/mL)	AVERAGE % RELAXATION AFTER (5.8 µg/mL) AumPEG (n=5)PEG alone n=5	Unpaired t-test with *AumPEG (2.9* µg/mL *)*	Unpaired t-test with *PEG alone (2.9* µg/mL *)*
$1x10^{-8}$	-8	11.28	5.35	15.95	0.28947	0.523013
$4x10^{-8}$	-7.4	24.01	16.03	23.98	0.30655	0.997323
$3.20x10^{-7}$	-6.5	35.00	28.01	31.00	0.36652	0.584608
$1.28x10^{-6}$	-5.9	38.81	32.07	34.04	0.39418	0.519861
$5.12x10^{-6}$	-5.3	47.12	42.68	39.47	0.57044	0.289176
$2.05X10^{-5}$	-4.7	50.98	46.81	42.67	0.62300	0.318654
$8.19X10^{-5}$	-4.1	54.72	49.39	46.34	0.63891	0.341705
$1.11x10^{-4}$	-3.8	59.74	52.93	52.88	0.73593	0.467099
$2.3x10^{-4}$	-3.5	66.22	59.52	61.46	0.76376	0.640546

Table 13: SNP responses BEFORE and AFTER incubation with AumPEG (n=5)(2.9 µg/mL) and Control (PSS) n=5 for 30 min.

SNP concentration	log[SNP]	AVERAGE % RELAXATION BEFORE	AVERAGE % RELAXATION AFTER	Paired t-test	Unpaired t-test
$1x10^{-10}$	-10	4.30	4.11	0.915561	0.9140
$8x10^{-10}$	-9.1	16.08	13.32	0.508209	0.5175
$3.2x10^{-9}$	-8.5	35.67	30.53	0.431169	0.3737
$1.28x10^{-8}$	-7.9	61.11	53.41	0.118424	0.1422
$5.12x10^{-8}$	-7.3	82.76	73.43	0.138817	0.1231
$2.05x10^{-7}$	-6.7	91.06	85.75	0.18574	0.1374

Table 14: SNP responses BEFORE and AFTER incubation with ($7.4x10^{-8}$g/ml) mPEG alone (n=4) (2.9 µg/mL) for 30 min.

SNP concentration	Log[SNP]	AVERAGE % RELAXATION BEFORE	AVERAGE % RELAXATION AFTER	Paired t-test
$6.66x10^{-8}$	-7.1	14.04	5.87	0.367756
$6.62x10^{-7}$	-6.2	26.58	18.81	0.30904
$6.60x10^{-6}$	-5.2	33.82	28.85	0.49722
$6.50x10^{-5}$	-4.2	37.62	33.01	0.39023
$6.50x10^{-4}$	-3.2	45.50	32.66	0.03059

Table 15: SNP response AFTER incubation with PEG alone(n=7) and Control (PSS) (n=5) for 30 min.

SNP concentration	log[SNP]	AVERAGE % RELAXATION AFTER CONTROL (PSS) (n=5)	AVERAGE % RELAXATION AFTER (PEG alone)(n=7)	Unpaired t-test
$1x10^{-10}$	-10.00	4.30	3.52	0.75875
$8x10^{-10}$	-9.10	16.08	9.46	0.22807
$3.2x10^{-9}$	-8.49	35.67	26.62	0.193659
$1.28x10^{-8}$	-7.89	61.11	46.78	0.049867
$5.12x10^{-8}$	-7.29	82.76	67.092	0.042663
$2.05x10^{-7}$	-6.69	91.06	79.43	0.02456